ASSIGNMENT OF PHOTOSYNTHETIC PARAMETERS IN ESTIMATION OF MARINE PHYTOPLANKTON PRODUCTION FROM REMOTE SENSING OF OCEAN COLOUR

by

Marie-Hélène Forget

Submitted in partial fulfillment of the
requirements for the degree of
Doctor of Philosophy

at

Dalhousie University
Halifax, Nova Scotia
August 2007

Your file Votre référence
ISBN: 978-0-494-31483-8
Our file Notre référence
ISBN: 978-0-494-31483-8

DALHOUSIE UNIVERSITY

To comply with the Canadian Privacy Act the National Library of Canada has requested that the following pages be removed from this copy of the thesis:

Preliminary Pages
- Examiners Signature Page (pii)
- Dalhousie Library Copyright Agreement (piii)

Appendices
- Copyright Releases (if applicable)

Table of Contents

List of Tables

List of Figures

Abstract

Photosynthesis (primary production) is the fundamental process by which solar photons are transformed into organic matter that is the source of energy for the entire food web. The first chapter of this thesis reviews the concepts that underpin models of marine primary production as well as the relevant parameters and their variation according to phytoplankton functional type. The application of the models to compute primary production from remotely-sensed images of ocean colour is then reviewed. The different approaches for assignment of the photosynthetic parameters in the model are presented and the advantages and disadvantages of each one of them are discussed. Particular emphasis is given to understanding the variability in photosynthesis-irradiance ($P - E$) parameters, which is the focus of the thesis.

In Chapter 2 and 4, new measurements of $P-E$ are presented for two ecologically-different regions of the North Atlantic: the tropical Caribbean waters and the temperate North-West Atlantic. The issues that have to be addressed for regional computations of primary production are examined, and results are presented for primary production in the two regions using remotely-sensed data on ocean colour. Chapter 3 presents a new method for extraction of the photosynthesis-response parameters from profiles of *in situ* phytoplankton production. The procedure, previously proposed but hitherto untested, is here implemented in various aquatic systems and a protocol is established for its use. The major conclusions and recommendations for future work are presented in the fifth and final chapter.

List of Abbreviations and Symbols Used

B	Chlorophyll a concentration in mg chla m^{-3}
B_0	background chlorophyll-a concentration in mg chla m^{-3}
B_Z	Water-column chlorophyll a concentration integrated over the euphotic zone in mg chla m^{-2}
D	Daylength in h
E_*^m	Dimensionless irradiance computed as surface irradiance at noon normalised to E_K in dimensionless units
E_K	The photo-acclimation parameter, where $E_K = P_m^B/\alpha^B$ in W m^{-2}
E_T	Daily irradiance (PAR) in mol photons m^{-2} d^{-1}
E_{max}	Daily PAR at the inflection point between light-limited and light-saturated production measured from *in situ* incubations (Behrenfeld and Falkowski, 1997) mol photons m^{-2} s^{-1}
H	Height of the chlorophyll peak at depth z_m in mg chla m^{-3}
K	Attenuation coefficient for downwelling irradiance (PAR) in m^{-1}
L	The thickness of a layer in m
P	Volumetric production in mg C m^{-3} d^{-1}
P^B	Production normalised to chlorophyll a concentration in mg C mg $chla^{-1}$ h^{-1}
P_m^B	The assimilation number, the chlorophyll-specific production at light saturation in mg C mg $chla^{-1}$ h^{-1}
P_{opt}^B	Maximum chlorophyll-specific carbon fixation measured from *in situ* incubations (Behrenfeld and Falkowski, 1997) in mg C mg $chla^{-1}$ h^{-1}
P_{ZT}	Daily integrated water-column production in mg C m^{-2} d^{-1}

R_S	Relative daily water-column production (Ryther 1956) in dimensionless units
T	Temperature in °C
Λ	Daily integrated water-column production normalised to water-column chlorophyll a (P_{ZT}/B_Z) in mg C mg chla^{-1} d^{-1}
Ψ	Water-column light utilisation index, the slope of the linear relationship between P_{ZT}/B_Z and E_T in g C g chla^{-1} (mol photons m^{-2})$^{-1}$
α^B	The initial slope of the production-irradiance relationship in mg C mg chla^{-1} (W m^{-2})$^{-1}$ h^{-1}
ϕ_f	Quantum yield of fluorescence in dimensionless units
ϕ_m	Maximum quantum yield of photosynthesis in dimensionless units
ρ	Measure of the relative importance of the maximum chlorophyll-a biomass compared with the background chlorophyll-a concentration, in dimensionless units
σ	defines the width of the DCM, where 4σ is the maximum width of the DCM peak in m
ξ	The intercept of the linear relationship between P_{ZT}/B_Z and E_T in g C g chla^{-1} d^{-1}
a_p^*	Chlorophyll-a specific absorption coefficient for phytoplankton in m^2 mg chla^{-1}
a_{676}^*	Chlorophyll-a specific absorption coefficient for phytoplankton at wavelength 676nm in m^2 mg chla^{-1}
b	Slope of the linear relationship between $f(E_*^m)$ and E_*^M in dimensionless units
c	Intercept of the linear relationship between $f(E_*^m)$ and E_*^m in dimensionless units
$f(E_*^m)$	Function of E_*^m in dimensionless units
h	integral under the Gaussian curve of the DCM peak, in mg chla m^{-2}
z_m	depth of the chlorophyll peak in m

z_p	Euphotic depth, where light is reduced to 1% of its value at the surface in m
ADP	Adenosine diphosphate
ATP	Adenosine triphosphate
AVHRR	Advance Very High Resolution Radiometer
C-SOLAS	Canadian branch of the Surface Ocean-Lower Atmosphere Study
CDOM	Chromophoric Dissolved Organic Matter
CTD	Conductivity, Temperature and Depth profiler
DCM	Deep Chlorophyll Maximum
DMS	Dimethylsulphide
FAO	Food and Agriculture Organization
HPLC	High Performance Liquid Chromatography
IOCCG	International Ocean-Colour Coordinating Group
LAPE	Lesser Antilles Pelagic Ecosystem
MERIS	Medium Resolution Imaging Spectrometer
MODIS	Moderate Resolution Imaging Spectroradiometer
NADPH	Reduced nicotinamide adenine dinucleotide phosphate
NASA	National Aeronautics and Space Administration
NOAA	National Oceanographic & Atmospheric Administration

NWCS	North West Coastal Shelf
PFT	Phytoplankton Functional Type
PSI	Photosystem I
PSII	Photosystem II
RMS	Root Mean Squared
Rubisco	Ribulose-1,5-biphosphate carboxylase/oxygenase
SeaDAS	SeaWiFS Data Analysis System
SeaWiFS	Sea-viewing Wide Field-of-view Sensor
SIDS	Small Island Developing States
SST	Sea Surface Temperature

Acknowledgements

First I would like to thank my supervisor, Dr. Shubha Sathyendranath, a talented scientist and a wonderful woman, who taught me, with a lot of patience, how to be rigorous and critical, two qualities that, I hope, will follow me throughout my scientific career. I would also like to thank Dr. Trevor Platt for his time, his advice and most importantly for believing in me. I am also grateful to my committee members for their availability and for their guidance, and the examiners, Dr. Bill Li, Dr. John Cullen and Dr. Ian Joint, for their valuable comments and for constructive discussions.

Thanks to Brian Irwin, who did the field work for the Caribbean project and processed the phytoplankton absorption analyses. Thanks to Dr. Edward Horne, who taught me and helped me with optical measurements. Thanks to Dr. George White for his support in processing satellite images. Thanks to Dr. Emmanuel Devred for his patience in teaching me IDL and other programming languages. Thanks to Dr. Cesar Fuentes-Yaco and Dr. Julien Pommier for their collaboration in the C-SOLAS project. Thanks to Dr. Venitia Stuart, Carla Caverhill and Dr. Anitha Nair for reading the manuscript and for moral support. And thanks to all scientific and technical staff of the Bedford Institute of Oceanography and to the C9 crew who helped with sampling, lab analyses and provided good advice. It was a great pleasure to conduct my study in such a stimulating environment.

The financial support for this thesis was provided by a grant from Natural Sciences and Engineering Research Council of Canada (NSERC) provided to Dr. Platt, a grant from the Canadian branch of the Surface Ocean-Lower Atmosphere Study (C-SOLAS) provided to Dr. Sathyendranath and a grant from Food and Agriculture Organization of the United Nations (FAO).

Finally, I would like, from the bottom of my heart, to thank my family, who supported me throughout this long adventure... thank you!

Chapter 1

INTRODUCTION

1.1 Photosynthesis

Primary production by phytoplankton, the first echelon of the trophic chain in aquatic systems, regulates energy available to higher trophic groups as well as the carbon and oxygen fluxes between the ocean and the atmosphere. Photosynthesis is the process by which autotrophic organisms transform photons (or solar energy) into organic matter:

$$H_2O + CO_2 + \text{light} \rightarrow (CH_2O) + O_2. \tag{1.1}$$

The organic matter is then available to heterotrophic organisms as a source of energy for respiration processes. Briefly, the photosynthesis reactions occur in two phases: the light and dark reactions. The light reactions involve absorption of photons by chlorophyll-a and accessory pigments found in the antenna. The solar energy is transferred to the reaction center of the photosystem II (PSII) where the energy is used by a chlorophyll molecule to dislocate electrons from molecules of water (H_2O) resulting in the emission of oxygen molecules (O_2) and protons (H^+). Then, a series of electron transfers follows until the electron reaches photosystem I (PSI), where a second light reaction occurs. The energy transfers following the Z scheme result in the emission of heat energy and production of a molecule of NADPH (reduced nicotinamide adenine dinucleotide phosphate). A third pathway of dissipation of the energy absorbed by the photosynthetic apparatus is fluorescence; this pathway represents only a small proportion of the energy dissipation (about 2-3%). The light reactions occur in the membrane of the thylakoid where the protein-based photosystems are countained. This membrane enables the physical segregation between the charges and allows the production, through ATP synthase, of molecules of ATP (adenosine triphosphate) from ADP (adenosine diphosphate) molecules. The light

reactions are limited mainly by light absorption, by the number of reaction centers available and by the number of open (as opposed to closed) reaction centers.

The dark reaction, which takes place in the stroma (or outside the thylakoid) involves the fixation of carbon through Rubisco (ribulose-1,5-bisphosphate carboxylase/oxygenase) enzyme catalysis following the Calvin-Benson cycle. Briefly, the carbon fixation follows four main steps: the carboxylation of one Rubisco protein to produce two molecules of 3-phosphoglycerate, the production of a molecule of triose phosphate (basic sugar) using the energy available from the NADPH and the ATP resulting from the light reactions, the conversion of the triose phosphate into a suite of complex sugar molecules, and finally the regeneration of a ribulose-1,5-busphosphate molecule. The assimilation of one molecule of CO_2 requires two molecules of NADPH and three molecules of ATP, two for the creation of the organic carbon compound, and one to allow the Rubisco enzyme to return to its initial state. The main limitations on the assimilation of carbon are the availability of CO_2 in the stroma, the amount of Rubisco protein available and the enzymatic activity of the Rubisco protein, which is strongly related to temperature.

Photosynthesis is the only mechanism to convert solar energy into chemical energy, and thus it is essential to quantify photosynthetic rate under natural conditions as accurately as possible. However not all autotrophic organisms have the same photosynthetic capacity. In the ocean macrophyte, periphyton and phytoplankton are primary producers; here we will focus on phytoplankton.

1.2 Phytoplankton Classification

Phytoplankton, the autotrophic organisms that drive primary production in the ocean ecosystems, are unicellular organisms that vary in size and function. The three main size classes are the pico-phytoplankton ($< 2\mu$m) the nano-phytoplankton (between 2 and 20μm) and the micro-phytoplankton ($> 20\mu$m). Two main phytoplankton groups constitute each one of these size classes (Table 1.1).

Owing to their smaller size, pico-phytoplankton absorb light more efficiently (a phenomenon known as the flattening effect, Duysens 1956) and thus are known to have higher photosynthetic capacity (Bouman *et al.* 2005). Moreover, because of their high surface to volume ratio, they are highly efficient at absorbing nutrients. Thus,

Table 1.1: Classification of phytoplankton groups according to their size classes.

Size classes	Phytoplankton classes	Phytoplankton groups
> 20 μm	Micro-phytoplankton	Diatoms Dinoflagellates
2 - 20 μm	Nano-phytoplankton	Nanoflagellates Cryptophytes
< 2 μm	Pico-phytoplankton	Green flagellates Cyanobacteria

pico-phytoplankton are predominant in oligotrophic conditions. On the other hand, micro-phytoplankton, diatoms more specifically, have the capacity of blooming when irradiance and nutrient concentrations are high, usually in the spring in temperate regions, when the water-column stratifies after the winter mixing. The phytoplankton biomass can reach chlorophyll concentrations of 30 to 100 mg m^{-3}. Because diatom blooms use nutrients imported from the deeper layers of the water column, the production performed during these events is known as new primary production. By contrast, the production of pico-phytoplankton in oligotrophic waters is known as regenerated primary production because the nutrient source is derived from the products of metabolism and from senescence of the phytoplankton.

Although the classification of phytoplankton by size is a very useful division of the phytoplankton community, phytoplankton groups often cross the size classes. For example, diatoms are usually considered as micro-phytoplankton, but depending on environmental conditions and on the species, some diatoms can be classified as nano-phytoplankton. Moreover, some phytoplankton groups, although they share the same size classes, have different functional properties. For example, diatoms and dinoflagellates share the same size class (micro-phytoplankton) but diatoms are silicifiers whereas dinoflagellates are DMS (dimethylsulphide) producers. Four main functional types are defined: nitrogen fixers, calcifiers, silicifiers, DMS producers (Table 1.2, see review by Nair *et al.* submitted). Again, some phytoplankton groups can be found in more than one class, such as the coccolithophores which can be classified both as a DMS-producer and as a calcifier.

Table 1.2: Classification of phytoplankton groups according to their functional type.

Phytoplankton functional type	Phytoplankton groups
Nitrogen fixers	cyanobacteria (*Trichodesmium*)
Calcifiers	haptophytes (coccolithophores)
Silicifiers	bacillariophyta (diatoms) chrysophyta silicoflagellates xantrophyta
DMS-producers	dinoflagellates haptophytes (coccolithophores)

Although this classification may not be perfect, it is certainly a very useful approach to modeling biogeochemical cycles (Le Quéré *et al.* 2005). Moreover, some of these phytoplankton functional types can now be detected by remote sensing of ocean colour (Subramaniam *et al.* 1999, Sathyendranath *et al.* 2004, Alvain *et al.* 2005), which represents a significant advantage to classification by functionality.

1.3 Primary Production From Remote Sensing of Ocean Colour

Remote sensing of ocean colour has proven to be valuable in providing synoptic fields of primary production (Longhurst *et al.* 1995, Antoine and Morel 1996, Antoine *et al.* 1996, Behrenfeld and Falkowski 1997, see also review from Joint and Groom 2000), from which it has been deduced that globally, oceanic primary production fixes from 36.5 to 50 gigatonnes of carbon every year, which is equivalent in magnitude to the terrestrial primary production (Longhurst *et al.* 1995, Behrenfeld *et al.* 2001, Cramer *et al.* 2001). Primary production can be computed using either empirical models (Joint and Groom 2000) or analytical models (Platt and Sathyendranath 1988, Platt *et al.* 1990, Antoine and Morel 1996, Behrenfeld and Falkowski 1997). To quantify primary production on synoptic scales from numerical analysis, remotely-sensed estimates of chlorophyll-a concentration, daily irradiance and attenuation coefficient have to be combined with the characteristics of pigment-biomass profiles and of photosynthetic response to light (Platt and Sathyendranath 1988, Sathyendranath and Platt 1993). Uncertainties associated with each of these functions generate uncertainties in production estimates from field data (Pemberton *et al.* 2006) and satellite application

(Platt *et al.* 1995, Joint and Groom 2000, Platt *et al.* submitted).

According to Sathyendranath and Platt (1993), the six steps to follow in computation of primary production are as follows (see Fig. 1.1):

- 1. Computation of light available at the surface.
- 2. Estimation of biomass at the surface.
- 3. Determination of the biomass profile.
- 4. Assignment of photosynthetic parameters.
- 5. Computation of underwater light transmission.
- 6. Computation of primary production.

Of all these steps, steps 1, 2, 5 and 6 are easy to handle. Step 1 could be estimated either by modelling (Bird 1984) or by satellite measurements. Further useful information is provided by satellite imagery to estimate the biomass at the surface (step 2). Various algorithms have been proposed to estimate chlorophyll-a concentration by remote sensing of ocean colour. Regional algorithms (Sathyendranath *et al.* 2004) should be preferred over global algorithms (O'Reilly *et al.* 1998) when the computation is intended to be limited to regional scales. Regarding step 5, good models are available to compute parameters of light distribution under water (Platt and Sathyendranath 1988). Sathyendranath and Platt (2007) have also shown by a comparison of models of photosynthesis-light models (step 6) that although they are classified into different groups of model (available light, absorbed light and biomass independant) they can all be interchanged and be written with the same set of parameters. Sathyendranath *et al.* (2007) have shown that a basic set of parameters is required to run any of the production models: α, P_m^B, the chlorophyll-a specific absorption coefficient a_B^* and the carbon-to-chlorophyll ratio. Steps 3 and 4 require assignment of parameters from *in situ* measurements. As chlorophyll-a concentration is a standard measurement at sea, biomass profiles are abundant. However, photosynthetic parameters are scarce, especially in the southern hemisphere, and thus represent an important limitation for computation of primary production

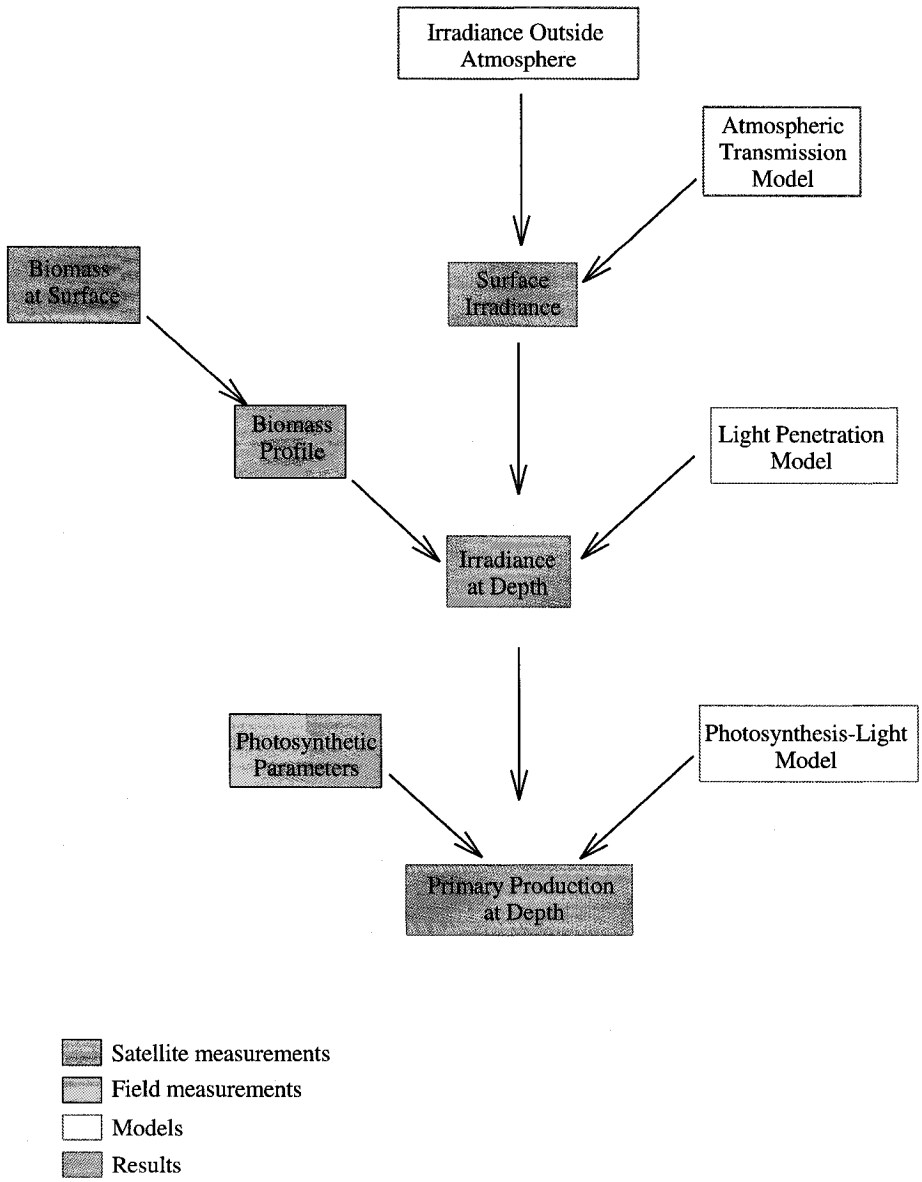

Figure 1.1: Flow chart showing the six steps required to compute primary production from remote sensing of ocean colour. Modified from Platt and Sathyendranath 1997

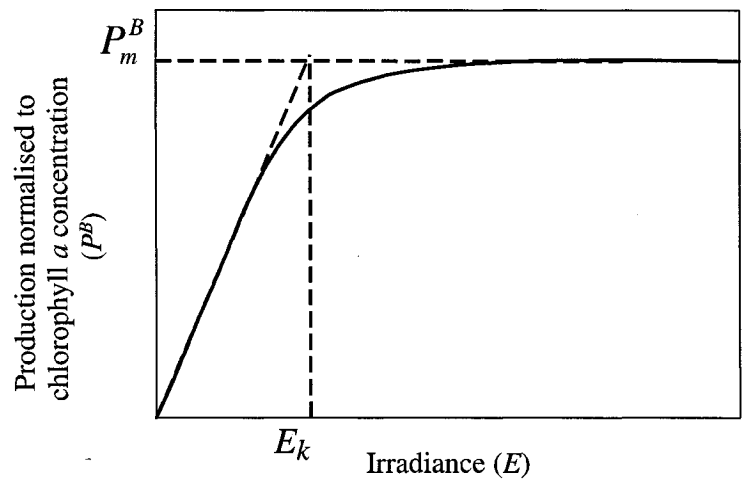

Figure 1.2: Relationship between irradiance (E) and production normalised to chlorophyll-a concentration (P^B) ($P - E$ curve) used to obtain the photosynthetic parameters α^B, the initial slope, and P_m^B, the assimilation number.

Photosynthetic parameters are extracted from photosynthesis-irradiance curves ($P-E$ curves) in which production P is normalised to chlorophyll-a concentration B (Fig. 1.2). The two parameters required to describe the $P-E$ relationship are α^B, the initial slope of the relationship, and P_m^B, the light-saturated production plateau. The projection on the abscissa of the intersection of the light-limited and the light-saturated parts of the $P-E$ curve provides the photoadaptation parameter E_k ($E_k = P_m^B/\alpha^B$). These parameters are derived from experiments made under light-controlled conditions in a light-gradient incubation box. Good estimates of phytoplankton production can be obtained by combining these photosynthetic parameters, when they are known, with the underwater irradiance field and biomass concentration (see for example Côté and Platt, 1984, Platt and Sathyendranath 1988, Kyewalyanga *et al.* 1997) implying that robust models are available for calculation of primary production.

It is another matter, however, to make calculations of primary production when the photosynthetic parameters are not known by direct measurement at the particular time and place of interest. Indeed, given that robust functions exist to calculate primary production from pigment biomass and irradiance, the principal difficulty in the calculation lies in the assignment of the photosynthetic parameters. Longhurst *et al.* (1995) have pointed out the paucity of data on these parameters, especially in some biogeochemical provinces of the southern hemisphere. In estimation of primary production using remotely-sensed data on ocean colour, where the primary production algorithms have to be implemented on a pixel-by-pixel basis, the required photosynthesis parameters are typically lacking.

Thus, a protocol for assignment of the photosynthetic parameters is needed so that primary production models may be implemented in instances when the parameters are unknown. I will now review the principal methods that have been used until now, and assess their limitations.

1.4 Survey of Protocols for Assignments of Photosynthetic Parameters

1.4.1 Background

Development of protocols for assigning photosynthetic parameters is governed by our view of the ecological and physiological issues involved and also on the tolerable uncertainty in the estimated parameters for calculation of primary production.

Ecologically, the magnitudes of the photosynthetic parameters at a particular time and place are under the control of many factors. These include the size and taxonomic status of the cells, temperature, nutrient status and the light history (review in Falkowski 1981). The parameter estimates must contain latent information on all these factors, but so far it has not been possible to extract the information in an unambiguous manner.

Physiologically, the two parameters α^B and P_m^B characterise different aspects of the photosynthesis process. The initial slope α^B is

$$\alpha^B = \lim_{E \to 0} \frac{\partial P^B}{\partial E}, \tag{1.2}$$

the increment in photosynthesis for a small change in irradiance at very low levels of irradiance. As such, it depends on the maximum quantum yield of photosynthesis ϕ_m. In principle, the maximum quantum yield ϕ_m is fixed by the biochemistry of photosynthesis (Platt and Jassby 1976) and one might propose that α^B is a universal constant. However, experience shows this is not so (Platt and Jassby 1976, Côté and Platt 1983, Kyewalyanga *et al.* 2002, and many more). Moreover, E is the *available* irradiance, such that the specific absorption coefficient of the cells, a_p^*, also plays a role (Platt and Jassby 1976):

$$\alpha^B = a_p^* \phi_m. \tag{1.3}$$

The specific absorption coefficient itself is highly variable, depending on numerous factors, in particular the size and pigment complement of the cell (Platt and Jassby 1976, Sathyendranath *et al.* 1987, Hoepffner and Sathyendranath 1992, Stuart *et al.* 1998, Ciotti *et al.* 2002). Cell size is especially important, in view of the phenomenon known as the packaging effect (Duysens 1956).

If α^B characterises the photochemical reactions of photosynthesis, the parameter P_m^B characterises the dark reactions of photosynthesis. These are enzyme-mediated reactions and therefore temperature-dependent, whereas photochemical reactions are not (Eppley, 1972). The magnitude of P_m^B is also related to the concentration of carboxylating enzymes in the cells, and can be regulated by the cells according to environmental factors (Glover and Morris 1979, review in Glover 1989).

In the absence of physiological models that express P_m^B and α^B explicitly as functions of variables such as light, temperature, nutrient and species composition (but see Geider *et al.* 1998), it has been no trivial matter to assign values to these parameters, on a pixel-by-pixel basis, in computation of primary production by remote sensing. Several approaches have been suggested in the literature.

1.4.2 Different Options for Assignment of Photosynthesis-Irradiance Parameters

The possible approaches to assignment of photosynthetic parameters were enumerated by Platt and Sathyendranath (1999):

- Globally uniform and always constant
- Globally uniform and seasonally constant
- Globally continuous
- Piecewise uniform
- Piecewise continuous

Many factors control the magnitude of the photosynthetic parameters, so assuming global uniformity and absolute constancy would be sweeping, and only justified for very approximate calculations. Nevertheless, there are examples where this assumption has been adopted in the literature (Morel and Berthon 1989).

The idea of continuity in parameter assignment, global or piecewise, implies that robust functions of environmental variables (for example temperature) are available for estimating parameter magnitudes. Because many factors affect the parameters, any one of them may be difficult to isolate for the construction of a predictive equation.

For example, it would not be unreasonable to suppose that P_m^B might be estimated from temperature given its status as characteristic of an enzyme-mediated reaction. However, in oceanography, local decreases in temperature are often associated with local increases in nutrient. Thus a decrease in temperature might directly decrease P_m^B but also be accompanied by an increase because of physiological changes in the cells due to enhanced nutrient conditions.

Thus estimating P_m^B from local temperature is difficult, yet considerable attention has been devoted to this method (Megard 1972, Balch *et al.* 1992, Antoine *et al.* 1996, Behrenfeld and Falkowski 1997). The most-frequently-cited paper is that of Behrenfeld and Falkowski (1997), and it has been applied to many oceanographic problems, even after the first author has distanced himself from it (Behrenfeld *et al.* 2002). On the other hand, Bouman *et al.* (2005) demonstrated that temperature predicts P_m^B very well in the Northwest Atlantic, but not in the tropical Arabian Sea.

Fewer authors have attempted to predict α^B from environmental variables. Unlike P_m^B, light-limited processes are not enzyme-mediated and thus should not be directly affected by temperature. Platt and Jassby (1976) have related the variability in the magnitude of α^B to changes in the light level averaged over three days prior to measurements. However, in the context of remote sensing of ocean-colour, primary production is usually estimated from composite images compiled over a period of two weeks. Thus light history over a short period of time is not suitable for assignment of this parameter. Behrenfeld *et al.* (2004) reviewed the variation of α^B and P_m^B and found that they covary in a significant proportion of field and laboratory results, implying that α^B could be assigned by estimating P_m^B. However, as they explain, this relationship is applicable only in variable environmental conditions and does not account for photoacclimation, which is in fact known to influence E_k (MacCaull and Platt, 1977).

Another means to predict α^B is through solar-induced chlorophyll fluorescence. The relationship between fluorescence and photosynthesis depends on pathways of energy conversion as described in biophysical models (Butler and Strasser 1977, Butler 1978, Topliss and Platt 1986, Kiefer *et al.* 1989, Krause and Weis 1991, Kiefer and Reinolds 1992, Doerffer 1993, Babin *et al.* 1995, Govindjee 1995, Babin *et al.* 1996, Maritorena *et al.* 2000, Morisson 2003). The quantum yield of fluorescence

(ϕ_f) is obtained as the total number of photons emitted divided by the total number of photons absorbed. The tripartite model (Butler and Strasser 1977, Butler 1978, Govindjee 1995) assumes that only three de-excitation pathways are possible for an excited chlorophyll-a molecule to return to its ground state: fluorescence, heat dissipation and photosynthesis. When all the reaction centres are open, the quantum yield of photosynthesis is maximal and the quantum yield of fluorescence is minimal. On the other hand, when all the reaction centres are closed, the quantum yield of photosynthesis is zero whereas that of fluorescence is maximal (Kiefer and Reynolds 1992). Thus, if heat dissipation remains constant, an inverse relationship between the quantum yield of photosynthesis and the maximum quantum yield of fluorescence is expected (Topliss and Platt, 1986). Huot *et al.* (2005) have proposed a method (as yet untested) to estimate quantum yields of fluorescence from satellite images of ocean colour. Westberry and Siegel (2003) studied the quantum yield of fluorescence and the quantum yield of photosynthesis in the Sargasso Sea, but found no relationship between them. However, it is worth mentioning that they used the actual quantum yield of photosynthesis rather than the maximum realised quantum yield of photosynthesis. Moreover, it has been shown that the quantum yield of fluorescence is species dependent, due to the distribution of pigments within the photosystems (Lutz *et al.* 1997, 2000). Most of the fluorescence occurs in photosystem II. Thus, it is not trivial to retrieve a relationship between the quantum yields of fluorescence and photosynthesis, especially in waters dominated by cyanobacteria such as the Sargasso Sea, because most chlorophyll-a molecules are associated with the photosystem I. Thus, no direct relationship between quantum yield of fluorescence and the maximum quantum yield of photosynthesis in time or space has been established for application to remote sensing of ocean colour. Furthermore, as the method based on solar-induced fluorescence would require measurements of quantum yield of photosynthesis to test the validity of the method, the need for measurements of photosynthesis-irradiance parameters would remain, at least until a robust method were established (which is far from being the case at present).

A distinction is made between globally-continuous and piecewise-continuous functions of environmental variables. Globally-continuous functions could be applied anywhere without modification of the functions. A piecewise-continuous function assumes

that the ocean is not the same everywhere, but is structured in ways that can be revealed through inspection and analysis. This view is implicit in the discipline of ocean biogeography: different parts of the ocean support different biological communities, in particular for the phytoplankton, and these communities show specific spatial (and temporal) patterns because of the spatial (and temporal) structure of the environment (Longhurst 1998). If autotrophic communities are structured over the globe, it can be expected that the ecophysiological parameters are also structured, given their dependence on cell size and taxonomic status. Then, the functions would change abruptly at the boundaries between autotrophic assemblages. This is the meaning of piecewise assignment.

A piecewise-continuous function of an environmental variable is somewhat vulnerable to the same criticism as a globally-continuous function. If the effect of the environmental independent variable (say temperature) is too difficult to isolate for construction of a predictive model, it might be abandoned in favour of an archive of measured parameters as a repository of information about the aggregate effect of all environmental factors on the parameter magnitude.

The rationale for assignment of photosynthetic parameters would then be as follows. The parameter values are controlled by many factors, varying regionally and seasonally, which are difficult to account for, from first principles. But the parameter magnitudes themselves reflect the aggregate effect of all these factors. Therefore, the best estimate of the parameters at a particular place and season would be selected from a parameter archive for that region and season. This is the basis for using biogeochemical provinces for calculation of global primary production (Longhurst *et al.* 1995). The principal weakness of the method, at present, is the paucity of data on such photosynthetic parameters.

It is easy to see that undersampling of photosynthetic parameters is a limitation on all existing protocols for assigning parameters, so we need to look elsewhere to augment the existing data. One possibility is to exploit the relatively-rich archive of data on *in situ* primary production, which predates the measurements of the photosynthetic parameters by many years (*in situ* experiments, Steemann-Nielsen 1952; photosynthetic parameters, early 70s) and is more widely measured even today.

In this thesis, I test various approaches to assigning photosynthetic parameters in two aquatic systems: a tropical ocean and the North Atlantic shelf. Three different assignment methods are examined: the regional approach, where parameters are kept constant over a determined area (Longhurst *et al.* 1995); a temperature model (Platt *et al.* 2005, Bouman *et al.* 2005); and the Nearest-Neighbour Method (Platt and Sathyendranath 2002, Platt *et al.* submitted), by which parameters are assigned according to temperature and chlorophyll fields and as a function of time of the year. I also develop and test, in a variety of aquatic systems, an approach to retrieve photosynthetic parameters from data on *in situ* production and the results are compared with the other approaches to assignment of parameters.

In Chapter 2, I present new data on photosynthesis-irradiance and profile parameters from a tropical ocean (the Caribbean Sea) and use them to compute primary production in the region using satellite data. In Chapter 3, I develop and evaluate a novel method for estimating the $P - E$ parameters from *in situ* primary production data using data from a variety of aquatic systems. In Chapter 4, I consider several methods for assignment of photosynthetic parameters and their impact on the estimation of primary production from satellite data is discussed. The results of the calculations are compared with primary production measured *in situ*. General conclusions and recommendations are presented in Chapter 5.

Chapter 2

PHYTOPLANKTON COMMUNITY STRUCTURE AND PRIMARY PRODUCTION IN THE CARIBBEAN WATERS: THE BIOLOGICAL COMPONENT OF THE LAPE PROJECT[1]

2.1 Introduction

Small Island Developing States (SIDS) depend highly on the resources of the ocean (FAO, 1999). Owing to their small land areas and high population density, fisheries in the Caribbean islands are an important source of income and a major source of food for the islanders (FAO, 1999). Thus, it is essential to manage the fisheries properly and understand the pelagic ecosystem to ensure a stable economy and sustainable development in these countries. The Lesser Antilles Pelagic Ecosystem (LAPE) project was designed to address these questions, using a multispecies ecosystem approach (FAO 2006a). The goal of the LAPE project is to quantify the energy available to the Caribbean food web and assess the fish biomass supported by these waters and that could be exploited in a sustainable way (FAO 2006a). A first step in implementing an ecosystem approach is to understand the flow of energy and material between different components of the ecosystem. This flow is studied in LAPE using the EcoPath model (FAO 2006b, and see www.ecopath.org) combined with an extensive sampling of the physicochemical environment, phytoplankton community structure, primary production, fish diet and fish biomass.

The EcoPath model is a mass-balance analysis of the ecosystem applied to a suite of functional types within the ecosystem (Bundy 2004). To implement the model, a systematic sampling of the fish community as well as a quantification of the food supply and the energy available to sustain the fish population are required. A key

[1]This chapter has been accepted as a technical report for Food and Agriculture Organization of the United Nations.

input to the EcoPath model is therefore the energy available to the ecosystem through primary production, the first level of production of energy in the food web. Primary production is traditionally estimated from ship-based experiments. However, this approach is expensive and provides only sparse measurements with limited temporal and spacial resolution. Using satellite-based methods developed in the eighties, primary production can now be computed on synoptic scale from remote sensing of ocean colour. For the LAPE area, primary production was computed at local scale (21 stations in April and May 2006) as well as from satellite images of ocean colour.

Here I present first the phytoplankton community structure assessed by pigment analyses. Then, the model used to compute primary production is explained, with a description of the five steps to compute primary production from satellite data. Monthly images of primary production are then presented over an annual cycle for 2006, using two methods of assignment of the model parameters.

2.2 Study Area and Sampling Design

The LAPE survey was conducted in the Caribbean waters in April and May 2006 within 56°W to 64°W longitude and 9°N and 21°N latitude. The estimation of primary production from ocean-colour data was carried out over a more extensive area (51-67°W and 7-24°N) to place the LAPE fields observations in a larger oceanographic context. The physical environment of the region (Fig. 2.1) presents deep waters towards the north with shallower waters around the Antilles, especially on the Caribbean coast as compared with the Atlantic coast.

A total of 52 stations were sampled for phytoplankton community properties (Fig. 2.1). At each of these stations, a Conductivity, Temperature and Depth (CTD) profiler was used. Casts of 500 m or less included *in situ* fluorometric measurements using a SeaTech FL500 fluorometer, which were used to determine the depth of the deep chlorophyll maximum (DCM) for sampling purposes. For stations deeper than 500 m, the deep chlorophyll maximum was assumed to be at the same depth as the previous station. This assumption had to be made for 12 stations. For each station, depth permitting, 10 depths were sampled using a rosette for chlorophyll-a Turner fluorometric analyses (10, 20, 40, 60, 80, 90, 100, 120, 140, 200 m) and 2 depths were sampled for HPLC and phytoplankton spectral absorption (20 m and at the deep

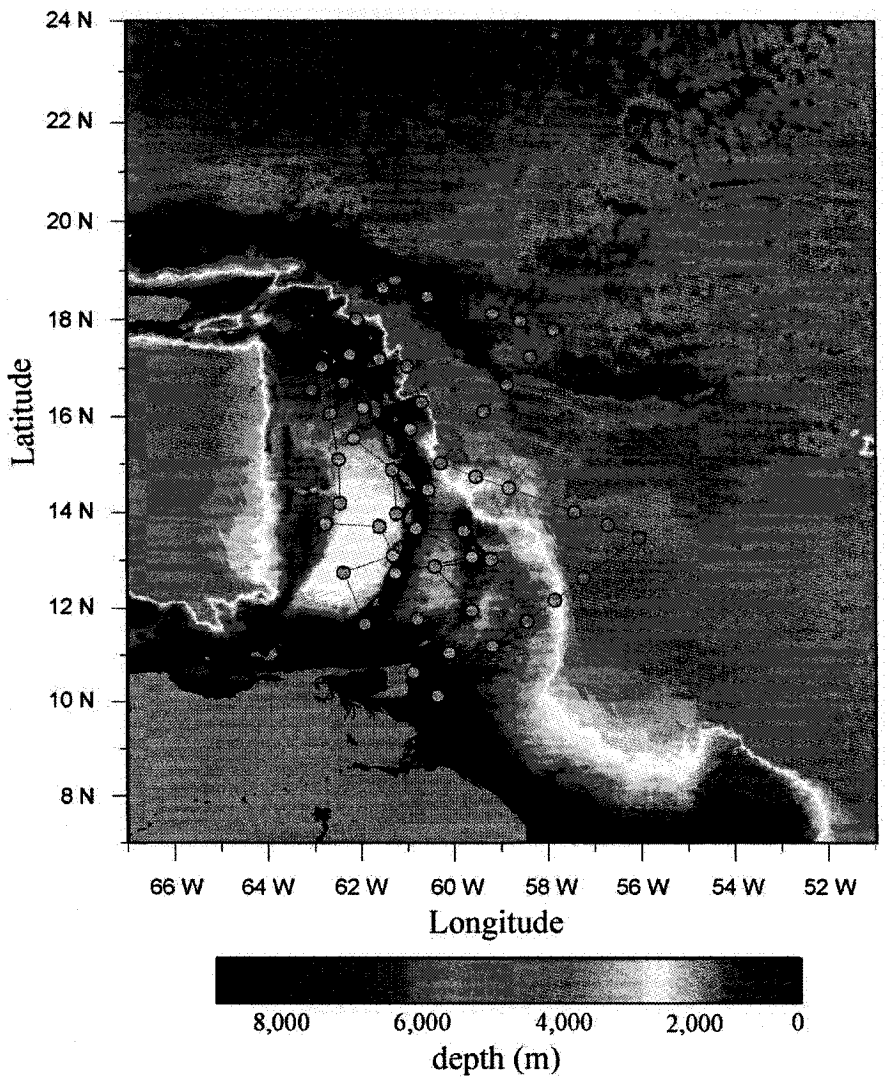

Figure 2.1: Bathymetry of the LAPE project. The sampling stations are superimposed.

chlorophyll maximum). For 22 stations, photosynthetic-light ($P - E$) experiments were performed using surface (20 m) samples. The study area could be partitioned into three regions: coastal (depth < 200 m), southern (lat $< 16°$N) and northern (lat $> 16°$N). The methods used for each of these measurements and the results obtained are described in the following sections.

2.3 Pigment Analyses

2.3.1 Chlorophyll-a Profile Parameters

The chlorophyll-a concentrations at 10 different depths at each station were used to determine the chlorophyll-a profile parameters assuming a shifted Gaussian function to describe the vertical structure in chlorophyll-a profile. The biomass B at depth z can then be estimated as follows:

$$B(z) = B_0 + \frac{h}{\sigma\sqrt{2\pi}} \exp\left[-\frac{(z - z_m)^2}{2\sigma^2}\right], \tag{2.1}$$

where B_0 is the background biomass, z_m is the depth of the biomass peak, σ defines the width of the peak and h is the integral under the Gaussian curve (Fig 2.2). The parameter H, the height of the biomass peak at depth z_m, can be calculated from h and σ as:

$$H = \frac{h}{\sigma\sqrt{2\pi}}. \tag{2.2}$$

An additional parameter ρ can be used to provide a measure of the relative importance of the maximum chlorophyll biomass compared with the background:

$$\rho = \frac{H}{(H + B_0)}. \tag{2.3}$$

The parameters ρ, σ and z_m can then be combined with the information on surface chlorophyll from remote sensing of ocean colour, to scale the chlorophyll profile to match actual values of chlorophyll-a concentration at specific pixels. Two profiles from the coastal region did not permit the retrieval of the parameters due to small sample numbers (shallow stations). The parameters estimated are tabulated in Appendix A and summarised in Table 2.1. Examples of northern and southern stations are presented in Figure 2.3

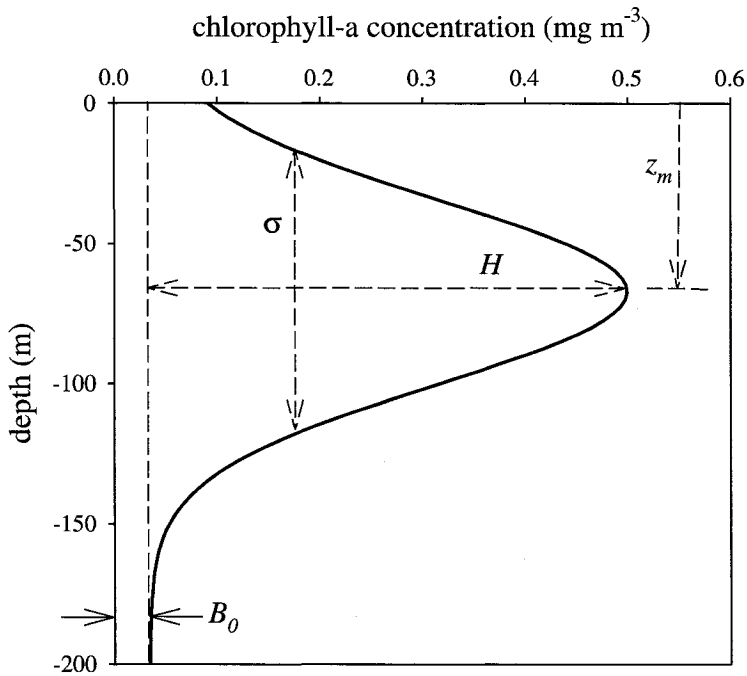

Figure 2.2: Chlorophyll-a profile parameters using a shifted Gaussian function, where B_0 is the background biomass, z_m is the depth of the biomass maximum, σ is the width of the peak and H is the height of the biomass peak at z_m.

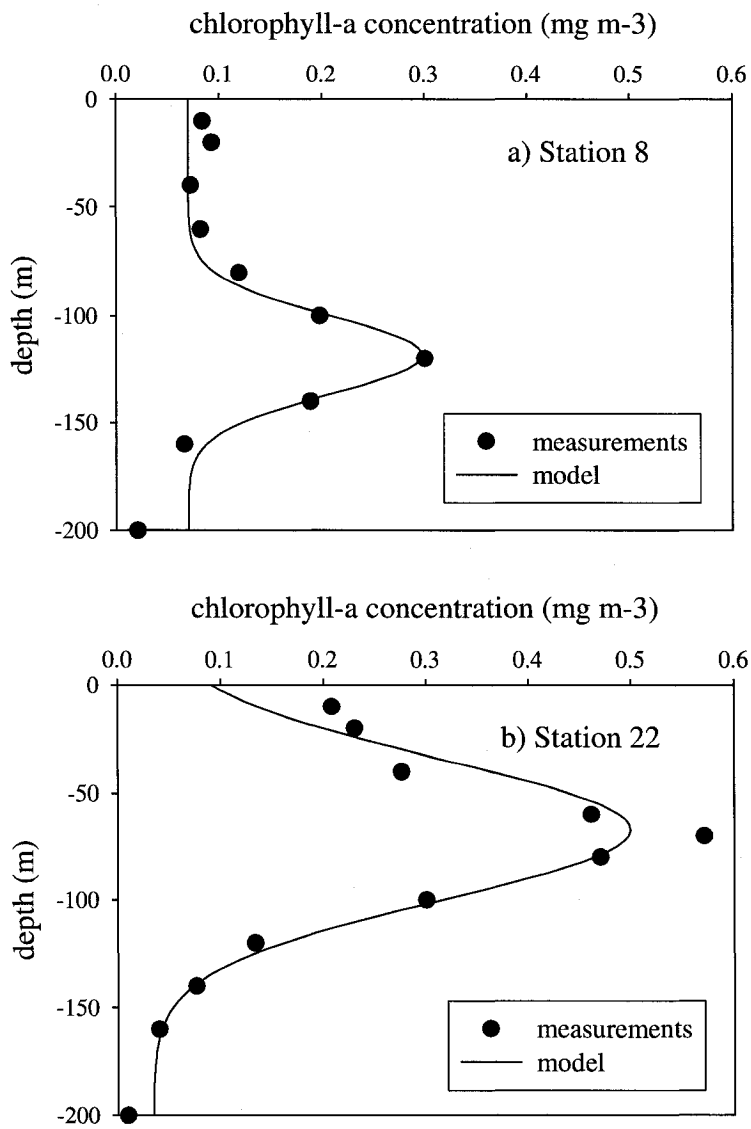

Figure 2.3: Examples of chlorophyll-a profile for two stations sampled during the LAPE projects. The parameters for station 8 (a) are $B_0 = 0.070$ mg m^{-3}, $H = 0.23$ mg m^{-3}, $\sigma = 18.5$ m, and $z_m = 118$ m and for station 22 (b) are $B_0 = 0.034$ mg m^{-3}, $H = 0.46$ mg m^{-3}, $\sigma = 32.8$ m, and $z_m = 67$ m.

Table 2.1: Chlorophyll-a profile parameters averaged ($\pm$ standard deviation) for the entire LAPE area (N=49) and averaged ($\pm$ standard deviation) over the three regions: coastal waters (N=1), open ocean south of 16°N (N=29) and open ocean north of 16°N (N=19).

region	B_0 mg m^{-3}	z_m m	σ m	h mg m^{-2}	H mg m^{-3}	ρ dimensionless
LAPE region	0.075 ($\pm$0.036)	83 ($\pm$23)	22.9 ($\pm$8.6)	20.7 ($\pm$9.8)	0.38 ($\pm$0.18)	0.82 ($\pm$0.10)
coastal	0.087 (N/A)	71 (N/A)	21.6 (N/A)	27.2 (N/A)	0.50 (N/A)	0.85 (N/A)
open ocean <16°N	0.076 ($\pm$0.042)	71 ($\pm$17)	22.5 ($\pm$9.15)	24.2 ($\pm$9.32)	0.46 ($\pm$0.17)	0.86 ($\pm$0.08)
open ocean >16°N	0.073 ($\pm$0.029)	103 ($\pm$19)	23.6 ($\pm$7.82)	14.9 ($\pm$7.86)	0.25 ($\pm$0.08)	0.76 ($\pm$0.11)

Overall, we found a significant difference (t-test, $p<0.001$) between the stations of the northern region (>16°N) compared with the southern region (<16°N) of the LAPE region for four of the six profile parameters (z_m, h, H and ρ). Northern stations generally had deeper chlorophyll maximum and lower chlorophyll-a concentration (Fig 2.3a) compared with southern stations (Fig 2.3b). Only one coastal station (maximum depth < 200 m) provided enough samples to fit the equation; thus no statistical analyses were possible to compare the coastal region with the two open-ocean regions.

2.3.2 Phytoplankton Community Structure

High Performance Liquid Chromatography (HPLC) analyses were used to quantify the concentrations of various phytoplankton pigments in the water samples. To perform the analyses, 1-L seawater samples were initially filtered onto a GF/F filter. Samples were stored in liquid nitrogen or in a Super-Freezer (-80°C) until analyses, within 6 months of sampling. The method used for the HPLC analyses is described in detail in SeaHARRES-2 (Hooker *et al.* 2005) under the Horn Point Laboratory section, where the samples were analysed. Briefly, the pigments are extracted in 95% acetone, then, using a C8 column and a linear gradient between solvent A (methanol) and solvent B (70:30 methanol: 28 nM aqueous tetrabutyl ammonium acetate), the

pigments were separated according to their polar/non-polar properties. Pigment concentrations are tabulated in Appendix B.

Three general types of pigments are found in phytoplankton cells: chlorophylls, carotenoids and biliproteins. Chlorophylls and carotenoids can be quantified by the Horn Point Laboratory HPLC method, whereas biliproteins are water soluble and thus could not be quantified by this method. However, biliproteins have absorption spectra that differ from those of carotenoids and chlorophylls and thus biliproteins can often be detected from the absorption spectra of phytoplankton. Phytoplankton cells contain various pigments for both photosynthetic and photo-protective purposes. Pigments differ among phytoplankton groups and thus using some diagnostic pigments, it is possible to identify the phytoplankton groups that are present in the water samples (Claustre 1994). Certain pigments present in more than one taxonomic group are a limitation of this approach. On the other hand, pigment analyses can assess community structure for phytoplankton of all size classes, unlike flow cytometry which is limited to cell size lower than 20 μm (pico- and nano-phytoplankton) or microscopic taxonomic counts that usually cannot identify pico-phytoplankton, and must rely on epifluorescence counts. These complementary approaches to assess community structure should increase the confidence in the identified community structure.

Using diagnostic pigments, phytoplankton cells were divided in three groups: pico-phytoplankton ($<2\,\mu$m), nano-phytoplankton ($>2\,\mu$m, $<20\,\mu$m) and micro-phytoplankton ($>20\,\mu$m) (Table 2.2, Vidussi *et al.* 2001). For each size class, the ratio of diagnostic pigments for the specific size class to the total diagnostic pigments yields the fraction of each size class in the water sample. This fraction was multiplied by the chlorophyll-a concentration to obtain the fraction of the chlorophyll-a associated with each size class (Fig. 2.4). Deep samples were not used in this analysis when the sample depth did not coincide with the depth of the DCM (10 stations).

We found a predominance of pico-phytoplankton in surface water (Fig. 2.4) with a significant but smaller contribution of nano-phytoplankton, whereas micro-phytoplankton were practically non-existent. It is important to point out that fucoxanthin, a diagnostic pigment of diatoms (micro-phytoplankton) is also present in prymnesiophytes and chrysophytes, two nano-phytoplankton groups. Thus, the presence in this study of micro-phytoplankton is unlikely, with the possible exception of

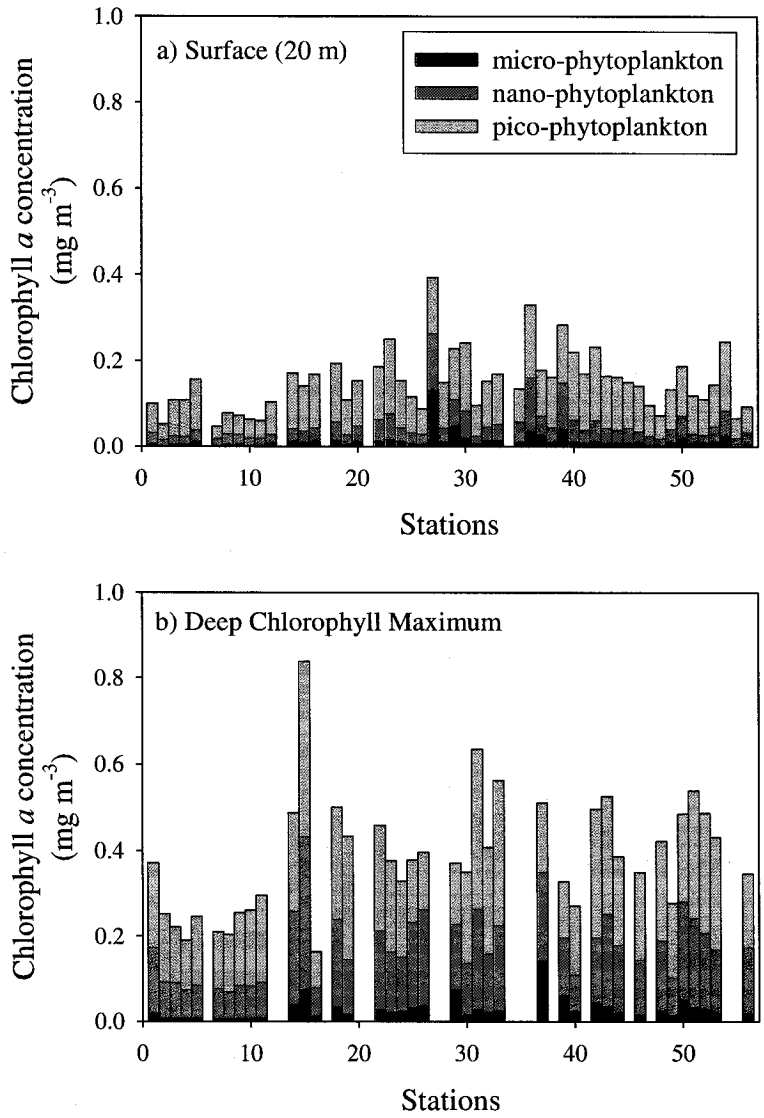

Figure 2.4: chlorophyll-a concentration associated with the three size classes, pico, nano, and micro-phytoplankton (a) at the surface (20 m) and (b) at the deep chlorophyll maximum. Note that 20 m depth is treated analogous to a surface sample, since the mixed-layer depth was always greater than 20 m

Table 2.2: Diagnostic pigments associated with major phytoplankton groups organised according to size-classes.

Phytoplankton classes	Phytoplankton groups	diagnostic pigments
Micro-phytoplankton	Diatoms	Fucoxanthin
	Dinoflagellates	Peridinin
Nano-phytoplankton	Nanoflagellates	19'Butanoyloxyfucoxanthin + 19'Hexanoyloxyfucuxanthin
	Cryptophytes	Alloxanthin
Pico-phytoplankton	Green flagellates	Chlorophyll-b
	Prochlorophytes	Divinyl-chlorophyll-b
	Synechococcus	Zeaxanthin

station 27, a coastal station. Micro-phytoplankton often represent a larger fraction of the chlorophyll-a biomass in coastal stations. The proportion of pico-phytoplankton at the deep chlorophyll maximum is much lower than at the surface, and an increase in the fraction of nano-phytoplankton is noted (Fig. 2.4). It is well recognised that smaller cells (*Prochlorococcus* and *Synechococcus*) are abundant in warm, stratified oligotrophic waters because of their high buoyancy and their limited need of nutrients (Chisholm et al. 1988). It has also been pointed out that, typically, nano- and pico-eukaryotes are more abundant below the mixed layer, where nutrients are available from the deeper, colder layer of the ocean, generating the deep chlorophyll maximum (Claustre and Marty, 1995).

Claustre and Marty (1995) proposed a pigment-based method to determine the fractions of *Prochlorococcus*, other cyanobacteria and flagellates in the total phytoplankton population in oligotrophic waters where micro-phytoplankton are not present. The chlorophyll-a associated with *Prochlorococcus* is estimated from the concentration of divinyl-chlorophyll-a, which is a typical marker of the group (Goericke and Repeta 1993). The chlorophyll-a associated with flagellates is estimated as the sum of 19'-hexanoyloxyfucoxanthin (19'-Hex) and 19'-butanoyloxyfucoxanthin (19'-But) multiplied by 0.75, the ratio of chlorophyll-a to (19'-Hex + 19'-but) as measured in Claustre *et al.* (1994) in flagellate populations. The remaing chlorophyll-a concentration is usually associated with the other cyanobacteria (Fig. 2.5). Obviously,

if other phytoplankton groups are present in the sample, then the chlorophyll-a concentration associated with the other cyanobacteria will be overestimated, thus in this study the remaining chlorophyll-a will be identified as other phytoplankton. The sum of the divinyl-chlorophyll-a and normal chlorophyll-a yields the total chlorophyll-a.

It can be noticed from this analysis that other phytoplankton represents the greatest fraction of surface samples (Fig. 2.5). The fraction of chlorophyll-a associated with *Prochlorococcus* and flagellates increases as it reaches the deep chlorophyll maximum.

The northern open-ocean stations (latitude north to 16°N) had chlorophyll-a concentration significantly lower than in the stations of the southern open-ocean (latitude south of 16°N). In the surface samples the proportion of *Prochlorococcus* in the north was only slightly less than that in the southern region, whereas the proportion of other phytoplankton and the flagellates remained stable across the two regions (Table 2.3). However, samples from the deep chlorophyll maximum presented a striking difference between northern and southern regions (Table 2.4). *Prochlorococcus* is more abundant in northern DCM region compared with those of the southern DCM region, which is the opposite of the trend found in surface samples. Moreover, DCM samples from northern stations show a much lower proportion of other phytoplankton compared with southern stations. For both northern and southern stations, a significant increase in eukaryotic flagellates in the DCM is found compared with surface samples. The community structure seems to undergo an important change over the water column which is more pronounced in the northern subregion of the LAPE area. This is most likely due to the presence of a deeper DCM in the northern region (see Table 2.1) compared with the southern region. The enhanced stratification of the water column allows a segregation of the deep phytoplanktonic community. Moreover, increased divinyl-chlorophyll-a with decreasing irradiance (Partenski *et al.* 1993) as a result of photoacclimation might explain why a higher proportion of *Prochlorococcus* was estimated at the DCM of the northern region. The increase in pigment may be at least partly indicative of photoacclimation, rather than increase in cell number.

HPLC analyses indicated the presence of two different phytoplankton communities in the northern and southern regions of the LAPE study area. Unfortunately, the limited number of stations in the coastal region (three stations, with only one DCM sample available) restricted the analysis of its community structure and prevented

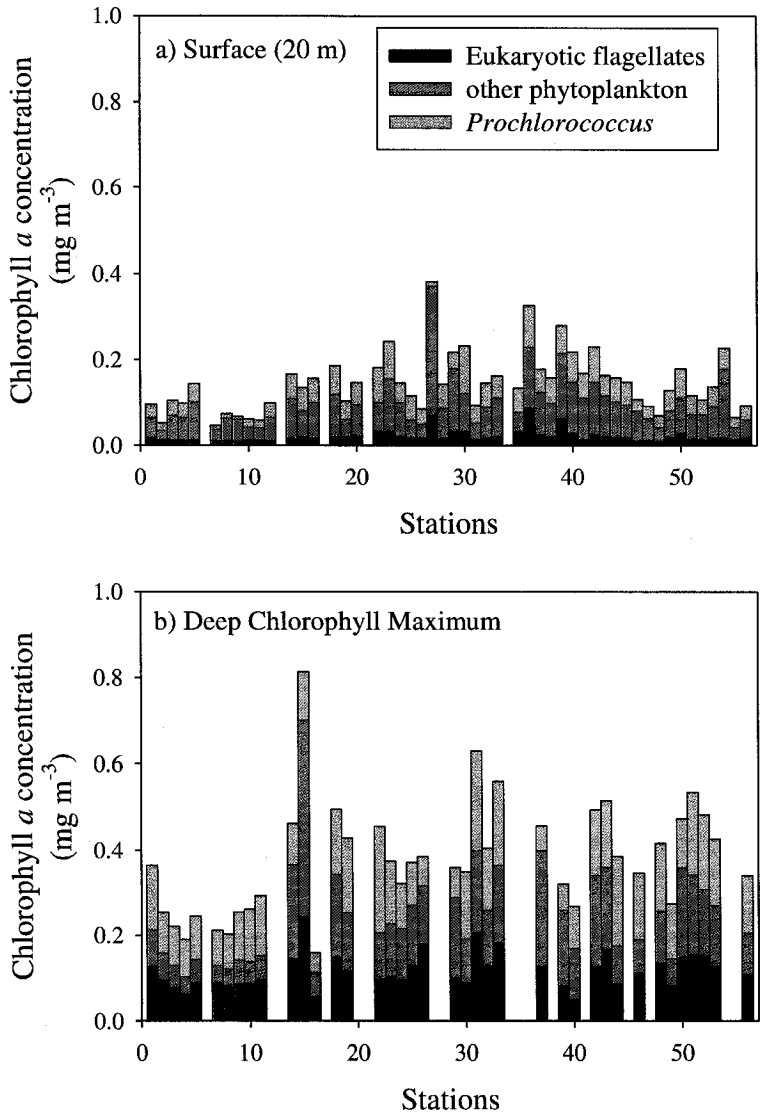

Figure 2.5: Chlorophyll-a concentration associated with the three phytoplankton groups, Eukaryotic flagellates, *Prochlorococcus* and other phytoplankton (a) at the surface (20 m) and (b) at the deep chlorophyll maximum.

Table 2.3: Description of the community structure for surface samples (20m) expressed as the proportions of each phytoplankton group (*Prochlorococcus*, eukaryotic flagellates and other phytoplankton) averaged ($\pm$ standard deviation) for the entire LAPE area (N=51) and averaged ($\pm$ standard deviation) over the three regions: coastal waters (N=3), open ocean north of 16°N (N=29) and open ocean south of 16°N (N=19).

region	*Prochlorococcus*	other phytoplankton	Eukaryotic flagellates
LAPE region	0.32 ($\pm$0.09)	0.52 ($\pm$0.10)	0.16 ($\pm$0.05)
coastal	0.24 ($\pm$0.19)	0.54 ($\pm$0.22)	0.22 ($\pm$0.04)
open ocean <16°N	0.35 ($\pm$0.06)	0.50 ($\pm$0.07)	0.15 ($\pm$0.03)
open ocean >16°N	0.28 ($\pm$0.08)	0.55 ($\pm$0.10)	0.17 ($\pm$0.06)

Table 2.4: Description of the community structure for deep chlorophyll maximum samples expressed as the proportion of each phytoplankton group (*Prochlorococcus*, eukaryotic flagellates and other phytoplankton) averaged ($\pm$ standard deviation) for the entire LAPE area (N=39) and averaged ($\pm$ standard deviation) over the three regions: coastal waters (N=1), open ocean north of 16°N (N=24) and open ocean south of 16°N (N=14).

region	*Prochlorococcus*	other phytoplankton	Eukaryotic flagellates
LAPE region	0.35 ($\pm$0.10)	0.33 ($\pm$0.11)	0.32 ($\pm$0.05)
coastal	0.17 (N/A)	0.36 (N/A)	0.47 (N/A)
open ocean <16°N	0.32 ($\pm$0.10)	0.39 ($\pm$0.10)	0.30 ($\pm$0.04)
open ocean >16°N	0.43 ($\pm$0.05)	0.23 ($\pm$0.03)	0.35 ($\pm$0.05)

comparison with the other two regions.

2.3.3 Phytoplankton Spectral Absorption

Particulate absorption was estimated following the filter technique described in the NASA protocols (Mitchell et al. 2002). Briefly, 1L of sea water was filtered onto a Whatman GF/F filter which was then stored in liquid nitrogen or in a Super-Freezer (-80°C) until analysed at the Bedford Institute of Oceanography. The samples were thawed and measured in a dual beam Shimadzu spectrophotometer using an integrating sphere to minimise loss of photons by scattering. Optical densities were measured with a 1 nm spectral resolution from 350 to 750 nm. This measurement represents total particle spectral absorbance. The samples were then extracted with 100% warm methanol, rinsed with filtered sea water, and measured again to estimate absorbance by detritus. By subtraction, the spectral absorbance by phytoplankton was estimated.

Optical density measurements are corrected for path-length amplification by applying the β-correction factor proposed by Hoepffner and Sathyendranath (1992, 1993) modified as in Kyewalyanga *et al.* (1998). The absorbance spectra are transformed into absorption spectra (m^{-1}) by accounting for volume of water filtered and the diameter of the filtered area on the GF/F filters. Absorption spectra are then normalised to chlorophyll-a concentration from HPLC analyses to obtain the chlorophyll-a specific absorption spectra. The flattening effect on the chlorophyll-a specific absorption spectra provide another index of cell size of the phytoplankton community, as larger cells typically show lower specific absorption spectra than smaller cells (Duysens 1956). This analysis complements our HLPC analyses of the community structure. The chlorophyll-a specific absorption at 676nm (a^*_{676}) is less affected by absorption from pigments other than chlorophyll-a that at other wavelengths and is therefore used here (Fig. 2.6) as the index of cell size (Hoepffner and Sathyendranath 1992, 1993; Bouman *et al.* 2000).

This analysis confirmed our findings from HPLC analysis, that all stations are mainly composed of pico- and nano-phytoplankton, with values of a^*_{676} around $0.02\,m^{-1}$ which is characteristic of small cells. Unfortunately, 15 samples were lost when transferred from the dewar where they were stored aboard the ship to the dry

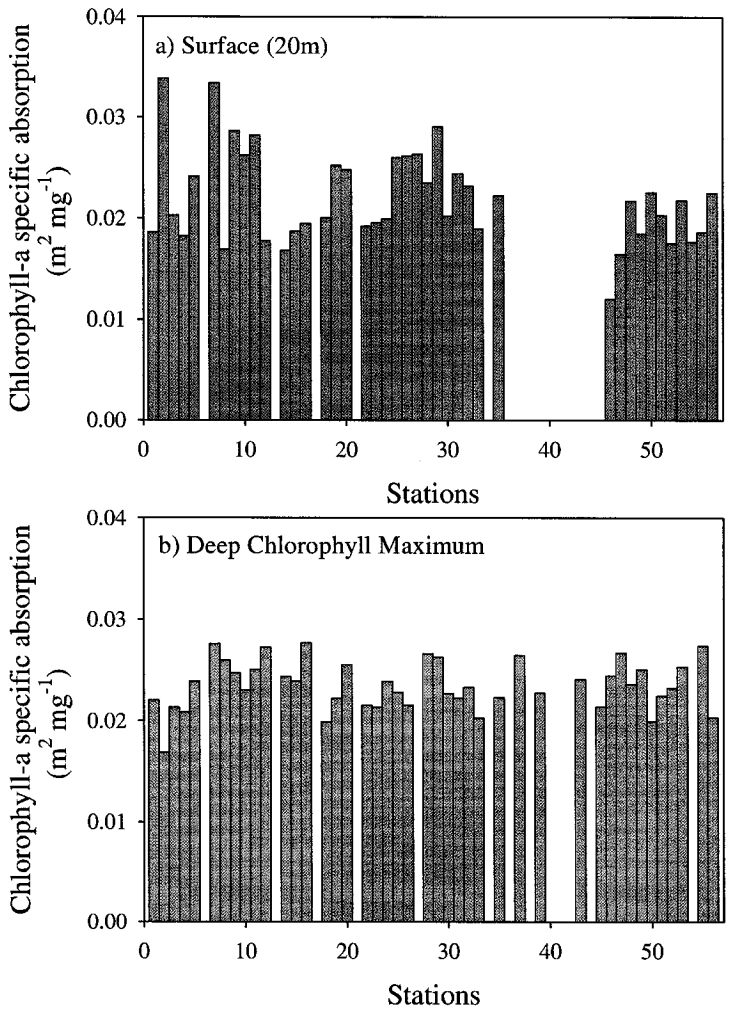

Figure 2.6: Chlorophyll-a specific absorption at 676 nm (a) for surface (20 m) samples and (b) for deep chlorophyll maximum samples.

shipper for shipment to the Bedford Institute of Oceanography.

2.4 Satellite Images

Chlorophyll-a concentration was estimated using the OC3M algorithm, the NASA global algorithm for the MODIS sensor. This algorithm uses the wavebands centered at 443, 490 and 550nm. Level 2 images provided by NASA were processed at the Bedford Institute of Oceanography using the SeaDAS software. The studied area is bounded by 7°-24°N and 51°-67°W (Fig. 2.7). The time series are given as monthly composite images over the annual cycle (Fig. 2.8, full-page versions can be found in Appendix C). Blank pixels represent areas where ocean-colour data are unavailable. This is mainly due to cloud cover but could also result from negative values of water-leaving radiances (due to processing error), sun glint or high aerosols. Only the June and July composite images have a high proportion of blank pixels, limiting the estimation of primary production for these two months. These months correspond to the rainy season, with increased cloud cover in this region.

Confidence in the data can be assessed from the number of data points available per pixel to estimate chlorophyll-a concentration for the composite image, the pixel depth (Figures 2.9 and 2.10; see also Appendix D). The average pixel depth is about 5, higher in winter and lower in summer, during the rainy season. Since five data points is better than weekly sampling frequency, we have confidence that the composite values represent reasonable monthly-mean values.

Chlorophyll-a concentration was extracted at 1 km resolution and averaged for each month of 2006. The composite image for May 2006 (Fig. 2.7) shows low chlorophyll-a concentrations (around 0.05 mg m^{-3}) in the northern part of the region. The values increase southward, and maximal values are found in the coastal area, probably due to the influence of the Orinoco and the Amazon Rivers. The very high chlorophyll-a concentrations in coastal waters may be biased by the high concentration of chromophoric dissolved organic matter (CDOM or yellow substances) and suspended particles in the river outflow, and therefore the values should be treated with caution. The computed values show a high overestimation of the satellite-derived chlorophyll-a concentration at stations 27 and 37, where the influence of the river outflows seem to be maximal (Fig. 2.11a). Excluding these two stations produces a more

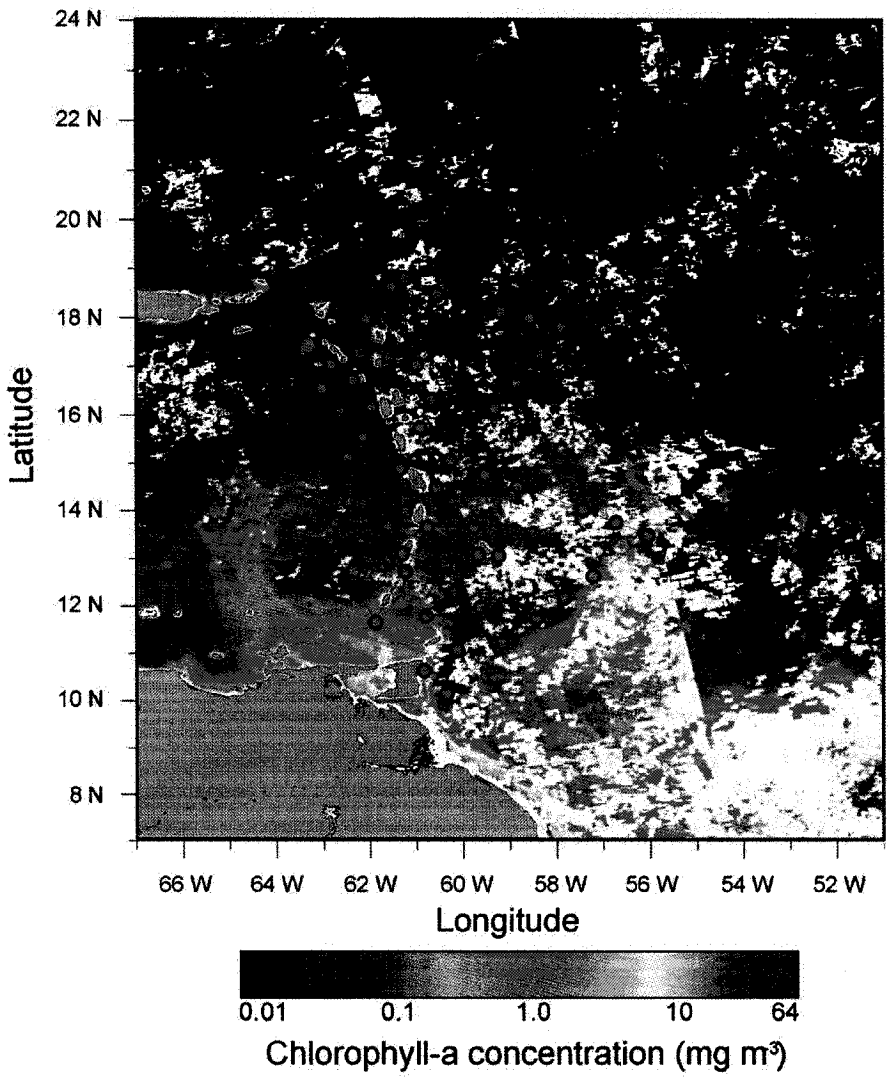

Figure 2.7: Monthly composite image of chlorophyll concentration for May 2006 for the LAPE study area. The sampling stations are superimposed.

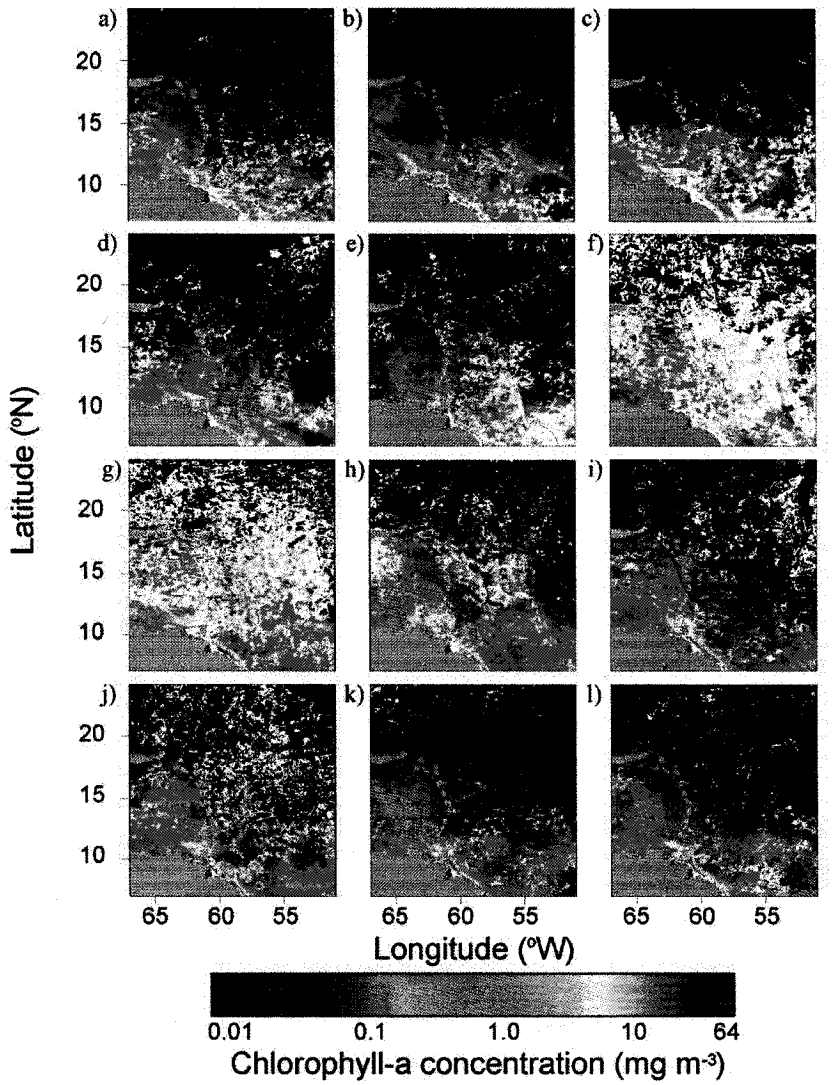

Figure 2.8: Monthly composite images of chlorophyll concentration over an annual cycle for the year 2006 for the LAPE study area (a) January, (b) February, (c) March, (d) April, (e) May, (f) June, (g) July, (h) August, (i) September, (j) October, (k) November and (l) December.

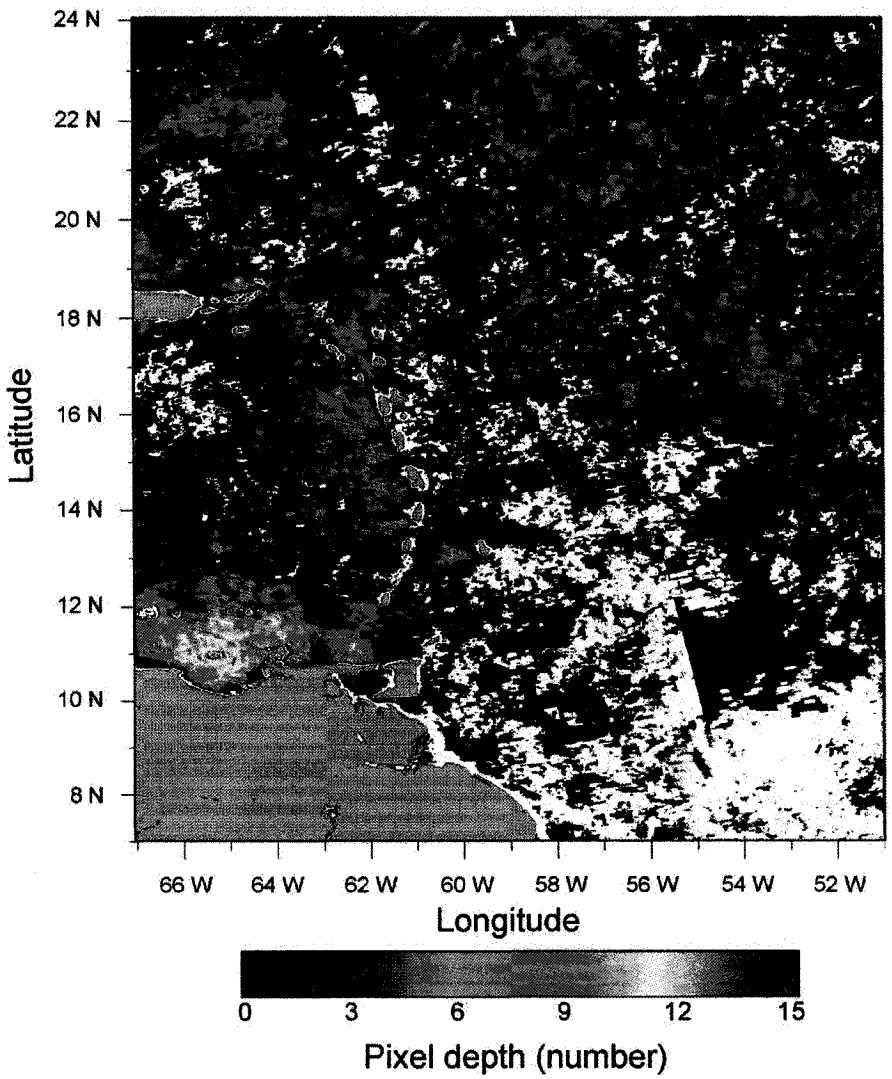

Figure 2.9: Pixel depth for monthly composite image of chlorophyll concentration for May 2006 for the LAPE study area.

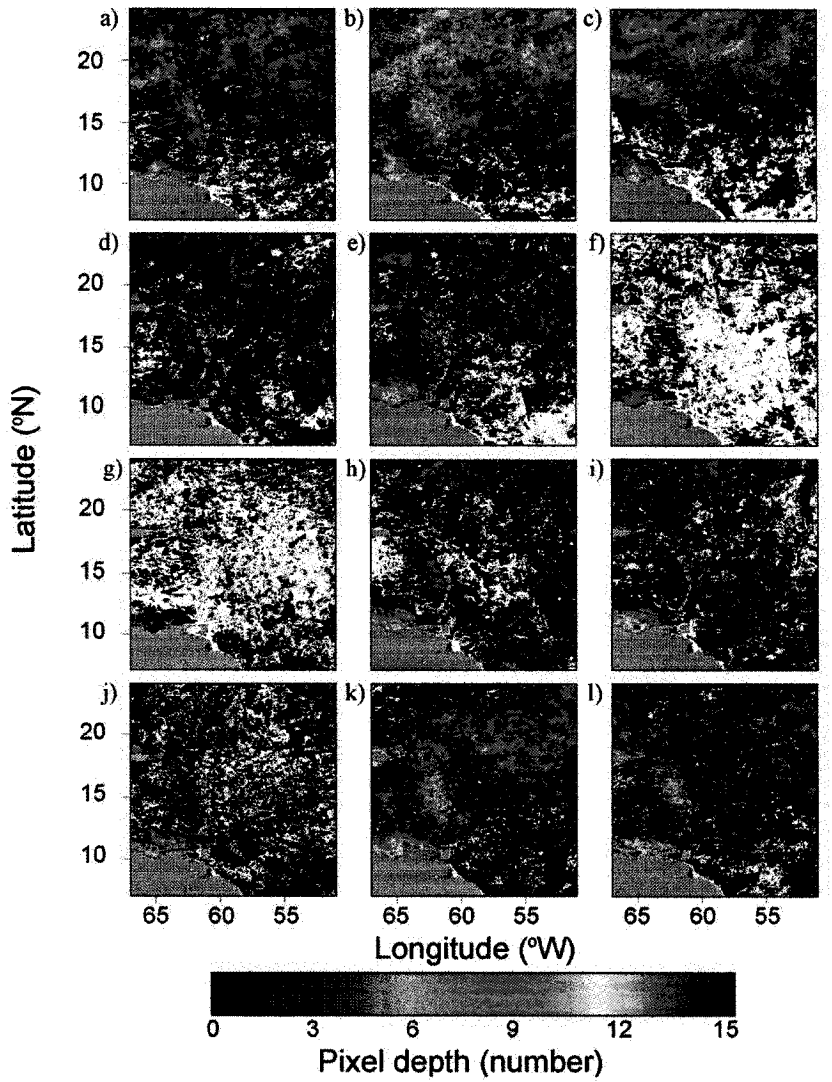

Figure 2.10: Pixel depth for monthly composite image of chlorophyll concentration over an annual cycle for the year 2006 for the LAPE study area (a) January, (b) February, (c) March, (d) April, (e) May, (f) June, (g) July, (h) August, (i) September, (j) October, (k) November and (l) December.

secure relationship with chlorophyll-a estimates from the satellite images that are biased only slightly low (Fig. 2.11b). Individual images were also used to compare chlorophyll retrieval with field measurements; however, only three stations coincided with the satellite passes. These points followed a pattern similar to those from the composite images, with slight underestimation as chlorophyll concentration increased (Figs. 2.11a and b).

The chlorophyll-a concentration appears to remain fairly stable over the annual cycle although a slight increase in chlorophyll concentration is noticed over most of the study area in August (Fig. 2.8). Strong chlorophyll-a concentrations are also found in the western part of the study area in September and October and remain fairly high in November and December.

Composite images of sea-surface temperature have also been generated over an annual cycle. The MODIS temperature data are estimated from the far infrared wavebands. The monthly composite images of sea-surface temperature are bounded, as for the chlorophyll-a concentration images, by the coordinates 7°-24°N and 51°-67°W. The monthly composite image for May 2006 illustrates the low spatial variability in sea-surface temperature (Fig. 2.12). Low temporal variability is also evident in the annual cycle of monthly composites (Fig. 2.13), although a general increase in sea-surface temperature is noticed in September and October. As in the annual cycle of chlorophyll concentration, there are more monthly blank pixels in June and July, most likely due to an increase in cloud cover. The monthly composite images of sea-surface temperature are presented in Appendix E in large format.

Overall, satellite images provide good estimates of chlorophyll concentration for the month of May 2006, except in coastal regions affected by river outflows, which lead to a serious overestimation of the chlorophyll concentration. The spatial pattern show overall low chlorophyll concentrations in the northern region and higher chlorophyll concentrations in the southern region. The annual cycle presents stable concentrations of chlorophyll, with some apparent blooming events in the southern regions, but they are most likely overestimations of chlorophyll-a related to river outflows. Temperature remains nearly stable over the LAPE study area over the annual cycle, averaging 28°C.

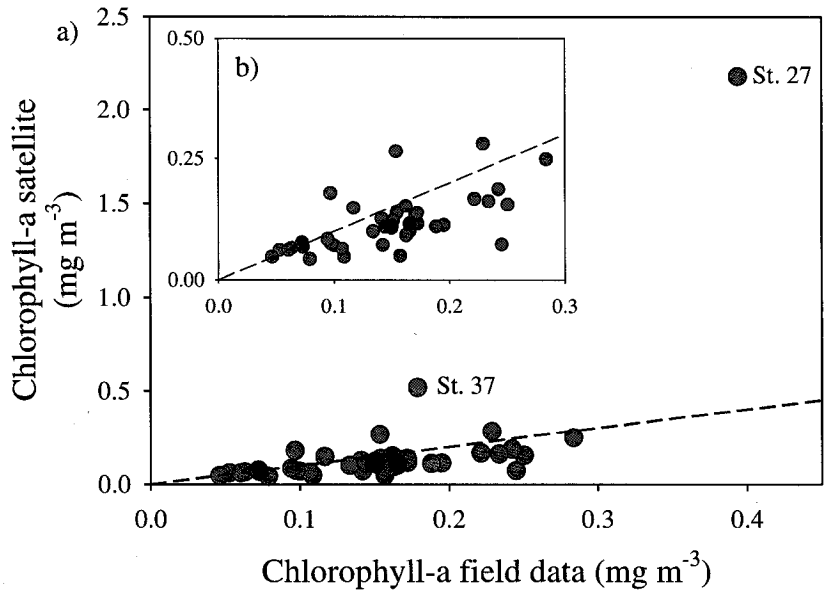

Figure 2.11: Comparison between chlorophyll-a estimated from remote sensing of ocean colour from individual images (red circles) and the monthly composite of May 2006 (green circle) with field measurements (HPLC) during the LAPE field study in May 2006. (a) all stations; and (b) excluding stations 27 and 37, two stations apparently affected by high chromophoric dissolved organic matter (CDOM) and suspended particles from river outflows. The dashed lines depict a 1:1 relationship.

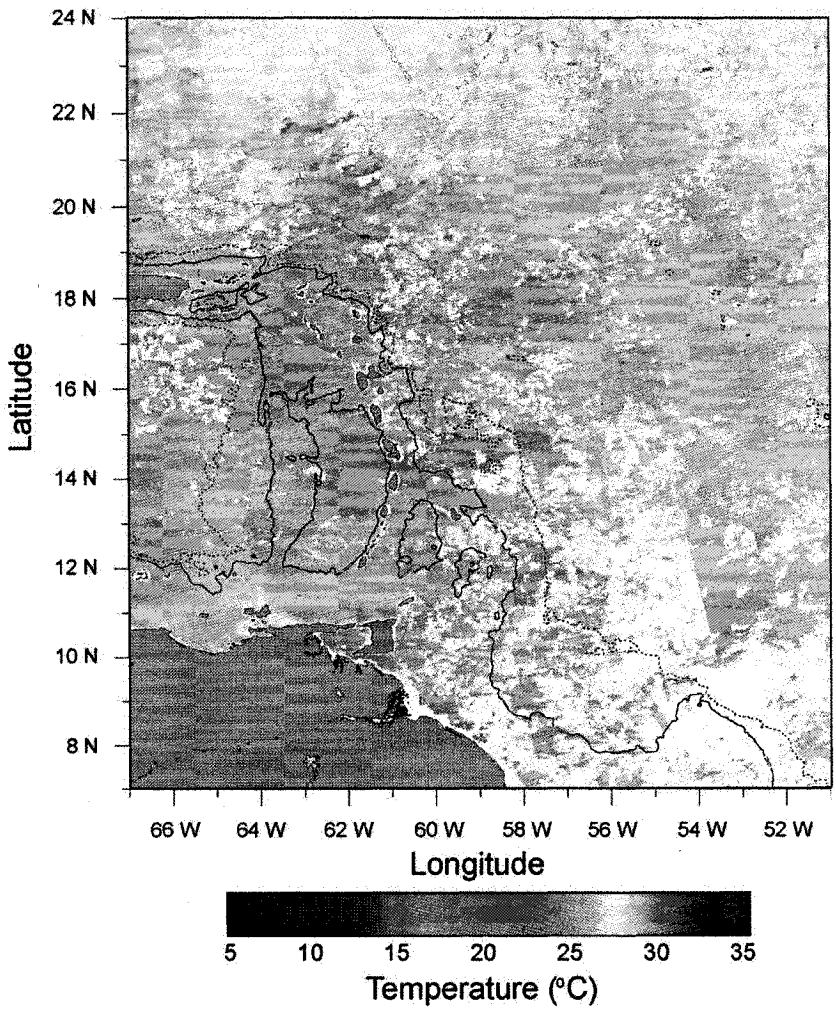

Figure 2.12: Monthly composite image of sea-surface temperature for May 2006 for the LAPE study area.

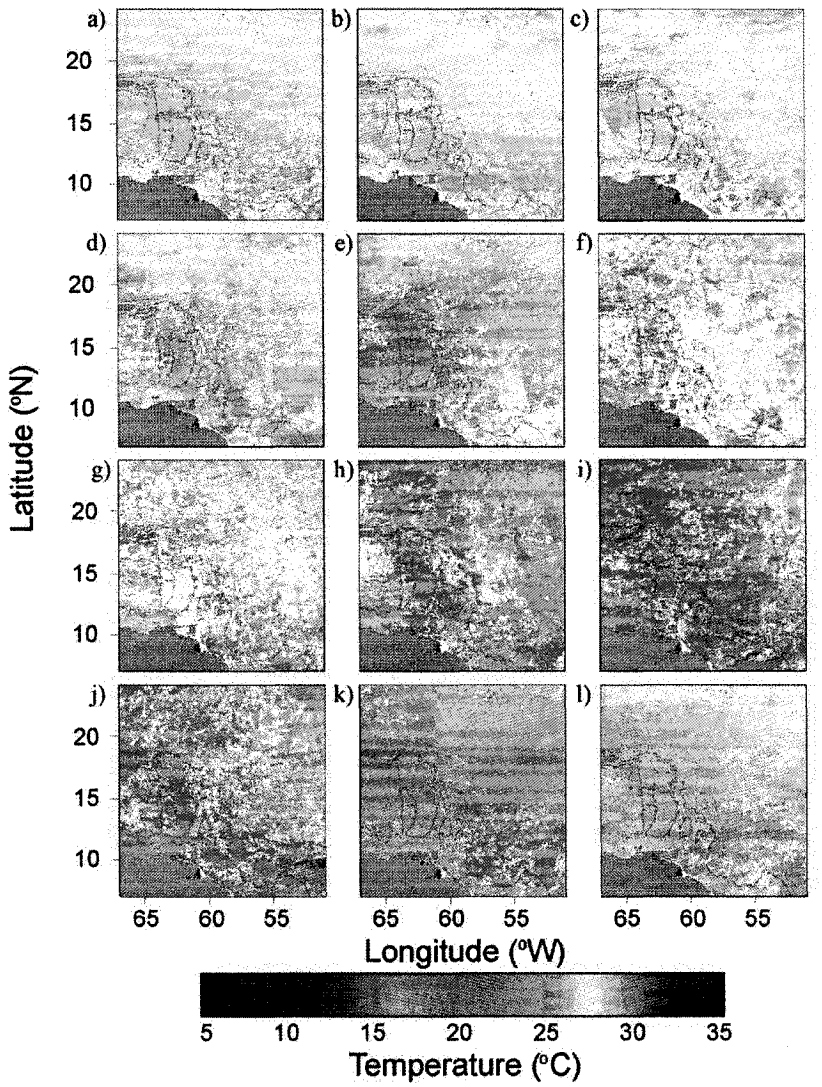

Figure 2.13: Monthly composite images of sea-surface temperature over an annual cycle for the year 2006 for the LAPE study area (a) January, (b) February, (c) March, (d) April, (e) May, (f) June, (g) July, (h) August, (i) September, (j) October, (k) November and (l) December.

2.5 Primary Production

2.5.1 Photosynthetic-Light Experiments

Primary production was measured using the photosynthetic-light ($P-E$) experiments. The water sample collected by a 10L Niskin bottle was divided into 10 transparent plastic bottles (750 ml each) and incubated for 3 hours in a light-gradient incubator, and carbon uptake during the experiment measured using ^{13}C. The ^{13}C and ^{12}C on filters were analysed using a mass spectrometer at Boston University. The photosynthetic parameters were estimated by fitting the equation of Platt *et al.* (1980) to the observations.

$$P^B = P_m^B \left(1 - \exp(-E\alpha^B / P_m^B)\right), \tag{2.4}$$

where biomass-normalised production (P^B) is a function of the initial slope, α^B, measured in light-limited conditions and the assimilation number, P_m^B, the plateau reached under light-saturating conditions, and where E is the incident irradiance (see examples in Fig. 2.14). The biomass B used to normalise production is the chlorophyll-a estimated by HPLC analysis. There were initial concerns over the use of ^{13}C in oligotrophic waters due to its lower sensitivity compared with ^{14}C, but the low level of noise in the $P-E$ curves gives confidence in the results.

The photosynthetic parameters are fairly stable over the LAPE area, although α^B has a wider range compared with P_m^B. The average values of the photosynthetic parameters among regions (Table 2.5) are not significantly different (t-test, $p > 0.05$). The full dataset is tabulated in Appendix F. The photosynthetic parameters measured during the LAPE cruise are similar to those measured in the Gulf of Mexico in March 1999 (unpublished data) and in the Caribbean waters in December 1984 (Irwin *et al.* 1987) and thus there is good agreement (Fig. 2.15) within the same biogeochemical province (Longhurst 1998) leading further confidence in the new dataset. Although temperature and chlorophyll-a concentration were significantly different among all the above three cruises (t-test $p < 0.05$), the photosynthetic parameters were not significantly different between the two Caribbean cruises. The α^B values for the Gulf of Mexico dataset were significantly lower, but the P_m^B significantly greater than those of the LAPE study (t-test, $p < 0.05$).

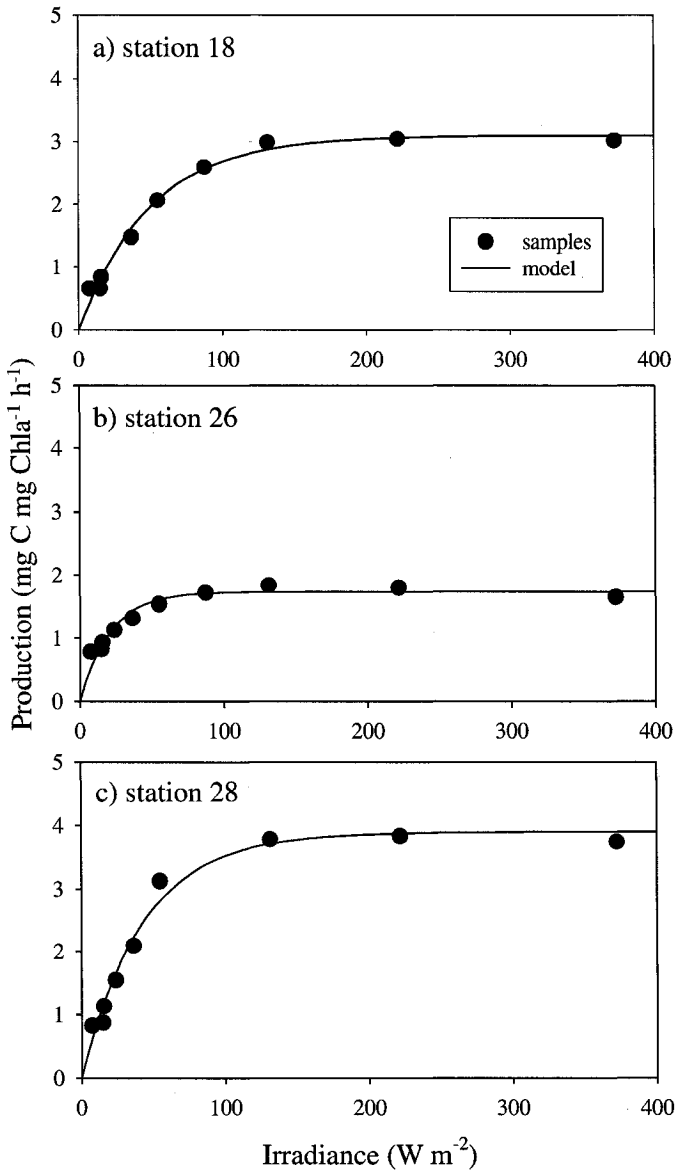

Figure 2.14: Examples of $P-E$ curves for three LAPE stations. The parameters are (a) for station 18: $\alpha^B = 0.062$ mg C mg chla^{-1} (W m^{-2})$^{-1}$ h^{-1} and $P_m^B = 3.10$ mg C mg chla^{-1} h^{-1}, (b) for station 26: $\alpha^B = 0.084$ mg C mg chla^{-1} (W m^{-2})$^{-1}$ h^{-1} and $P_m^B = 1.73$ mg C mg chla^{-1} h^{-1}, and (c) for station 28: $\alpha^B = 0.091$ mg C mg chla^{-1} (W m^{-2})$^{-1}$ h^{-1} and $P_m^B = 3.90$ mg C mg chla^{-1} h^{-1}.

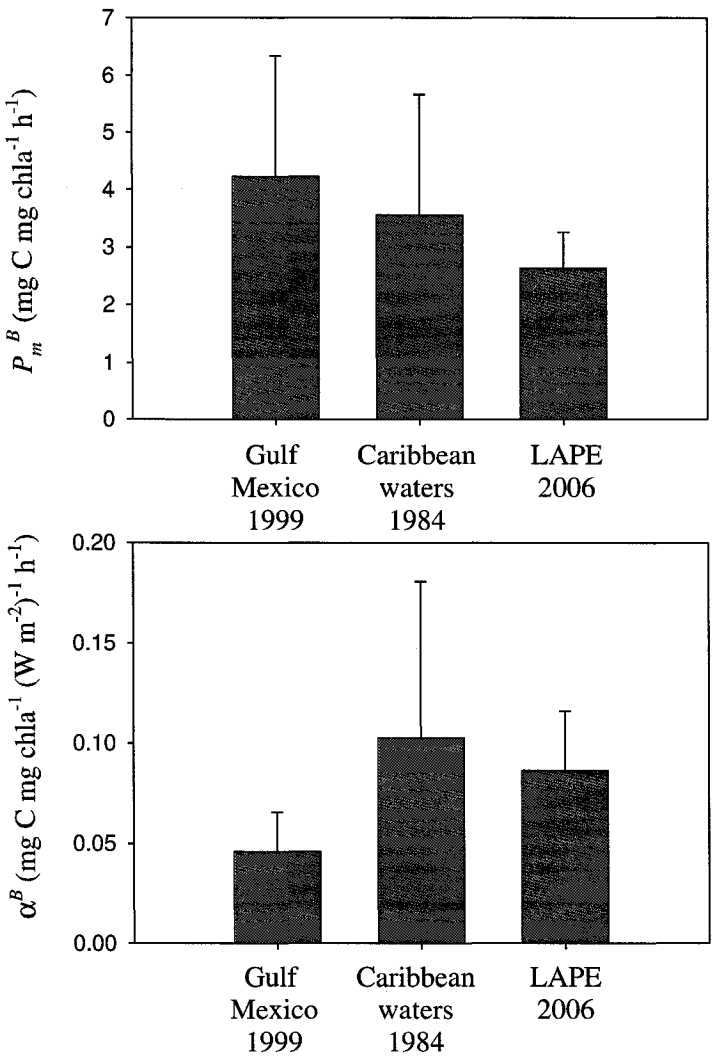

Figure 2.15: Comparison of photosynthetic parameters α^B and P_m^B estimated during the LAPE field programme (2006) and for the Caribbean waters in 1984 (cruise centered around 15°N and 65.5°W, Irwin *et al.* 1987) and for the Gulf of Mexico waters in 1999 (cruise centered around 22.7°N and 85.5°W, unpublished data) Heights of boxes indicate means. The standard deviations around the means are also shown as bars.

Table 2.5: Photosynthetic parameters averaged ($\pm$ standard deviation) for the entire LAPE area (N=22) and for three regions: coastal waters (N=2), open ocean north of 16°N (N=12) and open ocean south of 16°N (N=8).

region	α^B mg C mg chla^{-1}(W m^{-2})$^{-1}$ h^{-1}	P_m^B mg C mg chla^{-1} h^{-1}
Entire LAPE area	0.086 ($\pm$ 0.030)	2.64 ($\pm$ 0.64)
coastal	0.83 ($\pm$0.002)	2.24 ($\pm$0.72)
open ocean <16°N	0.076 ($\pm$0.015)	2.89 ($\pm$0.54)
open ocean >16°N	0.102 ($\pm$0.043)	2.35 ($\pm$0.65)

2.5.2 Assignment of Parameters

To compute primary production on synoptic fields, photosynthetic and profile parameters have to be assigned to each pixel. This could be achieved either by using temperature-based models for photosynthetic parameters (Antoine *et al.* 1996, Berhenfeld and Falkowski 1997, Bouman *et al.* 2005) or on chlorophyll-a concentrations for biomass profiles (Morel and Berthon 1989). The temperature-dependant models provide good estimates of the parameters in temperate regions; however, in tropical regimes, where the variation of sea-surface temperature is limited, they would be inadequate (Bouman *et al.* 2005). Another approach, proposed by Longhurst *et al.* (1995) and Sathyendranath *et al.* (1995), is to define regions that share similar physical and biological properties as a series of biogeochemical provinces and to apply a set of homogeneous photosynthetic and profile parameters to each province for each season. This approach, however, produces sharp discontinuities at the borders of each province. Platt *et al.* (submitted) have proposed a related approach, the Nearest-Neighbour Method, that matches the temperature and biomass at a pixel to the nearest neighbours in a corresponding *in situ* data base, and the parameter values are assigned based on their values at the nearest neighbours (Fig. 2.16). The Nearest-Neighbour approach is limited by the number of observations available in the *in situ* database.

Based on the variability of the profile parameters and on the spatial variation in chlorophyll-a concentration, three regions have been identified in the study area: open ocean south of 16°N (excluding shallow regions) and open ocean north of 16°N both excluding coastal waters (maximal depth < 200m). In one approach used here, mean

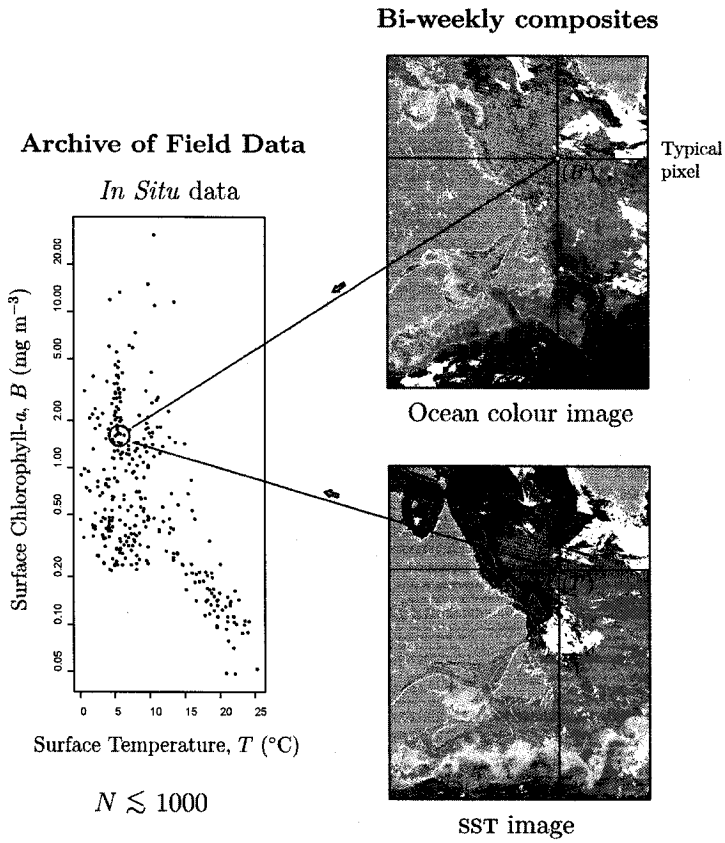

Figure 2.16: The Nearest-Neighbour Method. Satellite measurements of chlorophyll and sea-surface temperature are used to enter a database of chlorophyll, temperature and photosynthetic parameters. The parameter values associated with the nearest neighbours in chlorophyll-temperature space are selected from the database, and averaged over a number of nearest neighbours, usually 10. From Platt *et al.* (submitted).

parameters are assigned homogeneously within each of the three regions. To asses the agreement between the assigned and measured parameters, a comparison was conducted between the primary production estimated using both sets of parameters scaled to field chlorophyll. The root mean squared (RMS) error for this approach of assignment of the parameters was 26%.

To avoid the discontinuity at the border of the regions, a second approach to assigning the parameters was also assessed, where an average value of the parameters was applied homogeneously to the entire LAPE region if the values were not significantly different among regions. The values of the remaining parameters were estimated using linear functions of chlorophyll-a established by regression. In this approach the photosynthetic parameters and σ presented in Tables 2.1 and 2.5 were used for the entire area. The regressions that were used to assign z_m and ρ are given in Table 2.6. The values of chlorophyll-a concentration estimated by remote sensing of ocean colour was taken to be B_0, the DCM being on average deep enough to minimize its impact on satellite estimates. Although this method of assignment of the parameters provided maps that were free of boundaries, the RMS value was higher (RMS = 35%) than the regional approach. The use of mixed-layer depth (determined as the depth at which the density (σ_t) has decreased by one unit compared to the density at 5m) to explain the variability in parameters was also explored. However, the regressions between the mixed-layer depth and the parameters had lower r^2 and significance levels (p) than those obtained using chlorophyll-a concentration (Table 2.6). Moreover, chlorophyll concentration is available through remote sensing of ocean colour, whereas mixed layer depth would have to be estimated indirectly, either from archived climatology, or using models. Temperature, being stable over the entire area with a very small range, was found to be unsuitable for predicting variations in parameters.

The Nearest-Neighbour Method was also used to assign parameters. Although the Nearest-Neighbour Method provides a mean to avoid discontinuity in the map of primary production, this method is sensitive to the numbers of observations available in the database. In this study, a total of 49 profile parameters are available and only 22 photosynthetic parameters. Thereafter, observations from two other studies (Fig. 2.15) one conducted in the Gulf of Mexico in March 1999 (unpublished data)

Table 2.6: Regression between chlorophyll profile parameters (B_0 in mg m^{-3}, h in mg m^{-2}, H in mg m^{-3}, σ in m, z_m in m and ρ in dimensionless unit) and photosynthetic parameters (α^B in mg C mg $chla^{-1}$ (W $m^{-2})^{-1}$ h^{-1} and P_m^B in mg C mg $chla^{-1}$ h^{-1}) with chlorophyll-a concentration (B) in mg m^{-3} at the surface (20m) and the mixed layer depth (M) in meter for the LAPE region. The coefficient of determination (r^2), the confidence level (p value) and the number of stations (N) are also presented. Only significant relationships are presented.

Dependent variables	Equations	r^2	p value	N
z_m	122 - 270B	0.44	<0.001	49
h	4.98 + 110B	0.40	<0.001	49
ρ	0.690 + 0.902B	0.23	<0.001	49
σ	13.9 + 62.8B	0.16	0.003	49
H	0.238 + 0.988B	0.08	0.025	49
B_0	0.102-0.192B	0.07	0.037	49
α	0.114 - 0.184B	0.14	0.047	22
z_m	61.7 + 0.409M	0.11	0.011	49
h	29.0 - 0.154M	0.09	0.025	49

and one in Caribbean Waters in December 1984 (Irwin *et al.* 1987) were used to produce a database of 48 photosynthetic parameters for application using the Nearest-Neighbour method. This method is usually conducted using 10 nearest neighbours. However, due to the limited numbers of observations available in our database, using 10 values produced a high RMS value (27%). A decrease in the number of nearest neighbours returned better agreement between the primary production computed from the measured and assigned parameter (5 neighbours RMS = 23%, 4 neighbours RMS = 19%).

2.5.3 Computation of Primary Production From Satellite Data

Primary production was calculated using a spectral, non-uniform model (Sathyendranath *et al.* 1989) using the Ocean Primary Production software (see IOCCG website, http://www.ioccg.org/) with numerical integration, forced by Bird's clear sky spectral irradiance model (1984) with correction for cloud cover using NOAA monthly composite data (one degree grid). The ratio of yellow-substance absorption at 440 nm to that of phytoplankton absorption at the same wavelength was fixed at 30 %. Primary production was estimated for the LAPE region over an annual cycle for the

year 2006 from monthly composite images of chlorophyll-a concentration using both a regional approach and the Nearest Neighbour Method to assign photosynthetic and profile parameters. It is important to point out that the photosynthetic parameters, as well as the profile parameters, were measured only in April and May in the LAPE study and in March and December in the previous two studies used in the Nearest Neighbour Method. Thus, the estimates of primary production for any other month might be biased by the extrapolation of the physiological and profile parameters. However, if we compare the data with those from two previous studies in the same region (Irwin *et al.* 1987 and unpublished data, March 1999), the photosynthetic parameters seem to remain stable from year to year and season to season (Fig. 2.15). No comparison of the profile parameters has been made because datasets are lacking for this province. Water-column primary production has also been calculated for all 21 stations for which both photosynthetic parameters and profile parameters were available (tabulated in Appendix F).

In general, primary production maps showed similar features to chlorophyll composite images: low primary production in the north and higher primary production in the southern region. The coastal waters, due to the shallow water column (less than photic depth), presented in some cases a lower water-column primary production than that offshore, a different pattern from that observed in the chlorophyll images. The primary production maps computed using the regional approach (Figs. 2.17 left and 2.18) exhibit a discontinuity between the northern and the southern regions, a consequence of the difference between the profile parameters z_m and h. The discontinuity between the coastal region and the two open-ocean regions is less apparent. The use of the Nearest-Neighbour Method to assign parameters eliminated the discontinuity but produced lower primary production values (Figs. 2.17 right and 2.19 and Table 2.7). The Nearest-Neighbour Method assigns parameters from the temperature and chlorophyll fields. Thus, fewer pixels are available when using this approach compared with the regional approach because of the increased number of blank pixels in the temperature fields. Although the Nearest Neighbour Method provided lower estimates of production, especially in the northern region, compared with the regional approach, the two approaches overall returned similar patterns of primary production. Full-page versions of the annual cycle of primary production using the two different

Table 2.7: Comparison of the monthly mean ($\pm$ standard deviation) primary production estimated from ocean-colour data using two different approaches to assign parameters: the regional approach and the Nearest Neighbour Method.

Month	regional mg C m^{-2} d^{-1}	Nearest Neighbour mg C m^{-2} d^{-1}	difference %
January	239.28 $\pm$ 106.23	203.74 $\pm$ 152.82	14.9
February	261.57 $\pm$ 123.48	209.82 $\pm$ 171.26	19.8
March	270.84 $\pm$ 128.21	202.87 $\pm$ 171.37	25.1
April	308.31 $\pm$ 141.92	256.63 $\pm$ 186.64	16.8
May	300.86 $\pm$ 128.90	270.88 $\pm$ 155.46	10.0
June	336.62 $\pm$ 175.29	330.50 $\pm$ 163.28	1.8
July	378.91 $\pm$ 190.08	358.68 $\pm$ 220.52	5.3
August	352.03 $\pm$ 172.21	350.09 $\pm$ 174.13	0.6
September	319.54 $\pm$ 153.34	309.99 $\pm$ 164.34	3.0
October	297.99 $\pm$ 137.25	296.64 $\pm$ 153.93	0.5
November	255.30 $\pm$ 102.47	257.00 $\pm$ 136.30	-0.7
December	240.18 $\pm$ 103.13	208.39 $\pm$ 137.65	13.2
average	296.79	271.27	9.18

approaches to assign parameters are in Appendices G and H.

The magnitude of primary production in the LAPE region is characteristic of systems with low nutrient concentration; for exemple, Joint *et al.* (2001), in a Lagrangian study of a North-Atlantic off-shore water mass, found daily primary production varying between 249 mg C m^{-2} d^{-1} and 436 mg C m^{-2} d^{-1} and in Platt and Harrison (1985) for the Bermuda station where primary production averaging 225 mg C m^{-2} d^{-1}. Note also that monthly values of primary production are fairly stable over the annual cycle (Table 2.7) with a small increase in primary production in the summer months, when daylength and irradiance increased slightly, and a decrease in winter months. By contrast, in their study of the Bermuda waters Platt and Harrison (1985) found that primary production decreased by about two thirds in the summer and autumn compared with late winter and spring values. A possible explanation for the stable annual cycle in the present study might lie in the use of photosynthetic parameters from only three cruises (March, April, May and December) and the profile parameters from only one cruise (April and May 2006). However, Platt and Harrison (1985) found a decrease in nutrient levels at the end of March whereas nutrient levels in the Caribbean waters are expected to remain low throughout the annual cycle

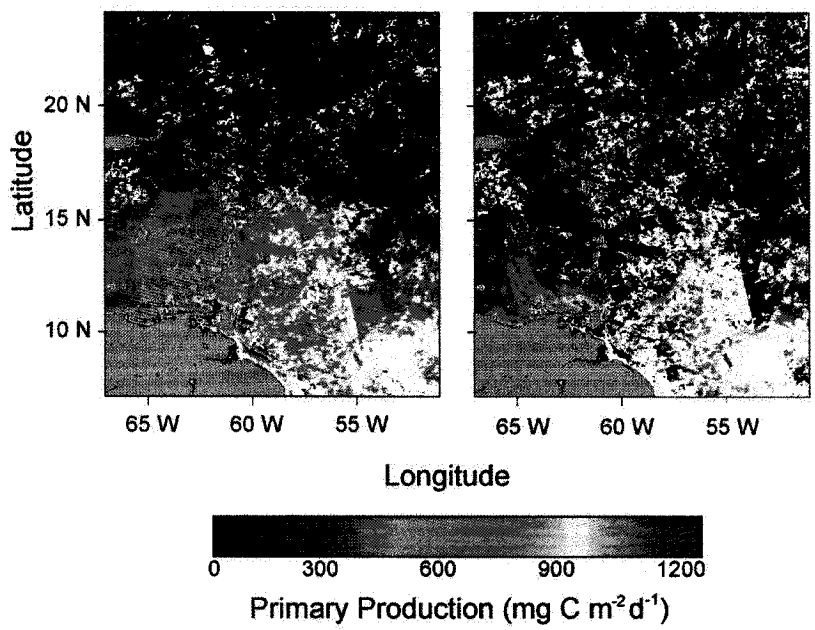

Figure 2.17: Primary production for May 2006 for the LAPE study area for different assignment of the photosynthetic parameters and the chlorophyll-a profile parameters. Left) Different parameters assigned to three subregions. Right) Parameters are assigned from the Nearest-Neighbour Method. The sampling stations are superimposed.

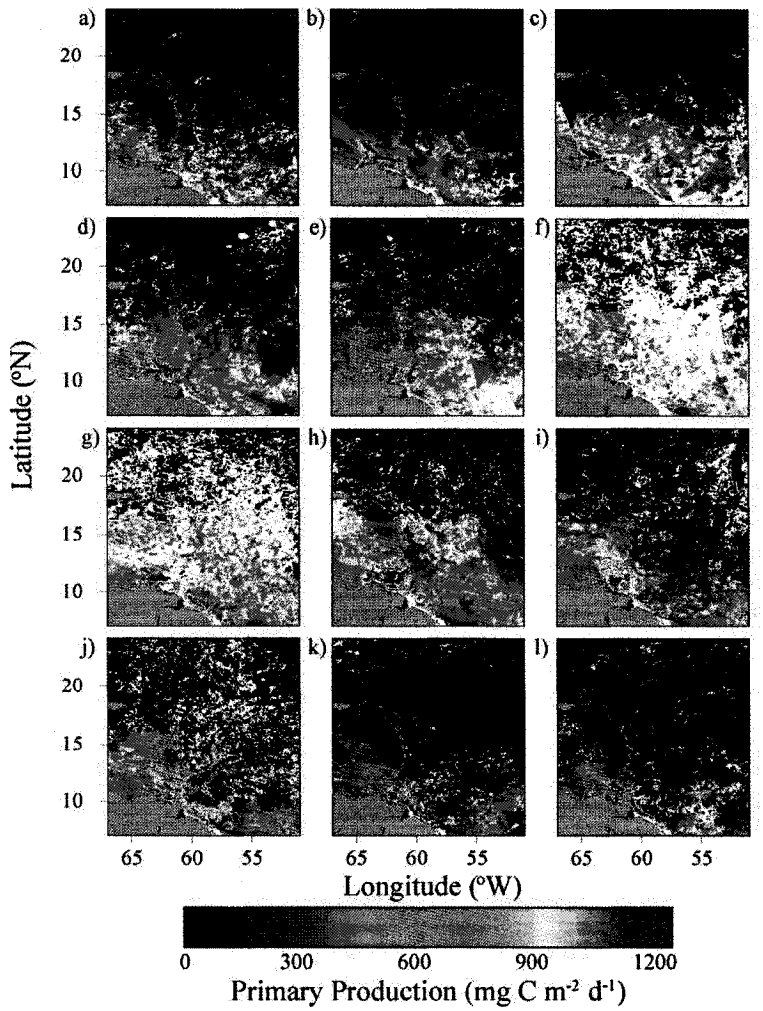

Figure 2.18: Primary production estimated from remote sensing of ocean colour with parameters assigned according to regions (coastal, southern or northern) over an annual cycle for the year 2006 for the LAPE study area (a) January, (b) February, (c) March, (d) April, (e) May, (f) June, (g) July, (h) August, (i) September, (j) October, (k) November, and (l) December.

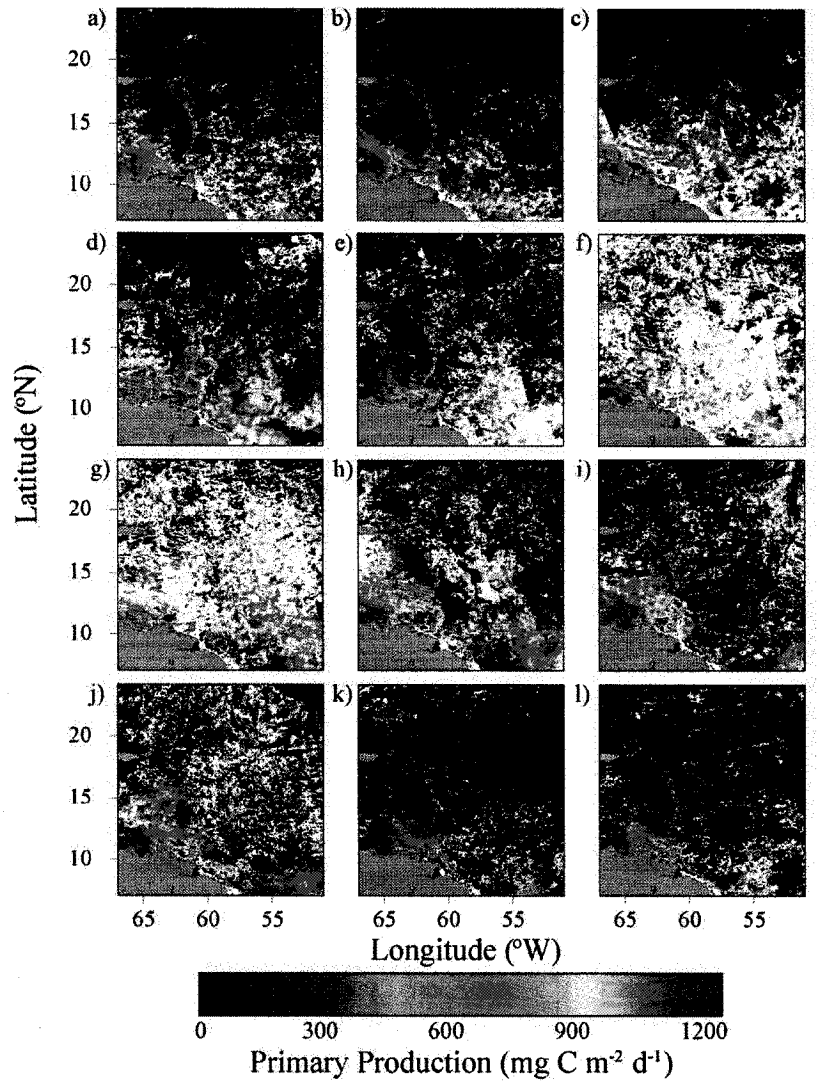

Figure 2.19: Primary production estimated from remote sensing of ocean colour using the Nearest Neighbour Method over an annual cycle for the year 2006 for the LAPE region a) January, b) February, c) March, d) April, e) May, f) June, g) July, h) August, i) September, j) October, k) November and l) December.

owing to its stable annual temperature cycle (Fig 2.13).

2.6 Conclusion

From pigment ratios and absorption analyses, it was determined that the phytoplankton community in the LAPE study was mainly pico-phytoplankton ($< 2\,\mu$m) and some nano-phytoplankton (between 2 and $20\,\mu$m), whose contribution to the pool of pigments increase at the deep chlorophyll maximum (DCM). Micro-phytoplankton ($> 20\,\mu$m) were practically absent. The pico-phytoplankton *Prochlorococcus* and the nano-flagellates dominated at the deep chlorophyll maximum whereas the other phytoplankton component increased at the surface. Statistical analyses indicated that the phytoplankton community was significantly different between the northern and southern regions.

Monthly composite images of chlorophyll-a were produced for 2006 from MODIS satellite imagery. The 1 km-resolution maps showed very low interference by cloud coverage, except for June and July (rainy season). Chlorophyll-a concentration was lower in the northern than the southern region. Maximum values were found along the coast, which is under the influence of the Amazon and Orinoco River outflows.

Field measurements allowed the parameterisation of the chlorophyll-a profile (shifted Gaussian curve) and the photosynthetic parameters. Primary production was calculated on the monthly composite images (2 km resolution) with the photosynthetic and profile parameters assigned using two different approaches, a regional approach and the Nearest Neighbour Method. Both approaches returned similar patterns of primary production, which followed the trend found in chlorophyll concentration, with lower primary production in the north than in the south.

Chapter 3

EXTRACTION OF PHOTOSYNTHESIS-IRRADIANCE PARAMETERS FROM PHYTOPLANKTON PRODUCTION DATA: DEMONSTRATION IN VARIOUS AQUATIC SYSTEMS[2]

3.1 Introduction

Primary production by phytoplankton regulates energy availability to higher trophic levels as well as carbon and oxygen fluxes between the ocean and the atmosphere. Remote sensing of ocean colour has proven to be valuable in providing synoptic fields of primary production (Longhurst *et al.* 1995; Antoine *et al.* 1996; Behrenfeld and Falkowski 1997), from which it has been estimated that global oceanic primary production fixes 36.5 to 50 gigatonnes of carbon every year, similar to global terrestrial primary production (Longhurst *et al.* 1995; Behrenfeld *et al.* 2001; Cramer *et al.* 2001). To quantify primary production on synoptic scales in this manner, remotely-sensed estimates of chlorophyll-a concentration, daily irradiance and attenuation coefficients have to be combined with the characteristics of pigment-biomass profiles and photosynthetic response (Platt and Sathyendranath 1988; Sathyendranath and Platt 1993). Under the simplified assumption of vertical homogeneity, only the photosynthetic parameters are required as auxiliary data (Platt and Sathyendranath 1993).

Photosynthetic parameters are extracted from production-irradiance curves ($P-E$ curves) in which production P is normalised to chlorophyll-a concentration as P^B which is taken as a surrogate for biomass, B (Fig. 1.2). The two parameters required to describe the $P-E$ relationship are α^B, the initial slope of the relationship, and P_m^B, the light-saturated production plateau. The projection on the abscissa of the intersection of α^B and P_m^B provides the photoacclimation parameter E_k. These

[2]This chapter has been published as an article in Journal of Plankton Research, Volume 29(3): p.249-262, 2007.

parameters are derived from experiments made under light-controlled conditions in a light-gradient incubation box. Good estimates of phytoplankton production can be obtained by combining photosynthetic parameters with the underwater irradiance field and biomass concentration (see for example Côté and Platt 1984; Platt and Sathyendranath 1988; Kyewalyanga *et al.* 1997). However, under-sampling of $P-E$ parameters, especially in some biogeochemical provinces in the southern hemisphere, has been pointed out as a circumstance that limits the applicability of the procedure at the global scale (Longhurst *et al.* 1995). At the same time, substantial existing databases provide data on water-column primary production from *in situ* or simulated *in situ* incubation (O'Reilly *et al.* 1987; see also Table III in Campbell *et al.* 2002). Thus, extracting the required photosynthetic parameters from *in situ* or simulated *in situ* measurements of primary production, would be an important contribution to satellite-based primary-production measurements.

One suggested approach (Behrenfeld and Falkowski 1997) is to use measured vertical biomass-specific profiles of primary production to extract a set of productivity parameters, P^B_{opt} and E_{max}. However, these parameters are different from those derived from production-irradiance curves, and cannot be easily extrapolated to other conditions since they can be influenced by daily variations in irradiance at the time of the incubation. Moreover, field measurements of P^B_m are usually unavailable for comparison with estimates of P^B_{opt}, as production data are generally for either *in situ* water-column production or $P-E$ experiments.

Here we explore and refine a new method for estimating the photosynthetic parameters, α^B and P^B_m, from a series of *in situ* and simulated *in situ* primary production measurements from different regions and seasons (Platt and Sathyendranath 1993). We show how the method can also be used to extract the photosynthetic parameters of two freshwater systems. We then apply the method to measurements of both *in situ* and simulated *in situ* water-column primary production in marine systems and find a generalisation that will simplify the retrieval of the photosynthetic parameters. Finally, we verify the method using independent data, from the Canadian Arctic waters.

3.2 Theoretical Considerations

Along with phytoplankton biomass, light is a major limiting factor for primary production. Thus, understanding the relationship between daily water-column primary production (P_{ZT}) and daily irradiance (E_T) is fundamental in computing water-column primary production (Fig. 3.1a). By calculating P_{ZT} from a hypothetical population at different times of the year, Ryther was first to show the curvilinear relationship between the daily relative water-column production (R_S) and the available light at the surface of the ocean (Ryther 1956). Many other authors have studied the relationship between P_{ZT} and E_T (Ryther and Yentsch 1957; Talling 1957; Rodhe 1965; Platt *et al.* 1990), and a canonical form has been found (Platt *et al.* 1990; Platt and Sathyendranath 1993) for this relationship:

$$P_{ZT} = \frac{BDP_m^B}{K} f(E_*^m), \tag{3.1}$$

where B is the chlorophyll-a concentration, D is daylength, K is the attenuation coefficient for downwelling irradiance and $f(E_*^m)$ is a function of E_*^m (dimensionless irradiance computed as surface irradiance at noon, E_0^m, normalised to E_K) (Fig. 3.1b), whose particular form depends on the equation selected to represent the photosynthesis-irradiance curve. The first part of the right-hand side of the equation, BDP_m^B/K, is a scale factor, whereas the second half, $f(E_*^m)$, provides the curvilinear shape of the relationship with a steep slope at low light levels, and a much lower slope at high irradiance.

The relationship between the daily water-column production normalised to chlorophyll-a concentration in the euphotic zone ($\Lambda = P_{ZT}/B_Z$) and daily irradiance (E_T) has been studied (e.g. Fig. 3.1a) for many years (Malone 1976; Morel 1978; Falkowski 1981; Jordan and Joint 1984; Platt 1986; Platt *et al.* 1988). In many respects, this relationship is similar to that of the $P - E$ curves, but deals with the production not only of a single water sample but of an entire ecosystem, often on a seasonal time-scale. The normalised production measured at low light is forced mainly by the light-limited properties of the phytoplankton community (α^B), whereas normalised production measured at high light is related more to light-saturated properties of the phytoplankton community (P_m^B). However, describing an

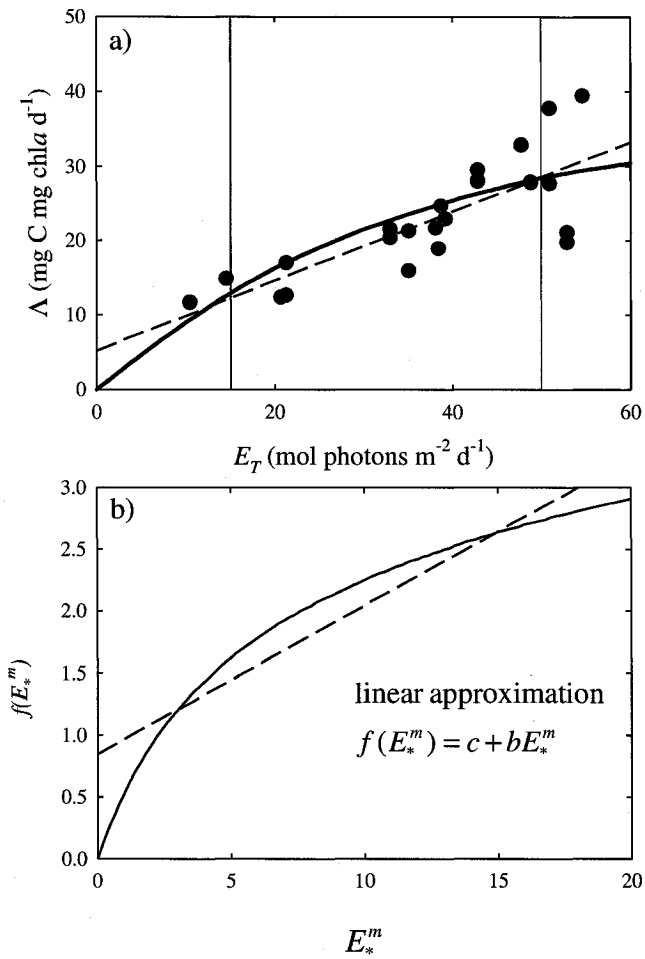

Figure 3.1: (a) Curvilinear relationship between daily irradiance (E_T) and the daily water-column production normalised to the water-column biomass Λ (P_{ZT}/B_Z) (solid line) and the linear approximation with the slope Ψ and the intercept ξ (dashed line). The data (red symbols) are from Lake Croche. The vertical lines correspond to E_T = 15 mol photons m^{-2} day^{-1} and E_T = 50 mol photons m^{-2} day^{-1}. Observations at E_T < 15 mol photons m^{-2} day^{-1} were used to estimate α^B and E_T > 50 mol photons m^{-2} day^{-1} were used to estimate P_m^B. (b) 5th−order polynomial function of E_*^m and the linear approximation for the entire range of E_*^m.

accurate curvilinear relationship with light-limited and light-saturated parameters is much more difficult for an entire ecosystem than for $P-E$ experiments, due to the limited range of daily surface irradiance encountered. Many authors (Malone 1976; Morel 1978; Falkowski 1981; Jordan and Joint 1984; Platt 1986; Platt *et al.* 1988) have proposed to represent this relationship using a linear approximation with a slope Ψ (Fig. 3.1a). The slope (Ψ) is referred to as the water-column light-utilisation index (Falkowski 1981), and it has been pointed out (Platt *et al.* 1988) that Ψ varies by only a factor of 2 in all the studies reviewed in their paper (0.29-0.52 g C (g Chl $a)^{-1}$ m^2 (mol quanta)$^{-1}$). It has been proposed that the linear approximation to the relationship between Λ and E_T carries information on the photosynthetic parameters (Platt and Sathyendranath 1993). However, the proposition has not yet been tested.

Suppose that, over a given range of E_*^m, the linear approximation of $f(E_*^m)$ is represented by

$$f(E_*^m) = bE_*^m + c, \tag{3.2}$$

with slope b and intercept c (Fig. 3.1b). It has been shown that Equations (3.1) and (3.2) can be combined and rewritten as a function of the photosynthetic parameters:

$$\Lambda = \frac{Dc}{4.6}P_m^B + \frac{b\pi}{9.2}\alpha^B E_T, \tag{3.3}$$

where the intercept contains P_m^B and the slope contains α^B (Platt and Sathyendranath 1993). Since b and c are unknown, the parameters α^B and P_m^B cannot be estimated directly from Equation (3.3), unless an iterative procedure is established. Here I develop and test such a method.

The procedure could be substantially simplified if a typical range of E_*^m were defined, such that values of b and c could be estimated from linear approximation of $f(E_*^m)$. It has been pointed out that a small range of E_*^m (from 5 to 8) might cover many situations in temperate latitudes (Platt and Sathyendranath 1993). Here we examine this suggestion using several data sets of primary production to determine the range of E_*^m they represent, and then calculate the corresponding values of b and c for each set. Next, we generalise the results and validate the resultant simplified approach using an independent data set.

Table 3.1: Description of the aquatic systems under study and of the types of production measurements (N = number of observations) included in the analyses. Production estimations are 1 for $P - E$ experiments, 2 for *in situ* measurements and 3 for simulated *in situ* measurements.

Systems	Lat.; Long.	Type	Season	methodology
Lac Croche[1]	45°59'N;74°01'W	Lacustrine	Summer	1 (N = 23)
St Lawrence River[1]	45°16'N;74°06'W	Fluvial	Summer	1 (N = 16)
Bedford Basin[2,3]	44°41'N;63°38'W	Coastal	Spring	1,2 (N = 23)
Canary Current[4]	31°04'N;10°50'W	Coastal	Autumn	1,2 (N = 7)
Sargasso Sea[5]	37°30'N;40°00'W	Open Ocean	Spring	1,2 (N = 8)
NW Atlantic shelf[6,7]	43°53'N;57°56'W	Open Ocean	Spring	1,3 (N = 9)
Canadian Arctic[8]	74°52'N;80°02'W	Open Ocean	Summer	1,2 (N = 5)

[1]Forget (2001)
[2]Platt (1986)
[3]Irwin *et al.* (1988)
[4]Kyewalyanga *et al.* (1997)
[5]Kyewalyanga *et al.* (1992)
[6]Unpublished data
[7]Pommier *et al.* (submitted)
[8]Irwin *et al.* (1985)

3.3 Methods

3.3.1 Study Sites

To test the above method and its applicability, six different datasets were used. The systems studied encompass a broad range of biogeochemical properties (Table 3.1), varying from lacustrine, fluvial and coastal to open-ocean systems. These systems were sampled at different times of the year and represented conditions from well mixed to fully stratified water columns. All of the systems studied are within eastern Canada and the Northwest Atlantic, except the Canary Current coastal province, which is located in the Northeast Atlantic Ocean. The Northwest Atlantic Shelf refers to a Lagrangian study (C-SOLAS) of the decline of a spring bloom located between 43°N and 44°N, and 57°W and 58.5°W (Pommier *et al.* submitted). During that study, a water mass containing the bloom was sampled daily from 25 April to 2 May of 2003 (d1 to d8, where d8 falls outside the studied water mass). The site was sampled again on 14 May 2003 (referred as d20).

3.3.2 Primary Production Measurements

Primary production was measured using three different techniques. First, $P-E$ experiments were performed by incubating samples for 3 to 4 hours in a light-gradient incubator, using either ^{14}C uptake (Irwin *et al.* 1985) or oxygen evolution (high precision Winkler method, Carignan *et al.* 1998). A photosynthetic quotient of 1.25 was used to transform oxygen production in carbon units (Williams and Robertson 1991). The photosynthetic parameters were obtained by fitting the equation of Platt *et al.* (1980) to the observations. Attenuation coefficients of photosynthetically active radiation in the water column were also measured. Second, *in situ* primary production was measured using the ^{14}C technique (Irwin *et al.* 1985). Water samples were collected from different depths, bottled and returned to their specific depth for incubation for 6 to 24 hours. Third, simulated *in situ* primary production was measured using a similar approach (Pommier *et al.* submitted), except that the bottles were incubated for 8-10 hours on deck in temperature-controlled chambers, shaded to mimic the different optical depths (100%, 50%, 30%, 15%, 5%, 1% and 0.2% of surface PAR). The water-column integrated production from *in situ* and simulated *in situ* incubations was computed as the sum of production P_i in each of the n layers where production was measured

$$\int P(z)dz = \sum_{i=1}^{n} P_i L_i, \tag{3.4}$$

where i represents the layer and L_i is the thickness of the i_{th} layer (Platt and Irwin 1968). When incubation time was less than the daylength, the computed production was scaled to obtain daily water-column production by multiplying by E_T and dividing by the total irradiance during the period of incubation. Similarly, mean chlorophyll-a in the euphotic zone was computed as

$$\sum_{i=1}^{n} B_i L_i / z_p, \tag{3.5}$$

where B_i is the measured chlorophyll concentration in the i_{th} layer and the integration is carried out over the euphotic depth to z_p where light is reduced to 1% of its surface value.

3.3.3 Iterative Procedure

For an initial test of the method, daily production in two freshwater systems was estimated from photosynthetic parameters using Fee's model (1990). This model consists of a numerical integration over depth and time and implies homogeneity of the water column, which corresponds to the premise of the model of Platt and Sathyendranath (1993). To start the iterative procedure, initial estimates of photosynthetic parameters were used to obtain initial values for E_*^m. Then $f(E_*^m)$ was computed (see Table A1 of Platt and Sathyendranath 1993) for each observation, and a linear approximation (Equation 3.2) was fitted to the values. This yielded initial values of b and c, which were then substituted into Equation (3.3) to obtain new values for α^B and P_m^B from the slope ($\Psi = b\pi\alpha^B/9.2$) and the intercept ($\xi = DcP_m^B/4.6$) of the linear equation fitted to Λ as a function of E_T. Then, through successive iterations, a final set of photosynthetic parameters should be estimated by convergence. We found, however, that trial fits to both parameters simultaneously did not lead to convergence, perhaps because the results were sensitive to initial guesses, as had been suggested earlier (Platt and Sathyendranath 1993). Therefore, Equation (3.3) was applied separately in each of two ranges of daily irradiance determined arbitrarily: less than 15 mol photons m^{-2} d^{-1} to obtain α^B and greater than 50 mol photons m^{-2} d^{-1} for P_m^B. This two-part estimation of parameters was accepted as the final result. This procedure led to successful convergence for the parameters. The same technique was then applied to the four sets of data from *in situ* or simulated *in situ* water-column incubations. When the observed irradiance range did not offer any data points in either of the two ranges, the two points from each of the lowest and highest irradiance levels were used for the estimation. This compromise had to be made in three of the six studied systems: the Canary Current coastal province, the Sargasso Sea and the Northwest Atlantic Shelf. For all of these systems, the photosynthetic parameters estimated by the iteration procedure were compared with the measurements from the $P - E$ curves.

3.4 Results

Prior to evaluating the results of the iterative procedure, estimates and measurements of water-column primary production were compared to establish whether the models used were capable of reproducing the observations well (Fig. 3.2). Estimates of water-column primary production from the two different models (Fee 1990; Platt *et al.* 1990) showed good agreement, with values tightly distributed around the one-to-one line, with a small but consistent over-estimation of primary production by the model of Platt *et al.* compared to that of Fee. *In situ* and simulated *in situ* measurements showed higher variability when compared with modelled production (Platt *et al.* 1990). Primary production in the Bedford Basin measured over a 24-hour incubation was much lower than measurements from 6-hour incubations, and from estimates using the model of Platt *et al.* (1990). Since measurements using ^{14}C did not account for planktonic respiration, such divergence between short and long incubations was expected: short incubations yield estimates closer to gross primary production whereas long incubations represent net primary production. Production estimates from the Canary Current coastal province and the Sargasso Sea were often higher than values computed using the model of Platt *et al.* (1990). However, results remained well distributed around the one-to-one line.

The iterative procedure (Fig. 3.3) was based on the relationship between normalised production (Λ) and daily irradiance (E_T). For all of the systems under study, the magnitudes of Λ were similar, except for the remarkably low Λ values from the Northwest Atlantic Shelf. Highest values were found in the two freshwater systems and the Sargasso Sea. To account for differences in duration of incubation, the daily production from longer *in situ* incubations (Bedford Basin, 24 h incubation and Northwest Atlantic Shelf, 8-10 h incubation) was corrected for respiration to match estimates from short (4-hour or less) $P - E$ incubations; we used the empirical relationship of Smith and Kemp between volumetric respiration and temperature (Smith and Kemp 1995). This relationship accounts only for temperature, which is a strong predictor of respiration in Chesapeake Bay (Sampou and Kemp 1994; Smith and Kemp 1995), although others (del Giorgio and Peters 1994; Carignan *et al.* 2000) have shown that biomass (chlorophyll-a concentration) is also an important factor regulating planktonic respiration. Corrected data yielded a positive linear relationship

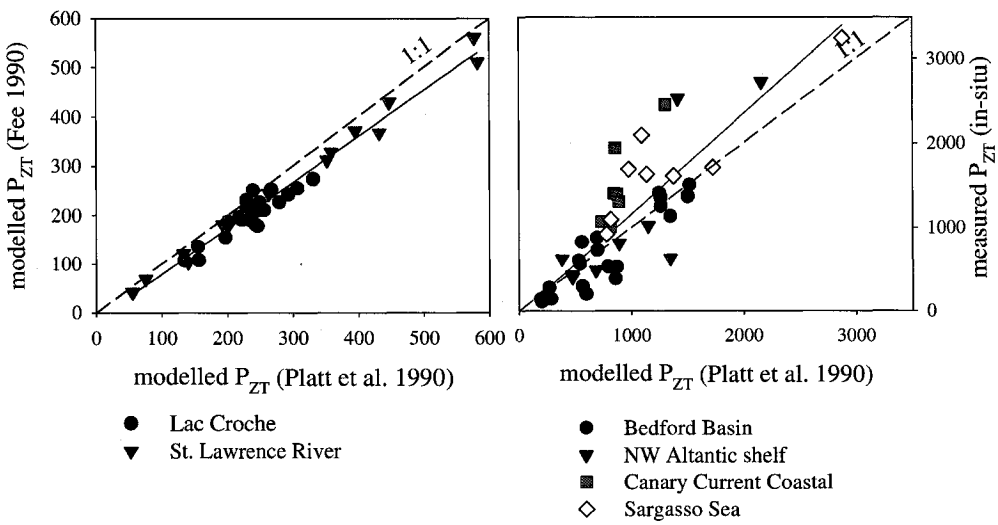

Figure 3.2: Relationship between water-column primary production estimated from models of Fee (1990) and Platt *et al.* (1990) where $y = 0.94x - 14.1$; $r^2 = 0.97$ (left), and relationship between water-column primary production measured from *in situ* incubation and that estimated from the model of Platt *et al.* (1990) where $y = 1.19x - 32.7$; $r^2 = 0.71$ (right). Units of production are mg C m^{-2} day^{-1}. In both graphs, the dashed line is the 1 to 1 line and the solid line represents the linear regression.

between Λ and E_T for all of the systems, with the exception of the two open-ocean systems (Sargasso Sea and Northwest Atlantic Shelf). For the Sargasso Sea dataset, daily irradiance was consistently high, and the low range of E_T limited any further analysis of light-dependent changes in production. In the Northwest Atlantic Shelf, the apparent decrease of Λ with light was counter-intuitive, which prompted further examination.

During the Northwest Atlantic Lagrangian time series (Fig. 3.4a) the average chlorophyll-a concentration integrated over the euphotic depth declined from d1 to d8. Observations from satellite images (Forget *et al.* in press, see Chapter 4) showed that these field measurements covered the decline of the spring bloom and that peak biomass occurred during the previous week. Total primary production integrated over the euphotic depth (Fig. 3.4b) was fairly high on d1 and d2 but dropped drastically on d3 after which it remained nearly constant until the end of the Lagrangian study and then increased slightly on d20 (Pommier *et al.* submitted). Normalised production (Λ) on d1 and d2 was higher than on d8 and d20, but significantly lower for d3 to d7 (t-test, $p < 0.01$). The time-series of water-column normalised production (Fig. 3.4c) along with its relationship with E_T (Fig. 3.5) allowed us to identify three groups of samples. *In situ* observations revealed that samples from group I were characteristic of a diatom bloom, which declined in samples from group II, followed in group III by a mixed phytoplankton population (Pommier *et al.* submitted). For the photosynthetic parameters (Fig. 3.4), group I and III presented higher mean values ($\pm$ standard deviation) of the photosynthetic parameters (group I: $\alpha^B = 0.024 \pm 0.014$ mg C mg chla^{-1} (W m^{-2})$^{-1}$ h^{-1}; $P_m^B = 1.04 \pm 0.43$ mg C mg chla^{-1} h^{-1}; group III: $\alpha^B = 0.024 \pm 0.0057$ mg C mg chla^{-1} (W m^{-2})$^{-1}$ h^{-1}; $P_m^B = 1.92 \pm 0.17$ mg C mg chla^{-1} h^{-1}) than the second group ($\alpha^B = 0.014 \pm 0.0035$ mg C mg chla^{-1} (W m^{-2})$^{-1}$ h^{-1}; $P_m^B = 0.84 \pm 0.15$ mg C mg chla^{-1} h^{-1}).

A positive linear relationship was observed between Λ (corrected for respiration) and E_T (Fig. 3.5) for group II (r^2=0.51, N=5); groups I and III were too small (both N=2) for statistical analyses. Therefore the regression for group II was used to estimate the photosynthetic parameters by iterative procedure for a decaying population of diatoms represented in the Northwest Atlantic Lagrangian study.

The photosynthetic parameters estimated from the iteration procedure were

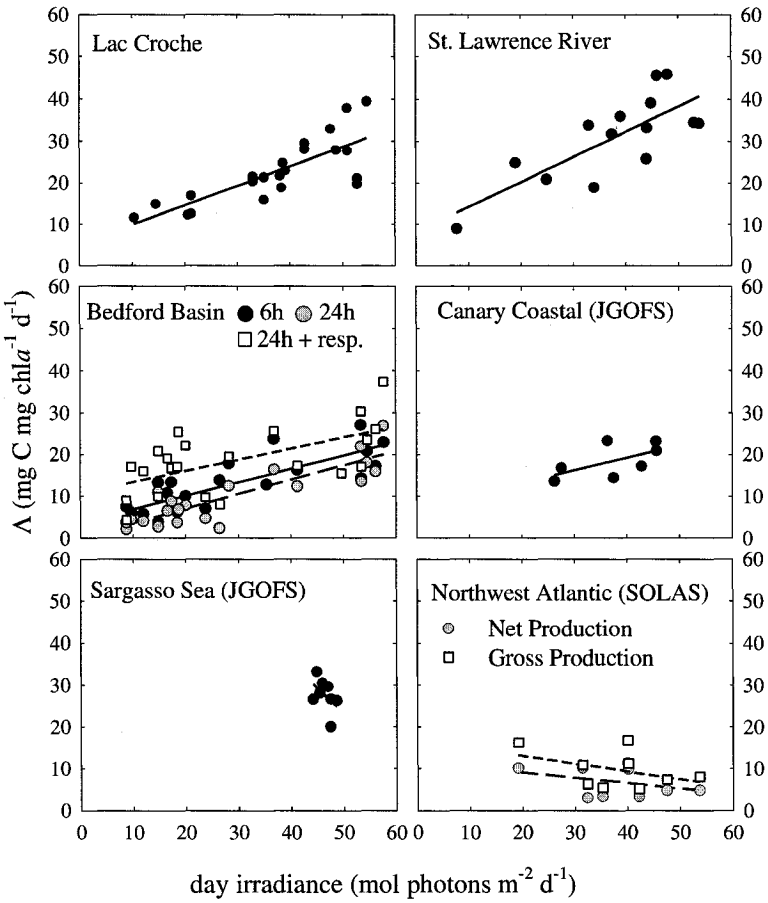

Figure 3.3: Relationship between the normalised daily water-column production Λ (P_{ZT}/B_Z) and daily irradiance (E_T) for the six systems studied. For Bedford Basin, the 6 h (filled circles) and 24 h (grey circles) incubations are presented, as well as the 24 h incubation corrected for planktonic respiration (blank squares). For the Northwest Atlantic Shelf, the net production (grey circles) and the gross production (blank squares) are presented. The parameters and r^2 of the regression lines are presented in Table 3.2.

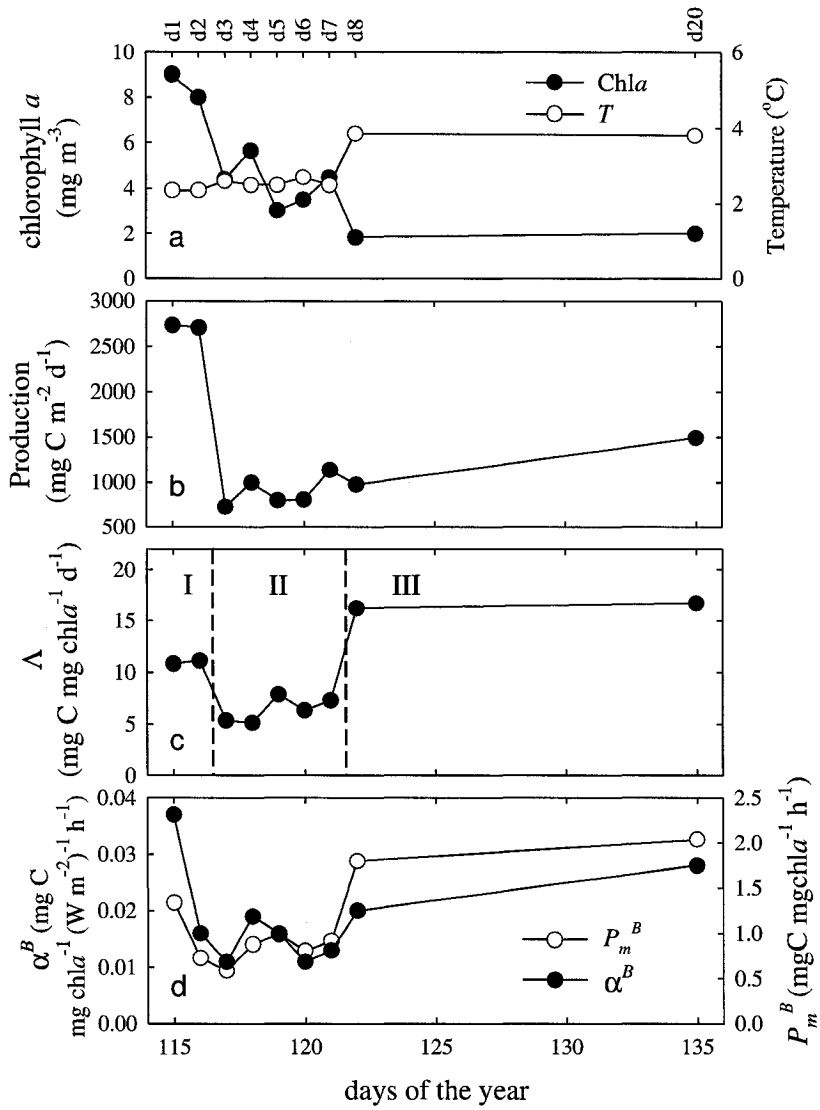

Figure 3.4: Lagrangian time-series carried out on the Northwest Atlantic Shelf from 24 April 2003 to 14 May 2003. (a) mean chlorophyll-a concentration integrated over the photic zone and mean temperature of the photic zone; (b) daily water-column primary production; (c) daily water-column primary production normalised to the water-column chlorophyll biomass; (d) photosynthetic parameters α^B and P_m^B . In panel c, the time-series has been divided into three groups according to Λ (P_{ZT}/B_Z).

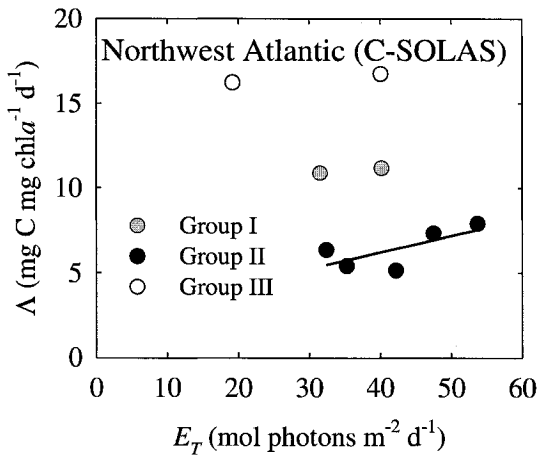

Figure 3.5: Relationship between the daily water-column production normalised to the water-column biomass Λ (P_{ZT}/B_Z) and the daily irradiance (E_T) for the Northwest Atlantic Shelf during the C-SOLAS Lagrangian study. Production values were corrected for respiration according to the empirical relationship of Smith and Kemp (1995). The data set is divided into three different groups according to their normalised production (Fig. 3.4c). The linear fit is applied to group II only, the parameters and r^2 values are presented in Table 3.2.

Table 3.2: Measurements of photosynthetic parameters (average$\pm$standard deviation) and ecosystem productivity parameters, where Ψ is the slope of the relationship between normalised production Λ and E_T whereas ξ is the intercept. The values of the slope Ψ and intercept ξ refer to Figs. 3.3 and 3.1; r^2 values are also presented. Sargasso sea data are excluded from the analyses due to the low range of daily irradiance. α^B is in $g\,C\,g\,Chla^{-1}\,(W\,m^{-2})^{-1}\,h^{-1}$, P_m^B is in $g\,C\,g\,Chla^{-1}\,h^{-1}$, Ψ is in $g\,C\,g\,Chla^{-1}\,(mol\,photons\,m^{-2})^{-1}$ and ξ is in $g\,C\,g\,Chla^{-1}\,d^{-1}$.

Systems	α^B	P_m^B	Ψ	ξ	r^2
Lac Croche	0.143$\pm$0.036	4.07$\pm$0.88	0.47	5.17	0.62
St Lawrence R.	0.149$\pm$0.037	6.72$\pm$1.53	0.60	8.10	0.60
Bedford Basin (6 h)	0.054$\pm$0.018	3.37$\pm$1.01	0.32	3.64	0.67
Canary Current	0.072$\pm$0.013	4.97$\pm$0.78	0.31	6.93	0.38
Sargasso Sea	0.097$\pm$0.024	7.41$\pm$2.09	21.16	81.93	0.21
NW Atlantic Shelf	0.014$\pm$0.004	0.84$\pm$0.15	0.09	2.31	0.51

fairly close to the photosynthetic parameters measured from the $P-E$ experiments (Fig. 3.6) usually falling within the 95% confidence interval for all the systems studied. Exceptions were for the Bedford Basin (samples were incubated *in situ* for a period of 24 hours), and in the Northwest Atlantic Shelf (8-10 h incubations). After correction for planktonic respiration, the estimated photosynthetic parameters were much closer to the measured values from the $P-E$ experiments. As explained earlier, estimated respiration rates only took temperature into account. Refining those estimates would probably give a better agreement between estimated and measured photosynthetic parameters. A similar correction should be applied to all ^{14}C *in situ* primary production measurements, when *in situ* incubation exceeds 6 hours. The implementation of the model requires that observations of production be made over a range of irradiance values to allow retrieval of parameters for light-limited and light-saturated conditions. Furthermore, the model assumes that the parameters remain stable throughout the experiments. When these conditions are satisfied, the iteration technique yields good estimates of the parameters (Fig. 3.6).

We have shown that the method proposed by Platt and Sathyendranath (1993) can yield useful estimates of photosynthetic parameters for vastly different aquatic systems. The question then arises, what generalisation could be made by combining results from all areas? Using the iteratively estimated photosynthetic parameters, we estimated b and c (Equation 3.3) from the linear fit between Λ and E_T for five of the

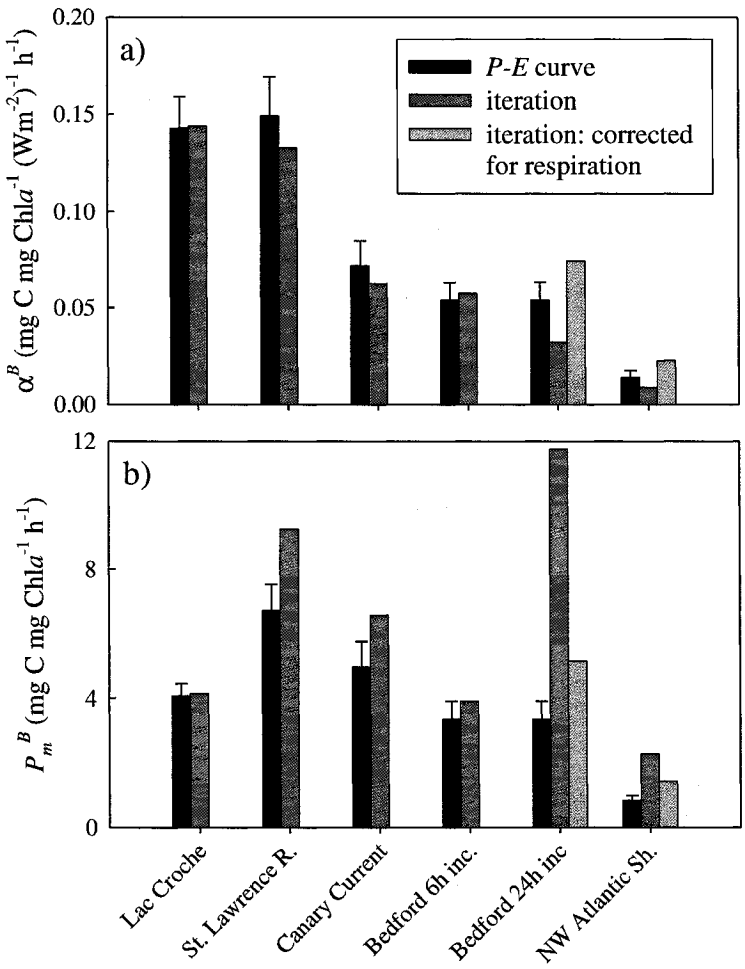

Figure 3.6: Photosynthetic parameters (α^B and P_m^B) estimated from *in situ* primary production using the iterative procedure (see text) and mean parameters (+95% confidence interval) estimated from PE experiments.

Table 3.3: Photosynthetic parameters retrieved by iterative procedure and linear approximation of the relationship between $f(E_*^m)$ and E_*^m as estimated from b and c (dimensionless) values for each ecosystem.

System	α^B (g C g chla^{-1} (W m^{-2})$^{-1}$ h^{-1})	P_m^B (g C g chla^{-1} h^{-1})	b	c
Lac Croche	0.144	4.14	0.164	0.382
St Lawrence R.	0.133	9.26	0.226	0.272
Bedford Basin	0.058	3.92	0.279	0.314
Canary Current	0.063	6.57	0.248	0.415
NW Atlantic Shelf	0.023	0.89	0.214	0.526
Average			0.23	0.38

six systems (Table 3.3); b and c could not be estimated for the Sargasso Sea system because the data did not span a sufficient irradiance range. The values of b and c varied about 2-fold and were thus more stable than the photosynthetic parameters themselves, which varied about 5-fold over the range of aquatic systems. As shown in Fig. 3.1b, values of b and c are expected to vary according to the range of E_*^m observed for each system.

Values of b and c can also be derived from the slope and the intercept of the regression of Λ on E_T in each system, given independent estimates of α^B and P_m^B, respectively. Note that such estimates are based on direct measurements of *in situ* production and of $P-E$ parameters, and therefore would be completely independent of the iteration method developed in this thesis. We can derive c from the intercept of Equation (3.3) if daylength D and P_m^B are known, and b from the slope, if α^B is known. From Fig. 3.7, we found that the slope Ψ varied linearly with α^B and the intercept ξ with P_m^B, suggesting that c and b were fairly stable among systems. Therefore, the best estimates of b and c were obtained using linear fits passing through the origin and the average daylength for all sampling days (14.1 h). These fits yielded values of 0.19 for b and of 0.41 for c (dimensionless units), which were very close to those obtained by averaging the b and c values for each aquatic system (Table 3.3: b=0.23, c=0.38). Plotting the linear approximation derived from these values of b and c superimposed on the full theoretical solution (curvilinear relationship between $f(E_*^m)$ and E_*^m) showed that our approximation was adequately close over a range of

Table 3.4: Photosynthetic parameters from Arctic water samples measured from PE experiments (values $\pm$ 95% confidence interval) and from equation (3.3) using fixed values of b and c from the common range of E_*^m for aquatic systems in the North Atlantic and Eastern Canada. The range of E_*^m is also provided (minmax values).

Methods	α^B (g C g chla^{-1} (W m^{-2})$^{-1}$ h^{-1})	P_m^B (g C g chla^{-1} h^{-1})	E_*^m Dimensionless
PE curves	0.090$\pm$0.008	1.40$\pm$0.035	1.11-1.63
Equation (3.3)	0.103	1.73	0-11

E_*^m between 0 and 11 (Fig. 3.8).

Using the above values of b and c established for aquatic systems in the North Atlantic (marine) and the Eastern Canada (freshwater), values of photosynthetic parameters were estimated using Equation (3.3) for an independent dataset, the Arctic Waters, for which both *in situ* production and P-E parameters were available (Table 3.4). The E_*^m values for the Arctic data set ranged from 1.1 to 1.6, which was at the lower end of the general E_*^m range observed for the system described earlier (Fig. 3.8). The photosynthetic parameters estimated from Equation (3.3) using fixed values of b and c were close to the measured values from $P-E$ experiments, with the P_m^B value falling within the 95% confidence interval.

3.5 Discussion

Primary production can be calculated using many different models, and ultimately estimated from satellite images of ocean colour to obtain global coverage of the global ocean. Following the approach of Longhurst (1998), the ocean can be divided into a suite of biogeochemical provinces, each one having its own specific physical, chemical and biological properties. Furthermore, these properties vary seasonally. Here, we have developed a method for estimating the photosynthetic parameters from *in situ* measurements of primary production that can be successfully applied across a wide range of marine and freshwater systems.

3.5.1 Inter-System Variations

In temperate regions, seasonal changes in temperature and wind induce the alternation of stratified (summer) and mixed (other seasons) water columns in lacustrine as

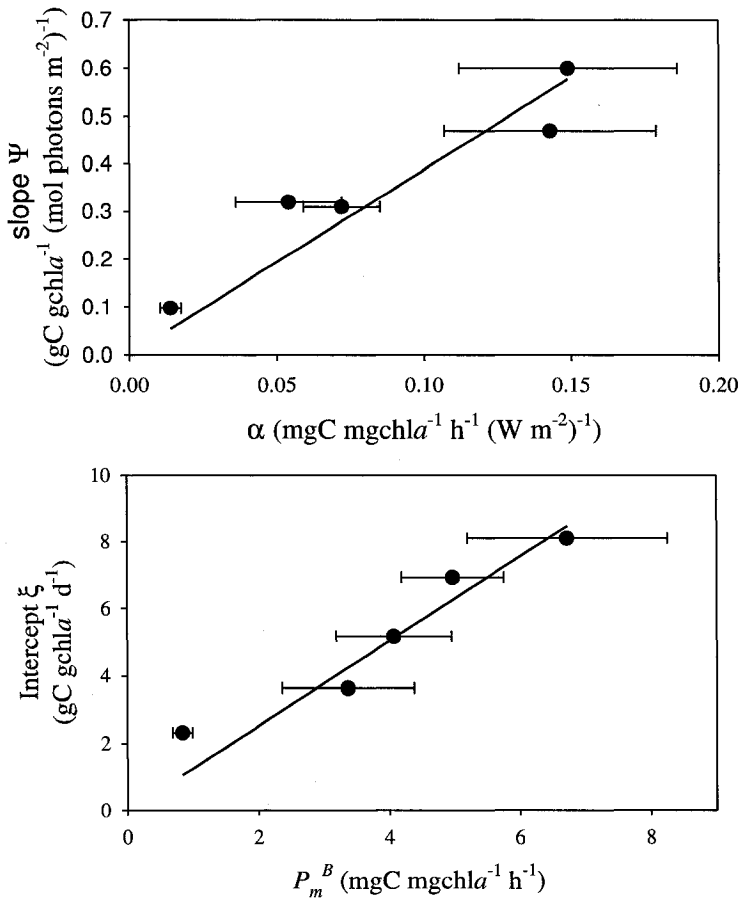

Figure 3.7: (Top panel) The linear regression between Ψ (g C g Chla^{-1} (mol photons m^{-2}) $^{-1}$) and α (g C g Chla^{-1} (W m^{-2})$^{-1}$ h^{-1}) is $y = 3.88x$, with a root mean squared (RMS) value of 0.15 g C g Chla^{-1} (mol photons m^{-2})$^{-1}$; (Bottom panel) the linear regression between the intercept ξ (g C g Chla^{-1} day^{-1}) and P_m^B (mg C mg Chla^{-1} h^{-1}) is $y = 1.26x$, with a root mean squared (RMS) value of 1.59 g C g Chla^{-1} day^{-1}. Values for b and c of the linear approximation of $f(E_*^m)$ as a function of E_*^m were estimated from equation (3.3) using the linear fit of the top panel to retrieve b and the linear fit of the bottom panel to retrieve c.

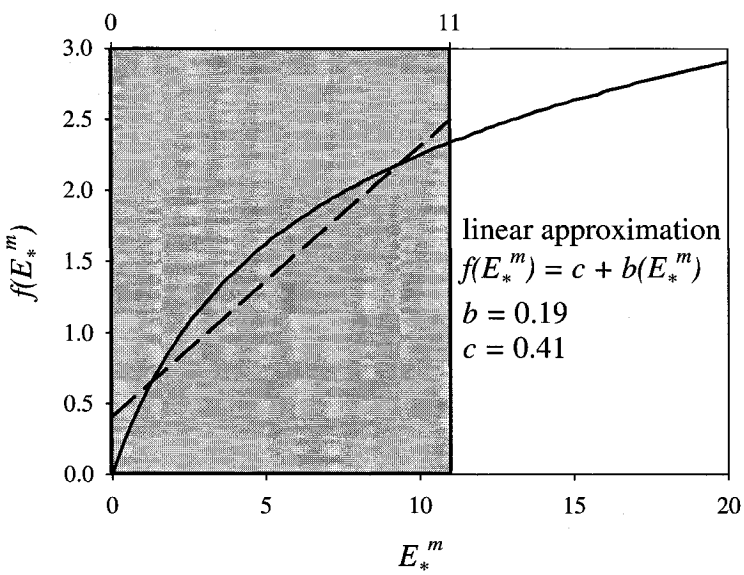

Figure 3.8: Linear approximation of the relationship between $f(E_*^m)$ and E_*^m for the range of E_*^m from all the systems studied (shaded area). Values of b and c were estimated from the linear relationships in Fig. 3.7. The corresponding E_*^m range is 0 to 11 (dimensionless).

well as oceanic systems. Our use of data sets derived from widely different aquatic systems allowed us to examine the effects of seasonal stratification (or lack thereof) on water-column primary production estimates. The models of both Platt and Sathyendranath (1993), used in the iteration procedure, and of Fee (1990) assume a vertically-homogeneous water column. This shared assumption partly explains the surprisingly good agreement between production estimates derived from those two models, which performed equally well when applied to a stratified (lacustrine) or a well-mixed (riverine) system (Fig. 3.2, left). In contrast, oceanic production estimates derived from the model of Platt *et al.* (1990) should differ most markedly from *in situ* measurements for samples from early autumn and summer due to water column stratification. In spite of seasonal differences in stratification, the agreement between *in situ* measurements and modelled primary production was high (Fig. 3.2, right).

The relationship between daily water-column production (normalised to chlorophyll-a concentration) and daily irradiance has been studied for many years (Malone 1976; Morel 1978; Falkowski 1981; Jordan and Joint 1984; Platt 1986; Platt *et al.* 1988). In this study (Fig. 3.3) the range of slope Ψ obtained (Table 3.2: 0.09 to 0.60 g C (g chl$a$)$^{-1}$ mol photons^{-1} m^2) was much wider than that reported earlier (Platt *et al.* 1988: 0.29 to 0.52 g C (g chl$a$)$^{-1}$ mol photons^{-1} m^2). The main difference comes from the Northwest Atlantic Lagrangian Study, which yielded a Ψ of 0.09 g C (g chl$a$)$^{-1}$ mol photons^{-1} m^2. The declining, post-bloom phytoplankton flora in the mixed layer at that study site reflected nutrient-limitation (Pommier *et al.* submitted). On the other hand, the St. Lawrence River, a freshwater system, exhibited the steepest slope (Ψ = 0.60 g C (g chl$a$)$^{-1}$ mol photons^{-1} m^2), indicative of eutrophic conditions. Given that the aquatic systems covered here included inland freshwater, coastal and open ocean systems, such a broad range in the ecosystem productivity parameters is not surprising and emphasizes the importance of a small number of common forcing variables on phytoplankton.

3.5.2 Extraction of Photosynthetic Parameters

The photosynthetic parameters derived from *in situ* experiments were fairly close to those measured in $P-E$ experiments (Fig. 3.6). Sometimes, α^B was slightly underestimated and P_m^B overestimated. The problem originated in the underestimation

of the initial slope of the $\Lambda - E_T$ relationship, resulting in an overestimation of P_m^B. The underestimation of the initial slope has two possible causes: insufficient data points at low light levels (Canary Current coastal province and Northwest Atlantic Shelf), or underestimation of the water-column primary production from long *in situ* incubations compared with $P - E$ experiments (4-hour incubations or less), as in Bedford Basin (24-hour incubations) or Northwest Atlantic Lagrangian site (8 to 10-hour incubations). Measurements from 24-hour incubations using ^{14}C are considered to be equivalent to the net primary production, whereas water-column primary production modelled from $P - E$ experiments and short (3-4 h) incubations are more representative of gross primary production, owing to negligible planktonic respiration (Peterson 1980). After correcting the net primary production for respiration, the $P - E$ parameter estimations were much closer to the actual measurements.

Using the retrieved photosynthetic parameters, we estimated the b and c values for each system (Table 3.4). The limited ranges of b and c implied that the range of E_*^m for all the aquatic systems under study was also restricted. However, these estimates of b and c are sensitive to errors in the estimation of the photosynthetic parameters from the iterative procedure. To avoid this source of error, b and c values were also estimated from the relationship of Ψ with α^B and ξ with P_m^B (see Fig. 3.7), using Equation (3.3) yielding $b = 0.19$; $c = 0.41$ in dimensionless units. These values would be applicable to a range of E_*^m from 0 to 11, which is broader than the restricted range of 5 to 8 previously proposed, as the usual range of E_*^m for marine ecosystems at temperate latitudes (Platt and Sathyendranath 1993). Photosynthetic parameters can thus be estimated directly from the linear relationship between Λ and E_T using Equation (3.3) and general values of b and c, which eliminates the need for the iterative procedure. Obviously, if the aquatic system presented unusual E_*^m values, outside the range from 0 to 11 (Fig. 3.8), this procedure would be inaccurate. The difficulty, of course, is that the values for E_*^m are unknown prior to the analyses. However, one could anticipate unusually high values of E_*^m if E_T values were unusually high. In such situations, the iterative approach would be preferred. Nevertheless, the range established here for E_*^m (0 to 11) should include most field situations, and my procedure should be generally applicable.

As an example, I verified the applicability of this direct procedure using an independent data set from the Canadian Eastern Arctic (Table 3.4). Although these data were from a different biogeochemical province from those previously discussed, with unique underwater light conditions and photophysiological responses of the phytoplanktonic community with low values of E_*^m (range of 1.1-1.6), the new procedure provided estimates of the photosynthetic parameters remarkably close to the measured values. This illustrates how the model could be applied globally.

3.5.3 Satellite Application

In situ or simulated *in situ* measurements of primary production provide information on this process at a particular location, at a particular time. Extraction of $P - E$ parameters from the data permits estimation of primary production at that location at different levels of biomass or light. A particular use for such prediction is for satellite-based estimates of primary production. Note that the estimated parameters, can even be used to estimate production in waters where the biomass shows vertical structure if an appropriate model is used, on condition that the parameters themselves do not show significant vertical structure.

The Lagrangian study on the Northwest Atlantic shelf illustrates well the applicability of this method to satellite-based estimation of primary production. The sampling took place at the end of a major spring bloom (Forget *et al.* in press, see Chapter 4), so the normalised production and photosynthetic parameters were not constant, but decreased through the tail-end of the bloom, a sign of increased nutrient limitation (Pommier *et al.* submitted), as observed in the decline of other blooms (Platt *et al.* 1992). The physiological state and the species composition of the phytoplankton community changed in time and space, being diatom-dominated early during the Lagrangian time-series (group I and II) and flagellate dominated in group III, outside the Lagrangian site (d8) and (d20) two weeks after the bloom (Pommier *et al.* submitted; Forget *et al.* in press see also Chapter 4). Species composition was determined by microscopic analyses and confirmed by satellite imagery (Pommier *et al.* submitted, Forget *et al.* in press, see also Chapter 4). Thus, spatial assignment of ecosystem productivity parameters could be made according to chlorophyll-a concentration maps combined with diatom-occurrence maps (Sathyendranath *et al.*

2004).

Estimates of the photosynthetic parameters from both the iteration procedure and its approximation using a general range of E_*^m correspond to average values for a specific region. One could argue that this iterative procedure would not provide data with a high level of precision. However, because the estimation of primary production from satellite images is usually performed from composite images (bimonthly, monthly or seasonally), computation from average values for a specific region and time period is appropriate. In the context of operational remote sensing of primary production, photosynthetic parameters are usually assigned from a database according to the time of the year and spatial proximity to the available data (Platt *et al.* submitted). The method developed here to estimate photosynthetic parameters from *in situ* primary production provides the means to augment such databases and enhance our ability to compute primary production from remotely-sensed data on ocean colour.

Chapter 4

COMPUTATION OF PRIMARY PRODUCTION FROM REMOTE SENSING OF OCEAN COLOUR AT THE LAGRANGIAN SITE OF C-SOLAS[3]

4.1 Introduction

Interaction between the surface layer of the ocean and the atmosphere is central to the SOLAS programme and its Canadian component, C-SOLAS. The main goal is to understand and quantify, at the global scale, the exchange of gases that affect processes in the atmosphere, such as DMS (dimethylsulphide) which triggers the formation of clouds (see review by Malin *et al.* 1992); O_2 which is essential to heterotrophic organisms; and CO_2 which is a major contributor to the enhanced greenhouse effect. Carbon assimilated through photosynthesis by phytoplankton cells in the ocean amounts to 50 gigatonnes of carbon per annum and is equivalent in magnitude to the terrestrial primary production (Longhurst *et al.* 1995, Behrenfeld and Falkowski 1997, Behrenfeld *et al.* 2001). Moreover, through the biological pump, a portion of this carbon will be stored in the ocean floor by sedimentation of organic material (Longhurst and Harrison 1989). Quantification of primary production in the ocean is therefore of central importance to programmes such as SOLAS.

Remote sensing of ocean colour is an effective method to compute primary production at the global scale (Longhurst *et al.* 1995, Antoine *et al.* 1996, Behrenfeld and Falkowski 1997). This method relies on the estimation of chlorophyll-a at the surface, the estimation of the attenuation coefficient for downwelling light and the assignment of parameters at each pixel describing the biomass profile as well as the photosynthetic response to available light (Platt and Sathyendranath 1988, Sathyendranath and Platt 1993). The first two requirements can be met directly from ocean-colour

[3]This chapter has been accepted for publication as an article in Marine Ecology Progress Series, manuscript number 7223.

algorithms (see Sathyendranath and Platt 1993), whereas parameter assignment relies largely on indirect approaches. Biomass profiles have been related to chlorophyll concentration at the surface (Morel and Berthon 1989). However, a global application of such relationship remains questionable (Longhurst *et al.* 1995). It has been shown that there is no significant relationship between either one of the photosynthetic parameters and chlorophyll-a concentration (Platt *et al.* 2005). Thus, using ocean colour directly to assign photosynthetic parameters is not a robust option. The use of temperature as a proxy to assign photosynthetic parameters (Antoine *et al.* 1996, Behrenfeld and Falkowski 1997) is attractive because sea-surface temperature can be retrieved from remote sensing in the far infra-red. However, changes in phytoplankton community structure and the increase in nutrient concentration that often accompanies a decrease in temperature may lead to trends that are not as expected from laboratory experiments (Eppley 1972).

To assign the photosynthetic parameters, some authors have proposed using archived data, either regrouping the parameters in space and time according to specific biogeochemical provinces (Longhurst *et al.* 1995, Sathyendranath *et al.* 1995) or alternatively arranging them according to temperature, chlorophyll and sampling season as a tool to recover parameters on a pixel-by-pixel basis using remotely-sensed temperature and chlorophyll as inputs (the Nearest-Neighbour Method, Platt and Sathyendranath 2002, Platt *et al.* submitted). Others have preferred to use environmental proxies such as temperature (Antoine *et al.* 1996, Behrenfeld and Falkowski 1997). Important limitations exist for each of these methods. Archived data on photosynthetic capacity are scarce, and particularly so in the southern hemisphere. However, in regions where the data are abundant, the assignment of photosynthetic parameters using the Nearest-Neighbour Method provides good estimates of primary production (Platt *et al.* submitted). Thus, expanding the archived database on parameters by deriving them from *in situ* production could increase its general applicability (Forget *et al.* 2007).

Here, we compare the photosynthetic parameters and the water-column production estimated using different approaches to assign parameters for the C-SOLAS spring cruise in the North West Atlantic. The photosynthetic parameters so obtained are used to establish a map of primary production for the Lagrangian site of C-SOLAS

(Northwest Atlantic shelf), during the spring bloom of 2003, where measurements of *in situ* production are available for comparison.

4.2 Assignment of the Parameters

4.2.1 Profile Parameters.

Biomass profiles can be parameterised using a shifted Gaussian function where four parameters are required: B_0 the background biomass; z_m the depth of the biomass peak maximum; σ which defines the width of the peak; and h the integral under the Gaussian curve (Platt *et al.* 1988, see also Chapter 2). Two additional parameters are also derived from the above set: H, the height of the biomass peak at depth z_m where $H = h/\sigma\sqrt{2\pi}$ and ρ that describes the shape of the profile ($\rho = H/(B_0 + H)$). In a remote sensing context, only three parameters are needed from the archive: z_m, σ and ρ, since information on surface and near surface biomass is available from ocean-colour data. In the following computations, we have assumed B at the surface, computed from the profile parameters, to be equal to satellite-derived chlorophyll concentration.

4.2.2 Photosynthetic Parameters.

The two photosynthetic parameters used for calculation of primary production are derived by fitting data from photosynthesis-irradiance ($P - E$) experiments to the equation of Platt *et al.* (1980):

$$P^B = P_m^B(1 - exp(-E\alpha^B/P_m^B)), \tag{4.1}$$

where biomass-normalised production (P^B) is function of the initial slope, α^B, measured in light-limited conditions, and the assimilation number, P_m^B, the plateau reached under light-saturating conditions of irradiance E.

Four methods of parameter assignment are compared in this study:

4.2.3 Nearest-Neighbour Method

The nearest-neighbour method assigns parameters by matching the values of chlorophyll and temperature at the desired pixel with their closest values in a database

Table 4.1: Probability p associated with paired t-tests between parameters measured at sea on the Scotian Shelf in Spring 2004 and parameters estimated using the Nearest-Neighbour Method with inputs either from field measurements or satellite measurements of chlorophyll and temperature. When the probability p exceeds the chosen confidence level of 0.05, the null hypothesis cannot be rejected, thus the two sets of data are equivalent.

Parameters	Probability p Field data	Probability p Satellite data
$P_m^B(\mathrm{mg\,C\,mg\,chl^{-1}\,h^{-1}})$	0.052	0.31
$\alpha^B(\mathrm{mg\,C\,mg\,chl^{-1}\,h^{-1}\,(\mu mol\,quantam^{-2}\,s^1)^{-1}})$	0.48	0.77
$z_m(\mathrm{m})$	0.35	0.26
$\sigma(\mathrm{m})$	0.98	0.89
ρ(dimensionless)	0.89	0.56

where photosynthetic parameters are archived as a function of chlorophyll and temperature (Platt *et al.* submitted, Fig. 2.16). The error involved in assignment of the parameters can be assessed by using station data not contained in the archive. We have used data from an oceanographic cruise to the continental shelf of Nova Scotia (May, 2004) for which some thirty stations are available (Figure 4.1a). All the parameters of the chlorophyll profile and the two photosynthesis parameters were measured on all stations, as were the surface temperature and surface chlorophyll. Using an archive of data not containing these thirty stations, otherwise containing 1638 observations of α^B, 1041 values of P_m^B (observations not deeper than 20m) and 1585 sets of profile parameters, and starting with the surface temperature and chlorophyll, we estimated all required parameters for each station using the nearest-neighbour method. We then compared the estimated parameters with the observed ones on a pairwise basis. The estimated sets were not significantly different (0.05 confidence level) from the observed sets (Table 4.1, Figure 4.2). Overall, these results are encouraging for the method of parameter assignment.

A more stringent test is to compare observed parameters with those estimated using the nearest-neighbour method where the inputs are not the observed temperature and chlorophyll but those captured by remote sensing. We prepared composite images of temperature (AVHRR) and chlorophyll (SeaWiFS) for the period May 1 to 15, 2004, covering the duration of the cruise. For pixels corresponding to the station

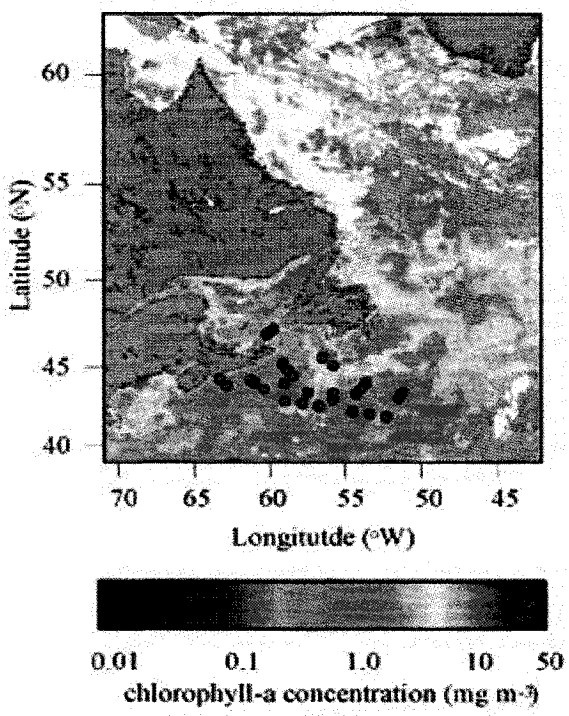

Figure 4.1: Composite image of chlorophyll concentration from SEAWiFS in the Northwest Atlantic Ocean for the first two weeks of May 2004. The location of the thirty oceanographic sampling stations mentioned in the text are superimposed.

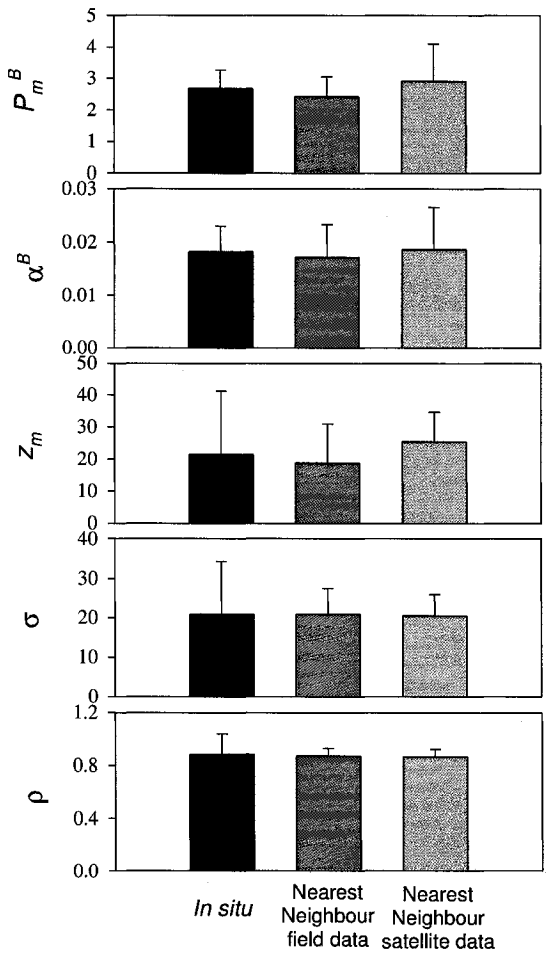

Figure 4.2: Photosynthetic-response and pigment-biomass-profile parameters from the Scotian Shelf measured in situ during the cruise from April 28 to May 08 2004 or assigned by the nearest-neighbour method using as input either field data or data from satellite images (1-15 May 2004). Photosynthesis parameters were measured from photosynthetic-irradiance experiments and biomass profiles from profiles of extracted chlorophyll-a. The error bars represent the standard deviation. Units are P_m^B (mg C(mg Chl)$^{-1}$ h^{-1}); α^B (mg C(mg Chl)$^{-1}$ h^{-1} (μmol quanta m^{-2} s^{-1})$^{-1}$); z_m (m); σ (m); ρ (dimensionless).

positions, temperature and chlorophyll were digitised. Using these as inputs, parameters were estimated by the nearest-neighbour method, and compared with observed parameters as before. In this case also (Table 4.1, Figure 4.2), the estimated parameter sets were not significantly different from the observed ones (0.05 confidence level).

Another way to evaluate the parameter assignment is through its influence on the estimation of primary production. For all thirty stations we established as the reference values of primary production those calculated with a spectral model (Platt and Sathyendranath 1988) using the observed photosynthesis parameters, observed biomass profile and clear-sky irradiance computed according to Bird (1984). We then estimated all required parameters by the nearest-neighbour method using as inputs the observed surface temperature and chlorophyll for each station. Primary production was calculated for all stations using these parameters and the same irradiance forcing as for the reference calculation. The differences between these estimates and the reference values could be ascribed only to the errors associated with parameter assignment. No other source of variance was present. We found that the mean relative difference (regardless of sign) between the estimates and the reference values was 27.0%. This is our best estimate of the relative error in the estimation of primary production arising from parameter assignment by the nearest-neighbour method. Generally, these estimates of primary production were low (under-estimated) compared with the reference values.

However, in operational use, parameter assignment use temperature and chlorophyll determined by remote sensing. We therefore made another set of estimates using parameters assigned in this way. There were now two sources of variance between these estimates and the reference values: errors from biomass retrieval and errors arising from parameter assignment. We found that the mean relative difference between these estimates and the reference values was 52.0%. This result, compared with 27.0% when only the errors were associated with parameter assignment were present leads to the conclusion that the error associated with biomass estimation is 25.0%. It is known that in the northwest Atlantic Ocean the SeaWiFS OC4 algorithm underestimates chlorophyll (Devred *et al.* 2005; Fuentes-Yaco *et al.* 2005), and this bias could account for some of the underestimation of primary production using the

operational procedure. Moreover, the remote sensing inputs are based on two-week composite images, whereas the ship observations represent particular days.

4.2.4 Temperature-Dependent Model

A relationship between surface (0 to 20 m) values of α^B (mg C mg chla^{-1} (W m^{-2})$^{-1}$ h^{-1}) and corresponding temperature (°C) was established in Platt *et al.* (2005) for data from 16 cruises on the Scotian Shelf and Labrador sea from 1997 to 2003. The fit, not provided in the original article, is significant and follows the relationship: $\alpha^B = 0.006T + 0.041$; $r^2 = 0.41$; $n = 416$, with $p < 0.001$ (Fig. 4.3a), where T is temperature. Similarly, Bouman *et al.* (2005) found that P_m^B (mg C mg chla^{-1} h^{-1}) could be well predicted for the North West Atlantic region using the relationship: $P_m^B = 0.034T + 1.15$; $r^2 = 0.66$; $n = 416$; $p < 0.001$ (Fig. 4.3b).

4.2.5 The Iterative Procedure

The iterative procedure for retrieval of photosynthetic parameters from *in situ* production was proposed initially by Platt and Sathyendranath (1993) and developed and implemented by Forget *et al.* (2007); see Chapter 3 where the model is fully described. Briefly, the iteration is applied to two sets of linear regressions: (1) between Λ (the water-column primary production normalised to the water-column chlorophyll-a) and the total irradiance at the surface (E_T); and (2) between a function f of E_*^m, the maximum irradiance at the surface normalised to E_k ($= P_m^B/\alpha^B$) the photo-acclimation parameter, and E_*^m itself. The procedure is applied in two parts: the initial slope α^B is estimated from a linear regression (forced through the origin) using points with daily irradiance lower than 15 mol quanta m^{-2} d^{-1}, and the assimilation number P_m^B is estimated using points with daily irradiance higher than 50 mol quanta m^{-2} d^{-1} (Forget *et al.* 2007). When the observed irradiance range did not offer any points in either of the two categories, the two points from the lowest and highest irradiance levels, respectively, are used for the estimation. The regressions are carried out first with an initial guess for E_k; the estimated parameter values are then used to recalculate E_*^m, and the iteration is repeated until convergence of the photosynthetic parameters.

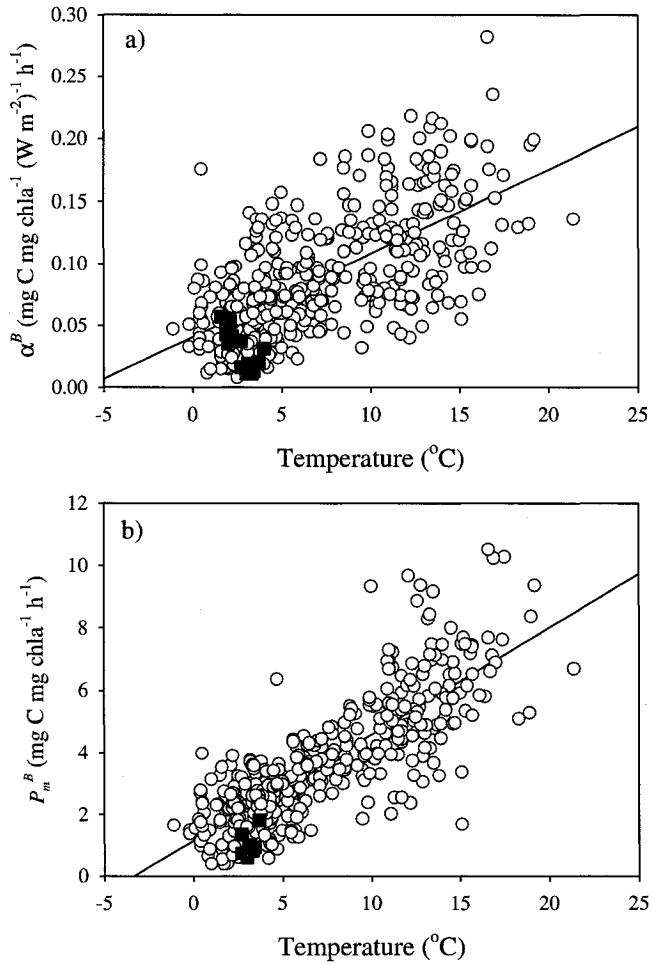

Figure 4.3: The relationship between surface (0 to 20 m) values of photosynthetic parameters (α^B in mg C mg chla^{-1} (W m^{-2})$^{-1}$ h^{-1} and P_m^B in mg C mg chla^{-1} h^{-1}) and corresponding temperature (°C) for 16 cruises on the Scotian Shelf and Labrador sea from 1997 to 2003 (open circles) (Platt *et al.* 2005, Bouman *et al.* 2005). (a) The fit between α^B and temperature, not provided in the original article (Platt *et al.* 2005), is significant and follows the relationship: $\alpha^B = 0.006T + 0.041$; $r^2 = 0.41$; N = 416. (b) The fit between P_m^B and temperature follows the relationship: $P_m^B = 0.034T + 1.15$; $r^2 = 0.66$; N = 416, (Bouman *et al.* 2005). The values measured during the Lagrangian study are superimposed on the previously-mentioned relationships (red squares).

4.2.6 Average of Measured Parameters

In this, the simplest of all the methods, the average parameters from the study area were assigned to all the pixels in the satellite image of the study area for which production is computed.

4.3 Material and Methods

4.3.1 Study Sites

The C-SOLAS Lagrangian study took place during the Spring of 2003 from April 25 to May 02 (D1-D8) on the Northwest Atlantic shelf between 43°N and 44°N, and 57°W and 58.5°W (Fig. 4.4). The same site was sampled again after two weeks (D20). A mooring followed the water mass from D1 to D7, and the phytoplankton in the water mass was dominated by diatoms in declining phase (Pommier *et al.* submitted). Contact with the water mass was lost on D8, when the cable connecting the mooring to the underwater sail was accidentally detached.

4.3.2 Primary Production Measurements

Photosynthesis was measured using two techniques. The first technique, the $P - E$ experiment, required incubating samples in a light-gradient incubator, and carbon assimilation was estimated using ^{14}C uptake (Irwin *et al.* 1990). The photosynthetic parameters were obtained by fitting equation (4.1) to the observations.

Secondly, the simulated *in situ* primary production was measured using the ^{14}C technique described by Pommier *et al.* (submitted). Briefly, the bottles were incubated for 8 to 10 hours on-deck in temperature-controlled chambers, shaded to mimic the light at different depths. Water-column production was then computed from the production P_i in each of the n layers, using equation (3.4)

4.3.3 Computation of Primary Production

Primary production was calculated at the C-SOLAS site using a spectral, non-uniform model (Sathyendranath *et al.* 1989). We used the Ocean Primary Production software (IOCCG website: http://www.ioccg.org/ 2007) with numerical integration forced by

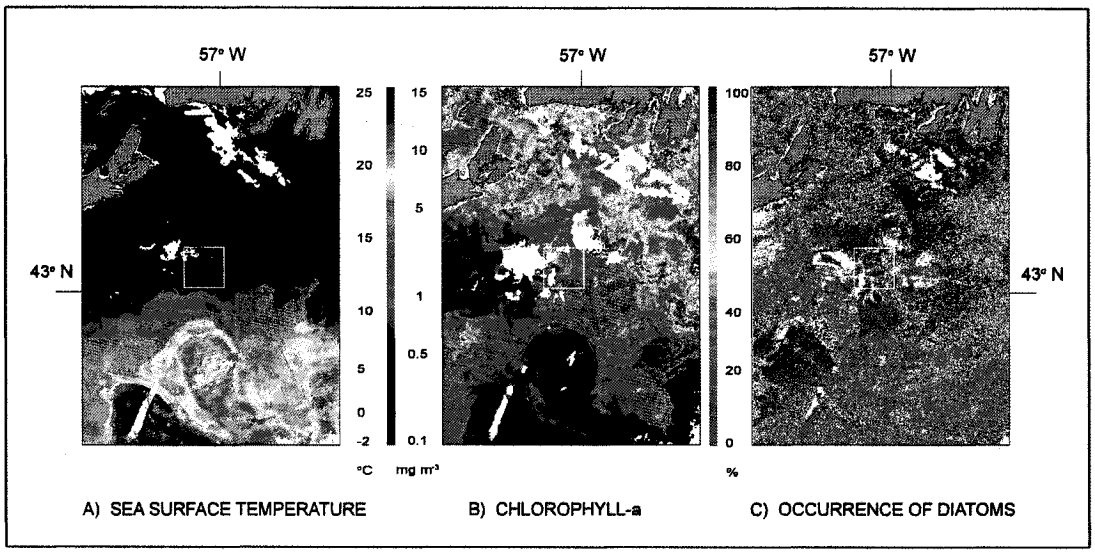

Figure 4.4: Composite image of (a) sea-surface temperature (SST) derived from AVHRR (°C) (b) chlorophyll-a derived from visible spectral radiometry (ocean colour) SeaWiFS, (mg chl-a m^{-3}) and (c) percentage of diatom-dominated pixels during the period of the study (Sathyendranath *et al.* 2004). This figure covers the time period between April 24th and May 2nd, 2003. The upper left corner of the image is 48°N and 62°W, the lower right: 39°N and 53°W. The Lagrangian site corresponds to the white box: lower right corner 43°N, 57°W and upper left corner 44°N, 58.5°W. This figure was provided by Dr. Cesar Fuentes-Yaco.

Bird's (1984) clear-sky spectral irradiance model to estimate light at the sea surface and the relative yellow-substance absorption at 440 nm was set at 30% of the phytoplankton absorption at that wavelength (Sathyendranath *et al.* 2001).

4.3.4 Satellite Application

Chlorophyll-a concentration was estimated from SeaWiFS images using the NASA OC4 version 4.3 algorithm to produce a composite image for the last 2 weeks of April 2003. The photosynthetic parameters were assigned using four different approaches: (1) spatially homogeneous, using the average of measured photosynthetic parameters; (2) spatially homogeneous, using the pair of parameters retrieved from the iteration approach; (3) spatially heterogeneous, using the Nearest-Neighbour Method; and (4) spatially heterogeneous using the temperature model. Results from the different approaches were compared with the independent *in situ* observations from C-SOLAS Lagrangian study.

4.4 Results

4.4.1 C-SOLAS Lagrangian Site

Composite images representing spatial features of SST, chlorophyll-a, and fields of diatom distribution during the Lagrangian study are shown in Fig. 4.4. The oceanographic features observed indicate that the Lagrangian study location was in the North Western Coastal Shelf (NWCS) province (Longhurst 1998). The images show warmer waters (Fig. 4.4a) with low phytoplankton pigment concentrations (Fig. 4.4b) south of the Lagrangian study area, corresponding to the Gulf Stream. Northern regions of NWCS are characterised by cooler and biologically-richer waters. Cold water (around 0 °C) and high pigment concentration ($> 10\,\mathrm{mg\ m^{-3}}$) were found north of 43°N, related to the southern Gulf of St. Lawrence and the Grand Banks of Newfoundland and the Northeastern Scotian Shelf. The diatom population was not homogeneously distributed over the Lagrangian study site, with high occurrences in the North West corner and the eastern portion of the Lagrangian site (Fig. 4.4c). As described from the time-series of satellite images, field measurements covered only the decline of the spring bloom, the peak having occurred in the previous week (Figs. 4.5).

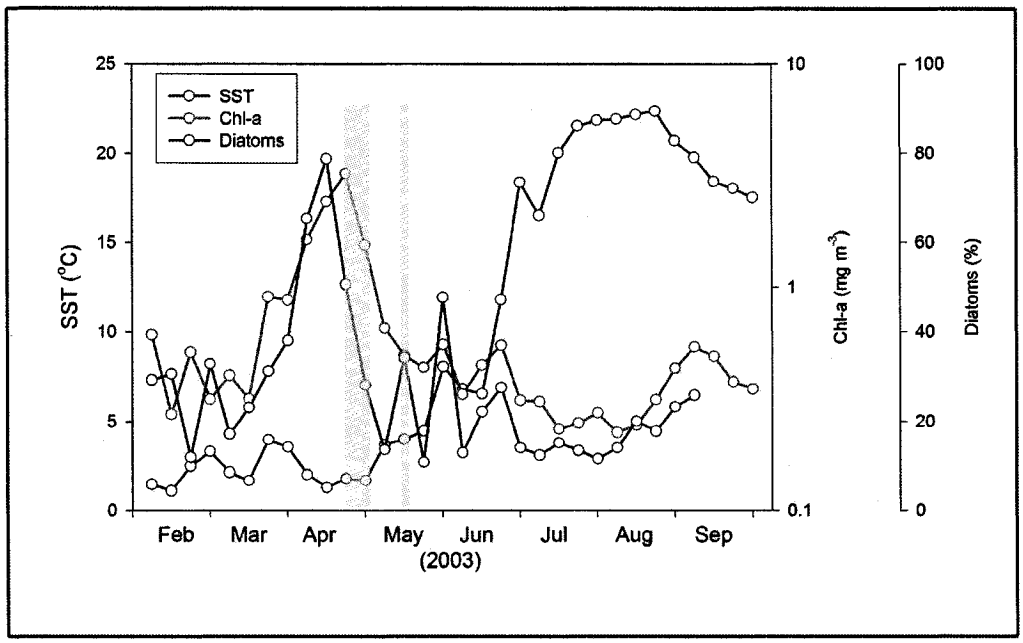

Figure 4.5: Average weekly values of satellite-derived SST (degrees Celsius), chlorophyll-a (mg m^{-3}) and percentage occurrence of diatom-dominated pixels between February and September, 2003 for the Lagrangian study area. The yellow bars indicate periods of in situ measurements: April 24th to May 2nd (D1-D8), and May 13th to 15th (D19-D21). This figure was provided by Dr. Cesar Fuentes-Yaco.

The Lagrangian time series showed a decline in chlorophyll-a concentration from day 1 to day 8 (D1 to D8) (Fig. 4.6a). The production was fairly high at D1 and D2 but decreased by D3 and stays stable for the remaining sampling period (Fig. 4.6b). The water-column production normalised to photic-zone chlorophyll (Λ) presented similar values at D1 and D2 to those at D8 and D20. However, days D3 to D7 showed significantly lower estimates (t test, $p < 0.01$). Based on the magnitude of Λ, three classes have been identified (Fig. 4.6b). We know from taxonomic counts that Class I is composed of diatom bloom samples, Class II of declining diatom samples and Class III of mixed population samples (Pommier *et al.* submitted). Pigment analyses matched the findings from taxonomic analyses (except for D8), with a ratio of fucoxanthin to chlorophyll-a above 0.4 (w w^{-1}) from D1-D8 and a decrease on D20 (Fig. 4.6c). A ratio of fucoxanthin to chlorophyll-a above 0.4 indicates samples dominated by diatom cells (Sathyendranath *et al.* 2004). Also, the chlorophyll-specific absorption by phytoplankton increases over the time period, which is an index of the decrease of the cell size of the phytoplankton community (Fig. 4.6c).

The photosynthetic parameters (Fig. 4.6d) of Classes I and III present higher average values than Class II (Mean $\pm$ standard deviation; Class I: $\alpha^B = 0.024 \pm 0.014$ mg C mg $chla^{-1}$ (W $m^{-2})^{-1}$ h^{-1}; $P_m^B = 1.04 \pm 0.43$ mg C mg $chla^{-1}$ h^{-1}; class III: $\alpha^B = 0.024 \pm 0.0057$ mg C mg $chla^{-1}$ (W $m^{-2})^{-1}$ h^{-1}; $P_m^B = 1.92 \pm 0.17$ mg C mg $chla^{-1}$ h^{-1}; class II $\alpha^B = 0.014 \pm 0.0035$ mg C mg $chla^{-1}$ (W $m^{-2})^{-1}$ h^{-1}; $P_m^B = 0.84 \pm 0.15$ mg C mg $chla^{-1}$ h^{-1}). Platt *et al.* (1992) reported a steady decrease in the photosynthetic parameters in the declining phase of a spring bloom in the Sargasso Sea, consistent with our findings. A positive correlation is found between Λ and P_m^B (r of Pearson = 0.89) with D2 as a probable outlier. However, no significant correlations were found between Λ and α^B, either from surface samples or from the deeper layers ($p > 0.05$ for both relationships). The iterative approach was applied only to Class II samples (declining bloom phase) because this was the only phase with a sufficient number of samples (only two data points for both Class I and III).

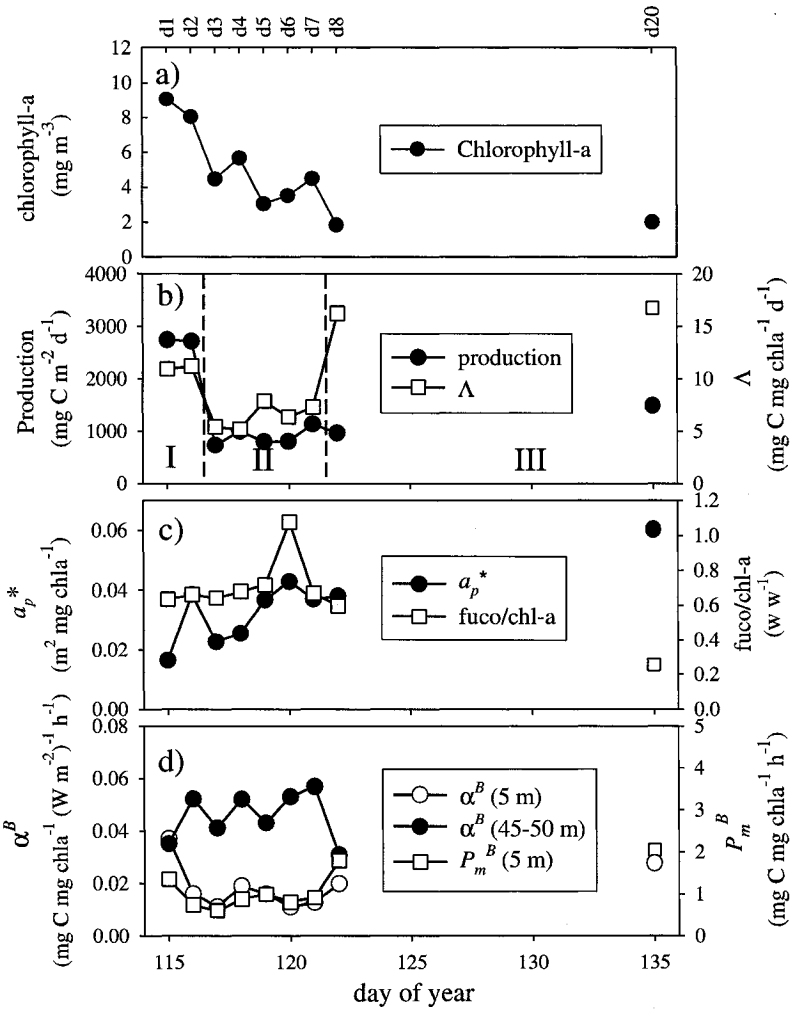

Figure 4.6: Northwest Atlantic shelf time-series April 24, 2003 - May 14, 2003. (a) average chlorophyll-a concentration over the photic depth (b) Daily water-column primary production (filled circles) and the same normalised to the photic zone chlorophyll biomass, Λ (open squares); (c) phytoplankton specific absorption at 440 nm (filled circles) and fucoxanthin: Chlorophyll-a ratio (open squares); (d) photosynthetic parameters α^B (circles) and P_m^B (squares). The time series has been divided into three classes according to Λ as described in Chapter 3.

Table 4.2: Photosynthetic parameter α^B (mg C mg chla^{-1} (W m^{-2})$^{-1}$ h^{-1}) and P_m^B (mg C mg chla^{-1} h^{-1}), $\pm$ standard deviation for the Lagrangian site on the Scotian Shelf (spring 2003) using three different approaches of parameter assignment compared with measured values. Confidence values (p values) associated with a paired t-test between the parameters assigned and the parameters measured using $P-E$ experiments are presented in parenthesis; a value below 0.05 implies that the parameters assigned are significantly different from the parameters measured, (n.s.) indicates a non-significant difference.

$P-E$ parameters	$P-E$ experiments	Nearest-Neighbour Method	Temperature model	Iteration from *in situ* production
P_m^B	1.01 ± 0.39	1.85 ± 0.26 ($p = 0.007$)	1.22 ± 0.02 (n.s.)	1.12 (n.s.)
α^B	0.032 ± 0.017	0.070 ± 0.011 ($p < 0.001$)	0.053 ± 0.003 ($p < 0.001$)	0.016 ($p < 0.001$)

4.4.2 Assignment of Photosynthetic Parameters

Photosynthetic parameters were assigned to the nine stations (D1 - D8 and D20) using three different approaches: the Nearest-Neighbour Method, the temperature-dependent model and the iterative approach, and the mean values of parameters thus obtained compared with means of the measured parameters (Table 4.2). In a previous study (Platt *et al.* submitted) that dealt with estimation of parameters in Spring 2004, good agreement was found between estimates of photosynthetic parameters using the Nearest-Neighbour Method and measured parameters. However, in this study, temperature model on average provided mean values closest to those of both measured parameters (Table 4.2).

Water-column primary production was computed for the nine stations using the three different approaches to assignment of the photosynthetic parameters combined with the measured chlorophyll-a profile parameters (Table 4.3). These estimates were compared with the water-column production measured from simulated *in situ* incubations and with the production calculated using the measured photosynthetic parameters. Owing to the high variability in the magnitude of the *in situ* production, the comparison has been extended on a class-by-class basis (I, II and III) representing the different phases of the diatom bloom (Class I is the blooming phase and Class II

Table 4.3: Comparison of water-column primary production computed with a spectral model using different approaches to assign photosynthetic parameters. The measured chlorophyll profile parameters were used for all assignment methods. Class I corresponds to diatom bloom (D1 and D2), Class II corresponds to decline of diatom bloom (D3-D7), and Class III corresponds to mixed population (D8 and D20). Confidence values (p values) associated with a paired t-test between the production computed from assigned parameters and *in situ* production are presented in parenthesis; a value below 0.05 implies that the estimated production is significantly different from the *in situ* production, (n.s.) indicates a non-significant difference.

	In situ	$P-E$ experiments	Nearest-Neighbour Method	Temperature model	Iteration from *in situ* production
Class I	2621 ± 140	824 ± 253 (p = 0.028)	1385 ± 143 (n.s.)	1099 ± 41 (p = 0.029)	597 ± 28 (p = 0.025)
Class II	548 ± 167	387 ± 90 (n.s.)	894 ± 176 (p = 0.045)	601 ± 130 (n.s.)	337 ± 78 (n.s.)
Class III	819 ± 282	466 ± 67 (n.s.)	712 ± 44 (n.s.)	509 ± 29 (n.s.)	278 ± 19 (n.s.)
average	1069 ± 902	502 ± 217 (p = 0.045)	963 ± 285 (n.s.)	691 ± 253 (n.s.)	381 ± 137 (p = 0.031)

is the declining phase) and the mixed population (Class III). In Class I, the production measured *in situ* was much higher than the mean production calculated using the photosynthetic parameters measured in Class I conditions. It seems that even the measured parameters did not capture the increased productivity of the blooming event. Of all the methods used to compute production, only the Nearest-Neighbour Method returned values that were not significantly different from the measured production. In Class II, the declining-diatom phase, the Nearest-Neighbour Method overestimated the water-column production whereas the other two approaches provided results that were not significantly different from the *in situ* measurements. In Class III, although the production estimated from all the methods was not significantly different from the *in situ* measurements, the Nearest-Neighbour Method provided estimates of water-column production that were closest to the *in situ* measurements.

4.4.3 Satellite Application

Water-column primary production was then computed for the Lagrangian study area from ocean-colour data using four methods for assignment of the parameters (Fig. 4.7). The fourth method corresponds to the use of average values of the measured photosynthetic parameters homogeneously applied over the Lagrangian study area. The four methods of parameter assignment returned similar trends in water-column production over the area, with high production in the northwest corner and in the center of the area. This qualitative consistency between all the maps reflects the pattern of chlorophyll-a concentration estimated from remote sensing of ocean colour. However, great differences in the magnitude of the estimated production were found among the four maps. The production estimated using the mean value of the measured parameters (Fig. 4.7a) or the set of parameters retrieved by iteration from the *in situ* production of Class II (Fig. 4.7b) gave maximum values of about 800 mg C m^{-2} d^{-1}, whereas the temperature-dependent model returned a maximum of about 1200 mg C m^{-2} d^{-1} (Fig. 4.7c) and the Nearest-Neighbour Method estimated a maximum of 2,000 mg C m^{-2} d^{-1} (Fig. 4.7d). When averaged over the entire region (Table 4.4), the water-column production estimated using the Nearest-Neighbour Method produced values closest to the mean value of production measured *in situ* whereas all the other approaches underestimated the production. However, when normalised to the water-column chlorophyll-a, estimated using the OC4 algorithm from ocean colour data combined over a two-week period (Table 4.4), the Nearest-Neighbour Method returned greatly overestimated the daily water-column production normalised to the photic zone chlorophyll (Λ) compared with the *in situ* measurements, whereas the iterative approach underestimated Λ for the studied area. The estimates made using the measured parameters and the temperature models both agreed well with the *in situ* production. This discrepancy between the estimates of Λ from the Nearest-Neighbour Method and the *in situ* measurements could be due to the higher resolution of the remote-sensing approach, which returned results from about 4500 pixels compared with the nine experiments of *in situ* incubation, as discussed in Joint *et al.* 2002 and in Platt *et al.* (submitted).

However, the discrepancy could also be due to the overestimation of the photosynthetic parameters in the declining phase of the diatom bloom (see Table 4.2

Table 4.4: Comparison of total water-column primary production and of water-column primary production normalised to water-column chlorophyll-a concentration using only the pixels common to all methods of assignment. The comparison is made between *in situ* measurements and corresponding values computed from satellite images of ocean colour using different approaches to assign photosynthetic parameters. Chlorophyll-a profile parameters were assigned to each pixel using the Nearest-Neighbour Method (Platt *et al.* submitted). Confidence values (p values) associated with a t-test on samples with unequal variances between the production computed from assigned parameters and *in situ* production are presented in parenthesis; a value below 0.05 implies that the estimated production is significantly different from the *in situ* production, (n.s.) indicates a non-significant difference.

Method of assignment	Production	P_{ZT}/B_Z
In situ	1076 ± 964	4.58 ± 2.43
$P - E$ experiments	593 ± 109 (n.s.)	3.58 ± 0.72 (n.s.)
Nearest-Neighbour	1260 ± 334 (n.s.)	7.68 ± 2.39 ($p = 0.015$)
Temperature model	802 ± 130 (n.s.)	4.90 ± 1.24 (n.s.)
Iteration from in situ production	454 ± 84 (n.s.)	2.74 ± 0.58 ($p = 0.032$)
Nearest-Neighbour + $P - E$ experiments	994 ± 491 (n.s.)	5.85 ± 2.82 (n.s.)
Nearest-Neighbour + iteration	944 ± 542 (n.s.)	5.52 ± 3.13 (n.s.)

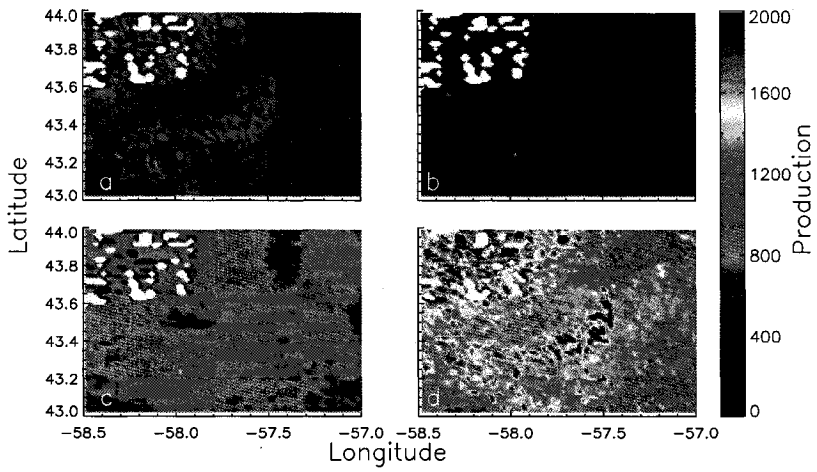

Figure 4.7: Water-column primary production (mg C m^{-2} d^{-1}) map from satellite images of ocean colour using four different approaches to assign photosynthetic parameters: (a) spatially-homogeneous, using the average of measured photosynthetic parameters; (b) spatially-homogeneous, using the pair of parameters retrieved by the iteration approach; (c) spatially-heterogeneous, using the temperature model; and (d) spatially-heterogeneous, using the Nearest-Neighbour Method.

and 4.3). To test this hypothesis, an intelligent (conditional branching) algorithm has been developed. In this algorithm, pixels were assigned to one of three possible classes using a combination of the diatom identification algorithm (Sathyendranath *et al.* 2004) and the rate of change in the remotely-sensed chlorophyll-a concentration over the two-week period (Fig. 4.8a). Class I pixels were identified as those with a probability of occurrence of diatoms over 25% and a stable or increasing chlorophyll-a concentration. Class II pixels were identified as those with a probability of occurrence of diatoms over 25% and a decreasing chlorophyll-a concentration (chlorophyll-a concentration in the second week was less than 75% of chlorophyll-a concentration of the first week of the study period), and Class III pixels were identified as those pixels where the probability of occurrence of diatoms was 25% or less. Partitioning the data into two separate weeks to assess the derivative in chlorophyll-a concentration resulted in an increase in pixels with no data due to cloud cover over the studied area. Water-column production was computed using the Nearest-Neighbour Method for Class I and Class III pixels and using either the measured parameters (Fig. 4.8b) or the parameters retrieved from the iterative approach for Class II pixels (Fig. 4.8c). The partitioning of the studied area returned a production map that is not as smooth as the maps previously produced. However, when averaged over the studied area, the magnitude of water-column production normalised to the water-column chlorophyll-a (Λ) compared well with the measurements from the *in situ* incubations (Table 4.4).

4.5 Discussion

Primary production can be calculated using many different approaches, and ultimately applied to satellite images of ocean colour to obtain synoptic fields of production in the global ocean (Longhurst *et al.* 1995, Antoine *et al.* 1996, Behrenfeld and Falkowski 1997). But to compute primary production, one needs to assign photosynthetic parameters, using either continuous or step-wise approaches (Platt and Sathyendranath 1999). The ocean can be divided in a suite of biogeochemical provinces, each with its own specific physical and biogeochemical properties, which could each be assigned sets of photosynthetic parameters specific for each season, as

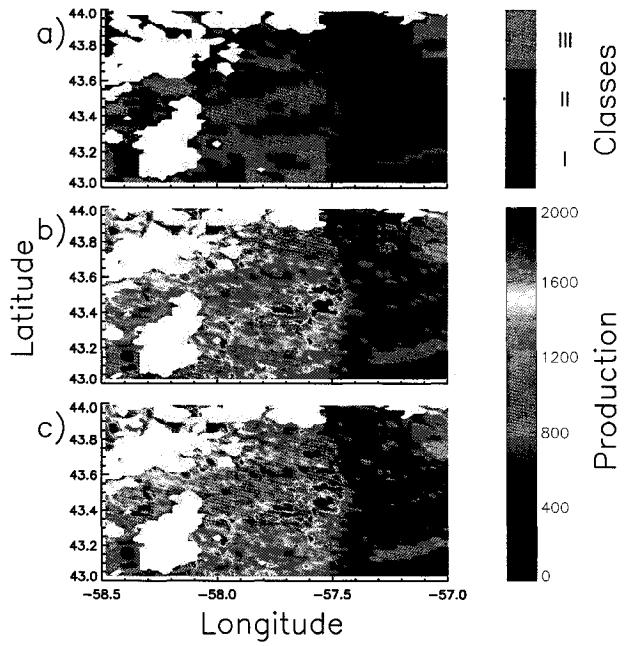

Figure 4.8: (a) Classification of the pixels according to the physiological state and the community structure of the phytoplankton population. Class I (blue) represents diatom blooming conditions, Class II (red) represents diatom declining conditions and Class III (green) represents mixed population conditions; (b) Water-column primary production (mg C m^{-2} d^{-1}) calculated using the Nearest-Neighbour Method for pixels identified as Classes I and III and using average photosynthesis-irradiance parameters for pixels identified as Class II; (c) Water-column primary production (mg C m^{-2} d^{-1}) calculated using the Nearest-Neighbour Method for pixels identified as Classes I and III and using the photosynthetic parameters retrieved using the iterative approach for pixels identified as Class II.

done by Longhurst *et al.* (1995) in the first estimate of global marine primary production by remote sensing. Obviously, this will introduce discontinuities at the boundaries of the provinces. This problem has been addressed in the Nearest-Neighbour Method (Platt *et al.* submitted), which assigns a set of photosynthetic parameters to a specific pixel by matching the values of biomass and temperature to those from a database using differences in the date of sampling and the date of the satellite image in a weighting function to calculate the parameter for each pixel. This approach has the advantage of providing values of photosynthetic parameters on a pixel-by-pixel basis and is used on archived data for the studied area. In other cases (Antoine *et al.* 1996, Behrenfeld and Falkowski 1997) photosynthetic parameters have been assigned from temperature-dependent models. Although using temperature as a proxy for phytoplankton metabolism has the advantage of providing photosynthetic parameters on a pixel-by pixel basis, for some biogeochemical provinces, using temperature to capture the variability in phytoplankton metabolism can be inappropriate, as shown by Bouman *et al.* (2005) for the Arabian Sea, where P_m^B was related only weakly to temperature. In the laboratory we expect to find an increase in cell metabolism with an increase in temperature (Eppley 1972). However, in the ocean, an increase in temperature is often associated with an increase in the stratification of the water column, which limits access to nutrients. These opposing effects of temperature, which can occur in different regions of the globe, are a strong limitation to modeling phytoplankton metabolism as a function of temperature (Behrenfeld *et al.* 2002). A second disadvantage of using temperature as a proxy for photosynthetic parameters is that, as for the Nearest-Neighbour Method, considerable data are needed to describe the variability in the metabolic data, posing a major problem in some parts of the world, especially in the southern hemisphere, where data on photosynthetic parameters are scarce, sometimes even non-existent. Here, we explore some of the possible approaches to assign photosynthetic parameters to estimate primary production from remote sensing of ocean colour.

The Lagrangian study on the Northwest Atlantic shelf captured a dynamic phytoplankton community. The sampling took place at the end of a major spring bloom (Figs. 4.5), so the productivity (as represented by Λ and photosynthetic parameters) was decreasing over the nutrient-limited terminal-phase of the bloom (Pommier *et*

al. submitted) as has been observed in the decline of other blooms (e.g. Platt *et al.* 1992). The physiological state of the phytoplankton populations evolved with time and the species composition of the community changed in time and space, being diatom-dominated during the Lagrangian Study and small-cell dominated on D8 and D20 (Figs. 4.4c and 4.6c; see also Pommier *et al.* submitted). Three classes of phytoplankton populations were distinguished: Class I the diatom bloom; Class II the declining diatom phase; and Class III consisting of small-cell dominated community. The species composition was observed by microscopic analyses (Pommier *et al.* submitted), by pigment analyses (Fig. 4.6c), as well as from satellite imagery (Fig. 4.4c). Not only was this system temporally dynamic, and spatially variable, but the seasonal progression proceeded at different rates, and with different phases, at different parts of the area. The composite images captured the spatial variation, whereas the temporal variability was averaged over a two-week period. Since the biomass was highly variable in the study area over the two-weeks study period, comparison between *in situ* and satellite-derived production should use the chlorophyll-a normalised production Λ (Table 4.4).

4.5.1 Iterative Approach

The iterative approach is not an assignment method of the photosynthetic parameters but rather a method to estimate photosynthetic parameters from *in situ* incubations (Forget *et al.* 2007, Chapter 3). We used this approach to validate the estimates of photosynthetic parameters, noting that parameters so retrieved could eventually be added to a database to enhance the Nearest-Neighbour Method or a temperature-dependent model. In this study, the iterative approach could be applied only to stations identified as Class II, the declining bloom phase, for which the number of *in situ* observations was sufficient. Thus the estimates of the parameters should not be considered representative of the other Classes, where the iterative approach strongly underestimates production compared with *in situ* measurements (Tables 4.3 and 4.4). However, when applied to Class II production (Table 4.3) the estimates compared well with results of both *in situ* measurements and computations from measured photosynthetic parameters.

4.5.2 Temperature-Dependent Model

It has been shown that P_m^B is related to temperature (Platt *et al.* 2005, Bouman *et al.* 2005), and α^B mainly to light history (Platt and Jassby 1976). For study of an entire ecosystem, temperature is an appropriate influence on productivity, but light history is more complex to interpret. Because we are not studying discrete water samples from specific depths, but the entire water column over a wide range of incident irradiance, light history cannot be treated in the same way as physical factors such as temperature. As reported by Platt and Jassby (1976) and Behrenfeld *et al.* (2004), the two photosynthetic parameters are found to be correlated in many aquatic systems. Thus, temperature probably could be a good indicator of α^B in large-scale studies (Fig. 4.3a). As temperature increases, there is a change in community structure, from larger cells in nutrient-rich cold waters to smaller cells in stratified warm waters. The photosynthetic parameter α^B is inversely dependent on light absorption. It is well accepted that decreasing the size of phytoplankton cells reduces the packaging effect, which returns higher specific absorption. Thus, if quantum yield were constant within phytoplankton groups, we would expect an increase in α^B when phytoplankton cell size is decreased. As shown by Platt *et al.* (2005), α^B is positively related to the specific absorption a^* at 676 nm, which increases inversely with cell size, and is negatively correlated to the proportion of micro-phytoplankton in the community. Thus, as the phytoplankton size class changes, both photosynthetic parameters, increase with a decrease in cell size (Platt *et al.* 2005).

On average, we found good agreement between the parameters estimated from the temperature model and parameters measured from the $P-E$ experiments (Table 4.2). The computed and measured water-column production compared well for Class II and Class III stations, but underestimated production, compared with simulated *in situ* measurements, for Class I stations. However, for average chlorophyll-a-normalised production over the studied area, the temperature model produced a mean value in good agreement with the mean value of the *in situ* incubation and with the production computed from measured parameters. The relationship developed by Platt *et al.* (2005) and Bouman *et al.* (2005) performed well for observations from the Northwest Atlantic. However, as stressed by Behrenfeld *et al.* (2002) and Bouman *et al.* (2005),

temperature-dependent models for photosynthetic capacity should be used with caution, and only in areas where the appropriate relationships have been established.

4.5.3 Nearest-Neighbour Method

The Nearest-Neighbour Method is not subject to the same limitation as a temperature model and thus is applicable to all regions where enough data on photosynthetic parameters, temperature and chlorophyll-a concentration is available (Platt and Sathyendranath 2002, Platt *et al.* submitted). The database used for this study covered the North Atlantic and included about 1500 entries. However, photosynthetic parameter data are scarce in certain parts of the globe (Longhurst *et al.* 1995). More photosynthesis-irradiance experiments should be performed in these regions to enhance the global database. Another option to augment the global database is to use *in situ* production experiments to retrieve photosynthetic parameters (Forget *et al.* 2007), since many *in situ* production data are available at the global scale (for example, from JGOFS studies).

The Nearest-Neighbour Method provided good estimates of the water-column production for mixed-population conditions (Class III) and in diatom blooming conditions (Class I). However, for the declining phase of the diatom bloom (Class II), water-column production was strongly overestimated (Table 4.3). As noted previously, the declining phase of a phytoplankton bloom shows lower photosynthetic capacity than during the blooming phase (Platt *et al.* 1992). The database represents the general trend of the physiological state of the phytoplankton community. The declining phase of a diatom population lasted for a period of only two weeks over the course of the year (Figs. 4.5). Thus, the database is not suitable for this specific short-term condition. Dividing database of photosynthetic parameters according to the physiological status and community structure of the phytoplankton would solve this problem. Use of a diatom-identification algorithm (Sathyendranath *et al.* 2004) supplemented by a temporal derivation of chlorophyll-a concentration provides a tool to map the different phases of the diatom bloom (blooming vs. declining) and the mixed phytoplankton population (Fig. 4.8). From this analysis, we found a substantial number of pixels classified as declining diatom conditions (Class II, red pixels in Fig. 4.8a). Averaging the estimates of primary production using a combination of

the Nearest-Neighbour Method for blooming (Class I) and mixed populations (Class III) conditions, and either the measured photosynthetic parameters (Fig. 4.8b) or the parameters retrieved from the iterative approach (Fig. 4.8c) provided estimates falling within the standard deviation of the *in situ* measurements (Table 4.4).

4.5.4 Remote-Sensing Applications

Over the past decade, there has been an increased interest in the partition of the marine microflora into phytoplankton functional types (PFTs) for modelling the carbon cycle (Le Quéré *et al.* 2005). Each PFT potentially presents a different photosynthesis response to available light. They also differ in pigment composition and packaging effect, and thus in their optical properties (Nair *et al.* submitted). These optical properties can be tracked by remote sensing of ocean colour using algorithms tuned to identify particular PFTs such as diatoms (Sathyendranath *et al.* 2004), *Trichodesmium* (Subramaniam *et al.* 1999) and other phytoplankton groups (Alvain *et al.* 2005). Using such algorithms, along with the time derivative of the chlorophyll-a concentration, one could partition the global ocean according to the dominant PFT and according to the occurrence of blooming or declining-bloom conditions. Provided that a database of photosynthetic parameters were available for each of these conditions and for the various PFTs, one could improve modelling of primary production at the global scale using the Nearest-Neighbour Method (Platt *et al.* submitted) to assign the photosynthetic and chlorophyll-a profile parameters. The future would seem to lie in the development of intelligent (conditional branching) algorithms for this purpose, along the lines of the first steps described here.

Chapter 5

CONCLUSION

There has been substantial progress during the last few decades in primary production modelling, including applications of remotely-sensed data on ocean colour (see review of Joint and Groom 2000). The development of photosynthesis-light models (Platt and Jassby 1976, Sathyendranath *et al.* 1989), the quantification of chlorophyll concentration from satellite imagery (CZCS) in the late seventies and the launch of many sensors in the most recent decades, and finally the development of methods to assign the parameters, such as the Nearest Neighbour Method (Platt *et al.* submitted) have all led to the progress. The field is now at the level that allows operational computation of primary production, at regional and global scales (Platt *et al.* submitted). In estimating primary production, one of the main problems resides in the estimation of chlorophyll-a concentration from global algorithms, which has uncertainties of the order of 35% (Hooker and McClain 2000). Global algorithms cannot capture regional variability, so further progress needs the development of regional algorithms to account for variation, at the appropriate scale, of different phytoplankton types. Another main limitation in computing primary production is the scarcity (or absence at some seasons) of photosynthetic parameters, in many biogeochemical provinces. Any of the assignment procedures requires extensive databases, either to develop and test empirical relationships, or to implement the Nearest-Neighbour Methods.

In this thesis I have reviewed the different approaches that have been proposed to assign photosynthetic parameters, and illustrated them by computing primary production in two quite different marine ecosystems: the tropical Caribbean and the North West Atlantic following the spring phytoplankton bloom.

A research cruise in April and May 2006 assessed the marine ecosystem in eastern Caribbean waters. The phytoplankton portion of the study was mainly to describe the community structure and quantify primary production from satellite imagery. The community structure, assessed by analysis of pigment data (High Performance Liquid

Chromatography, HPLC) and phytoplankton absorption spectra, showed a dominance of pico-phytoplankton and an increase in nano-phytoplankton at the deep chlorophyll maximum. For computation of primary production, data on biomass profiles and on photosynthesis-irradiance ($P - E$) parameters were obtained during the cruise. Monthly composites of chlorophyll-a concentration were produced using data from the MODIS satellite sensor for 2006. Based on the chlorophyll concentration, three regions were distinguished in the study area: coastal, and open ocean north and south. After sensitivity analyses on the possible approaches to assignment of the parameters, two methods (a regional approach and the Nearest-Neighbour Method) were selected for computation of primary production. Monthly images of primary production were then produced from remote sensing of ocean colour over the annual cycle for 2006.

At the C-SOLAS Lagrangian Study site in the North West Atlantic, the phytoplankton community was dominated by diatoms in declining-bloom conditions, characterised by decreasing primary production. Photosynthesis was measured using both photosynthesis-light experiments and simulated *in situ* incubations. Several methods were used to assign photosynthetic parameters for estimation of primary production from remote sensing of ocean colour: the Nearest-Neighbour Method, a temperature-dependent model and an iterative approach to retrieve photosynthetic parameters from *in situ* measurements of phytoplankton production. Owing to the decline and patchyness of the diatom population, the primary production measured from *in situ* incubations was highly variable. In blooming conditions, all methods underestimated production relative to simulated *in situ* measurements; however, the Nearest-Neighbour Method estimates were closest to the *in situ* measurements. In the declining bloom phase, the Nearest-Neighbour Method overestimated primary production, whereas the iterative method estimates were in good agreement with the *in situ* observations. In conditions of mixed-phytoplankton populations, the Nearest-Neighbour Method estimates agreed with the observations. Based on these results, a new method was proposed to classify the image pixels using remote sensing, according to the phase of the diatom bloom (blooming *vs.* declining conditions) and community structure (diatom *vs.* mixed population). Primary production was recomputed, partitioning the *in situ* data base into two pools, one representing the

general phytoplankton community and one representing the declining diatom conditions. The resulting estimates of chlorophyll-a normalised water-column production were in good agreement with the *in situ* observations.

For both the tropical Caribbean and the temperate North-West Atlantic, the Nearest-Neighbour Method for assignment of the photosynthetic parameters to compute primary production gave the best results according to RMS errors. Although the database for assigning parameters for the Caribbean waters comprised only about 50 entries, compared with about 1500 for the North Atlantic, a lower root mean squared (RMS) error was found for former Caribbean (RMS error = 27%, NW Atlantic RMS error = 52%). This is due mainly to the very stable conditions in the tropical system.

All the methods available for assignment of photosynthetic parameters in calculation of primary production from remote sensing of ocean colour have significant limitations, principally from a paucity of direct measurements of the photosynthetic parameters for protocol development. As a way to mitigate the lack of data, I have introduced a new method, to extract the parameters from *in situ* data on primary production, for which a substantial archive already exists. The method has sound theoretical basis, has been tested on data from a variety of aquatic regimes and verified with a completely independent data set.

For photosynthetic parameters, the chlorophyll-a profile parameters assigned to each pixel are a source of uncertainties which needs to be addressed. However, chlorophyll-a concentration is more often measured and profile parameters are usually more abundant than photosynthetic parameters although the Southern Ocean remains greatly under-sampled (Uitz *et al.* 2006). Morel and Berthon (1989) and more recently Uitz *et al.* (2006) assigned profile parameters based on surface chlorophyll concentration. Both studies found generally good agreement between the estimated and measured water-column chlorophyll-a concentration, although the validation with the profile parameters was lacking excepted for z_m, which showed poor accuracy of the estimated values. Extrapolation of this empirical approach to regions where measurements are unavailable could give biased estimates of chlorophyll-a concentration in those regions. Another approach is the Nearest-Neighbour Method (Platt *et al.* submitted, Chapter 4), which assigned profile parameters in good agreement with measured ones for a North Atlantic cruise.

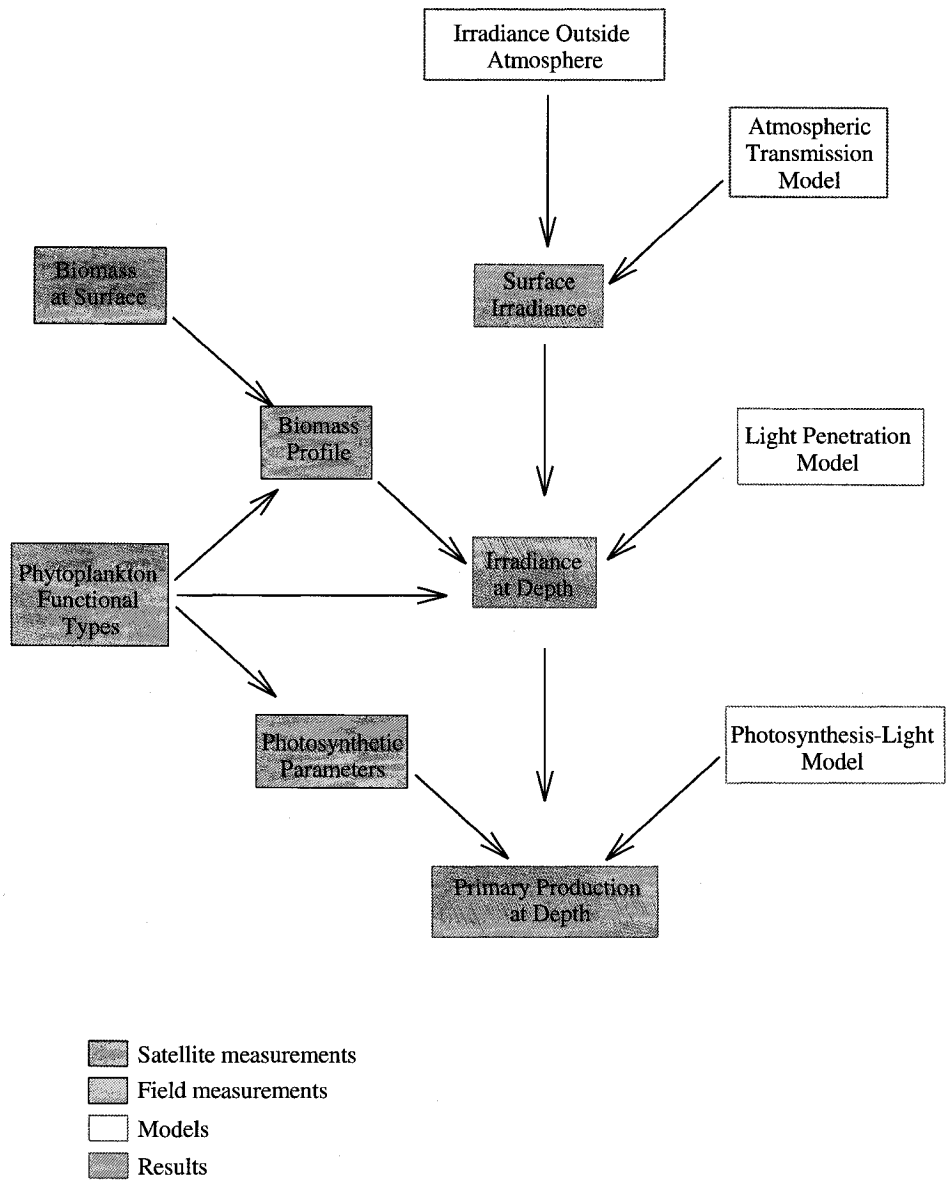

Figure 5.1: Flow chart showing the six steps required to compute primary production from remote sensing of ocean colour. The impact of phytoplankton functional types on computation of primary production have been added. Modified from Platt and Sathyendranath 1997

In the introduction, I presented the many steps required to compute primary production from remote sensing of ocean colour (Figs. 1.1 and 5.1) where the models (Fig. 5.1 in yellow) require inputs from field measurements (Fig. 5.1 in red) and from satellite imagery (Fig. 5.1 in blue). However, as noted in Chapter 4, phytoplankton functional types (PFTs) and their physiological status impact the photosynthetic parameters. Different PFTs also have a different vertical distribution: for example, diatoms are most likely to be well mixed in the water column, whereas picophytoplankton are usually stratified in oligotrophic waters. Moreover, the variation in the absorption spectra from pigment composition of different phytoplankton functional types is known to impact the light field in the water column (Sathyendranath and Platt 2007). Different approaches have been proposed to identify and map PFTs from remote sensing of ocean colour (Subramaniam *et al.* 1999, Sathyendranath *et al.* 2004, Alvain *et al.* 2005), all relying on the absorption spectra of the different phytoplankton types. The introduction of hyperspectral sensors such as HERO (Hyperspectral Environment and Resource Observers) planned to be launched by the Canadian Space Agency in the next few years, will allow the refinement of the existing algorithms and the development of new algorithms to identify other phytoplankton types.

Another approach to assigning photosynthetic parameters that remains to be explored is the use of solar-induced fluorescence and its potential relationship with the quantum yield of photosynthesis. When a chlorophyll-a molecule absorbs a photon, only three de-excitation pathways are possible for its return to ground level: photosynthesis, heat emission and fluorescence (Butler and Strasser 1977, Butler 1978). Thus, assuming a stable quantum yield of heat emission, the quantum yield of photosynthesis and fluorescence should be inversely related (Topliss and Platt 1986). Quantum yield of fluorescence can be tracked from remote sensing of ocean colour (Huot *et al.* 2005), using MODIS or MERIS sensors. Therefore, a relationship between the quantum yield of fluorescence and photosynthesis would provide a means to assign α^B on synoptic fields, offering a further refinement to the estimation of primary production in the operational mode.

Bibliography

Alvain, S., Moulin, C., Dandonneau, Y., & Bréon, F. M. (2005). Remote sensing of phytoplankton groups in case 1 waters from global SeaWiFS imagery. *Deep-Sea Research I, 52*, 1989–2004.

Antoine, D., André, J. M., & Morel, A. (1996). Oceanic primary production 2. Estimation at global scale from satellite (coastal zone color scanner) chlorophyll. *Global Biogeochemical Cycles, 10*(1), 57–69.

Antoine, D. & Morel, A. (1996). Oceanic primary production 1. Adaptation of a spectral light-photosynthesis model in view of application to satellite chlorophyll observations. *Global Biogeochemical Cycles, 10*(1), 43–55.

Babin, M., Morel, A., & Gentili, B. (1996). Remote sensing of sea surface sun-induced chlorophyll fluorescence: consequences of natural variations in the optical characteristics of phytoplankton and the quantum yield of chlorophyll *a* fluorescence. *International Journal of Remote Sensing, 17*(12), 2417–2448.

Babin, M., Therriault, J. C., Legendre, L., Nieke, B., Reuter, R., & Condal, A. (1995). Relationship between the maximum quantum yield of carbon fixation and the minimum quantum yield of chlorophyll *a in vivo* fluorescence in the Gulf of St. Lawrence. *Limnology and Oceanography, 40*(5), 956–968.

Balch, W., Evans, R., Brown, J., Feldman, G., McClain, C., & Esaias, W. (1992). The remote sensing of ocean primary productivity: Use of a new data compilation to test satellite algorithms. *Journal of Geophysical Research, 97*(C2), 2279–2293.

Behrenfeld, M. J. & Falkowski, P. G. (1997). Photosynthetic rates derived from satellite-based chlorophyll concentration. *Limnology and Oceanography, 42*(1), 1–20.

Behrenfeld, M. J., Marañón, E., Siegel, D. A., & Hooker, S. B. (2002). Photoacclimation and nutrient-based model of light-saturated photosynthesis for quantifying oceanic primary production. *Marine Ecology Progress Series, 228*, 103–117.

Behrenfeld, M. J., Prasil, O., Babin, M., & Bruyant, F. (2004). In search of a physiological basis for covariations in light-limited and light-saturated photosynthesis. *Journal of Phycology, 40*(1), 4–25.

Behrenfeld, M. J., Randerson, J. T., McClain, C. R., Feldman, G. C., Los, S. O., Tucker, C. J., Falkowski, P. G., Field, C. B., Frouin, R., Esaias, W. E., Kolber, D. D., & Pollack, N. H. (2001). Biospheric primary production during an ENSO transition. *Science, 291*, 2594–2597.

Bird, R. E. (1984). A simple, solar spectral model for direct-normal and diffuse horizontal irradiance. *Solar Energy, 32*, 461–471.

Bouman, H., Platt, T., Kraay, G. W., Sathyendranath, S., & Irwin, B. D. (2000). Bio-optical properties of the subtropical North Atlantic. I. Vertical variability. *Marine Ecology Progress Series, 2000*, 3–18.

Bouman, H., Platt, T., Sathyendranath, S., & Stuart, V. (2005). Dependence of light-saturated photosynthesis on temperature and community structure. *Deep-Sea Research I, 52*, 1284–1299.

Bundi, A. (2004) Mass balance models of the eastern Scotian Shelf before and after the cod collapse and other ecosystem changes. *Canadian Technical Report of Fiahesries and Aquatic Sciences, 2520*, xii+193pp.

Butler, W. L. (1978). Energy distribution in the photochemical apparatus of photosynthesis. *Annual Review of Plant Physiology, 29*, 345–378.

Butler, W. L. & Strasser, R. J. (1977). Tripartite model for the photoshemincal apparatus of green plant photosynthesis. *Proceedings of the Naional Academy of Sciences of the United States of America, 74*, 3382–3385.

Campbell, J., Antoine, D., Armstrong, R., Arrigo, K., Balch, W., Barber, R., Behrenfeld, M., Bidigare, R., Bishop, J., Carr, M. E., Esaias, W., Falkowski, P., Hoepffner, N., Iverson, R., Kiefer, D., Lohrenz, S., Marra, J., Morel, A., Ryan, J., Vedernikov, V., Waters, K., Yentsch, C., & Yoder, J. (2002). Comparison of algorithms for estimating ocean primary production from surface chlorophyll, temperature, and irradiance. *Global Biogeochemical Cycles, 16*(3).

Carignan, R., Blais, A. M., & Vis, C. (1998). Measurement of primary production and community respiration in oligotrophic lakes using the Winkler method. *Canadian Journal of Fisheries and Aquatic Sciences, 55*(5), 1078–1084.

Carignan, R., Planas, D., & Vis, C. (2000). Planktonic production and respiration in oligotrophic Shield lakes. *Limnology and Oceanography, 45*(1), 189–199.

Chisholm, S. W., Olson, R. J., Zettler, E. R., Goericke, R., Waterbury, J. B., & Welschmeyer, N. A. (1988). A novel free-living prochlorophyte abundant in the oceanic euphotic zone. *Nature, 334*(6180), 340–343.

Ciotti, A. M., Lewis, M. R., & Cullen, J. J. (2002). Assessment of the relationships between dominant cell size in natural phytoplankton communities and the spectral shape of the absorption coefficient. *Limnology and Oceanography*, (47).

Claustre, H. (1994). The trophic status of various oceanic provinces as revealed by phytoplankton pigment signatures. *Limnology and Oceanography, 39*(5), 1206–1210.

Claustre, H., Kerhervé, P., Marty, J. C., & Prieur, L. (1994). Phytoplankton photoadaptation related to some frontal physical processes. *Journal of Marine Systems*, *5*, 251–265.

Claustre, H. & Marty, J. C. (1995). Specific phytoplankton biomasses and their relation to primary production in the tropical North Atlantic. *Deep-Sea Research I*, *42*, 1475–1493.

Coté, B. & Platt, T. (1983). Day-to-day variations in the spring-summer photosynthetic parameters of coastal marine phytoplankton. *Limnology and Oceanography*, *28*(2), 320–344.

Coté, B. & Platt, T. (1984). Utility of the light-saturation curve as an operational model for quantifying the effects of environmental conditions on phytoplankton photosynthesis. *Marine Ecology Progress Series*, *18*, 57–66.

Cramer, W., Bondeau, A., Woodward, F. I., Prentice, I. C., Betts, R. A., Brovkin, V., Cox, P. M., Fisher, V., Foley, J. A., Friend, A. D., Kucharik, C., Lomas, M. R., Ramankutty, N., Sitch, S., Smith, B., White, A., & Young-Molling, C. (2001). Global response of terrestrial ecosystem structure and function to CO_2 and climate change: results from six dynamic global vegetation models. *Global Change Biology*, *7*(4), 357–373.

Del Giorgio, P. A. & Peters, R. H. (1994). Patterns in planktonic P-R ratios in lakes - Influence of lake trophy and dissolved organic carbon. *Limnology and Oceanography*, *39*(4), 772–787.

Devred, E., Fuentes-Yaco, C., Sathyendranath, S., Caverhill, C., Maass, H., Stuart, V., & Platt, T. (2005). A semi-analytic, seasonal algorithm to retrieve chlorophyll-a concentration in the North West Atlantic from seawifs data. *Indian Journal of Marine Sciences*, *34*, 356–367.

Doerffer, R. (1993). Estimation of primary production by observation of solar-stimulated fluorescence. In W. K. W. Li & S. Y. Maestrini (Eds.), *Measurement of Primary Production from the Molecular to the Global Scale*, volume 197 (pp. 104–113). Copenhagen: International Council for the Exploration of the Sea.

Duysens, L. N. M. (1956). The flattening of the absorption spectrum of suspensions, as compared to that of solutions. *Biochimica et Biophysica Acta*, *19*, 1–12.

Eppley, R. W. (1972). Temperature and phytoplankton growth in the sea. *Fishery Bulletin*, *70*(4), 1063–1085.

Falkowski, P. G. (1981). Light-shade adaptation and assimilation numbers. *Journal of Plankton Research*, *3*(2), 203–216.

Fee, E. J. (1990). Computer programs for calculating *in situ* phytoplankton photosynthesis. *Canadian technical report of fisheries and aquatic sciences*, *1740*, 1–27.

Food and Agriculture Organization of the United Nation (F.A.O.) (1999) Report of the Twenty-third Session of the Committee on Fisheries. *FAO Fisheries Report 595* 70p.

Food and Agriculture Organization of the United Nation (F.A.O.) (2006)a Scientif basis for ecosystem-masked management in the lesser antilles including interactions with marine mammals and other top predator: cruise report for the LAPE ecosystem survey on RV Celtic Explorer (CE0607). *FAO Field document 5* viii+99p.

Food and Agriculture Organization of the United Nation (F.A.O.) (2006)b Scientif basis for ecosystem-masked management in the lesser antilles including interactions with marine mammals and other top predator: Report of the first meeting of the ecosystem modelling working group. *FAO Field document 4* x+48p.

Forget, M.-H. (2001). *La variation journalière et saisonnière de la respiration planctonique et des paramètres photosynthétiques dans différents milieux aquatiques.* Masters thesis, University of Montreal.

Forget, M.-H., Fuentes-Yaco, C., Sathyendranath, S., Platt, T., Pommier, J., & Devred, E. (in press). Computation of primary production from remote sensing of ocean colour at the lagrangian site of C-SOLAS. *Marine Ecology Progress Series.*

Forget, M.-H., Sathyendranath, S., Platt, T., Pommier, J., Vis, C., Kyewalyanga, M., & Hudon, C. (2007). Extraction of photosynthesis-irradiance parameters from phytoplankton production data: Demonstration in various aquatic systems. *Journal of Plankton Research, 29*(3) 249–262.

Fuentes-Yaco, C., Devred, E., Sathyendranath, S., Platt, T., Payzant, L., Caverhill, C., Porter, C., Maass, H., & White, G. N. (2005). Comparison of in situ and remote sensing-derived (SeaWiFS) chlorophyll-a in the Northwest Atlantic. *Indian Journal of Marine Sciences, 34* 341–355.

Geider, R. J., MacIntyre, H. L., & Kana, T. M. (1998). A dynamic regulatory model of phytoplanktonic acclimation to light, nutrients and temperature. *Limnology and Oceanography, 43*(4), 679–694.

Glover, H. E. (1989). Ribulosebisphosphate carboxylase/oxygenase in marine organisms. *International Review of Cytology, 115*, 67–138.

Glover, H. E. & Morris, I. (1979). Photosynthetic carboxilating enzymes in marine phytoplankton. *Limnology and Oceanography, 24*, 510–519.

Goericke, R. & Repeta, D. (1993). The pigments of *Prochlorococcus marinus*: the presence of divinyl-chlorophyll *a* and *b* in a marine prokaryote. *Limnology and Oceanography, 37*, 425–433.

Govindjee (1995). Sixty-three years since kautsky: chlorophyll *a* fluorescence. *Australian Journal of Plant Physiology, 22*, 131–160.

Hoepffner, N. & Sathyendranath, S. (1992). Bio-optical characteristics of coastal waters: Absorption spectra of phytoplankton and pigment distribution in the western North Atlantic. *Limnology and Oceanography, 37*(8), 1660–1679.

Hoepffner, N. & Sathyendranath, S. (1993). Determination of the major groups of phytoplankton pigments from the absorption spectra of total particulate matter. *Journal of Geophysical Research, 98*(C12), 22,789–22,803.

Hooker, S. B. & McClain, C. R. (2000). The calibration and validation of SeaWiFS data. *Progress in Oceanography, 45*, 427–465.

Hooker, S. B., Van Heukelem, L., Thomas, C. S., Claustre, H., Ras, J., Barlow, R., Sessions, H., Schluter, L., Perl, J., Trees, C., Stuart, V., Head, E., Clementson, L., Fishwick, J., Llewellym, C., & Aiken, J. (2005). The second SeaWiFS HPLC analysis round-robin experiment (SeaHARRE-2). NASA/TM-20050212787, Goddard Space Flight Center, Greenbelt, Maryland 20771, USA. August 2005, (pp. 112)

Huot, Y., Brown, C. A., & Cullen, J. J. (2005). New algorithms for MODIS sun-induced chlorophyll fluorescence and a comparison with present data products. *Limnology and Oceanography-Methods, 3*, 108–130.

Irwin, B., Anning, J., Caverhill, C., Escribano, R., & Platt, T. (1988). Carbon and oxygen primary production in Bedford Basin from January to April 1986. *Canadian Data Report of Fisheries and Aquatic Sciences, 719*, iv+34.

Irwin, B., Anning, J., Caverhill, C., & Platt, T. (1990). Primary production on the Labrador Shelf and in the Strait of Belle Isle in May 1988. *Canadian Data Report of Fisheries and Aquatic Sciences, 784*, iv+96pp.

Irwin, B., Caverhill, C., Anning, J., & Platt, T. (1987). Primary production and related measurements at a fixed station in the Caribbean Sea in December 1984. *Canadian Data Report of Fisheries and Aquatic Sciences, 671*, iv+161pp.

Irwin, B., Platt, T., & Caverhill, C. (1985). Primary production and other related measurements in the Eastern Canadian Arctic during the summer of 1983. *Canadian Data Report of Fisheries and Aquatic Sciences, 510*, iv+143pp.

Joint, I. R. & Groom, S. B. (2000). Estimation of phytoplankton production from space: current status and future potential of satellite remote sensing. *J Exp Mar Biol Ecol, 250*, 233–255.

Joint, I. R., Groom, S. B., Wollast, R., Chou, L., Tilstone, G. H., Figueiras, F. G., Loijens, M., Smyth, T. J. (2002). The response of phytoplankton production to periodic upwelling and relaxation events at the Iberian shelf break: estimates by the ^{14}C method and by satellite remote sensing. *Journal of Marine Systems, 32*, 219–238.

Joint, I. R., Rees, A. P., Woodward, M. S. (2001). Primary production and nutrient assimilation in the Iberian upwelling in August 1998. *Progress in Oceanography, 51*, 303–320.

Jordan, M. B. & Joint, I. R. (1984). Studies on phytoplankton distribution and primary production in the western English Channel in 1980 and 1981. *Continental Shelf Research, 3*(1), 25–34.

Kiefer, D. A., Chamberlin, W. S., & Booth, C. R. (1989). Natural fluorescence of chlorophyll *a*: Relationship to photosynthesis and chlorophyll concentration in the western south pacific gyre. *Limnology and Oceanography, 34*(5), 868–881.

Kiefer, D. A. & Reynolds, R. A. (1992). Advances in understanding phytoplankton fluorescence and photosynthesis. In P. G. Falkowski & A. D. Woodhead (Eds.), *Primary Production and Biogeochemical Cycles in the Sea* (pp. 155–174). New York: Plenum Press.

Krause, G. H. & Weis, E. (1991). Chlorophyll fluorescence and photosynthesis - the basics. *Annual Review of Plant Physiology and Plant Molecular Biology, 42*, 313–349.

Kyewalyanga, M., Platt, T., & Sathyendranath, S. (1992). Ocean primary production calculated by spectral and broad-band models. *Marine Ecology Progress Series, 85*, 171–185.

Kyewalyanga, M., Platt, T., Sathyendranath, S., Lutz, V. A., & Stuart, V. (1998). Seasonal variations in physiological parameters of phytoplankton across the North Atlantic. *Journal of Plankton Research, 20*, 17–42.

Kyewalyanga, M. N., Platt, T., & Sathyendranath, S. (1997). Estimation of the photosynthetic action spectrum: implications for primary production models. *Marine Ecology Progress Series, 146*(1–3), 207–223.

Kyewalyanga, M., Sathyendranath, S., & Platt, T. (2002). Effect of *Mesodinium rubrum* (=*Myrionecta rubra*) on the action and absorption spectra of phytoplankton in a coastal marine inlet. *Journal of Plankton Research, 24*(7), 687–702.

Le Quéré, C., Harrison, S. P., Prentice, I. C., Buitenhuis, E. T., Aumont, O., Bopp, L., Claustre, H., da Cunha, L. C., Geider, R., Giraud, X., Klaas, C., Kohfeld, K. E., Legendre, L., Manizza, M., Platt, T., Rivkin, R. B., Sathyendranath, S., Uitz, J., Watson, A. J., & Wolf-Gladrow, D. (2005). Ecosystem dynamics based on plankton functional types for global ocean biogeochemistry models. *Global Change Biology, 11*, 2016–2040.

Longhurst, A. (1998). *Ecological Geography of the Sea.* San Diego: Academic Press.

Longhurst, A., Sathyendranath, S., Platt, T., & Caverhill, C. (1995). An estimate of global primary production in the ocean from satellite radiometer data. *Journal of Plankton Research, 17*(6), 1245–1271.

Longhurst, A. R. & Harrison, W. G. (1989). The biological pump: profiles of plankton production and consumption in the upper ocean. *Progress in Oceanography, 22*, 47–123.

Lutz, V., Sathyendranath, S., Head, E. J. H., & Li, W. K. W. (1997). Differences between *in vivo* absorption and fluorescence excitation spectra in natural samples of phytoplankton. *Journal of Phycology, 34*, 214–227.

Lutz, V. A., Sathyendranath, S., Head, E. J. H., & Li, W. K. W. (2000). Changes in the *in vivo* absorption and fluorescence excitation spectra with growth irradiance in three species of phytoplankton. *Journal of Plankton Research, 23*(6), 555–569.

MacCaull, W. A. & Platt, T. (1977). Diel variations in the photosynthetic parameters of coastal marine phytoplankton. *Limnology and Oceanography, 22*(4), 723–731.

Malin, G., Turner, S. M., & Liss, P. S. (1992). Sulfur - the plankton climate connection. *Journal of Phycology, 28*(5), 590–597.

Malone, T. C. (1976). Phytoplankton productivity in the apex of the new york bight: environmental regulation of productivity/chlorophyll *a*. In M. G. Gross (Ed.), *The Middle Atlantic Continental Shelf and New York Bight* (pp. 260–272). Limnology and Oceanography Special Symposium, 2.

Maritorena, S., Morel, A., & Gentili, B. (2000). Determintation of the fluorescence quantum yield by oceanic phytoplankton in their natural habitat. *Applied Optics, 39*(36), 6725–6737.

Megard, R. O. (1972). Phytoplankton, photosynthesis, and phosphorus in Lake Minnetonka, Minnesota. *Limnology and Oceanography, 17*(1), 68–87.

Mitchell, B. G., Kahru, M., Wieland, J., & Stramska, M. (2002). Determination of spectral absorption coefficients of particles, dissolved material and phytoplankton for discrete water samples. In J. L. Mueller & G. S. Fargion (Eds.), *Ocean Optics Protocols for Satellite Ocean Color Sensor Validation*, volume 2 (pp. 231–257). Maryland: National Aeronotics and Space Administration.

Morel, A. (1978). Available, usable, and stored radiant energy in relation to marine photosynthesis. *Deep-Sea Research I, 25*, 673–688.

Morel, A. & Berthon, J. F. (1989). Surface pigments, algal biomass profiles, and potential production of the euphotic layer: Relationships reinvestigated in view of remote-sensing applications. *Limnology and Oceanography, 34*(8), 1545–1562.

Morrison, J. R. (2003). *In situ* determination of the quantum yield of phytoplankton chlorophyll *a* fluorescence: A simple algorithm, observations, and a model. *Limnology and Oceanography, 48*(2), 618–631.

Nair, A., Sathyendranath, S., Platt, T., Morales, J., Stuart, V., Forget, M.-H., Devred, E. & Bouman, H. (submitted). Remote sensing of phytoplankton fundtional types. *Remote Sensing of Environment.*

O'Reilly, J. E., Evans-Zetlin, C., & Busch, D. A. (1987). Primary production. In R. H. Backus (Ed.), *Georges Bank* (pp. 220–233). Cambridge, Massachusetts: M.I.T. Press.

O'Reilly, J. E., Maritorena, S., Mitchel, B. G., Siegel, D., Carder, K. L., Garver, S., Kahru, M. & McClain, C. (1987). Ocean color chlorophyll algorithms for SeaWiFS. *Journal of Geophysical Research 103*(C11) 24937–24953.

Partenski, F., Hoepffner, N., Li, W. K. W., Ulloa, O., & Vaulot, D. (1993). Photoacclimation of *Prochlorococcus* sp. (Prochlorophyta) strains isolated from the North Atlantic and the Mediterranean Sea. *Plant Physiology, 101*, 285–296.

Pemberton, K. L, Clarke, K. R. & Joint, I. (2006). Quantifying uncertainties associated with the measurement of primary production. *Marine Ecology Progress Series, 322*, 51–59.

Peterson, B. J. (1980). Aquatic primary productivity and the ^{14}C-CO_2 method - a history of the productivity problem. *Annual Review of Ecology and Systematics, 11*, 359–385.

Platt, T. (1986). Primary production of the ocean water column as a function of surface light intensity: Algorithms for remote sensing. *Deep-Sea Research I, 33*(2), 149–163.

Platt, T., Bouman, H., Devred, E., Fuentes-Yaco, C., & Sathyendranath, S. (2005). Physical forcing and phytoplankton distributions. *Scientia Marina, 69*(1), 55–73.

Platt, T., Gallegos, C. L., & Harrison, W. G. (1980). Photoinhibition of photosynthesis in natural assemblages of marine phytoplankton. *Journal of Marine Research, 38*(4), 687–701.

Platt, T., & Harrison, W. G. (1985). Biogenic fluxes of carbon and oxygen in the ocean. *Nature, 318*, 55–58.

Platt, T. & Irwin, B. (1968). Primary productivity measurements in St. Margarets Bay. *Technical Report Fisheries Research Board of Canada, 77.*

Platt, T. & Jassby, A. D. (1976). The relationship between photosynthesis and light for natural assemblages of coastal marine phytoplankton. *Journal of Phycology, 12*(4), 421–430.

Platt, T. & Sathyendranath, S. (1988). Oceanic primary production: Estimation by remote sensing at local and regional scales. *Science, 241*, 1613–1620.

Platt, T. & Sathyendranath, S. (1993). Estimators of primary production for interpretation of remotely sensed data on ocean color. *Journal of Geophysical Research, 98*(C8), 14,561–14,576.

Platt, T. & Sathyendranath, S. (1997). Modelling primary production IV (in japanese). *Aquabiology, 19*(3), 229–232.

Platt, T. & Sathyendranath, S. (1999). Spatial structure of pelagic ecosystem processes in the global ocean. *Ecosystems, 2*, 384–394.

Platt, T. & Sathyendranath, S. (2002). Modelling primary production XXX (in japanese). *Aquabiology, 141*, 341–345.

Platt, T., Sathyendranath, S., Caverhill, C. M., & Lewis, M. R. (1988). Ocean primary production and available light: Further algorithms for remote sensing. *Deep-Sea Research I, 35*(6), 855–879.

Platt, T., Sathyendranath, S., Forget, M.-H., White, G., Caverhill, C., Bouman, H. A., Devred, E., & Son, S. (submitted). Operational mode estimation of primary production at large geographical scales. *Remote Sensing of Environment.*

Platt, T., Sathyendranath, S., & Longhurst, A. (1995). Remote sensing of primary production in the oceans: promise and fulfilment. *Philos. Trans. R. Soc. Lond. Ser. B, 348*, 191–202.

Platt, T., Sathyendranath, S., & Ravindran, P. (1990). Primary production by phytoplankton: analytic solutions for daily rates per unit area of water surface. *Proceedings of the Royal Society of London, Series B: Biological Sciences, 241*, 101–111.

Platt, T., Sathyendranath, S., Ulloa, O., Harrison, W. G., Hoepffner, N., & Goes, J. (1992). Nutrient control of phytoplankton photosynthesis in the Western North Atlantic. *Nature, 356*, 229–231.

Pommier, J., Gosselin, M., & Michel, C. (submitted). Size-fractionated phytoplankton production and biomass during the decline of the Northwest Atlantic spring bloom. *Marine Ecology-Progress Series.*

Rodhe, W. (1965). Standard correlations between pelagic photosynthesis and light. In C. R. Goldman (Ed.), *Primary Productivity in Aquatic Environments* (pp. 365–381). Berkeley: University of California Press.

Ryther, J. H. (1956). Photosynthesis in the ocean as a function of light intensity. *Limnology and Oceanography, 1*, 61–70.

Ryther, J. H. & Yentsch, C. S. (1957). The estimation of phytoplankton production in the ocean from chlorophyll and light data. *Limnology and Oceanography, 11*(3), 281–286.

Sampou, P. & Kemp, W. M. (1994). Factors regulating plankton community respiration in Chesapeake Bay. *Marine Ecology-Progress Series, 110*(2-3), 249–258.

Sathyendranath, S., Cota, G., Stuart, V., Maass, H., & Platt, P. (2001). Remote sensing of phytoplankton pigments: a comparison of empirical and theoretical approaches. *Int. J. Remote Sens., 22*, 249–273.

Sathyendranath, S., Lazzara, L., & Prieur, L. (1987). Variations in the spectral values of specific absorption of phytoplankton. *Limnology and Oceanography, 32*(2), 403–415.

Sathyendranath, S., Longhurst, A., Caverhill, C. M., & Platt, T. (1995). Regionally and seasonally differentiated primary production in the North Atlantic. *Deep-Sea Research I, 42*(10), 1773–1802.

Sathyendranath, S. & Platt, T. (1993). Remote sensing of water-column primary production. In W. K. W. Li & S. Y. Maestrini (Eds.), *Measurement of Primary Production from the Molecular to the Global Scale* (pp. 236–243). Copenhagen: ICES Marine Science Symposia, Vol. 197.

Sathyendranath, S. & Platt, T. (2007). Spectral effects in bio-optical control on the ocean system. *Oceanologia 49* 5–39.

Sathyendranath, S., Platt, T., Caverhill, C. M., Warnock, R. E., & Lewis, M. R. (1989). Remote sensing of oceanic primary production: Computations using a spectral model. *Deep-Sea Research I, 36*(3), 431–453.

Sathyendranath, S., Platt, T., & Forget, M.-H. (2007). Oceanic primary production: comparison of models. *Prcoeeding of the Institute of Electrical and Eloctronics Engineering IEEE*, Aberdeen, Scotland, June 2007.

Sathyendranath, S., Watts, L., Devred, E., Platt, T., Caverhill, C., & Maass, H. (2004). Discrimination of diatoms from other phytoplankton using ocean-colour data. *Marine Ecology Progress Series, 272*, 59–68.

Smith, E. M. & Kemp, W. M. (1995). Seasonal and regional variations in plankton community production and respiration for Chesapeake Bay. *Marine Ecology-Progress Series, 116*(1-3), 217–231.

Steemann Nielsen, E. (1952). The use of radioactive carbon (^{14}C) for measuring organic production in the sea. *J. Cons. perm. int. Explor. Mer, 18*, 117–14.

Stuart, V., Sathyendranath, S., Platt, T., Maass, H., & Irwin, B. D. (1998). Pigments and species composition of natural phytoplankton populations: Effect on the absorption spectra. *Journal of Plankton Research, 20*(2), 187–217.

Subramaniam, A., Carpenter, E. J., & Falkowski, P. G. (1999). Bio-optical properties of the marine diazotrophic cyanobacteria *Trichodesmium* spp. II. A reflectance model for remote sensing. *Limnology and Oceanography, 44*(3), 618–627.

Talling, J. F. (1957). The phytoplankton population as a compound photosynthetic system. *New Phytologist, 56*, 133–149.

Topliss, B. J. & Platt, T. (1986). Passive fluorescence and photosynthesis in the ocean: implications for remote sensing. *Deep-Sea Research I, 33*(7), 849–864.

Uitz, J., Claustre, H., Morel, A. & Hooker, S. B. (2006). Vertical distribution of phytoplankton communities in open ocean: An assessment based on surface chlorophyll. *Journal of Geophysical Research, 111*(C8), 10.1029/2005JC003207.

Vidussi, F., Claustre, H., Manaca, B. B., Luchetta, A., & Marty, J. C. (2001). Phytoplankton pigment distribution in relation to upper thermocline circulation in the eastern mediterranean sea during winter. *Journal of Geophysical Research, 106*(C9), 19,939–19,956.

Westberry, T. K. & Siegel, D. A. (2003). Phytoplankton natural fluorescence variability in the sargasso sea. *Deep-Sea Research I, 50*, 417–434.

Williams, P. J. L. & Robertson, J. E. (1991). Overall planktonic oxygen and carbon dioxide metabolisms: the problem of reconciling observations and calculations of photosynthetic quotients. *Journal of Plankton Research, 13*, 153–169.

Appendix A

CHLOROPHYLL-a PROFILE PARAMETERS FOR THE LAPE PROJECT

Table A.1: Chlorophyll-a profile parameters for the LAPE project, April and May 2006. The classes are also presented, where 1 is coastal waters (maximal depth < 200m), 2 is the open ocean stations south to 16°N and 3 is the open ocean stations north to 16°N.

station	class	B_0	z_m	σ	h
		mg chla m^{-3}	m	m	mg chla m^{-2}
CE0607-01	3	0.112	114	11.9	6.1
CE0607-02	3	0.066	114	26.5	10.7
CE0607-03	3	0.082	102	13.0	11.2
CE0607-04	3	0.085	105	20.4	7.7
CE0607-05	3	0.116	104	28.2	16.5
CE0607-07	3	0.069	114	24.2	11.1
CE0607-08	3	0.070	118	18.5	10.5
CE0607-09	3	0.058	120	23.5	13.3
CE0607-10	3	0.075	120	23.5	14.3
CE0607-11	3	0.072	119	27.2	16.1
CE0607-12	3	0.068	109	21.7	11.9
CE0607-14	2	0.103	75	13.8	35.9
CE0607-15	2	0.102	52	7.7	17.2
CE0607-16	2	0.154	87	7.8	15.7
CE0607-18	2	0.109	89	28.6	28.0
CE0607-19	2	0.091	82	21.3	23.9
CE0607-20	2	0.026	61	30.7	27.9
CE0607-22	2	0.034	67	32.8	38.2
CE0607-23	2	0.049	59	32.1	34.3
CE0607-24	2	0.034	68	31.4	32.3
CE0607-25	2	0.067	68	26.0	26.5

station	class	B_0 mg chla m^{-3}	z_m m	σ m	h mg chla m^{-2}
CE0607-26	1	0.087	71	21.6	27.2
CE0607-27	1	N/A	N/A	N/A	N/A
CE0607-28	2	0.086	79	22.9	21.2
CE0607-29	2	0.093	37	17.3	23.5
CE0607-30	2	0.007	67	47.5	48.8
CE0607-31	2	0.079	84	20.3	30.2
CE0607-32	2	0.120	81	16.5	11.3
CE0607-33	2	0.140	85	16.9	14.2
CE0607-35	2	0.125	114	8.3	9.1
CE0607-36	1	N/A	N/A	N/A	N/A
CE0607-37	2	0.040	49	20.5	27.6
CE0607-38	2	0.112	72	15.9	17.4
CE0607-39	2	0.009	42	35.0	32.7
CE0607-40	2	0.012	55	32.0	27.5
CE0607-41	2	0.106	104	26.1	17.9
CE0607-42	2	0.014	55	25.3	28.8
CE0607-43	2	0.085	69	19.4	18.0
CE0607-44	3	0.045	70	31.1	25.9
CE0607-45	3	0.131	117	28.8	9.3
CE0607-46	3	0.081	116	16.7	10.2
CE0607-47	3	0.085	77	24.1	16.8
CE0607-48	3	0.080	101	16.3	14.7
CE0607-49	2	0.067	74	23.1	17.3
CE0607-50	2	0.037	66	26.8	32.2
CE0607-51	2	0.112	82	18.5	17.8
CE0607-52	2	0.076	76	16.3	17.2
CE0607-53	2	0.107	73	11.6	10.5
CE0607-54	3	0.009	74	47.6	39.0
CE0607-55	3	0.064	94	21.5	11.6
CE0607-56	3	0.025	63	23.9	26.5

Appendix B

TABULATION OF PIGMENT DATA FOR SURFACE (20 M) AND DEEP CHLOROPHYLL MAXIMUM SAMPLES FOR THE LAPE PROJECT FROM TURNER ANALYSES AND FROM HIGH PERFORMANCE LIQUIDE CHROMATOGRAPHY (HPLC)

Table B.1: Pigment data (Turner chlorophyll-a, chlrophyll-c3, chlorophyll-c2, chlorophyll-c1, chlorophyllide-a and Pheophorbide-a) for surface samples (20m) analysed from Turner fluorescence and high performance liquid chromatography (HPLC) for the LAPE project, April and May 2006.

Station	Chl a(Turner) mg m^{-3}	Chl c_3 mg m^{-3}	Chl c_2 mg m^{-3}	Chl c_1 mg m^{-3}	Chlide a mg m^{-3}	Phide a mg m^{-3}
CE0607-01	0.110	0.0055	0.0062	0.0017	0.0042	0.0041
CE0607-02	0.079	0.0037	0.0045	0.0001	0.0001	0.0001
CE0607-03	0.118	0.0043	0.0049	0.0013	0.0036	0.0016
CE0607-04	0.107	0.0037	0.0047	0.0010	0.0088	0.0059
CE0607-05	0.173	0.0045	0.0059	0.0011	0.013	0.0059
CE0607-07	0.067	0.0031	0.0041	0.0001	0.0001	0.0001
CE0607-08	0.093	0.0034	0.0042	0.0008	0.0050	0.0049
CE0607-09	0.074	0.0030	0.0035	0.0004	0.0052	0.0001
CE0607-10	0.078	0.0036	0.0056	0.0001	0.0012	0.0001
CE0607-11	0.087	0.0047	0.0052	0.0001	0.0010	0.0001
CE0607-12	0.110	0.0031	0.0049	0.0005	0.0043	0.0020
CE0607-14	0.154	0.0060	0.0078	0.0013	0.0073	0.0026
CE0607-15	0.179	0.0064	0.0081	0.0008	0.0067	0.0024
CE0607-16	0.183	0.0066	0.0073	0.0013	0.0114	0.0059
CE0607-18	0.214	0.0071	0.0093	0.0013	0.0094	0.0031
CE0607-19	0.144	0.0063	0.0080	0.0008	0.0043	0.0019
CE0607-20	0.167	0.0076	0.0096	0.0004	0.0075	0.0001
CE0607-22	0.231	0.0108	0.0140	0.0001	0.0036	0.0001
CE0607-23	0.262	0.0112	0.0112	0.0031	0.0078	0.0035
CE0607-24	0.150	0.0065	0.0072	0.0013	0.0077	0.0050
CE0607-25	0.151	0.0061	0.0069	0.0001	0.0014	0.0001

Station	Chl a(Turner) mg m^{-3}	Chl c_3 mg m^{-3}	Chl c_2 mg m^{-3}	Chl c_1 mg m^{-3}	Chlide a mg m^{-3}	Phide a mg m^{-3}
CE0607-26	0.113	0.0071	0.0083	0.0001	0.0012	0.0001
CE0607-27	0.513	0.0490	0.0408	0.0036	0.0118	0.0178
CE0607-28	0.218	0.0070	0.0067	0.0025	0.0067	0.0027
CE0607-29	0.359	0.0175	0.0179	0.0020	0.0107	0.0109
CE0607-30	0.284	0.0112	0.0108	0.0065	0.0089	0.0038
CE0607-31	0.119	0.0048	0.0051	0.0014	0.0024	0.0001
CE0607-32	0.177	0.0065	0.0075	0.0026	0.0065	0.0020
CE0607-33	0.185	0.0069	0.0095	0.0008	0.0078	0.0047
CE0607-35	0.148	0.0120	0.0102	0.0028	0.0011	0.0001
Barbados	0.634	0.0353	0.0453	0.0101	0.0018	0.0102
CE0607-36	0.337	0.0374	0.0275	0.0072	0.0032	0.0128
CE0607-37	0.192	0.0121	0.0127	0.0001	0.0014	0.0001
CE0607-38	0.243	0.0068	0.0071	0.0019	0.0042	0.0001
CE0607-39	0.322	0.0299	0.0225	0.0040	0.0022	0.0053
CE0607-40	0.202	0.0090	0.0087	0.0031	0.0026	0.0001
CE0607-41	0.128	0.0046	0.0050	0.0018	0.0034	0.0001
CE0607-42	0.234	0.0088	0.0094	0.0021	0.0029	0.0001
CE0607-43	0.178	0.0076	0.0066	0.0020	0.0024	0.0001
CE0607-44	0.237	0.0051	0.0064	0.0015	0.0042	0.0016
CE0607-45	0.148	0.0066	0.0059	0.0019	0.0009	0.0001
CE0607-46	0.093	0.0036	0.0050	0.0018	0.0337	0.0119
CE0607-47	0.106	0.0040	0.0043	0.0009	0.0059	0.0044
CE0607-48	0.227	0.0038	0.0040	0.0015	0.0028	0.0001
CE0607-49	0.130	0.0069	0.0082	0.0006	0.0043	0.0035
CE0607-50	0.209	0.0110	0.0106	0.0025	0.0090	0.0037
CE0607-51	0.131	0.0047	0.0062	0.0014	0.0019	0.0001
CE0607-52	0.113	0.0044	0.0058	0.0010	0.0053	0.0022
CE0607-53	0.182	0.0058	0.0077	0.0013	0.0068	0.0077
CE0607-54	0.162	0.0064	0.0078	0.0023	0.0173	0.0083
CE0607-55	0.085	0.0045	0.005	0.0009	0.0009	0.0001
CE0607-56	0.110	0.0063	0.0086	0.0001	0.0010	0.0001

Table B.2: Pigment data (Peridinin, 19'Butanoyloxyfucoxanthin, Fucoxanthin, Neoxanthin, Prasinoxanthin, violaxanthin and 19'hexanoyloxyfucoxanthin) for surface samples (20m) analysed from high performance liquid chromatography (HPLC) for the LAPE project, April and May 2006.

Station	Perid	But Fuco	Fuco	Neo	Pras	Viola	Hex Fuco
	mg m^{-3}	mg m^{-3}	mg m^{-3}	mg m^{-3}	mg m^{-3}	mg m^{-3}	mg m^{-3}
CE0607-01	0.0025	0.0052	0.0042	0.0001	0.0001	0.0001	0.0210
CE0607-02	0.0023	0.0035	0.0025	0.0001	0.0001	0.0001	0.0136
CE0607-03	0.0025	0.0035	0.0043	0.0001	0.0001	0.0009	0.0138
CE0607-04	0.0001	0.0028	0.0048	0.0001	0.0001	0.0001	0.0132
CE0607-05	0.0029	0.0034	0.0058	0.0001	0.0001	0.0001	0.0148
CE0607-07	0.0019	0.0033	0.0023	0.0001	0.0001	0.0001	0.0125
CE0607-08	0.0019	0.0029	0.0020	0.0001	0.0001	0.0007	0.0130
CE0607-09	0.0019	0.0024	0.0017	0.0001	0.0001	0.0001	0.0112
CE0607-10	0.0022	0.0038	0.0032	0.0001	0.0001	0.0012	0.0154
CE0607-11	0.0025	0.0035	0.0026	0.0001	0.0001	0.0009	0.0170
CE0607-12	0.0015	0.0033	0.0061	0.0001	0.0001	0.0001	0.0141
CE0607-14	0.0035	0.0043	0.0060	0.0001	0.0001	0.0010	0.0183
CE0607-15	0.0023	0.0059	0.0076	0.0001	0.0001	0.0010	0.0215
CE0607-16	0.0030	0.0050	0.0063	0.0001	0.0001	0.0001	0.0209
CE0607-18	0.0034	0.0055	0.0089	0.0001	0.0001	0.0012	0.0233
CE0607-19	0.0023	0.0059	0.0055	0.0001	0.0001	0.0001	0.0221
CE0607-20	0.0047	0.0072	0.0061	0.0001	0.0001	0.0011	0.0245
CE0607-22	0.0053	0.0089	0.0061	0.0001	0.0001	0.0013	0.0354
CE0607-23	0.0058	0.0076	0.0072	0.0001	0.0001	0.0013	0.0359
CE0607-24	0.0044	0.0055	0.0066	0.0001	0.0001	0.0012	0.0223
CE0607-25	0.0029	0.0045	0.0058	0.0001	0.0001	0.0001	0.0191

Station	Perid	But Fuco	Fuco	Neo	Pras	Viola	Hex Fuco
	mg m^{-3}	mg m^{-3}	mg m^{-3}	mg m^{-3}	mg m^{-3}	mg m^{-3}	mg m^{-3}
CE0607-26	0.0031	0.0054	0.0034	0.0001	0.0001	0.0001	0.0192
CE0607-27	0.0059	0.0197	0.0982	0.0074	0.0001	0.0036	0.0761
CE0607-28	0.0030	0.0046	0.0062	0.0001	0.0001	0.0001	0.0200
CE0607-29	0.0049	0.0144	0.0323	0.0025	0.0001	0.0029	0.0313
CE0607-30	0.0077	0.0098	0.0076	0.0001	0.0001	0.0001	0.0337
CE0607-31	0.0026	0.0040	0.0060	0.0001	0.0001	0.0001	0.0161
CE0607-32	0.0043	0.0060	0.0075	0.0001	0.0001	0.0007	0.0194
CE0607-33	0.0033	0.0058	0.0084	0.0001	0.0001	0.0010	0.0241
CE0607-35	0.0061	0.0098	0.0046	0.0001	0.0001	0.0009	0.0341
Barbados	0.0177	0.0226	0.0577	0.0072	0.0001	0.0037	0.0858
CE0607-36	0.0064	0.0321	0.0275	0.0033	0.0059	0.0034	0.0823
CE0607-37	0.0039	0.0088	0.0180	0.0001	0.0001	0.0019	0.0255
CE0607-38	0.0017	0.0054	0.0076	0.0001	0.0001	0.0011	0.0239
CE0607-39	0.0044	0.0226	0.0289	0.0030	0.0001	0.0028	0.0629
CE0607-40	0.0033	0.0073	0.0073	0.0001	0.0001	0.0018	0.0320
CE0607-41	0.0021	0.0038	0.0049	0.0001	0.0001	0.0001	0.0168
CE0607-42	0.0044	0.0068	0.0074	0.0001	0.0001	0.0014	0.0294
CE0607-43	0.0029	0.0053	0.0058	0.0001	0.0001	0.0001	0.0239
CE0607-44	0.0019	0.0051	0.0066	0.0001	0.0001	0.0009	0.0202
CE0607-45	0.0028	0.0061	0.0053	0.0001	0.0001	0.0009	0.0211
CE0607-46	0.0032	0.0033	0.0027	0.0001	0.0001	0.0001	0.0132
CE0607-47	0.0020	0.0033	0.0030	0.0001	0.0001	0.0008	0.0134
CE0607-48	0.0020	0.0033	0.0028	0.0001	0.0001	0.0001	0.0123
CE0607-49	0.0039	0.0058	0.0060	0.0001	0.0001	0.0008	0.0227
CE0607-50	0.0052	0.0087	0.0094	0.0001	0.0001	0.0013	0.0303
CE0607-51	0.0022	0.0049	0.0081	0.0001	0.0001	0.001	0.0171
CE0607-52	0.0024	0.0037	0.0052	0.0001	0.0001	0.0007	0.0146
CE0607-53	0.0031	0.0046	0.0066	0.0001	0.0001	0.0008	0.0221
CE0607-54	0.0033	0.0045	0.0082	0.0001	0.0001	0.0011	0.0223
CE0607-55	0.0021	0.0036	0.0030	0.0001	0.0001	0.0009	0.0164
CE0607-56	0.0032	0.0056	0.0043	0.0001	0.0001	0.0008	0.0212

Table B.3: Pigment data (Diadinoxanthin, Alloxanthin, Diatoxanthin, Zeaxanthin and Lutein) for surface samples (20m) analysed from high performance liquid chromatography (HPLC) for the LAPE project, April and May 2006.

Station	Diadino mg m^{-3}	Allo mg m^{-3}	Diato mg m^{-3}	Zea mg m^{-3}	Lut mg m^{-3}
CE0607-01	0.0039	0.0001	0.0001	0.0544	0.0001
CE0607-02	0.0040	0.0001	0.0001	0.0398	0.0001
CE0607-03	0.0049	0.0001	0.0001	0.0665	0.0001
CE0607-04	0.0083	0.0001	0.0012	0.0651	0.0001
CE0607-05	0.0068	0.0001	0.0001	0.0686	0.0001
CE0607-07	0.0066	0.0001	0.0001	0.0255	0.0001
CE0607-08	0.0042	0.0001	0.0001	0.0263	0.0001
CE0607-09	0.0040	0.0001	0.0001	0.0222	0.0001
CE0607-10	0.0092	0.0001	0.0001	0.0425	0.0001
CE0607-11	0.0063	0.0001	0.0001	0.0449	0.0001
CE0607-12	0.0062	0.0001	0.0001	0.0585	0.0001
CE0607-14	0.0120	0.0001	0.0001	0.0813	0.0001
CE0607-15	0.0066	0.0001	0.0001	0.0911	0.0001
CE0607-16	0.0059	0.0001	0.0001	0.0870	0.0001
CE0607-18	0.0108	0.0001	0.0001	0.0851	0.0001
CE0607-19	0.0062	0.0001	0.0001	0.0858	0.0001
CE0607-20	0.0080	0.0001	0.0001	0.0740	0.0001
CE0607-22	0.0096	0.0001	0.0001	0.0847	0.0001
CE0607-23	0.0078	0.0001	0.0001	0.1022	0.0001
CE0607-24	0.0072	0.0001	0.0001	0.0827	0.0001
CE0607-25	0.0043	0.0001	0.0001	0.0653	0.0001

Station	Diadino mg m^{-3}	Allo mg m^{-3}	Diato mg m^{-3}	Zea mg m^{-3}	Lut mg m^{-3}
CE0607-26	0.0054	0.0001	0.0001	0.0491	0.0001
CE0607-27	0.0159	0.0055	0.0024	0.0268	0.0001
CE0607-28	0.0069	0.0001	0.0001	0.0644	0.0001
CE0607-29	0.0091	0.0001	0.0001	0.0578	0.0001
CE0607-30	0.0055	0.0001	0.0001	0.0789	0.0001
CE0607-31	0.0054	0.0001	0.0001	0.0692	0.0001
CE0607-32	0.0048	0.0001	0.0001	0.0687	0.0001
CE0607-33	0.0078	0.0001	0.0001	0.0778	0.0001
CE0607-35	0.0043	0.0001	0.0001	0.0520	0.0001
Barbados	0.0148	0.0069	0.0001	0.0902	0.0001
CE0607-36	0.0218	0.0039	0.0001	0.0694	0.0001
CE0607-37	0.0063	0.0001	0.0001	0.0593	0.0001
CE0607-38	0.0082	0.0001	0.0001	0.0864	0.0001
CE0607-39	0.0101	0.0024	0.0001	0.0609	0.0001
CE0607-40	0.0137	0.0001	0.0001	0.1092	0.0001
CE0607-41	0.0073	0.0001	0.0001	0.0834	0.0001
CE0607-42	0.0145	0.0001	0.0023	0.1141	0.0001
CE0607-43	0.0088	0.0001	0.0001	0.0898	0.0001
CE0607-44	0.0073	0.0001	0.0001	0.0937	0.0001
CE0607-45	0.0062	0.0001	0.0001	0.0670	0.0001
CE0607-46	0.0066	0.0001	0.0001	0.0556	0.0001
CE0607-47	0.0060	0.0001	0.0001	0.0546	0.0001
CE0607-48	0.0039	0.0001	0.0001	0.0504	0.0001
CE0607-49	0.0083	0.0001	0.0001	0.0704	0.0001
CE0607-50	0.0073	0.0001	0.0001	0.0633	0.0001
CE0607-51	0.0070	0.0001	0.0001	0.0844	0.0001
CE0607-52	0.0057	0.0001	0.0001	0.0683	0.0001
CE0607-53	0.0072	0.0001	0.0001	0.0646	0.0001
CE0607-54	0.0093	0.0001	0.0001	0.0599	0.0001
CE0607-55	0.0079	0.0001	0.0001	0.0456	0.0001
CE0607-56	0.0052	0.0024	0.0001	0.0490	0.0001

Table B.4: Pigment data (Total chlorophyll-b, Divinyl chlorophyll-b, Divinyl chlorophyll-a, chlorophyll-a, Phaeophytin-a, Carotenes and Total chlorophyll-a) for surface samples (20m) analysed from high performance liquid chromatography (HPLC) for the LAPE project, April and May 2006.

Station	Total Chl b mg m^{-3}	Div Chl b mg m^{-3}	Div Chl a mg m^{-3}	Chl a mg m^{-3}	Phytin a mg m^{-3}	Caro mg m^{-3}	Total Chl a mg m^{-3}
CE0607-01	0.0086	0.0038	0.0301	0.0658	0.0001	0.0097	0.1001
CE0607-02	0.0055	0.0021	0.0167	0.0355	0.0001	0.0059	0.0528
CE0607-03	0.0091	0.0040	0.0336	0.0714	0.0001	0.0143	0.1086
CE0607-04	0.0068	0.0033	0.0322	0.0659	0.0001	0.0130	0.1069
CE0607-05	0.0094	0.0047	0.0416	0.1024	0.0026	0.0191	0.1570
CE0607-07	0.0044	0.0001	0.0096	0.0367	0.0001	0.0047	0.0463
CE0607-08	0.0037	0.0001	0.0088	0.0651	0.0001	0.0082	0.0789
CE0607-09	0.0027	0.0001	0.0058	0.0617	0.0001	0.0074	0.0728
CE0607-10	0.0075	0.0026	0.0176	0.0444	0.0001	0.0062	0.0632
CE0607-11	0.0063	0.0021	0.0165	0.0429	0.0001	0.0060	0.0604
CE0607-12	0.0071	0.0036	0.0326	0.0664	0.0001	0.0134	0.1033
CE0607-14	0.0111	0.0060	0.0555	0.1095	0.0026	0.0214	0.1722
CE0607-15	0.0117	0.0063	0.0542	0.0802	0.0001	0.0185	0.1411
CE0607-16	0.0106	0.0058	0.0553	0.1016	0.0025	0.0213	0.1683
CE0607-18	0.0123	0.0075	0.0660	0.1196	0.0026	0.0256	0.1950
CE0607-19	0.0104	0.0052	0.0413	0.0631	0.0001	0.0131	0.1086
CE0607-20	0.016	0.0079	0.0495	0.0966	0.0024	0.0175	0.1536
CE0607-22	0.0224	0.012	0.0809	0.1008	0.0001	0.0202	0.1853
CE0607-23	0.0232	0.0136	0.0871	0.1555	0.0033	0.0282	0.2505
CE0607-24	0.0108	0.0055	0.0455	0.1009	0.0001	0.0192	0.1541
CE0607-25	0.0124	0.0067	0.0545	0.0609	0.0001	0.0139	0.1167

Station	Total Chl b mg m^{-3}	Div Chl b mg m^{-3}	Div Chl a mg m^{-3}	Chl a mg m^{-3}	Phytin a mg m^{-3}	Caro mg m^{-3}	Total Chl a mg m^{-3}
CE0607-26	0.0113	0.0052	0.0342	0.0518	0.0001	0.0101	0.0873
CE0607-27	0.0732	0.0031	0.0095	0.3728	0.0063	0.0218	0.3942
CE0607-28	0.0143	0.0080	0.0555	0.0887	0.0001	0.0181	0.1509
CE0607-29	0.0320	0.0081	0.0390	0.1793	0.0031	0.0208	0.2290
CE0607-30	0.0287	0.0194	0.1118	0.1217	0.0054	0.0286	0.2424
CE0607-31	0.0108	0.0056	0.0404	0.0539	0.0001	0.0121	0.0967
CE0607-32	0.0141	0.0080	0.0563	0.0897	0.0028	0.0175	0.1526
CE0607-33	0.0135	0.0068	0.0510	0.1113	0.0001	0.0204	0.1700
CE0607-35	0.0200	0.0105	0.0562	0.0784	0.0024	0.0129	0.1357
Barbados	0.0953	0.0239	0.1172	0.3881	0.0068	0.0405	0.5071
CE0607-36	0.0864	0.0358	0.0964	0.2308	0.0057	0.0316	0.3305
CE0607-37	0.0225	0.0082	0.0526	0.125	0.0033	0.0167	0.1789
CE0607-38	0.0111	0.0062	0.0575	0.1002	0.0025	0.0202	0.1619
CE0607-39	0.0470	0.0138	0.0654	0.2162	0.0042	0.0237	0.2838
CE0607-40	0.0164	0.0086	0.0692	0.1497	0.0045	0.0261	0.2215
CE0607-41	0.0097	0.0057	0.0558	0.1127	0.0029	0.0218	0.1719
CE0607-42	0.0177	0.0100	0.0806	0.1504	0.0033	0.0281	0.2338
CE0607-43	0.0118	0.0056	0.0462	0.1167	0.0027	0.0208	0.1652
CE0607-44	0.0113	0.0063	0.0543	0.1038	0.0032	0.0111	0.1623
CE0607-45	0.0150	0.0077	0.0522	0.0966	0.0021	0.0190	0.1497
CE0607-46	0.0078	0.0037	0.0264	0.0819	0.0001	0.0209	0.1420
CE0607-47	0.0078	0.0033	0.0268	0.0648	0.0001	0.0119	0.0975
CE0607-48	0.0063	0.0029	0.0266	0.0428	0.0001	0.0092	0.0722
CE0607-49	0.0141	0.0066	0.0472	0.0820	0.0001	0.0142	0.1336
CE0607-50	0.0219	0.0097	0.0657	0.1135	0.0027	0.0220	0.1882
CE0607-51	0.0093	0.0041	0.0435	0.0727	0.0001	0.0138	0.1181
CE0607-52	0.0083	0.0040	0.0337	0.0723	0.0001	0.0137	0.1113
CE0607-53	0.0109	0.0055	0.0454	0.0922	0.0026	0.0176	0.1444
CE0607-54	0.0124	0.0061	0.0488	0.1791	0.0049	0.0273	0.2452
CE0607-55	0.0066	0.0025	0.0216	0.0437	0.0001	0.0071	0.0662
CE0607-56	0.0128	0.0046	0.0312	0.0621	0.0001	0.0099	0.0943

Table B.5: Pigment data (Turner chlorophyll-a, chlrophyll-c3, chlorophyll-c2, chlorophyll-c1, chlorophyllide-a and Pheophorbide-a) for deep chlorophyll maximum (DCM) samples analysed from Turner fluorescence and high performance liquid chromatography (HPLC) for the LAPE project, April and May 2006.

Station	depth	Chl a (Turner)	Chl c_3	Chl c_2	Chl c_1	Chlide a	Phide a
	m	mg m^{-3}	mg m^{-3}	mg m^{-3}	mg m^{-3}	mg m^{-3}	mg m^{-3}
CE0607-01	120	0.292	0.0530	0.0343	0.0106	0.0068	0.0039
CE0607-02	130	0.208	0.0432	0.0221	0.0099	0.0001	0.0001
CE0607-03	120	0.206	0.0341	0.0184	0.0072	0.0010	0.0001
CE0607-04	120	0.210	0.0262	0.0174	0.0056	0.0001	0.0001
CE0607-05	140	0.236	0.0412	0.0210	0.0111	0.0001	0.0001
CE0607-07	140	0.172	0.0391	0.0201	0.0067	0.0001	0.0001
CE0607-08	140	0.189	0.0355	0.0183	0.0081	0.0001	0.0001
CE0607-09	140	0.247	0.039	0.0209	0.0100	0.0011	0.0001
CE0607-10	140	0.256	0.0416	0.0204	0.0148	0.0009	0.0001
CE0607-11	140	0.286	0.0461	0.0239	0.0129	0.0013	0.0001
CE0607-12	140	0.130	0.0278	0.0122	0.0063	0.0001	0.0001
CE0607-14	60	0.659	0.0629	0.0436	0.0137	0.0256	0.0203
CE0607-15	50	0.973	0.1163	0.0826	0.0216	0.0249	0.0450
CE0607-16	70	0.223	0.0303	0.0156	0.0057	0.0049	0.0074
CE0607-18	100	0.526	0.0717	0.0448	0.0113	0.0038	0.0101
CE0607-19	100	0.399	0.0535	0.0333	0.0159	0.0045	0.0058
CE0607-20	100	0.154	0.0274	0.0146	0.0070	0.0011	0.0001
CE0607-22	70	0.571	0.0381	0.0270	0.0101	0.0032	0.0013
CE0607-23	80	0.427	0.0478	0.0283	0.0126	0.0022	0.0001
CE0607-24	90	0.374	0.0484	0.0295	0.0076	0.0056	0.0056
CE0607-25	70	0.500	0.0607	0.034	0.0055	0.0051	0.0095

Station	depth	Chl a (Turner)	Chl c_3	Chl c_2	Chl c_1	Chlide a	Phide a
	m	mg m^{-3}	mg m^{-3}	mg m^{-3}	mg m^{-3}	mg m^{-3}	mg m^{-3}
CE0607-26	60	0.539	0.0736	0.0549	0.0028	0.0113	0.0075
CE0607-28	140	0.047	0.0075	0.0047	0.0001	0.0001	0.0001
CE0607-29	50	0.492	0.0611	0.0406	0.0025	0.0133	0.0145
CE0607-30	90	0.412	0.0416	0.0240	0.0096	0.0017	0.0023
CE0607-31	90	0.655	0.0897	0.0540	0.0196	0.0049	0.0069
CE0607-32	90	0.397	0.0637	0.0357	0.0127	0.0027	0.0001
CE0607-33	90	0.515	0.0804	0.0530	0.0170	0.0025	0.0095
CE0607-35	90	0.182	0.0048	0.0058	0.0021	0.0047	0.0024
CE0607-37	50	0.652	0.0943	0.0613	0.0054	0.0524	0.0477
CE0607-38	50	0.275	0.0171	0.0143	0.0047	0.0008	0.0001
CE0607-39	70	0.357	0.0480	0.0306	0.0027	0.0053	0.0154
CE0607-40	50	0.286	0.0186	0.0177	0.0047	0.0028	0.0001
CE0607-41	60	0.196	0.0126	0.0110	0.0026	0.0015	0.0001
CE0607-42	70	0.455	0.0720	0.0485	0.0112	0.0021	0.0212
CE0607-43	70	0.528	0.0845	0.0492	0.0115	0.0112	0.0233
CE0607-44	80	0.423	0.0347	0.0205	0.0115	0.0001	0.0001
CE0607-45	70	0.170	0.0111	0.0111	0.0001	0.0019	0.0001
CE0607-46	120	0.329	0.0517	0.0291	0.0110	0.0034	0.0063
CE0607-47	120	0.180	0.0252	0.0139	0.0074	0.0009	0.0001
CE0607-48	100	0.462	0.0650	0.0361	0.0134	0.0043	0.0073
CE0607-49	100	0.186	0.0364	0.0214	0.0112	0.0016	0.0001
CE0607-50	80	0.535	0.0774	0.0477	0.0087	0.0115	0.0200
CE0607-51	90	0.505	0.0691	0.0469	0.0124	0.0041	0.0064
CE0607-52	80	0.496	0.0721	0.0419	0.0165	0.0029	0.0093
CE0607-53	80	0.419	0.0581	0.0373	0.0112	0.0034	0.0025
CE0607-55	140	0.055	0.0269	0.0136	0.0059	0.0022	0.0017
CE0607-56	90	0.399	0.0506	0.0319	0.0063	0.0044	0.0038

Table B.6: Pigment data (Peridinin, 19'Butanoyloxyfucoxanthin, Fucoxanthin, Neoxanthin, Prasinoxanthin, violaxanthin and 19'hexanoyloxyfucoxanthin) for deep chlorophyll maximum (DCM) samples analysed from high performance liquid chromatography (HPLC) for the LAPE project, April and May 2006.

Station	Perid	But Fuco	Fuco	Neo	Pras	Viola	Hex Fuco
	mg m^{-3}	mg m^{-3}	mg m^{-3}	mg m^{-3}	mg m^{-3}	mg m^{-3}	mg m^{-3}
CE0607-01	0.0045	0.0708	0.0176	0.0001	0.0001	0.0001	0.0990
CE0607-02	0.0038	0.0562	0.0084	0.0001	0.0001	0.0001	0.0719
CE0607-03	0.0040	0.0415	0.0069	0.0001	0.0001	0.0001	0.0629
CE0607-04	0.0029	0.0379	0.0069	0.0001	0.0001	0.0001	0.0469
CE0607-05	0.0039	0.0568	0.0084	0.0016	0.0001	0.0001	0.0638
CE0607-07	0.0045	0.0513	0.0079	0.0001	0.0001	0.0001	0.0681
CE0607-08	0.0034	0.0487	0.0081	0.0001	0.0001	0.0001	0.0610
CE0607-09	0.0035	0.0555	0.0065	0.0001	0.0001	0.0001	0.0622
CE0607-10	0.0031	0.0566	0.0088	0.0017	0.0001	0.0001	0.0622
CE0607-11	0.0043	0.0642	0.0101	0.0001	0.0001	0.0001	0.0684
CE0607-12	0.0029	0.0339	0.0048	0.0001	0.0001	0.0001	0.0473
CE0607-14	0.0090	0.0574	0.0285	0.0098	0.0196	0.0066	0.1387
CE0607-15	0.0128	0.1413	0.059	0.0302	0.0398	0.0096	0.1871
CE0607-16	0.0026	0.0314	0.0146	0.0001	0.0001	0.0001	0.0453
CE0607-18	0.0077	0.0836	0.0262	0.0065	0.0090	0.0016	0.1195
CE0607-19	0.0060	0.0741	0.0164	0.0050	0.0001	0.0001	0.0812
CE0607-20	0.0038	0.0405	0.0083	0.0001	0.0001	0.0001	0.0397
CE0607-22	0.0090	0.0283	0.0110	0.0026	0.0001	0.0001	0.1017
CE0607-23	0.0053	0.0645	0.0168	0.0034	0.0001	0.0001	0.0768
CE0607-24	0.0066	0.0618	0.0174	0.0047	0.0001	0.0001	0.0691
CE0607-25	0.0076	0.0633	0.0213	0.0050	0.0001	0.0014	0.1132

Station	Perid	But Fuco	Fuco	Neo	Pras	Viola	Hex Fuco
	mg m^{-3}	mg m^{-3}	mg m^{-3}	mg m^{-3}	mg m^{-3}	mg m^{-3}	mg m^{-3}
CE0607-26	0.0086	0.0720	0.0321	0.0058	0.0001	0.0018	0.1680
CE0607-28	0.0001	0.0120	0.0031	0.0001	0.0001	0.0001	0.0110
CE0607-29	0.0047	0.0512	0.0636	0.0040	0.0001	0.0016	0.0874
CE0607-30	0.0059	0.0462	0.0104	0.0032	0.0001	0.0001	0.0756
CE0607-31	0.0096	0.1048	0.0236	0.0073	0.0121	0.0025	0.1710
CE0607-32	0.0087	0.0688	0.0202	0.0059	0.0077	0.0016	0.1051
CE0607-33	0.0101	0.0930	0.0226	0.0078	0.0064	0.0022	0.1527
CE0607-35	0.0016	0.0037	0.0063	0.0001	0.0001	0.0007	0.0152
CE0607-37	0.0082	0.0567	0.1115	0.0061	0.0001	0.0020	0.1131
CE0607-38	0.0065	0.0122	0.0110	0.0001	0.0001	0.0012	0.0486
CE0607-39	0.0046	0.0376	0.0472	0.0037	0.0001	0.0016	0.0735
CE0607-40	0.0088	0.0128	0.0115	0.0010	0.0001	0.0016	0.0551
CE0607-41	0.0056	0.0091	0.0078	0.0001	0.0001	0.0001	0.0377
CE0607-42	0.0116	0.0801	0.0414	0.0096	0.0133	0.0025	0.0907
CE0607-43	0.0069	0.0889	0.0329	0.0073	0.0001	0.0023	0.1350
CE0607-44	0.0059	0.0262	0.0094	0.0023	0.0001	0.0011	0.0901
CE0607-45	0.0055	0.0110	0.0049	0.0001	0.0001	0.0001	0.0347
CE0607-46	0.0050	0.0646	0.0130	0.0001	0.0001	0.0001	0.0867
CE0607-47	0.0029	0.0390	0.0078	0.0001	0.0001	0.0001	0.0379
CE0607-48	0.0081	0.0748	0.0199	0.0038	0.0001	0.0001	0.1058
CE0607-49	0.0052	0.0507	0.0128	0.0001	0.0001	0.0001	0.0600
CE0607-50	0.0102	0.0715	0.0378	0.0085	0.0001	0.0031	0.1301
CE0607-51	0.0083	0.0782	0.0262	0.0069	0.0071	0.0022	0.1292
CE0607-52	0.0093	0.0830	0.0252	0.0056	0.0001	0.0014	0.1224
CE0607-53	0.0074	0.0716	0.0175	0.0081	0.0001	0.0016	0.0992
CE0607-55	0.0034	0.0364	0.0053	0.0001	0.0001	0.0001	0.0407
CE0607-56	0.0055	0.0598	0.0157	0.0030	0.0001	0.0001	0.0886

Table B.7: Pigment data (Diadinoxanthin, Alloxanthin, Diatoxanthin, Zeaxanthin and Lutein) for deep chlorophyll maximum (DCM) samples analysed from high performance liquid chromatography (HPLC) for the LAPE project, April and May 2006.

Station	Diadino mg m^{-3}	Allo mg m^{-3}	Diato mg m^{-3}	Zea mg m^{-3}	Lut mg m^{-3}
CE0607-01	0.0080	0.0021	0.0001	0.0505	0.0001
CE0607-02	0.0055	0.0001	0.0001	0.0207	0.0001
CE0607-03	0.0053	0.0001	0.0001	0.0239	0.0001
CE0607-04	0.0039	0.0001	0.0001	0.0250	0.0001
CE0607-05	0.0054	0.0001	0.0001	0.0236	0.0001
CE0607-07	0.0047	0.0001	0.0001	0.0164	0.0001
CE0607-08	0.0046	0.0001	0.0001	0.0170	0.0001
CE0607-09	0.0055	0.0001	0.0001	0.0269	0.0001
CE0607-10	0.0048	0.0001	0.0001	0.0294	0.0001
CE0607-11	0.0059	0.0001	0.0001	0.0352	0.0001
CE0607-12	0.0035	0.0001	0.0001	0.0097	0.0001
CE0607-14	0.0138	0.0035	0.0001	0.0584	0.0001
CE0607-15	0.0182	0.0143	0.0001	0.0648	0.0001
CE0607-16	0.0039	0.0021	0.0001	0.0152	0.0001
CE0607-18	0.0100	0.0053	0.0001	0.0477	0.0001
CE0607-19	0.0078	0.0044	0.0001	0.0534	0.0001
CE0607-20	0.0038	0.0001	0.0001	0.0151	0.0001
CE0607-22	0.0085	0.0001	0.0001	0.0770	0.0001
CE0607-23	0.0070	0.0018	0.0001	0.0443	0.0001
CE0607-24	0.0071	0.0031	0.0001	0.0322	0.0001

Station	Diadino mg m^{-3}	Allo mg m^{-3}	Diato mg m^{-3}	Zea mg m^{-3}	Lut mg m^{-3}
CE0607-25	0.0102	0.0001	0.0001	0.0307	0.0001
CE0607-26	0.0137	0.0044	0.0001	0.0399	0.0001
CE0607-28	0.0012	0.0001	0.0001	0.0023	0.0001
CE0607-29	0.0095	0.0016	0.0001	0.0325	0.0001
CE0607-30	0.0070	0.0001	0.0001	0.0462	0.0001
CE0607-31	0.0151	0.0051	0.0001	0.0993	0.0001
CE0607-32	0.0088	0.0041	0.0001	0.0432	0.0001
CE0607-33	0.0111	0.0078	0.0001	0.0697	0.0001
CE0607-35	0.0060	0.0001	0.0013	0.0668	0.0001
CE0607-37	0.0160	0.0049	0.0001	0.0335	0.0001
CE0607-38	0.0060	0.0001	0.0001	0.0937	0.0001
CE0607-39	0.0084	0.0027	0.0001	0.0366	0.0001
CE0607-40	0.0086	0.0001	0.0001	0.0973	0.0001
CE0607-41	0.0071	0.0001	0.0001	0.0960	0.0001
CE0607-42	0.0093	0.0073	0.0001	0.0482	0.0001
CE0607-43	0.0125	0.0065	0.0001	0.0598	0.0001
CE0607-44	0.0066	0.0001	0.0001	0.0617	0.0001
CE0607-45	0.0050	0.0001	0.0001	0.0449	0.0001
CE0607-46	0.0075	0.0017	0.0001	0.0481	0.0001
CE0607-47	0.0036	0.0001	0.0001	0.0183	0.0001
CE0607-48	0.0108	0.0048	0.0001	0.0503	0.0001
CE0607-49	0.0055	0.0001	0.0001	0.0339	0.0001
CE0607-50	0.0126	0.0091	0.0001	0.0413	0.0001
CE0607-51	0.0110	0.0056	0.0001	0.0711	0.0001
CE0607-52	0.0105	0.0063	0.0001	0.0590	0.0001
CE0607-53	0.0082	0.0051	0.0001	0.0516	0.0001
CE0607-55	0.0032	0.0001	0.0001	0.0113	0.0001
CE0607-56	0.0075	0.0022	0.0001	0.0404	0.0001

Table B.8: Pigment data Total chlorophyll-b, Divinyl chlorophyll-b, Divinyl chlorophyll-a, chlorophyll-a, Phaeophytin-a, Carotenes and Total chlorophyll-a) for deep chlorophyll maximum (DCM) samples analysed from high performance liquid chromatography (HPLC) for the LAPE project, April and May 2006.

Station	Total Chl b mg m^{-3}	Div Chl b mg m^{-3}	Div Chl a mg m^{-3}	Chl a mg m^{-3}	Phytin a mg m^{-3}	Caro mg m^{-3}	Total Chl a mg m^{-3}
CE0607-01	0.1703	0.1334	0.1522	0.2129	0.0061	0.0447	0.3720
CE0607-02	0.2157	0.1936	0.0935	0.1601	0.0047	0.0409	0.2541
CE0607-03	0.1401	0.1090	0.0896	0.1316	0.0032	0.0283	0.2222
CE0607-04	0.1223	0.0992	0.0861	0.1046	0.0036	0.0266	0.1906
CE0607-05	0.2246	0.1896	0.1009	0.1456	0.0048	0.0404	0.2465
CE0607-07	0.2060	0.1781	0.0820	0.1297	0.0049	0.0337	0.2117
CE0607-08	0.2142	0.1774	0.0806	0.1226	0.0047	0.0333	0.2032
CE0607-09	0.2274	0.1852	0.1115	0.1430	0.0035	0.0392	0.2556
CE0607-10	0.2479	0.2097	0.1215	0.1398	0.0044	0.0448	0.2622
CE0607-11	0.2796	0.2391	0.1402	0.1543	0.0058	0.0513	0.2959
CE0607-12	0.1585	0.1495	0.0603	0.0853	0.0027	0.0273	0.1456
CE0607-14	0.1506	0.0496	0.0958	0.3681	0.0071	0.0424	0.4896
CE0607-15	0.3225	0.0750	0.1108	0.7028	0.0159	0.0566	0.8386
CE0607-16	0.0854	0.0600	0.0452	0.1144	0.0031	0.0185	0.1645
CE0607-18	0.2142	0.1381	0.1527	0.3445	0.0081	0.0529	0.5011
CE0607-19	0.3060	0.2307	0.1748	0.2542	0.0092	0.0635	0.4335
CE0607-20	0.1477	0.1252	0.0657	0.1065	0.0029	0.0278	0.1734
CE0607-22	0.0964	0.0641	0.2499	0.2066	0.0075	0.0514	0.4598
CE0607-23	0.1696	0.1225	0.1467	0.2284	0.0055	0.0435	0.3773
CE0607-24	0.1518	0.0937	0.1057	0.2174	0.0058	0.035	0.3287
CE0607-25	0.0972	0.0417	0.0993	0.2732	0.0054	0.0297	0.3777

Station	Total Chl b mg m^{-3}	Div Chl b mg m^{-3}	Div Chl a mg m^{-3}	Chl a mg m^{-3}	Phytin a mg m^{-3}	Caro mg m^{-3}	Total Chl a mg m^{-3}
CE0607-26	0.1040	0.0599	0.0666	0.3179	0.0056	0.0294	0.3959
CE0607-28	0.0299	0.0236	0.0095	0.0267	0.0001	0.0048	0.0362
CE0607-29	0.0976	0.0494	0.0689	0.2905	0.0061	0.0275	0.3726
CE0607-30	0.1675	0.1202	0.1567	0.1931	0.0073	0.0446	0.3514
CE0607-31	0.3402	0.2339	0.2295	0.4002	0.0093	0.0767	0.6346
CE0607-32	0.2800	0.2066	0.1449	0.2609	0.0089	0.0527	0.4086
CE0607-33	0.3571	0.2659	0.1939	0.3668	0.0108	0.0709	0.5632
CE0607-35	0.0105	0.0055	0.0508	0.0850	0.0031	0.0165	0.1404
CE0607-37	0.0996	0.0363	0.0578	0.4006	0.0147	0.0366	0.5108
CE0607-38	0.0351	0.0233	0.1191	0.1132	0.0034	0.0248	0.2331
CE0607-39	0.0734	0.0319	0.0609	0.2613	0.0053	0.0252	0.3274
CE0607-40	0.0320	0.0178	0.0988	0.1702	0.0051	0.0275	0.2718
CE0607-41	0.0240	0.0136	0.0811	0.1014	0.0028	0.0221	0.1841
CE0607-42	0.3038	0.2018	0.1530	0.3424	0.0128	0.0600	0.4976
CE0607-43	0.2300	0.1426	0.1535	0.3618	0.0092	0.0527	0.5265
CE0607-44	0.0896	0.0600	0.2097	0.1761	0.0064	0.0414	0.3858
CE0607-45	0.0199	0.0094	0.0516	0.0826	0.0001	0.0123	0.1361
CE0607-46	0.1941	0.1504	0.1546	0.1921	0.0047	0.0452	0.3502
CE0607-47	0.1325	0.1104	0.0718	0.0976	0.0031	0.0257	0.1703
CE0607-48	0.2115	0.1533	0.1601	0.2574	0.0052	0.0498	0.4218
CE0607-49	0.1821	0.1465	0.1282	0.1474	0.0056	0.0395	0.2773
CE0607-50	0.1467	0.0623	0.1142	0.3605	0.0082	0.0372	0.4862
CE0607-51	0.2307	0.1493	0.1933	0.3422	0.0096	0.0572	0.5396
CE0607-52	0.2698	0.1963	0.1753	0.3090	0.0101	0.0575	0.4872
CE0607-53	0.2575	0.1789	0.1549	0.2723	0.0073	0.0511	0.4306
CE0607-55	0.1634	0.1420	0.0592	0.0901	0.0035	0.0277	0.1515
CE0607-56	0.1294	0.0882	0.1343	0.2073	0.0049	0.0363	0.3461

Appendix C

MONTHLY COMPOSITE IMAGES OF CHLOROPHYLL CONCENTRATION FROM MODIS FOR THE LAPE REGION

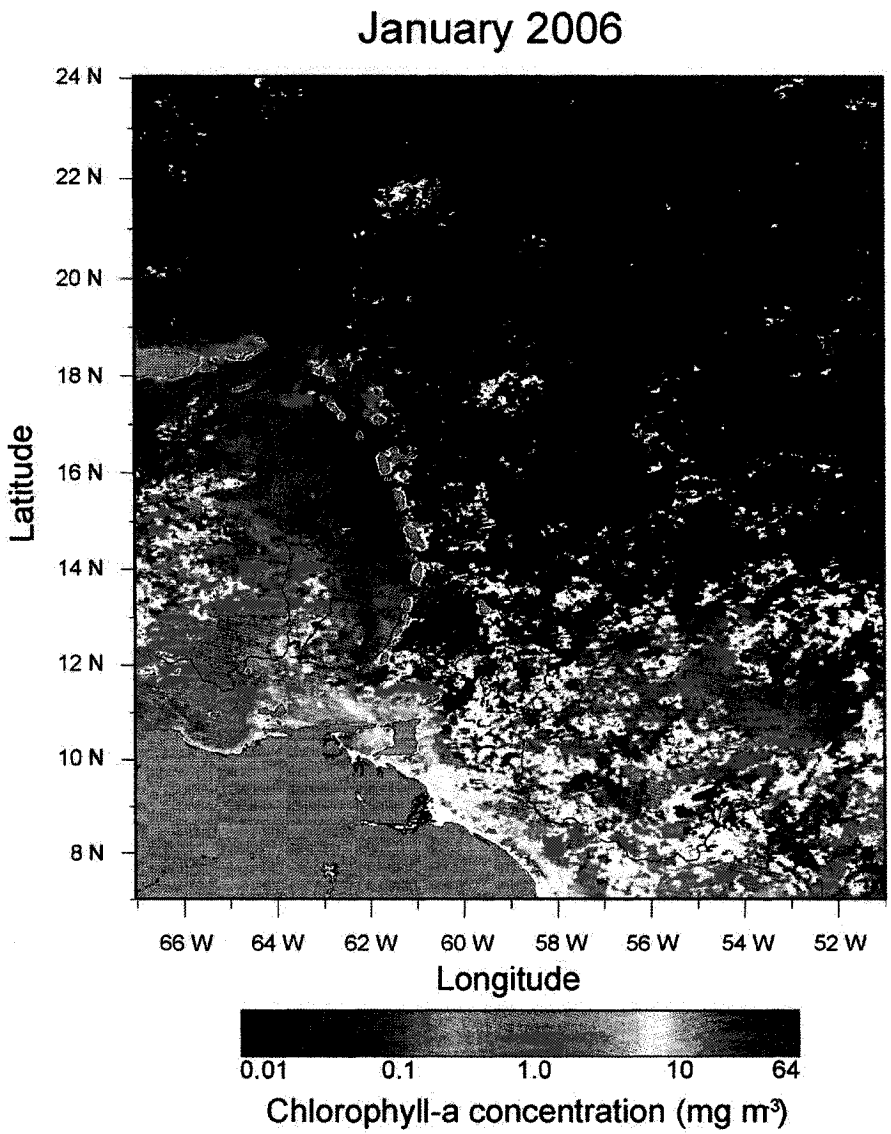

Figure C.1: Monthly composite image of chlorophyll concentration for January 2006 for the LAPE region.

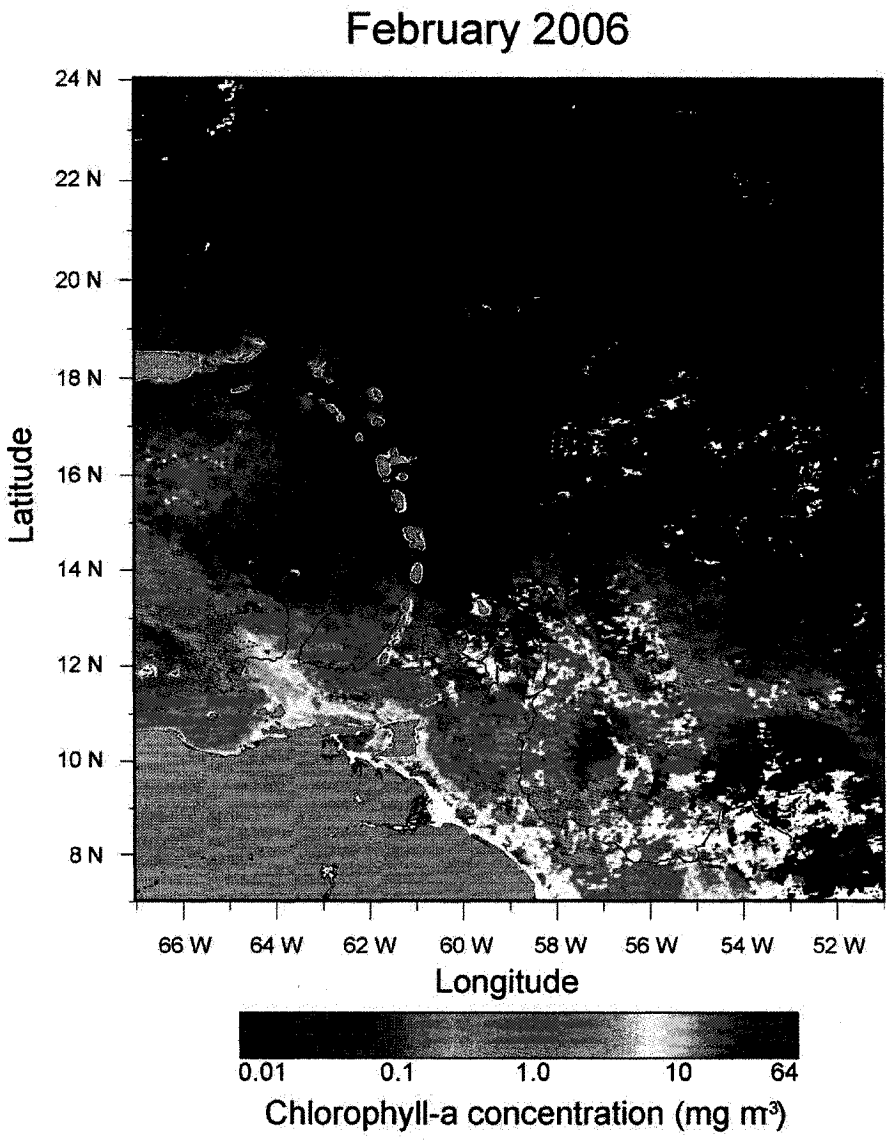

Figure C.2: Monthly composite image of chlorophyll concentration for February 2006 for the LAPE region.

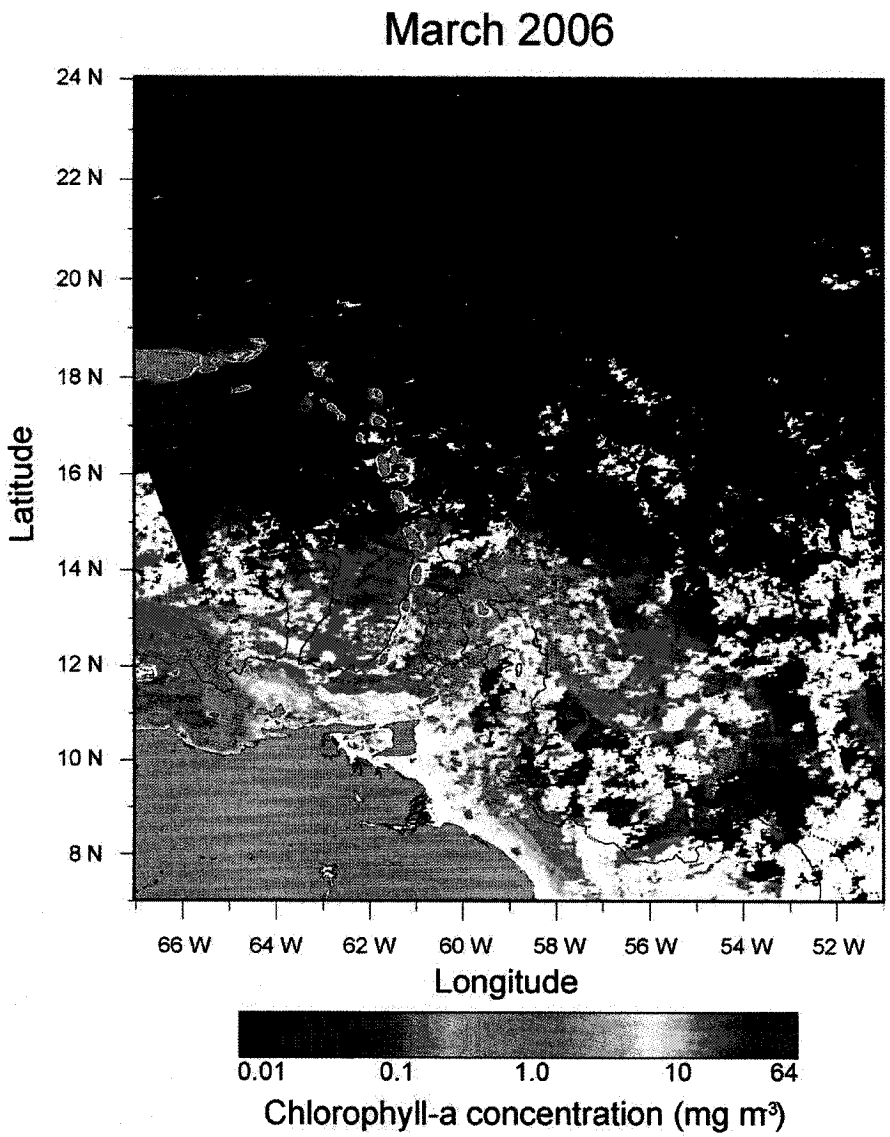

Figure C.3: Monthly composite image of chlorophyll concentration for March 2006 for the LAPE region.

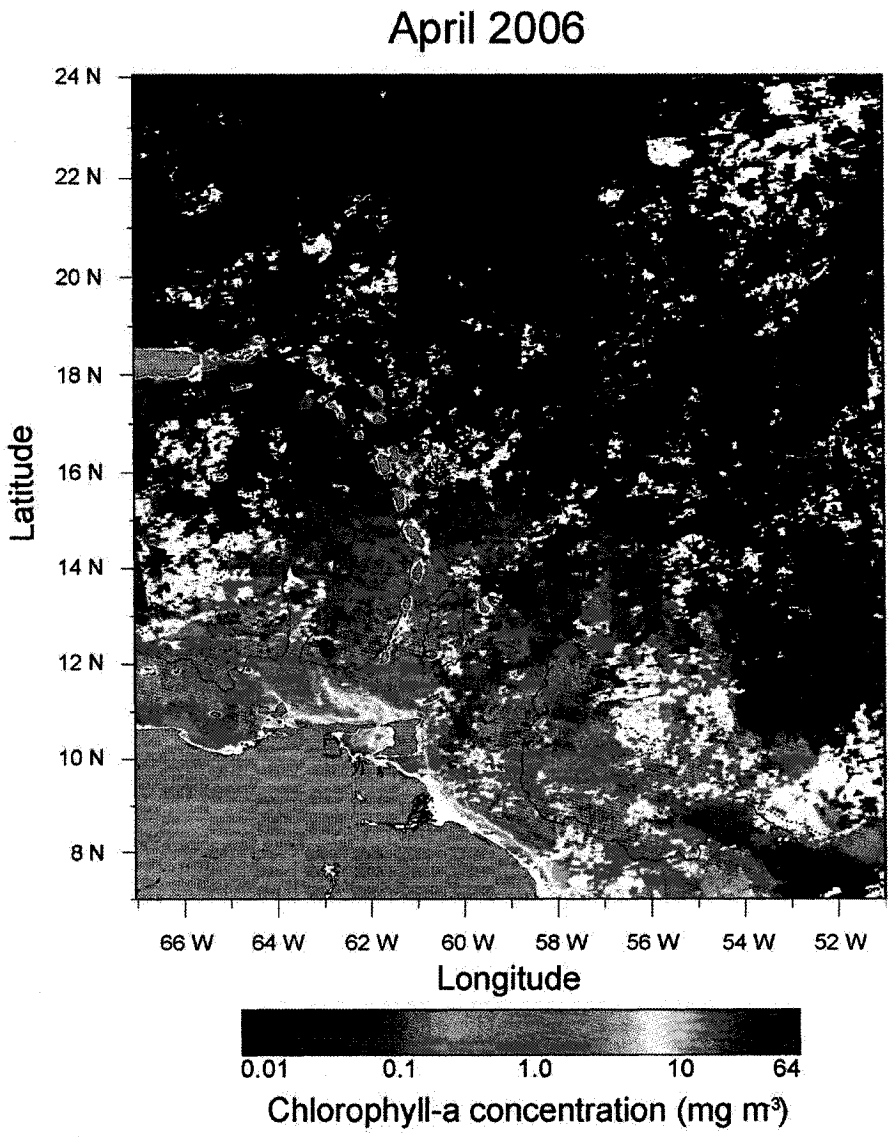

Figure C.4: Monthly composite image of chlorophyll concentration for April 2006 for the LAPE region.

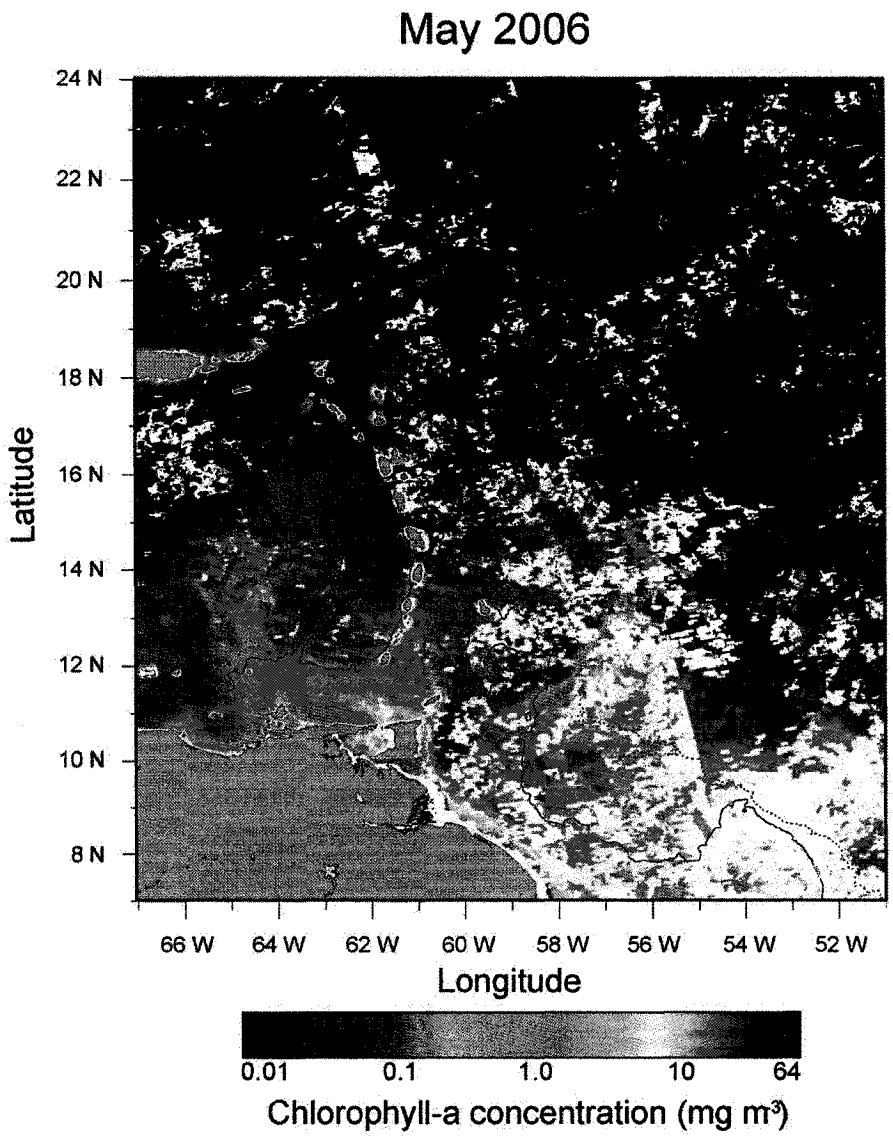

Figure C.5: Monthly composite image of chlorophyll concentration for May 2006 for the LAPE region.

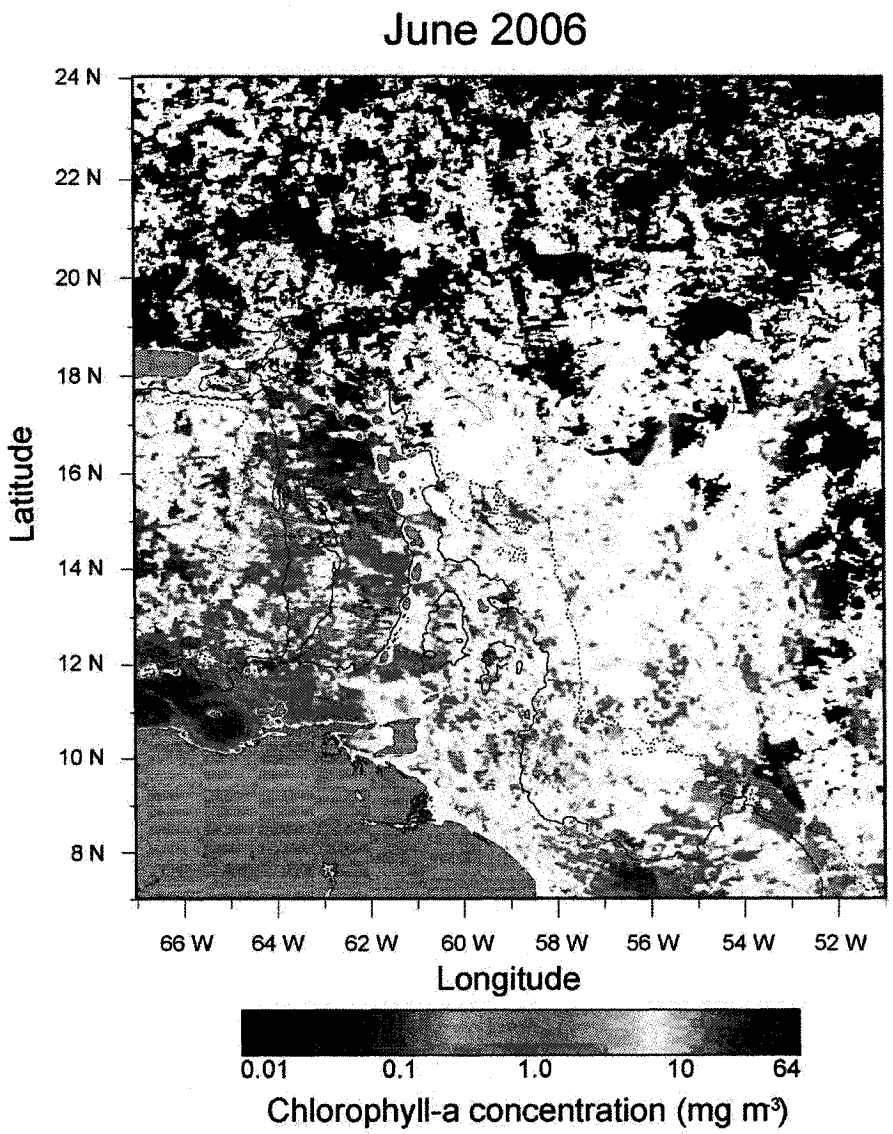

Figure C.6: Monthly composite image of chlorophyll concentration for June 2006 for the LAPE region.

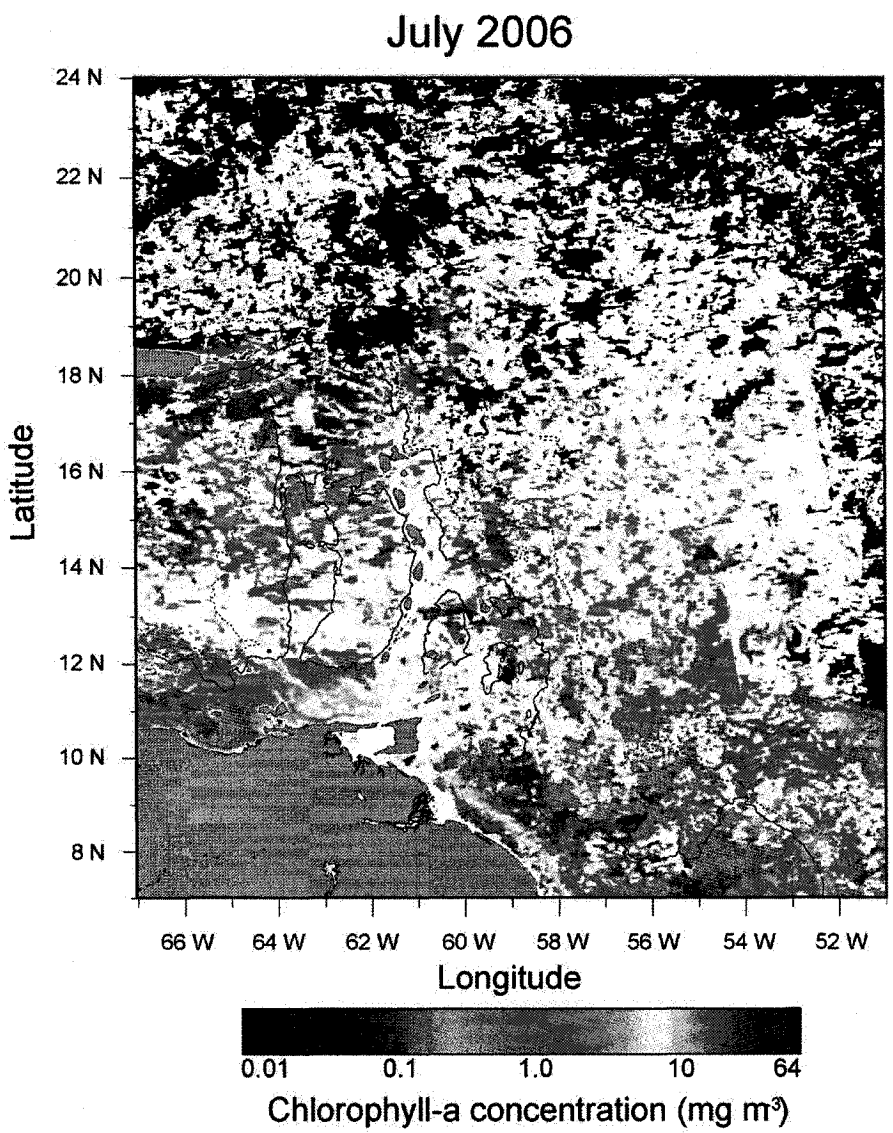

Figure C.7: Monthly composite image of chlorophyll concentration for July 2006 for the LAPE region.

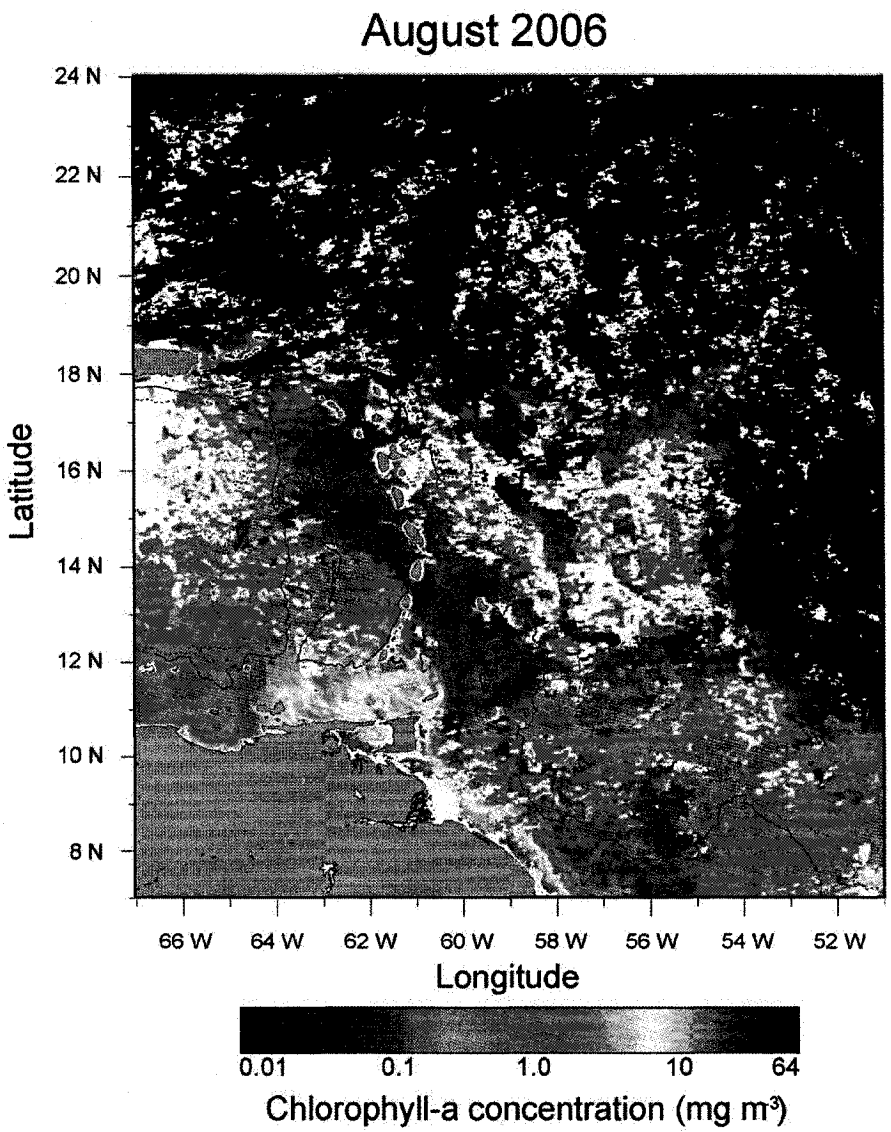

Figure C.8: Monthly composite image of chlorophyll concentration for August 2006 for the LAPE region.

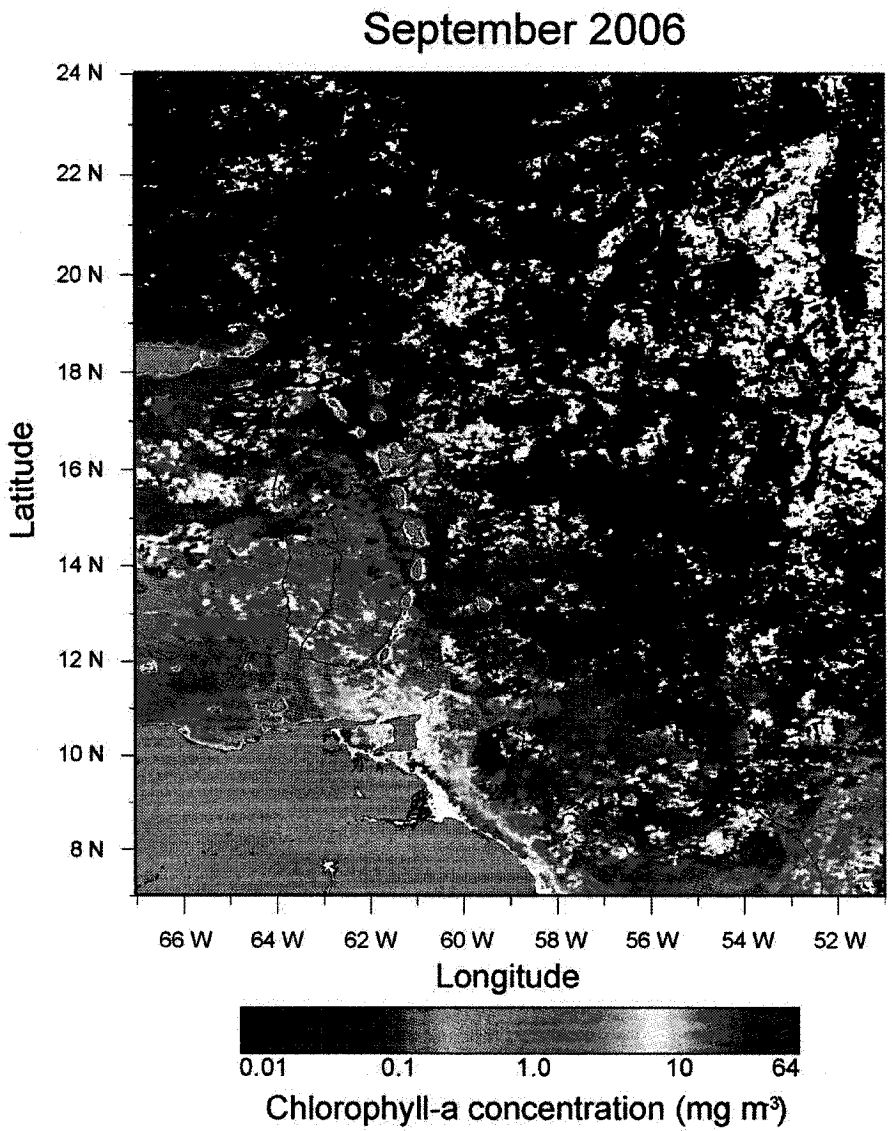

Figure C.9: Monthly composite image of chlorophyll concentration for September 2006 for the LAPE region.

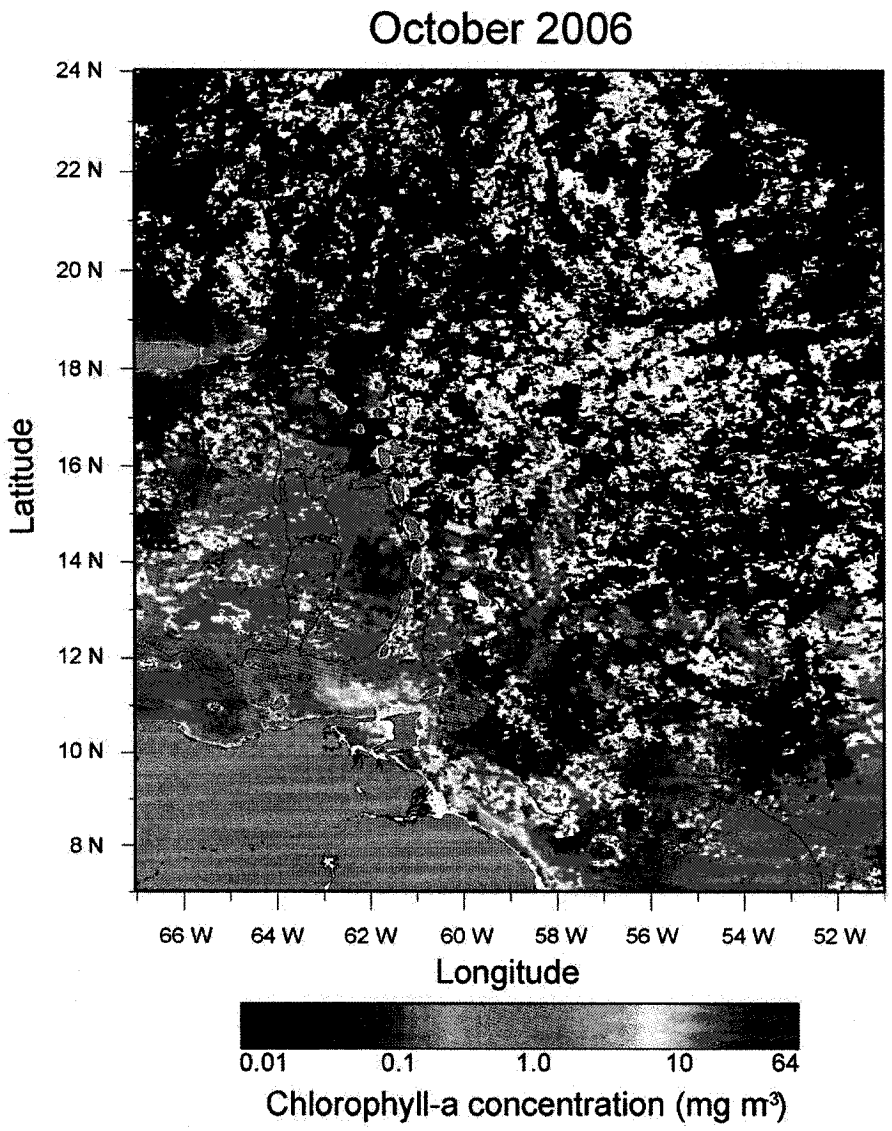

Figure C.10: Monthly composite image of chlorophyll concentration for October 2006 for the LAPE region.

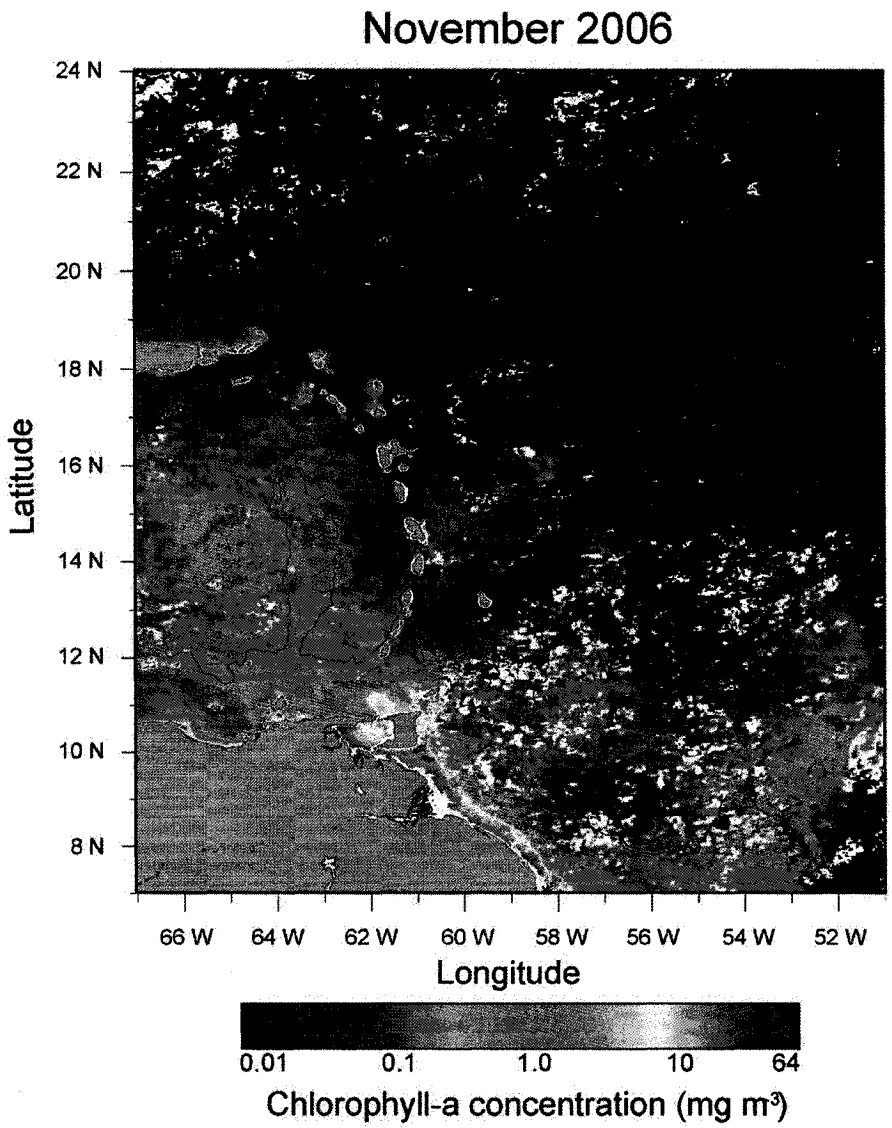

Figure C.11: Monthly composite image of chlorophyll concentration for November 2006 for the LAPE region.

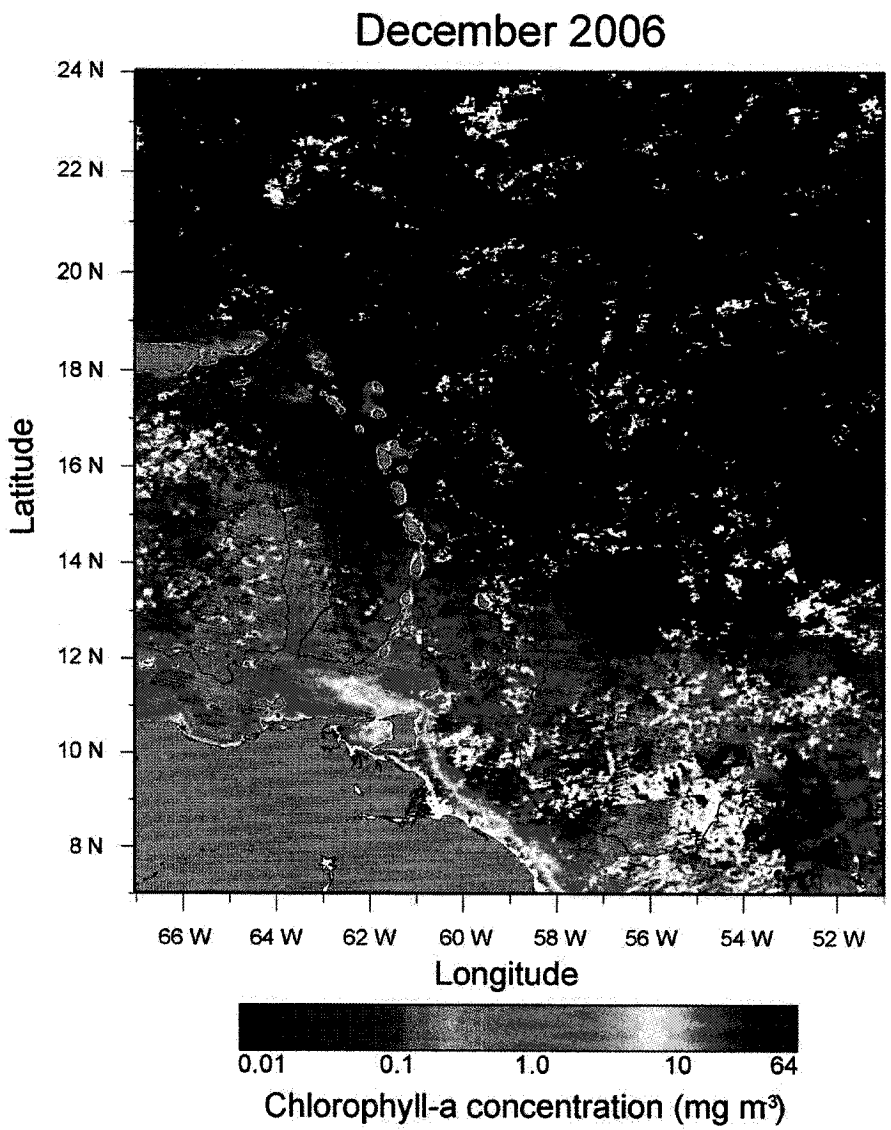

Figure C.12: Monthly composite image of chlorophyll concentration for December 2006 for the LAPE region.

Appendix D

PIXEL DEPTH FOR MODIS MONTHLY COMPOSITE IMAGES OF CHLOROPHYLL CONCENTRATION FOR THE LAPE REGION

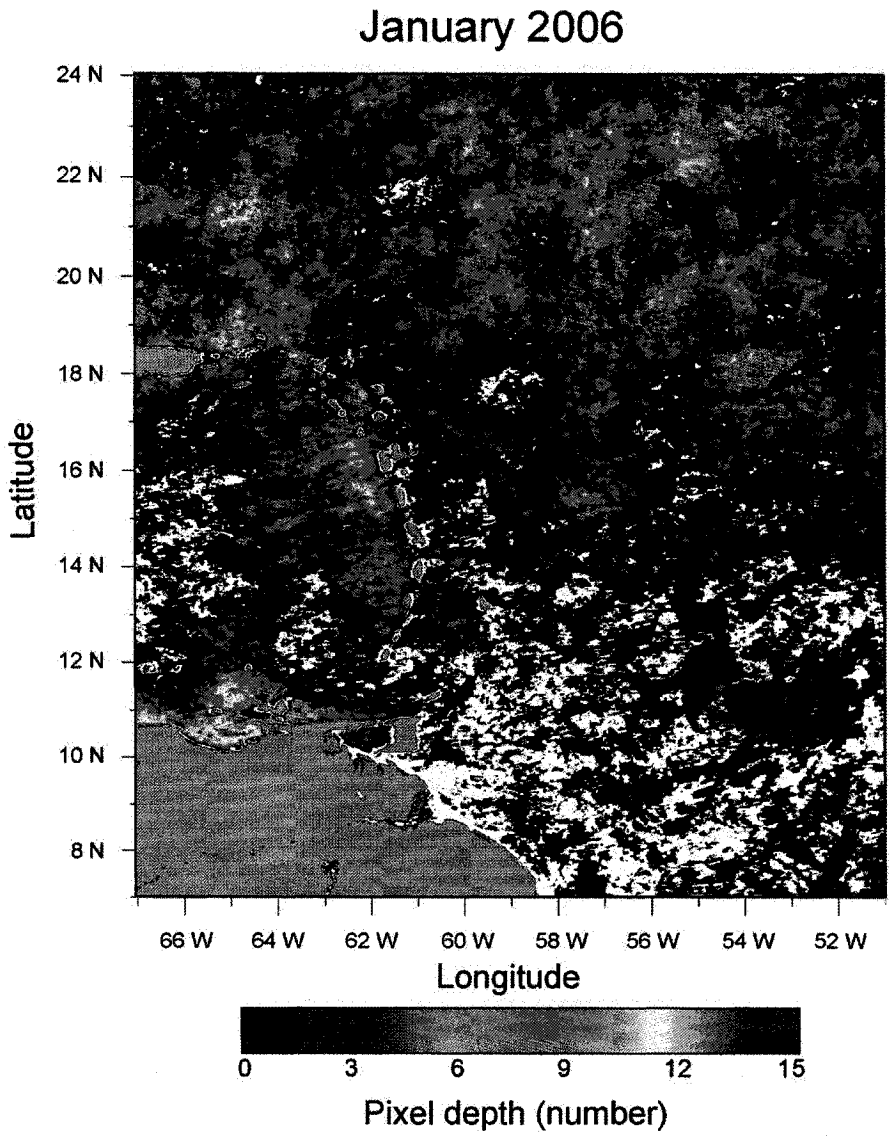

Figure D.1: Pixel depth for monthly composite image of chlorophyll concentration for January 2006 for the LAPE region.

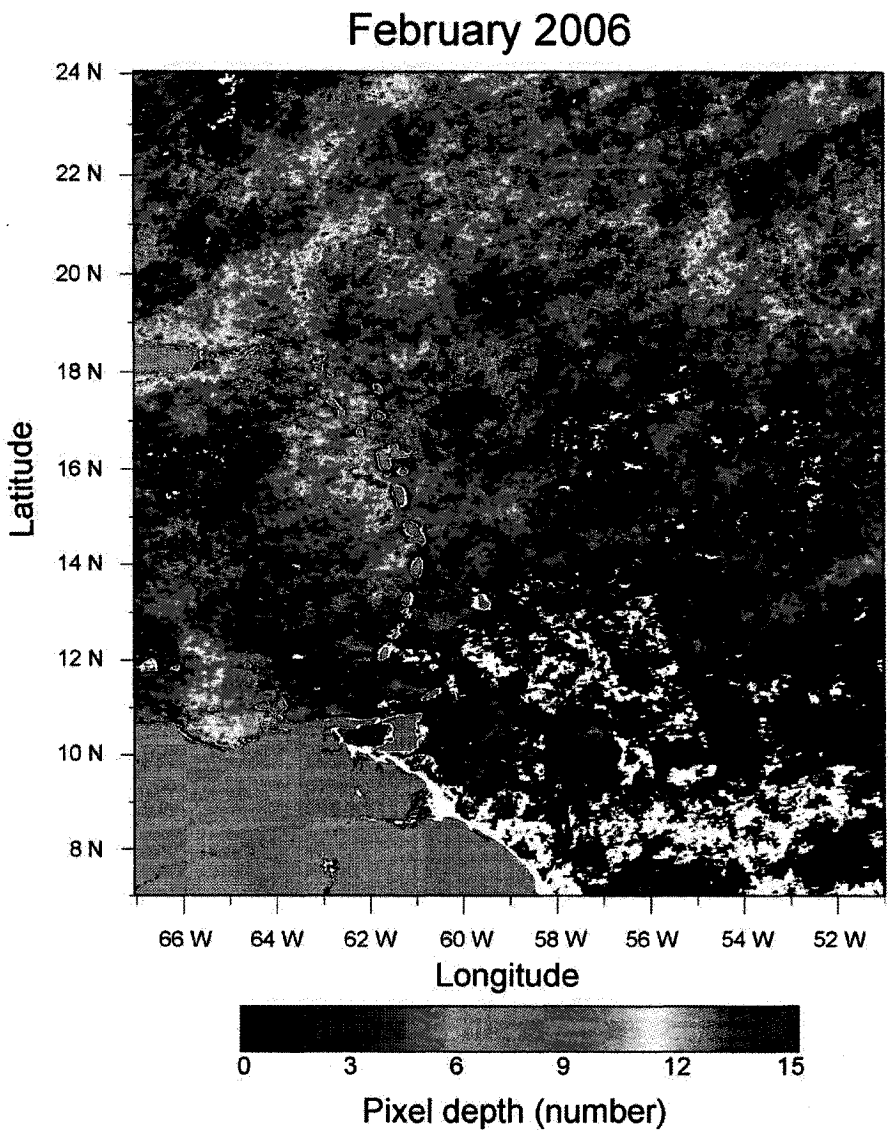

Figure D.2: Pixel depth for monthly composite image of chlorophyll concentration for February 2006 for the LAPE region.

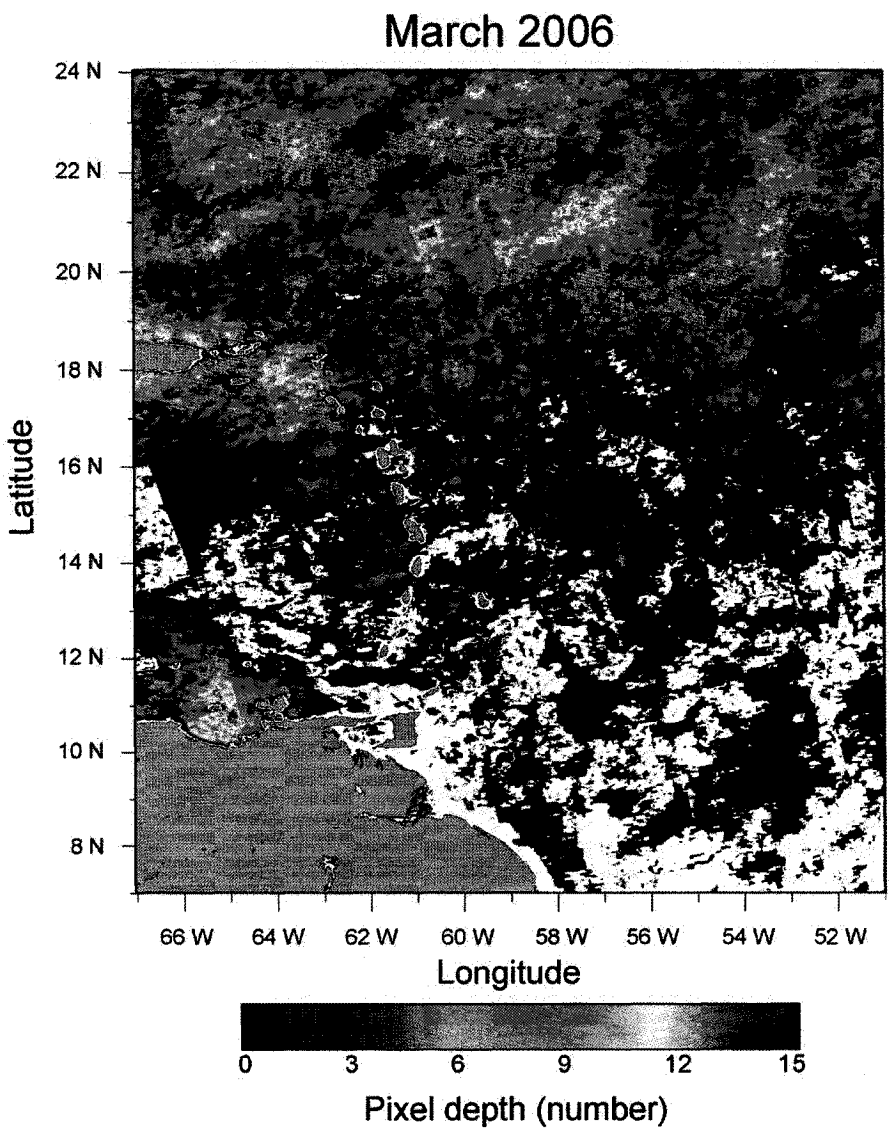

Figure D.3: Pixel depth for monthly composite image of chlorophyll concentration for March 2006 for the LAPE region.

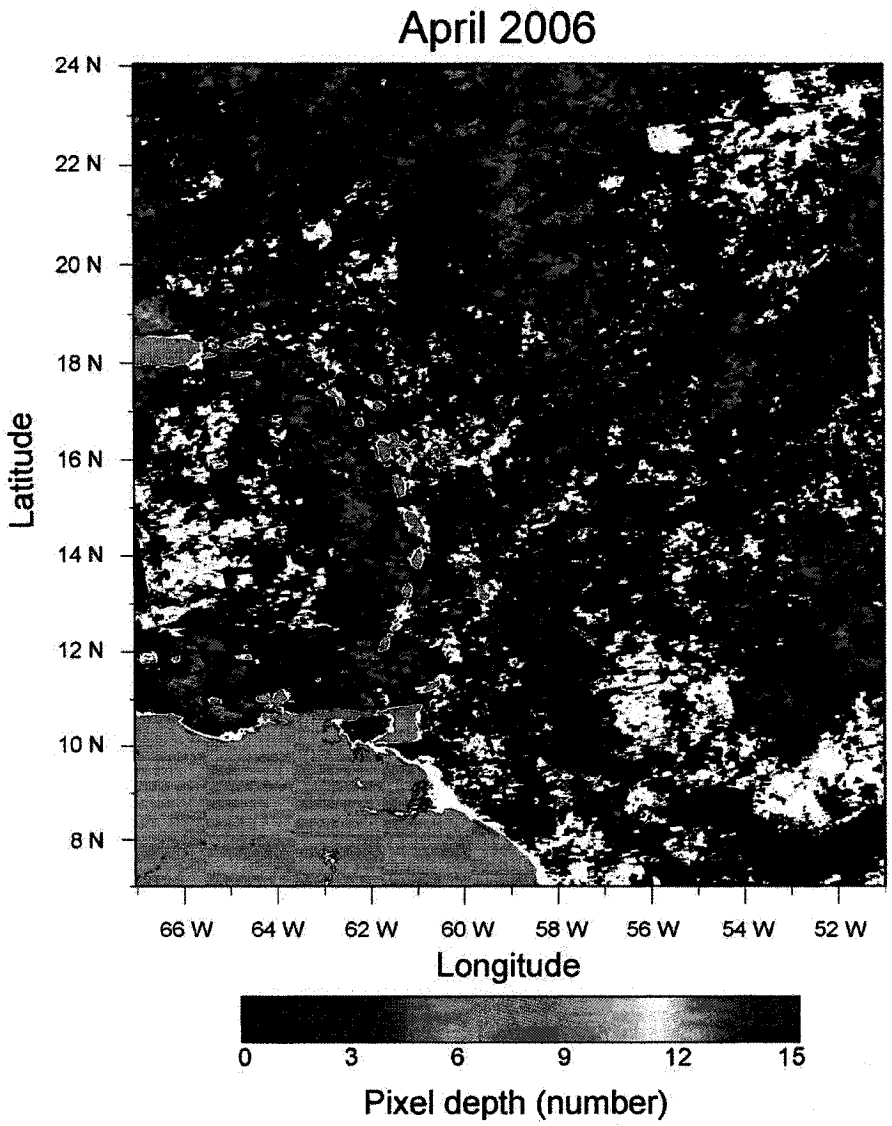

Figure D.4: Pixel depth for monthly composite image of chlorophyll concentration for April 2006 for the LAPE region.

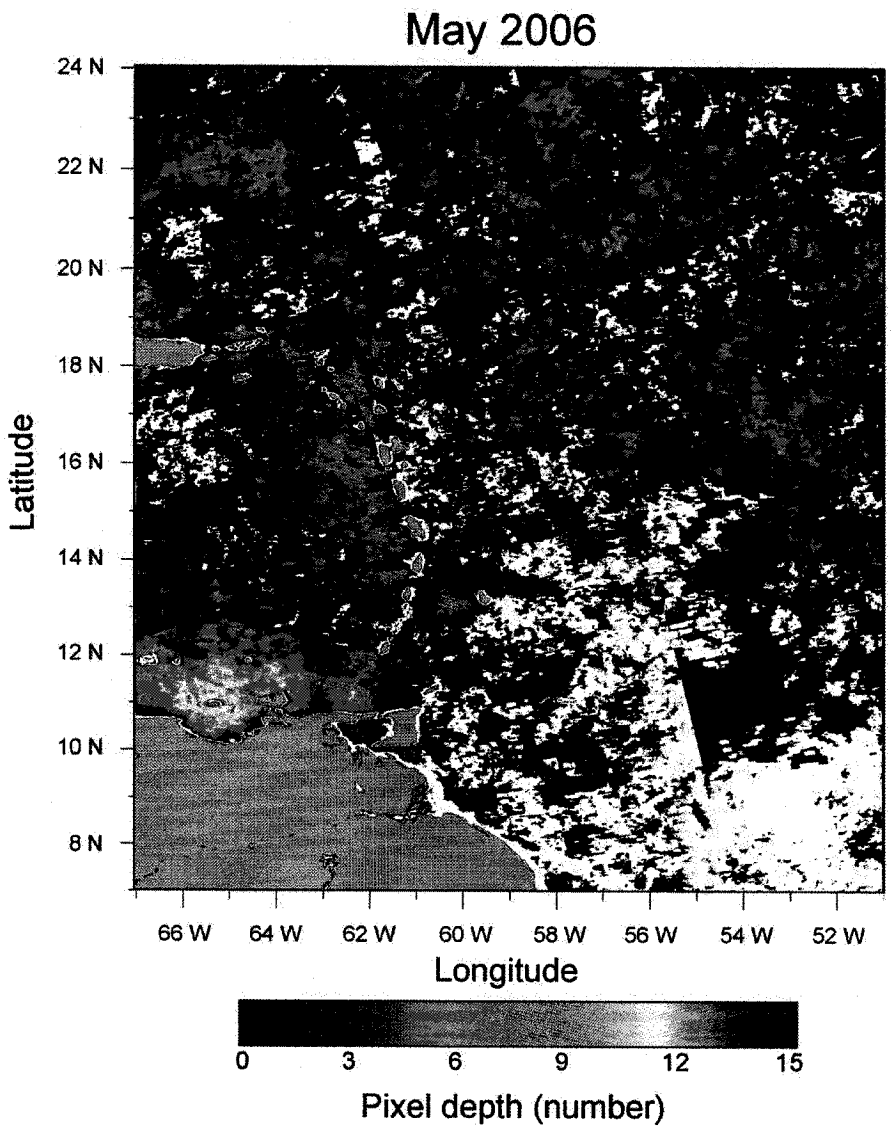

Figure D.5: Pixel depth for monthly composite image of chlorophyll concentration for May 2006 for the LAPE region.

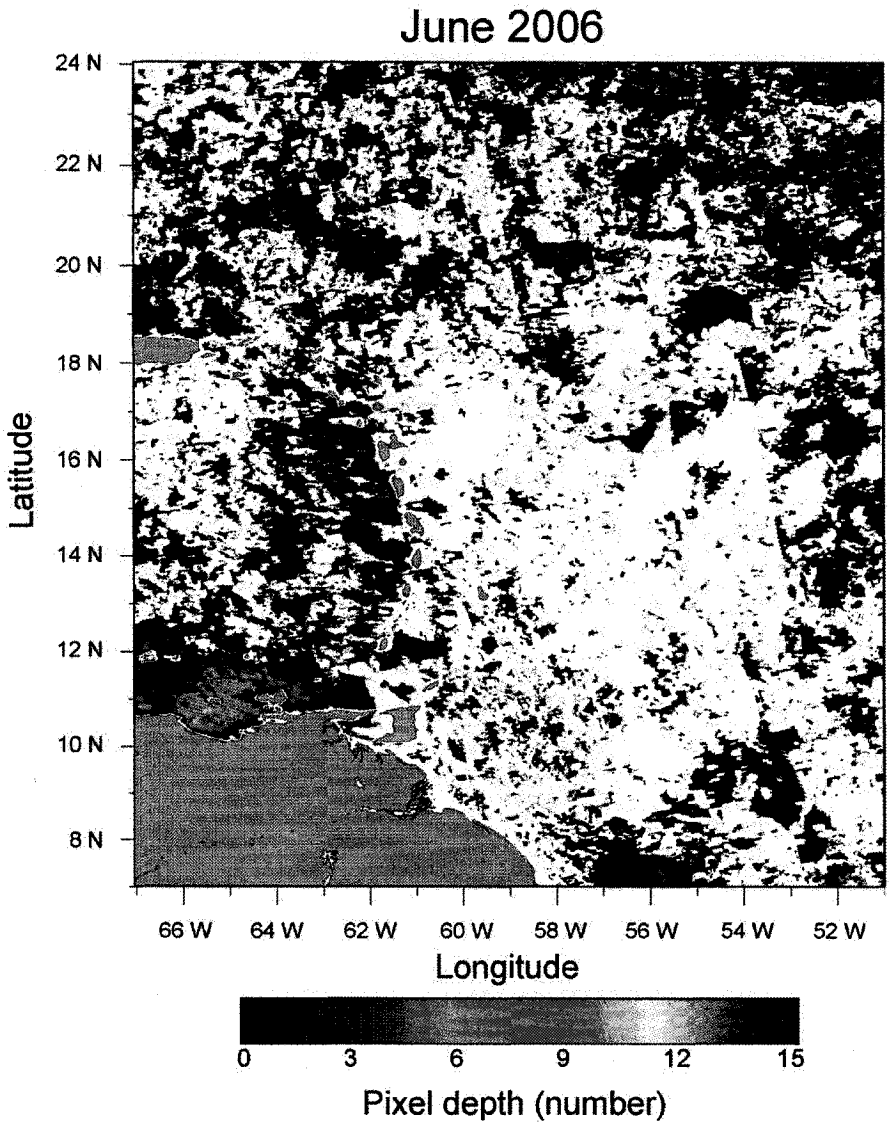

Figure D.6: Pixel depth for monthly composite image of chlorophyll concentration for June 2006 for the LAPE region.

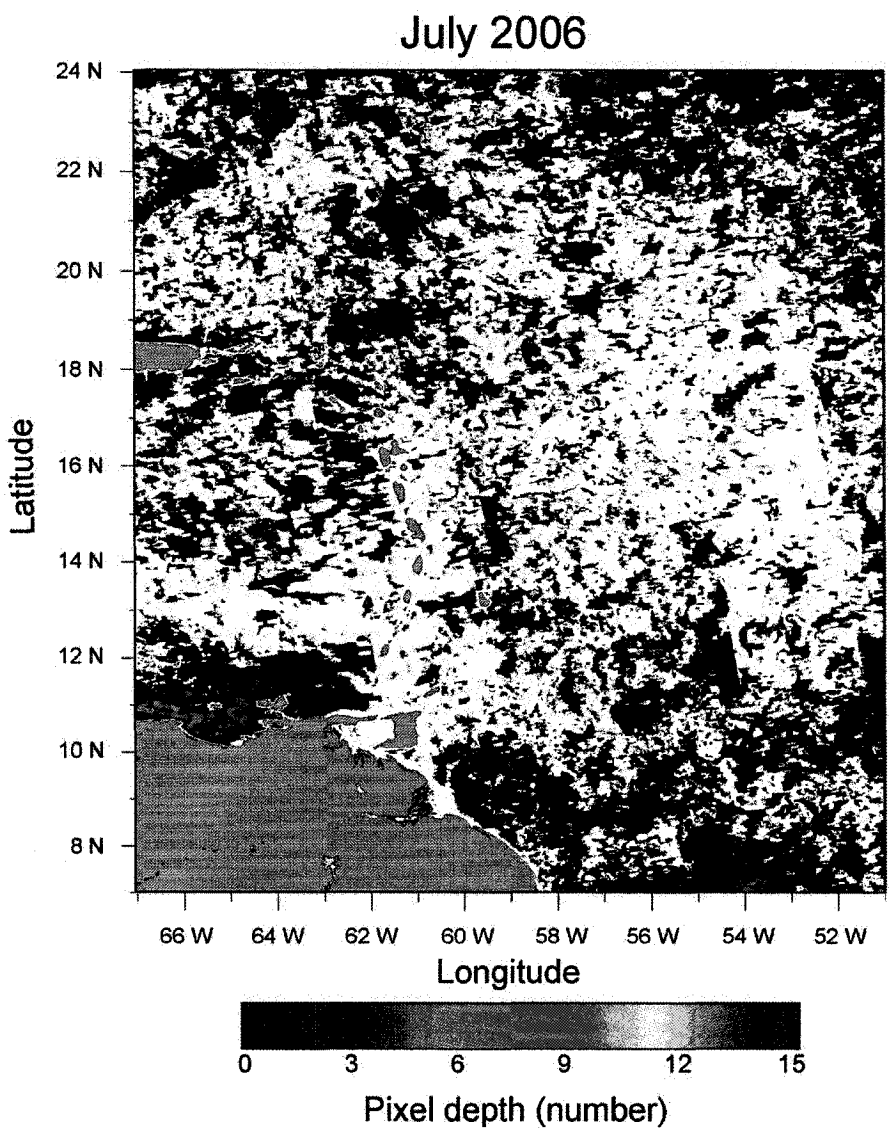

Figure D.7: Pixel depth for monthly composite image of chlorophyll concentration for July 2006 for the LAPE region.

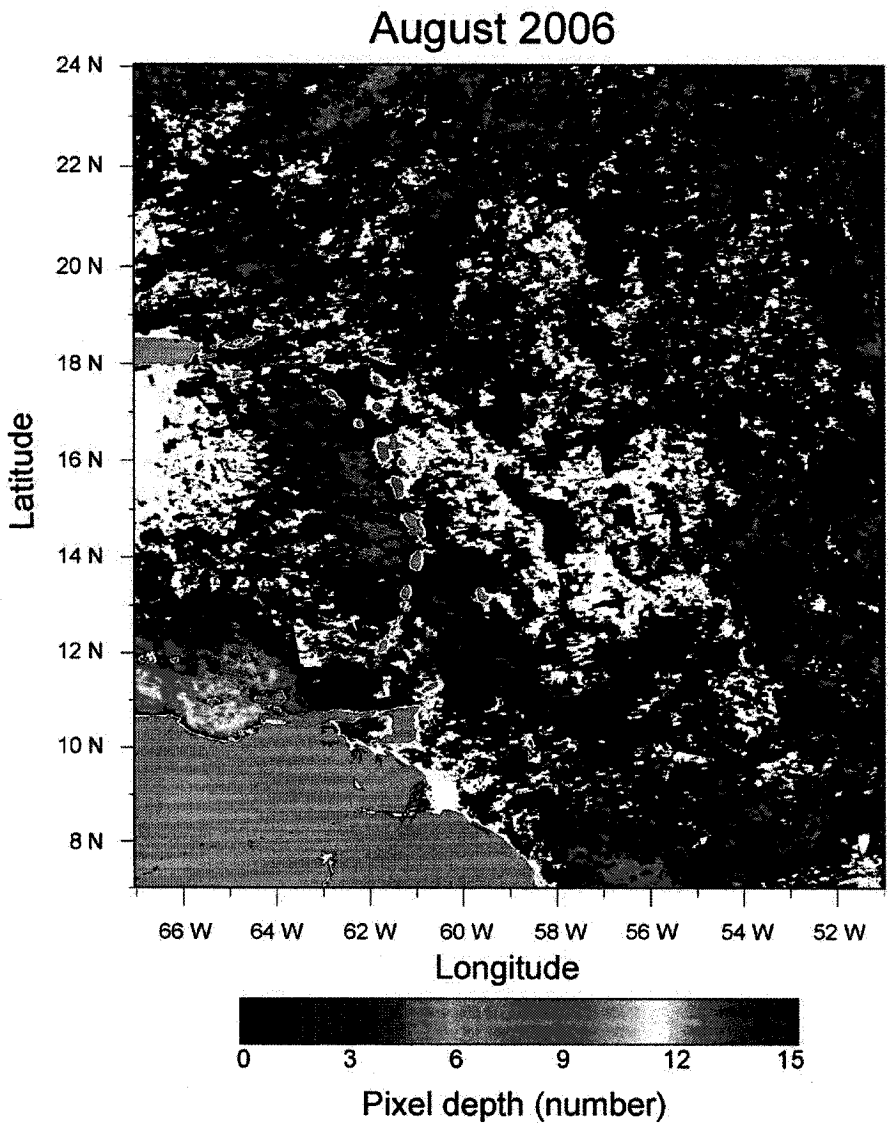

Figure D.8: Pixel depth for monthly composite image of chlorophyll concentration for August 2006 for the LAPE region.

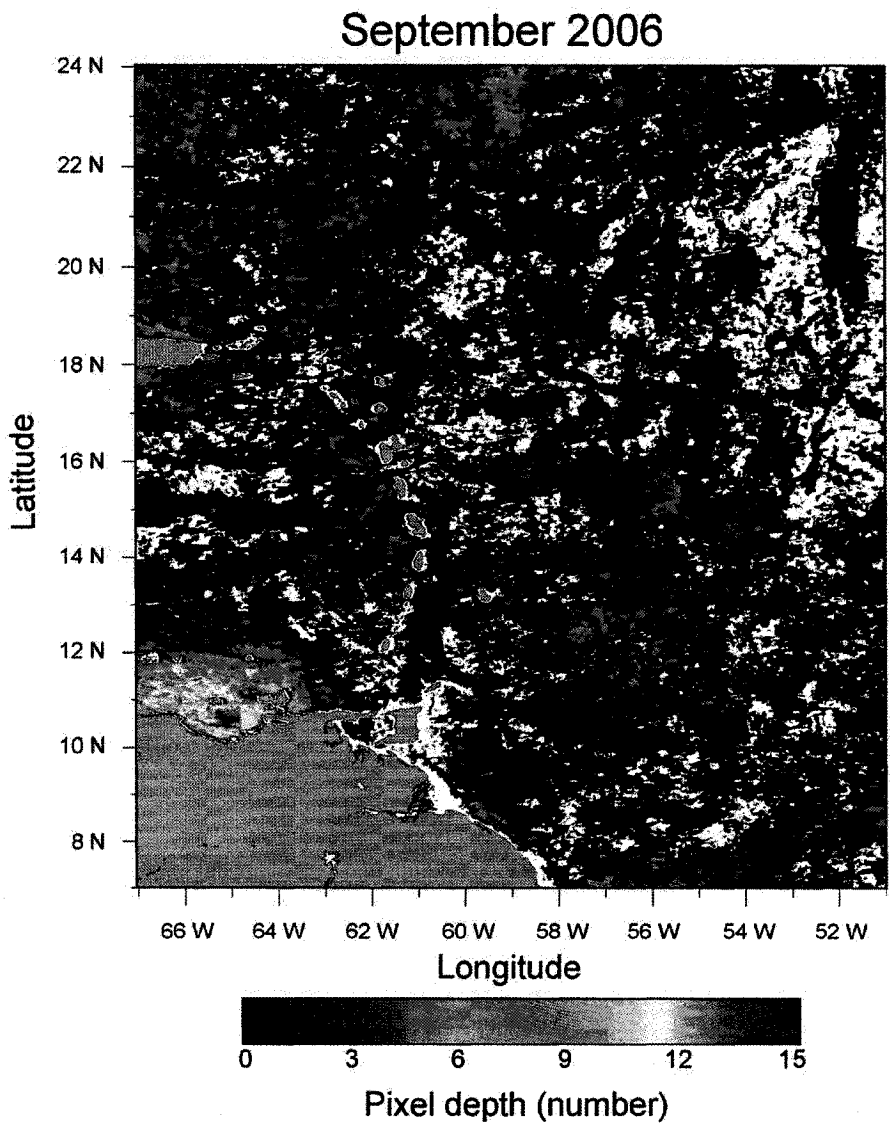

Figure D.9: Pixel depth for monthly composite image of chlorophyll concentration for September 2006 for the LAPE region.

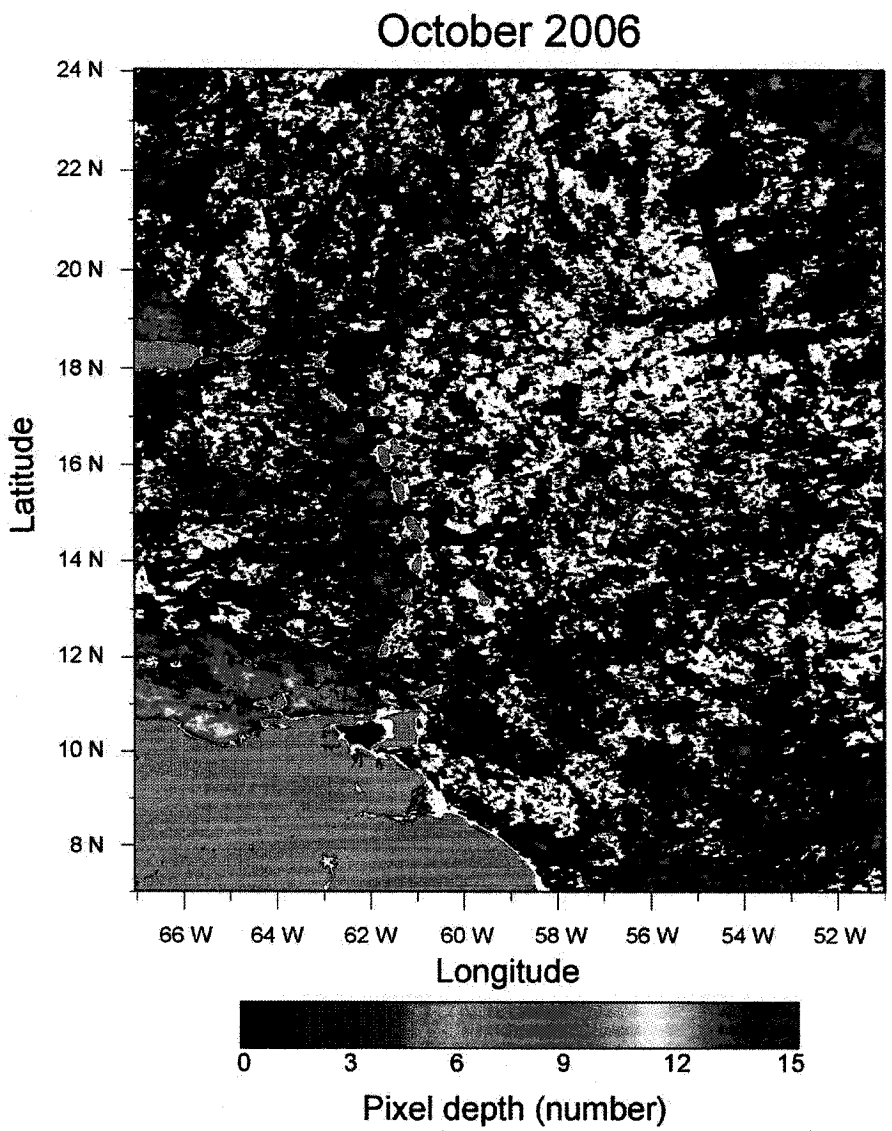

Figure D.10: Pixel depth for monthly composite image of chlorophyll concentration for October 2006 for the LAPE region.

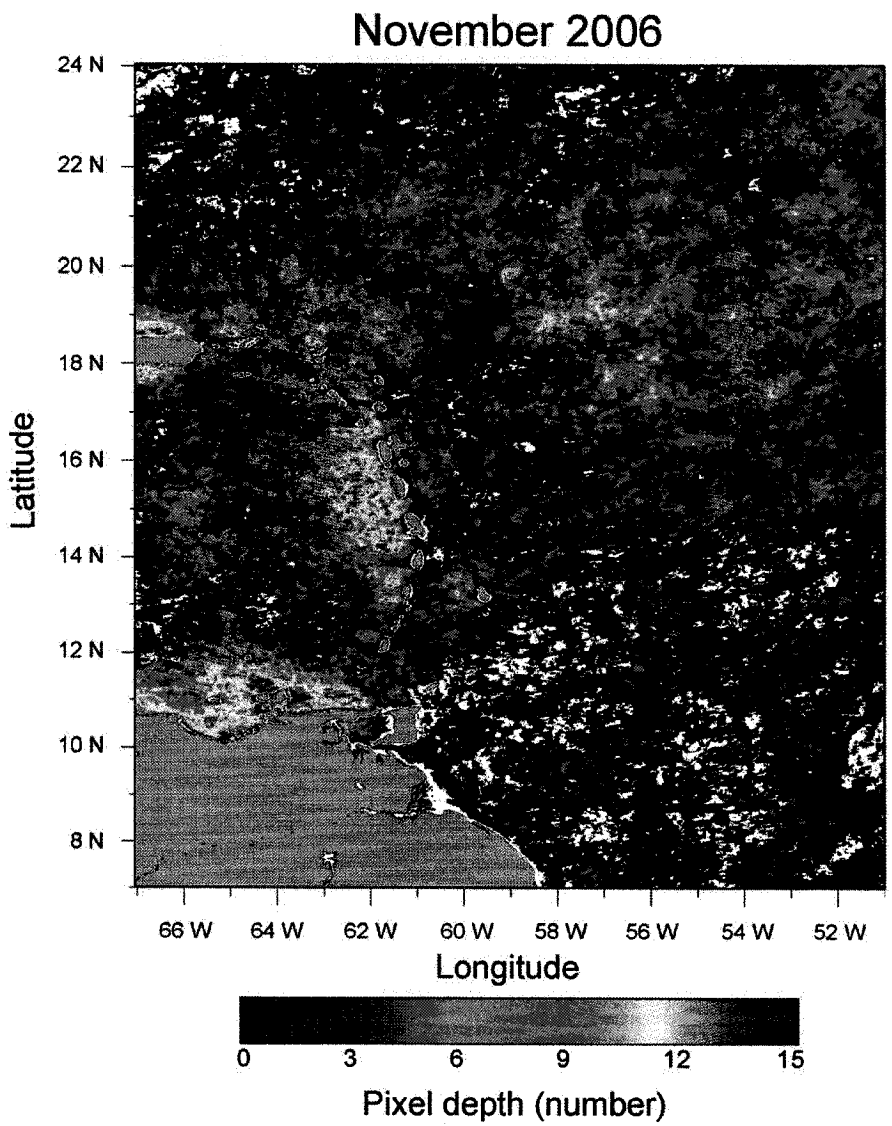

Figure D.11: Pixel depth for monthly composite image of chlorophyll concentration for November 2006 for the LAPE region.

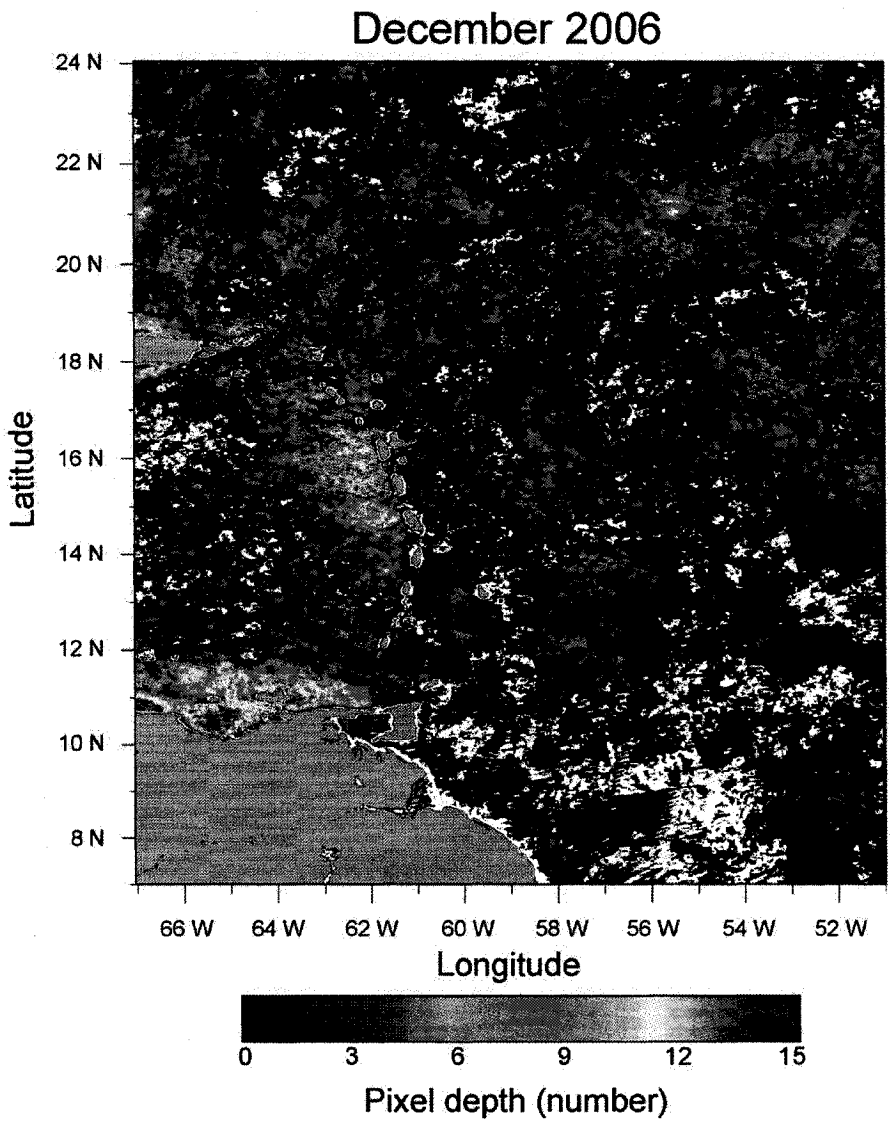

Figure D.12: Pixel depth for monthly composite image of chlorophyll concentration for December 2006 for the LAPE region.

Appendix E

MONTHLY COMPOSITE IMAGES OF SEA-SURFACE TEMPERATURE FROM MODIS FOR THE LAPE REGION

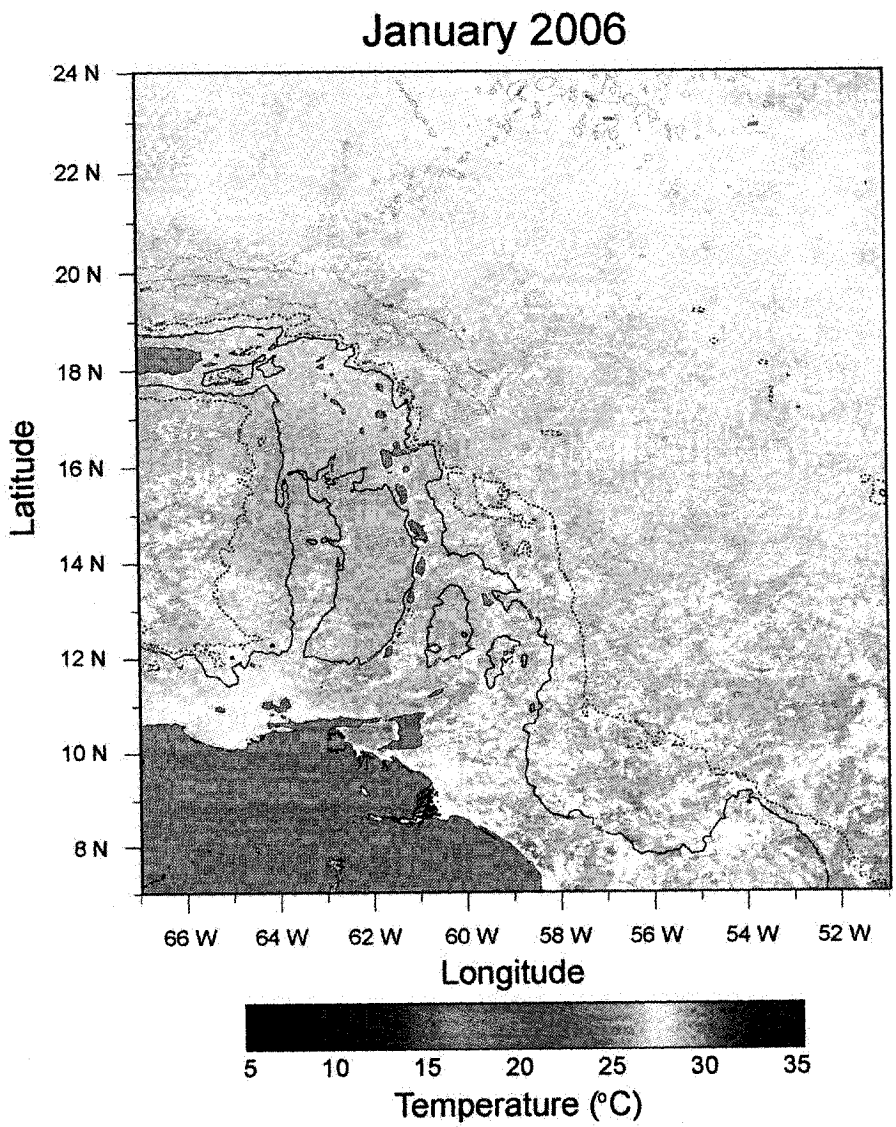

Figure E.1: Monthly composite image of sea surface temperature for January 2006 for the LAPE region.

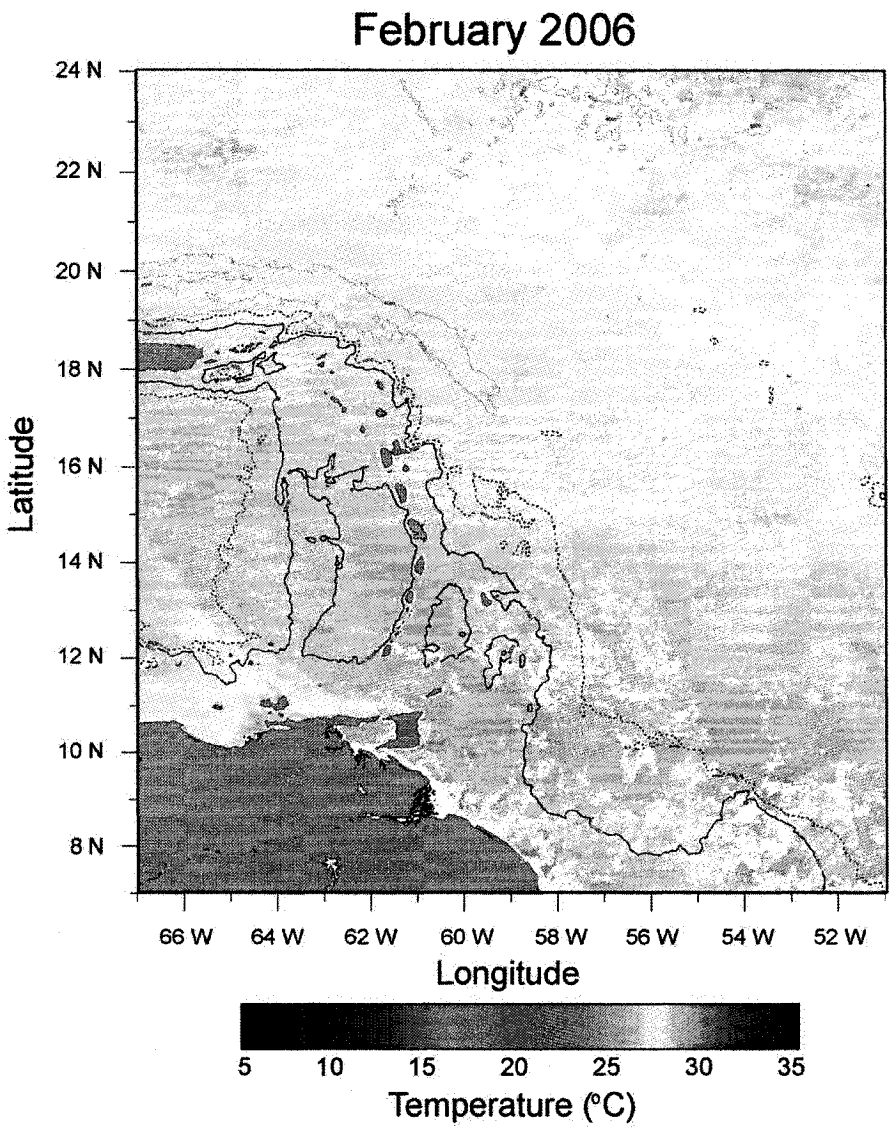

Figure E.2: Monthly composite image of sea surface temperature for February 2006 for the LAPE region.

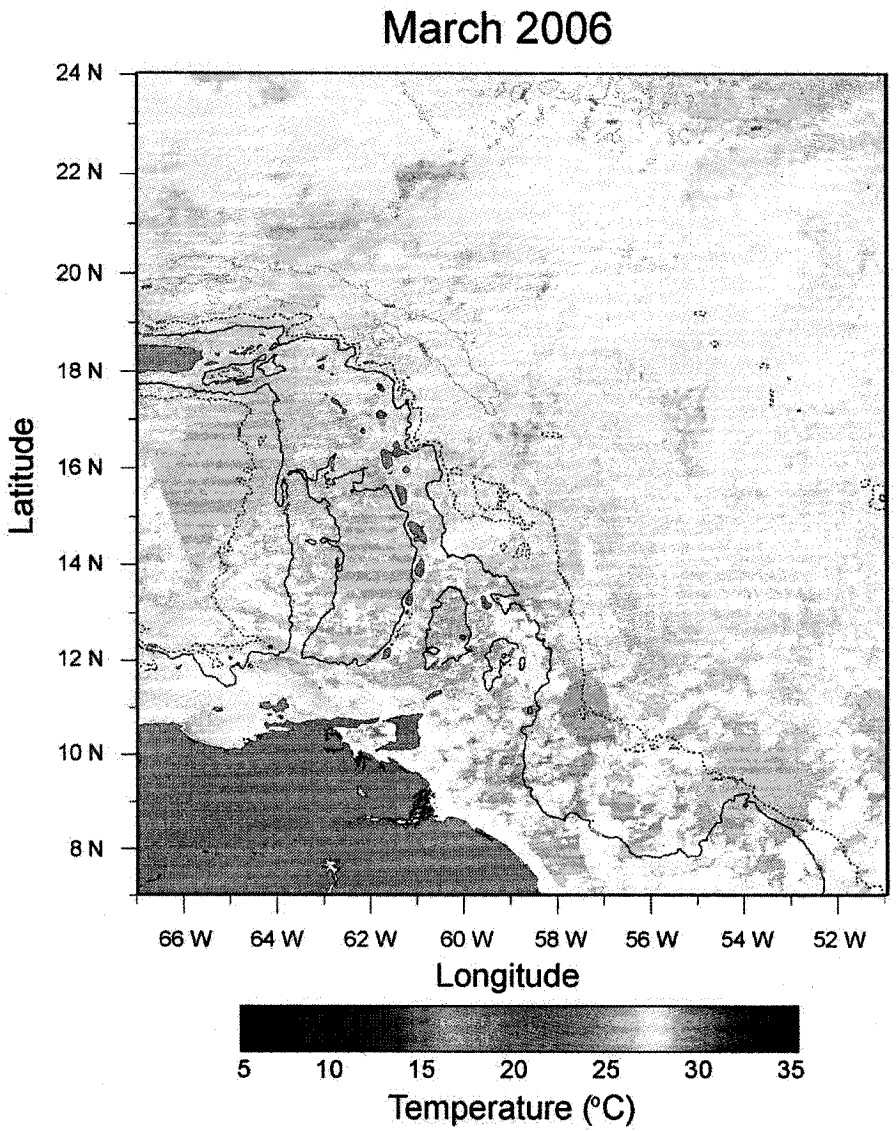

Figure E.3: Monthly composite image of sea surface temperature for March 2006 for the LAPE region.

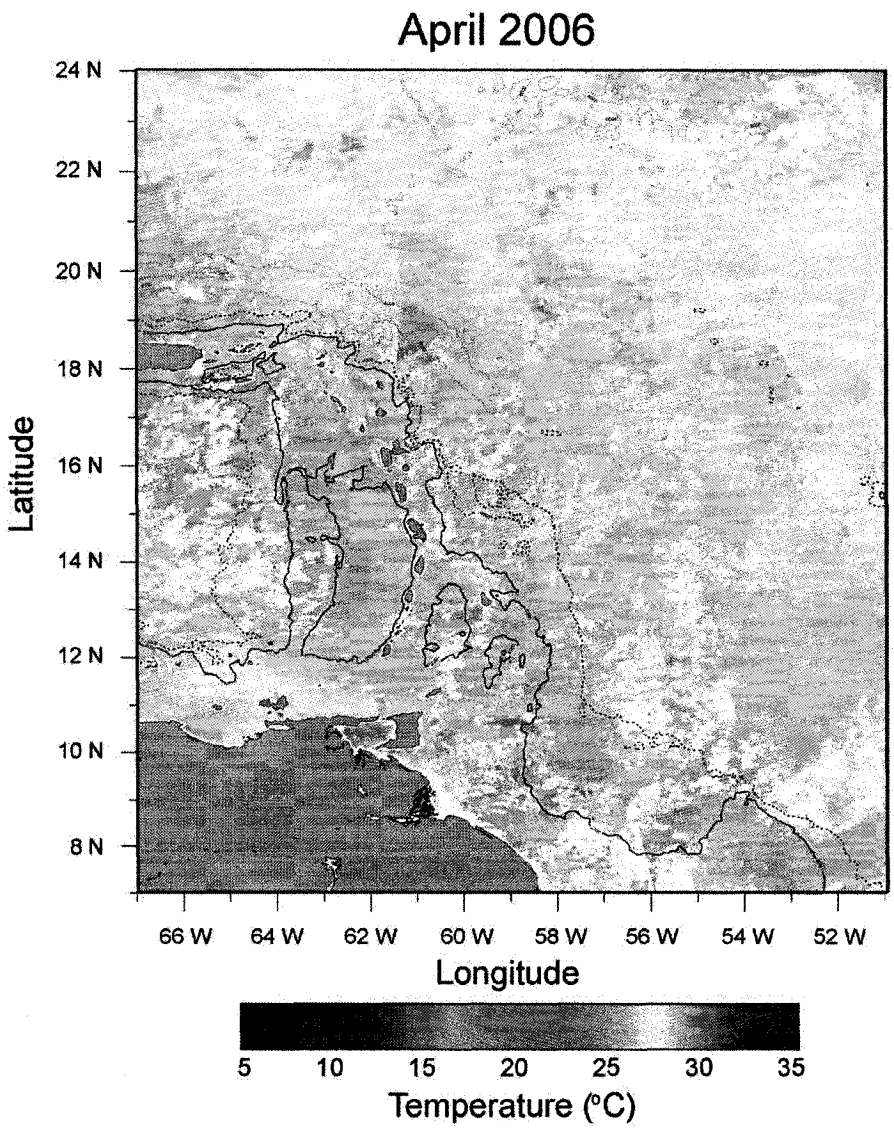

Figure E.4: Monthly composite image of sea surface temperature for April 2006 for the LAPE region.

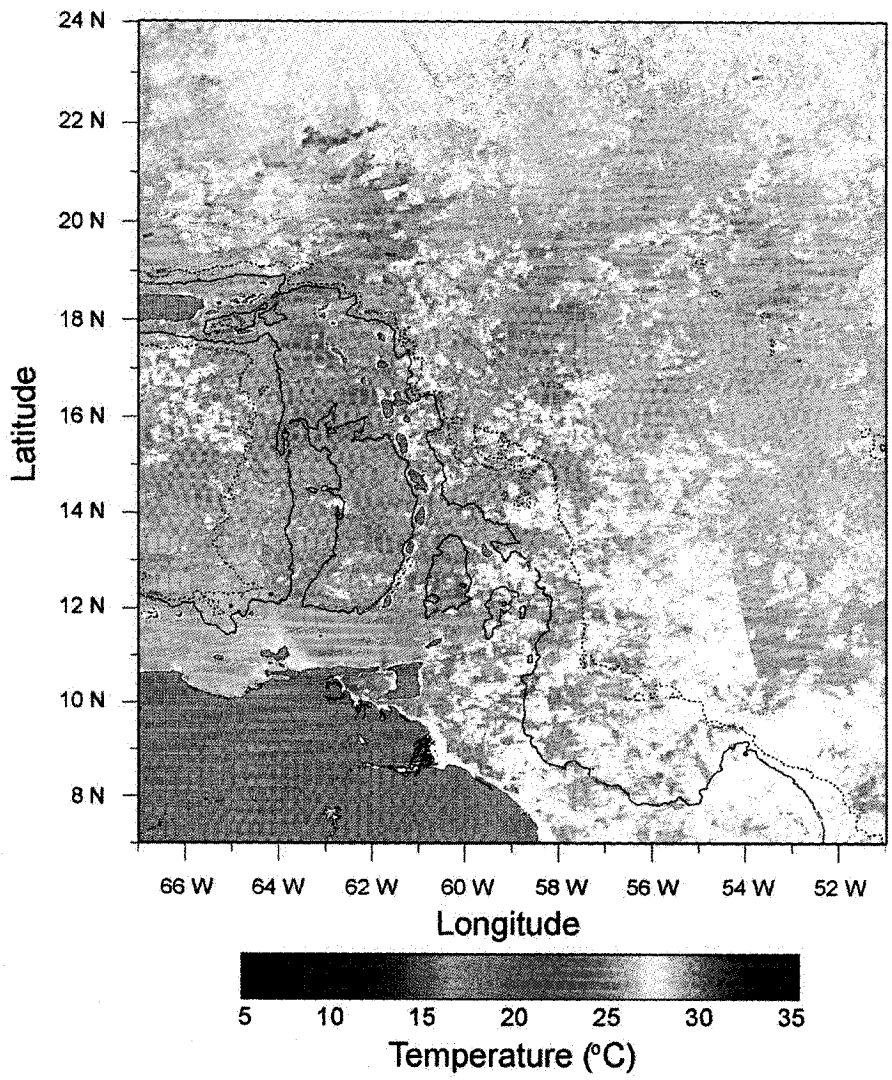

Figure E.5: Monthly composite image of sea surface temperature for May 2006 for the LAPE region.

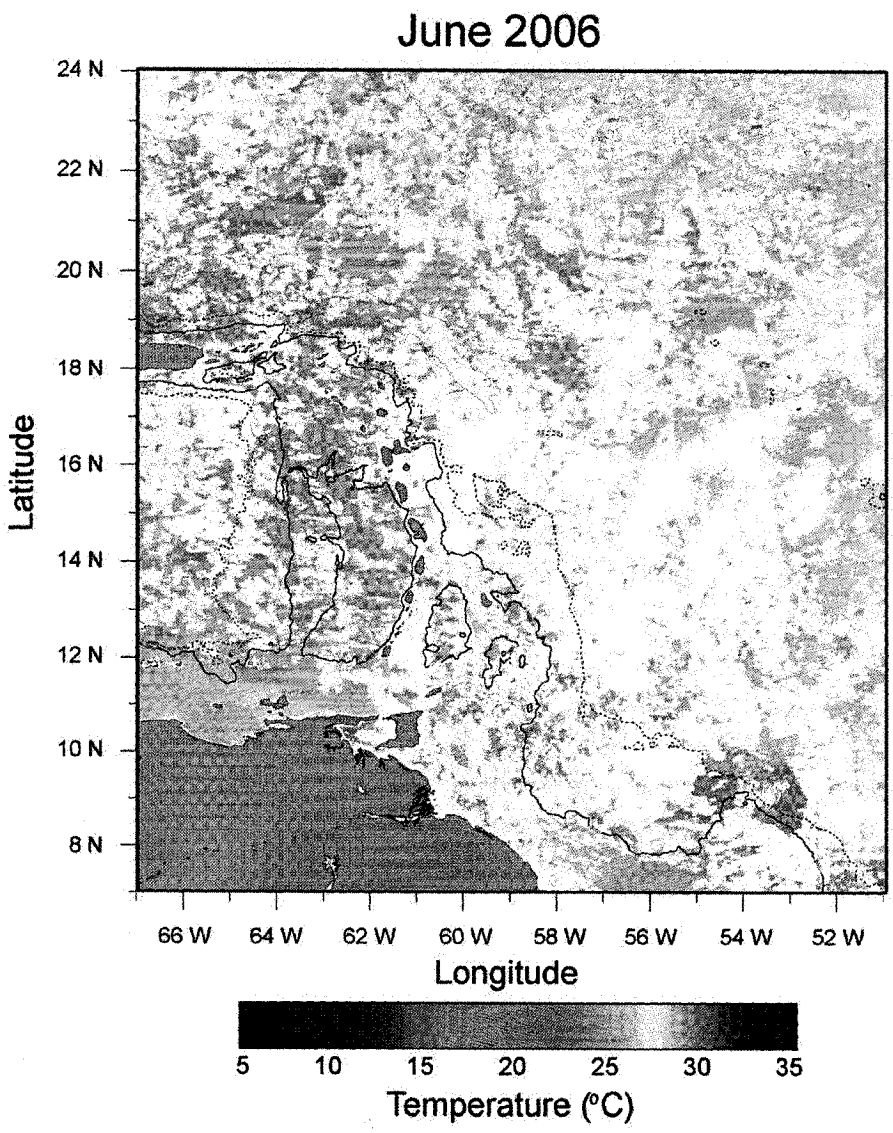

Figure E.6: Monthly composite image of sea surface temperature for June 2006 for the LAPE region.

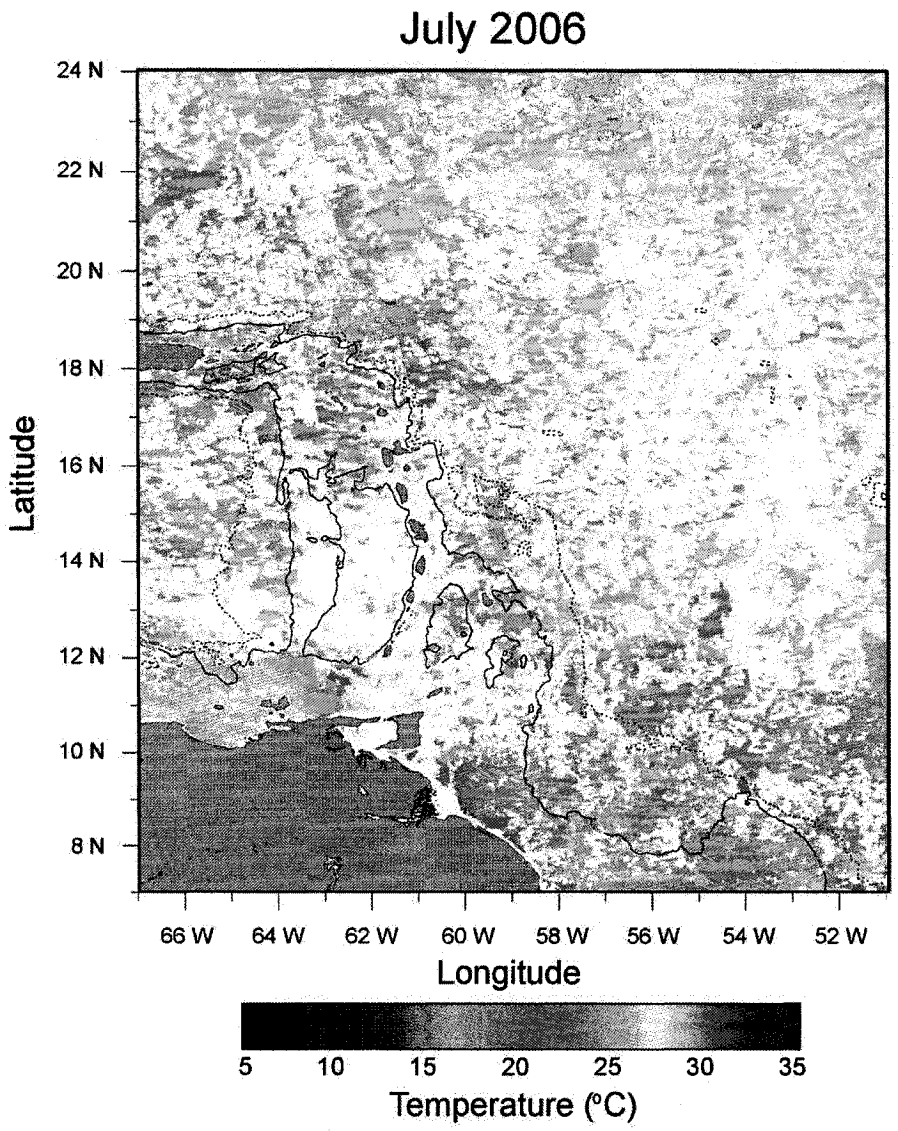

Figure E.7: Monthly composite image of sea surface temperature for July 2006 for the LAPE region.

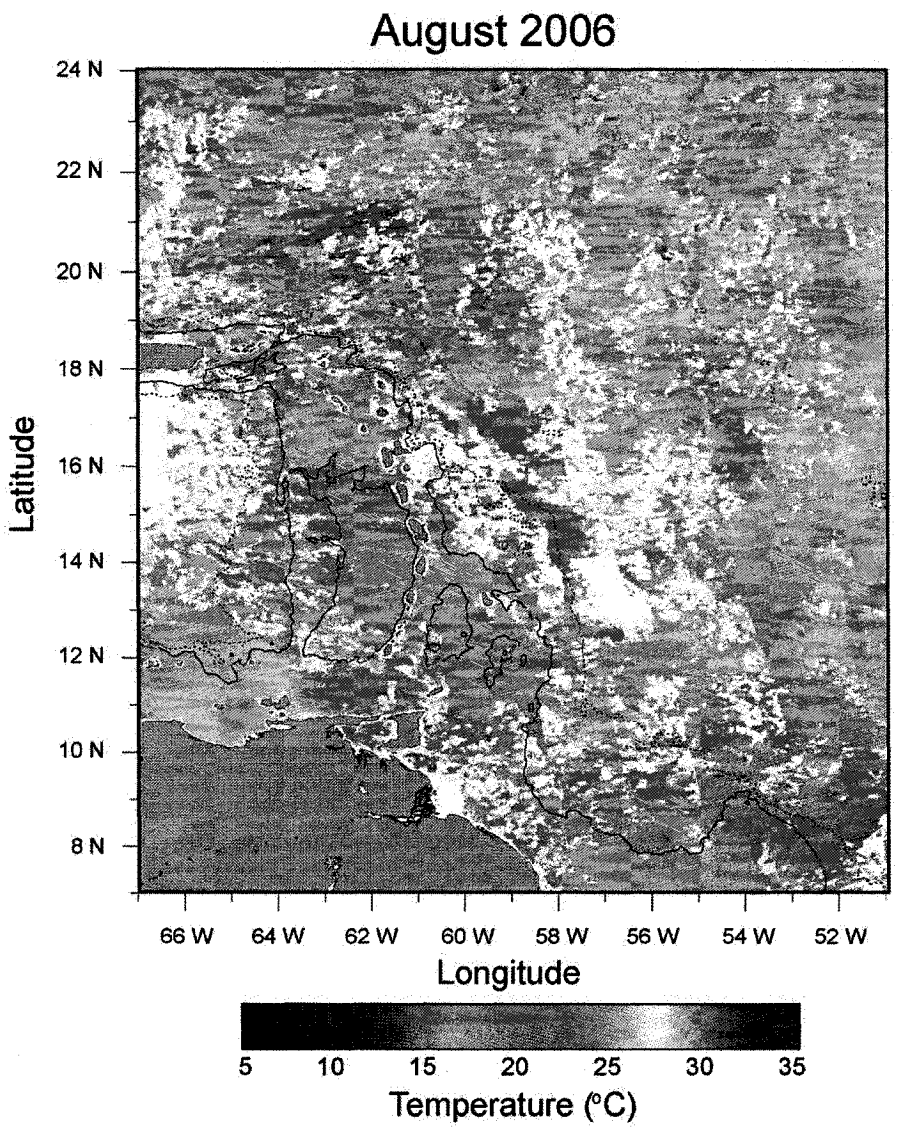

Figure E.8: Monthly composite image of sea surface temperature for August 2006 for the LAPE region.

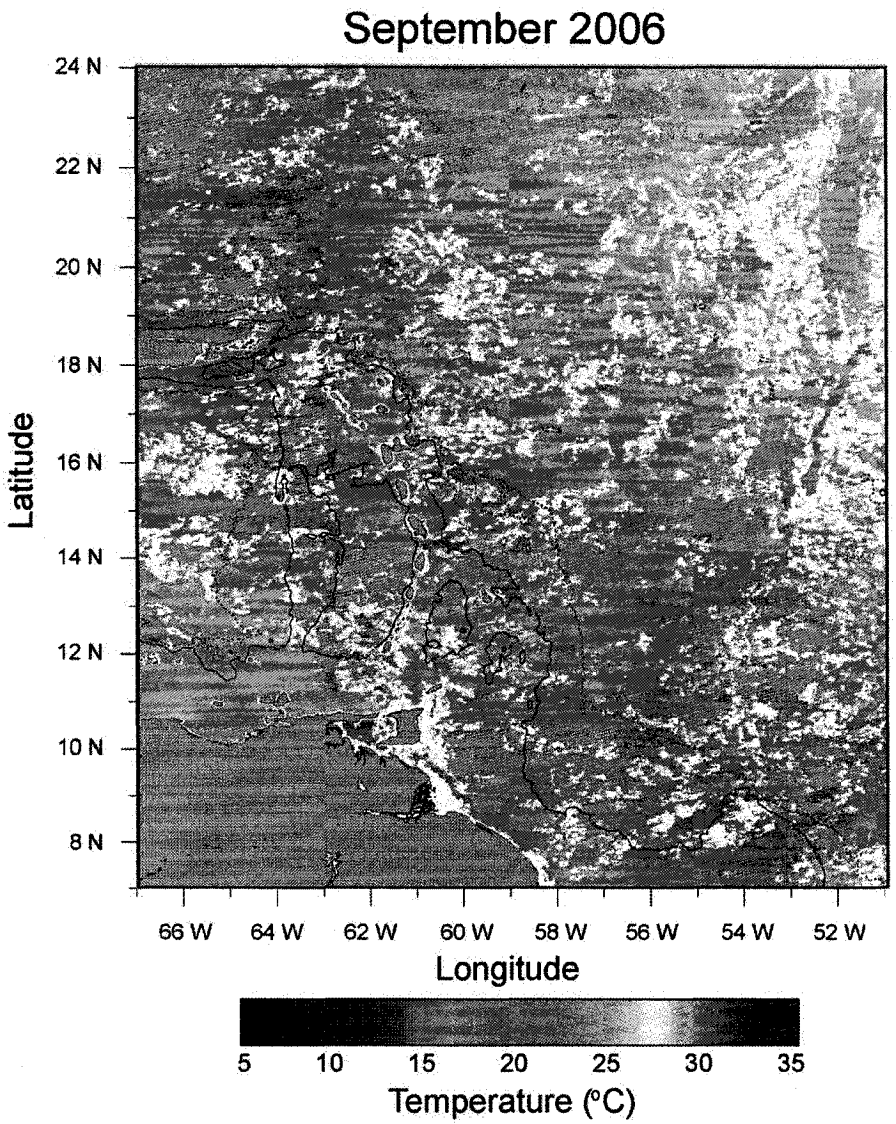

Figure E.9: Monthly composite image of sea surface temperature for September 2006 for the LAPE region.

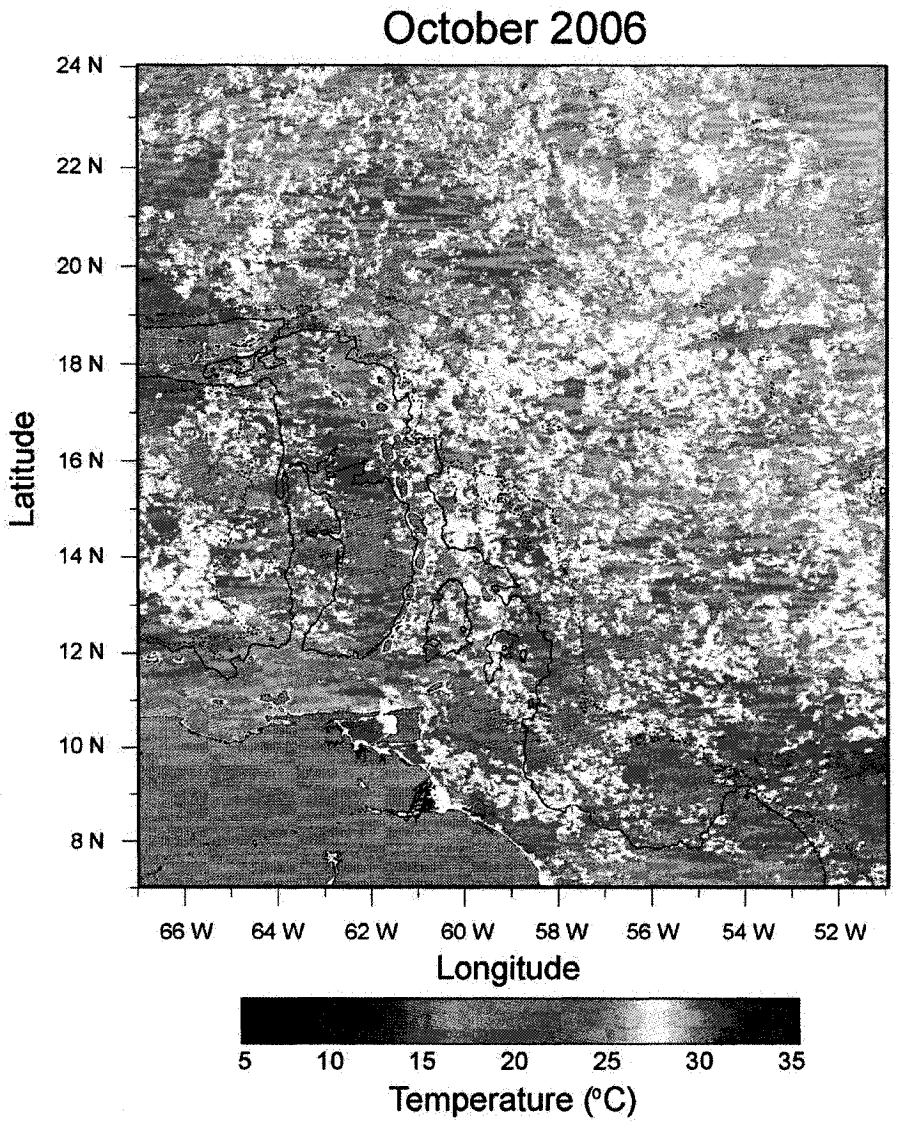

Figure E.10: Monthly composite image of sea surface temperature for October 2006 for the LAPE region.

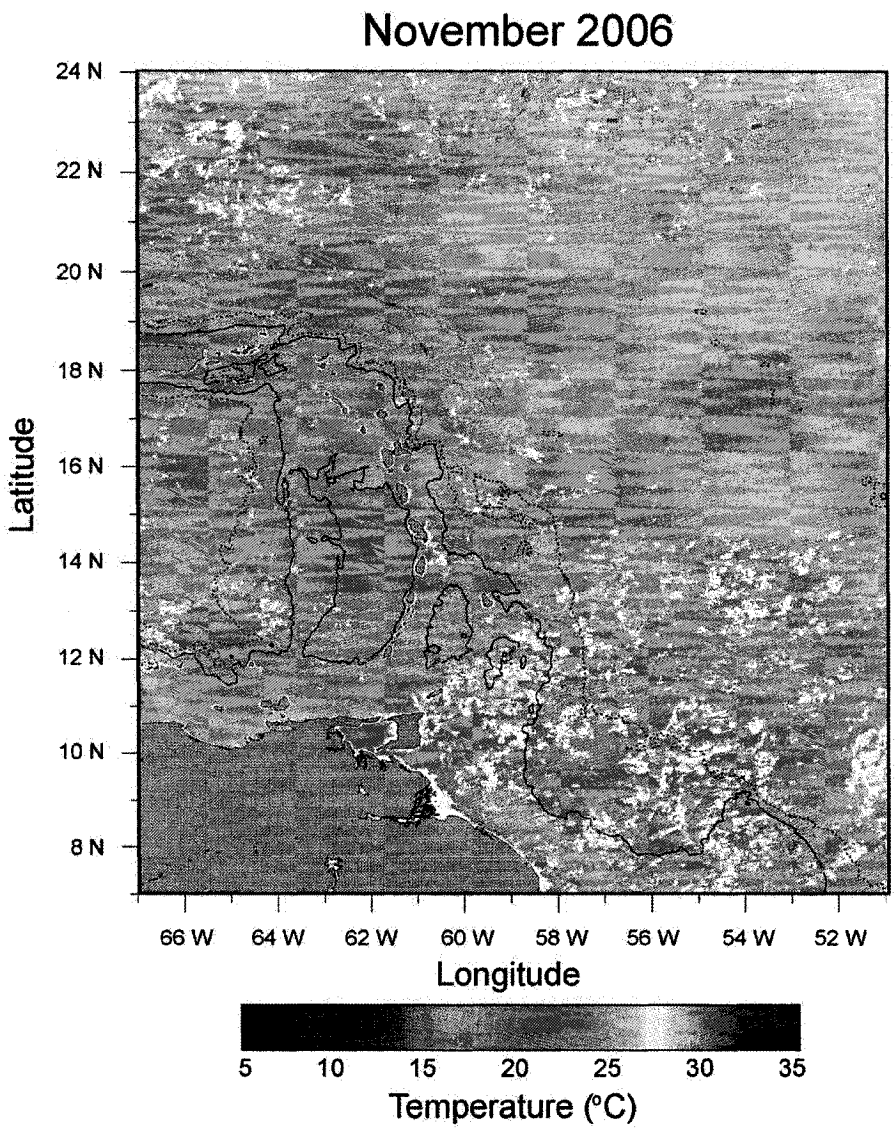

Figure E.11: Monthly composite image of sea surface temperature for November 2006 for the LAPE region.

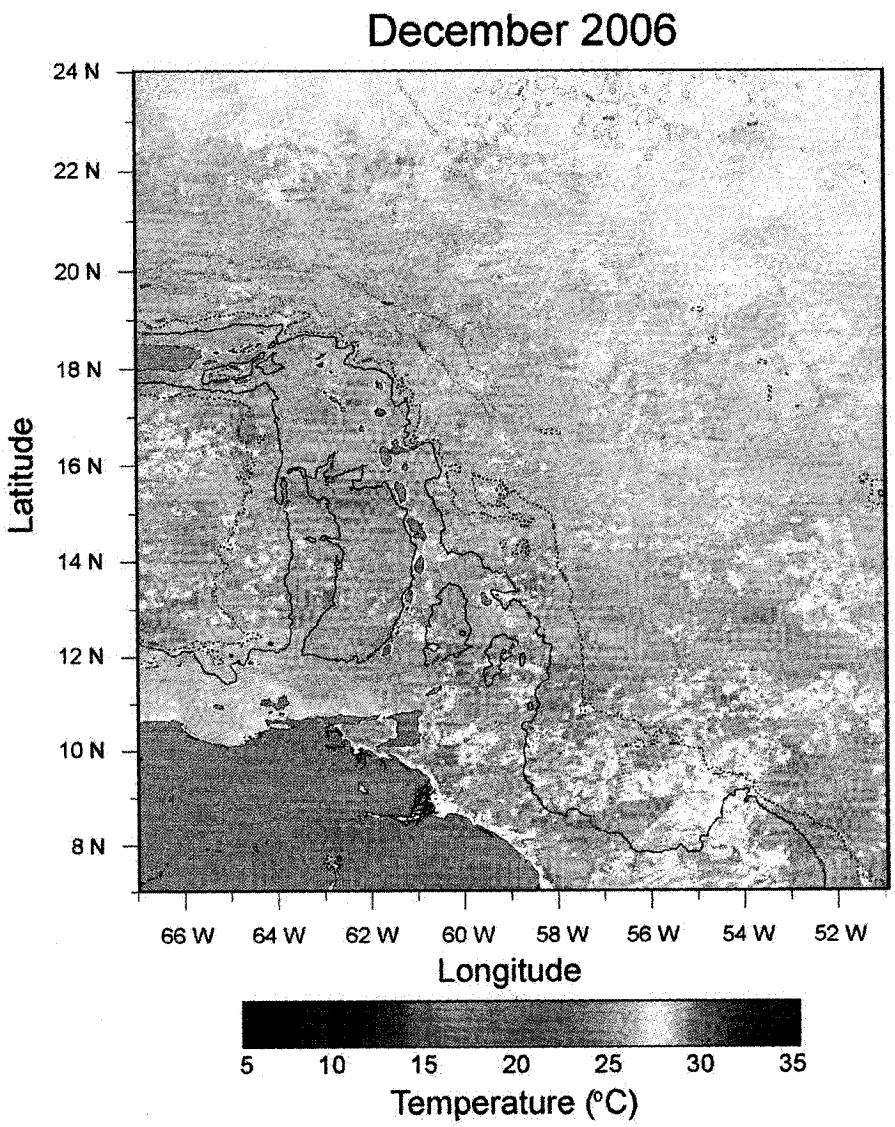

Figure E.12: Monthly composite image of sea surface temperature for December 2006 for the LAPE region.

Appendix F

PHOTOSYNTHETIC PARAMETERS AND PRIMARY PRODUCTION FOR TWENTY-ONE STATIONS FOR THE LAPE PROJECT

Table F.1: Photosynthetic parameters for the LAPE project, April and May 2006. The classes associated to each station are presented, where 1 is coastal waters (maximal depth < 200m), 2 is the open ocean stations south to 16°N and 3 is the open ocean stations north to 16°N. Water-column primary production (P_{ZT} and production to biomass ratio (P/B) are also presented.

station	class	P_m^B mg C mg chla^{-1} h^{-1}	α^B mg C mg chla^{-1} (W m^{-2})$^{-1}$ h^{-1}	P_{ZT} mg C m^{-2} d^{-1}
CE0607-01	3	2.35	0.130	267.9
CE0607-04	3	1.46	0.039	125.1
CE0607-07	3	2.42	0.098	229.8
CE0607-10	3	2.27	0.141	251.4
CE0607-14	2	3.38	0.054	337.9
CE0607-18	2	3.10	0.062	318.7
CE0607-22	2	2.84	0.071	372.9
CE0607-26	1	1.73	0.084	273.5
CE0607-28	2	3.90	0.091	412.3
CE0607-30	2	2.02	0.071	309.2
CE0607-32	2	2.73	0.086	313.4
CE0607-35	2	2.55	0.061	230.3
CE0607-36	1	2.75	0.082	
CE0607-37	2	3.16	0.086	471.2
CE0607-40	2	3.11	0.096	420.7
CE0607-42	2	3.00	0.069	382.9
CE0607-44	3	2.20	0.080	299.9
CE0607-46	3	1.61	0.057	149.5
CE0607-48	3	3.30	0.166	385.7
CE0607-51	2	3.00	0.073	322.4
CE0607-53	2	1.96	0.098	274.4
CE0607-55	3	3.19	0.106	312.2

Appendix G

PRIMARY PRODUCTION ESTIMATED FROM REMOTE SENSING OF OCEAN COLOUR FOR THE LAPE REGION USING THE SUBREGIONAL APPROACH TO ASSIGN THE PARAMETERS

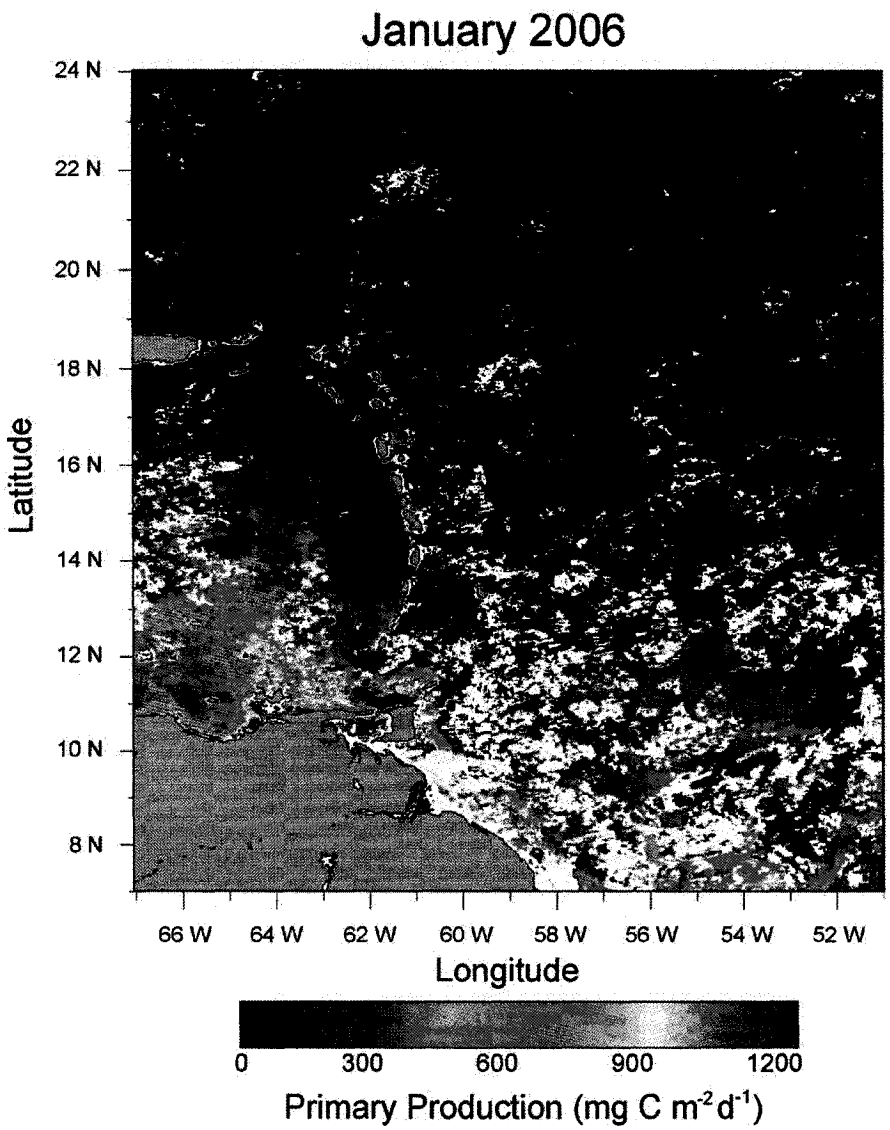

Figure G.1: Primary production with parameters assigned from three regions (coastal, north of 16°N and south of 16°N) for January 2006 for the LAPE region.

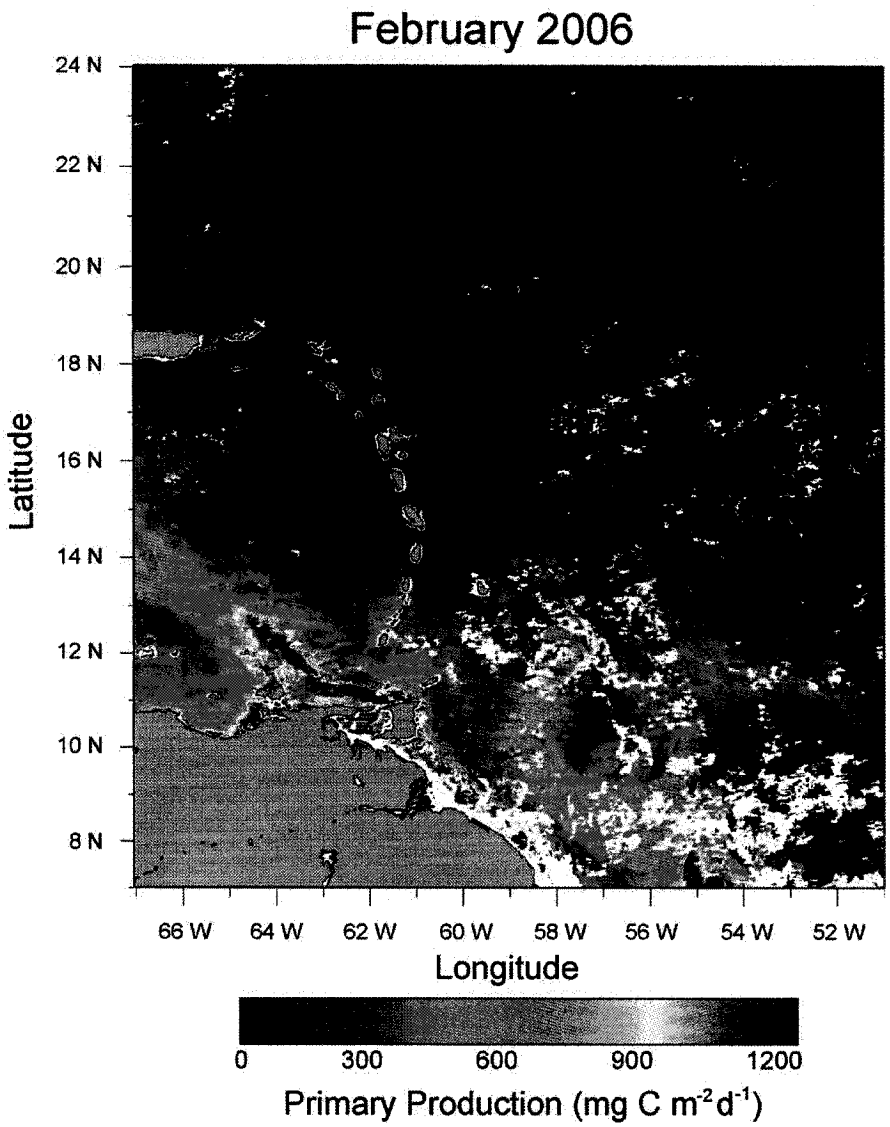

Figure G.2: Primary production with parameters assigned from three regions (coastal, north of 16°N and south of 16°N) for February 2006 for the LAPE region.

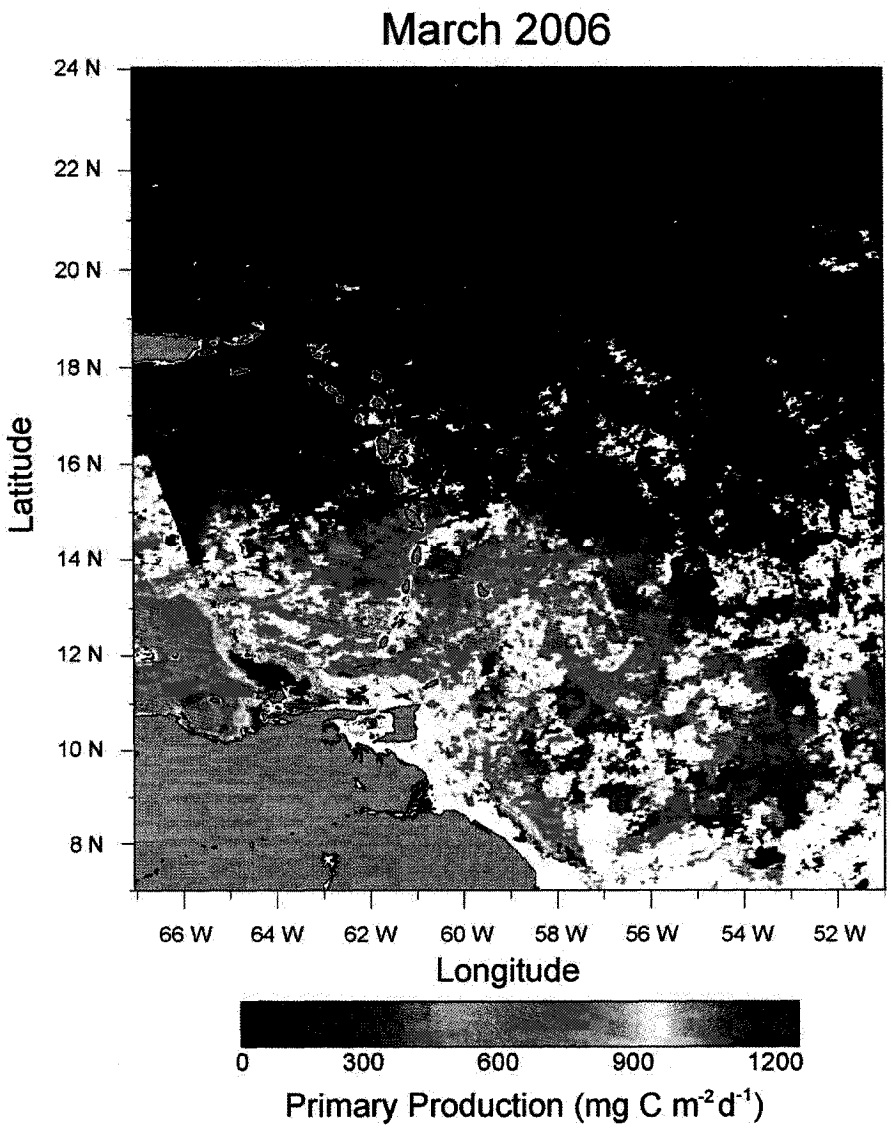

Figure G.3: Primary production with parameters assigned from three regions (coastal, north of 16°N and south of 16°N) for March 2006 for the LAPE region.

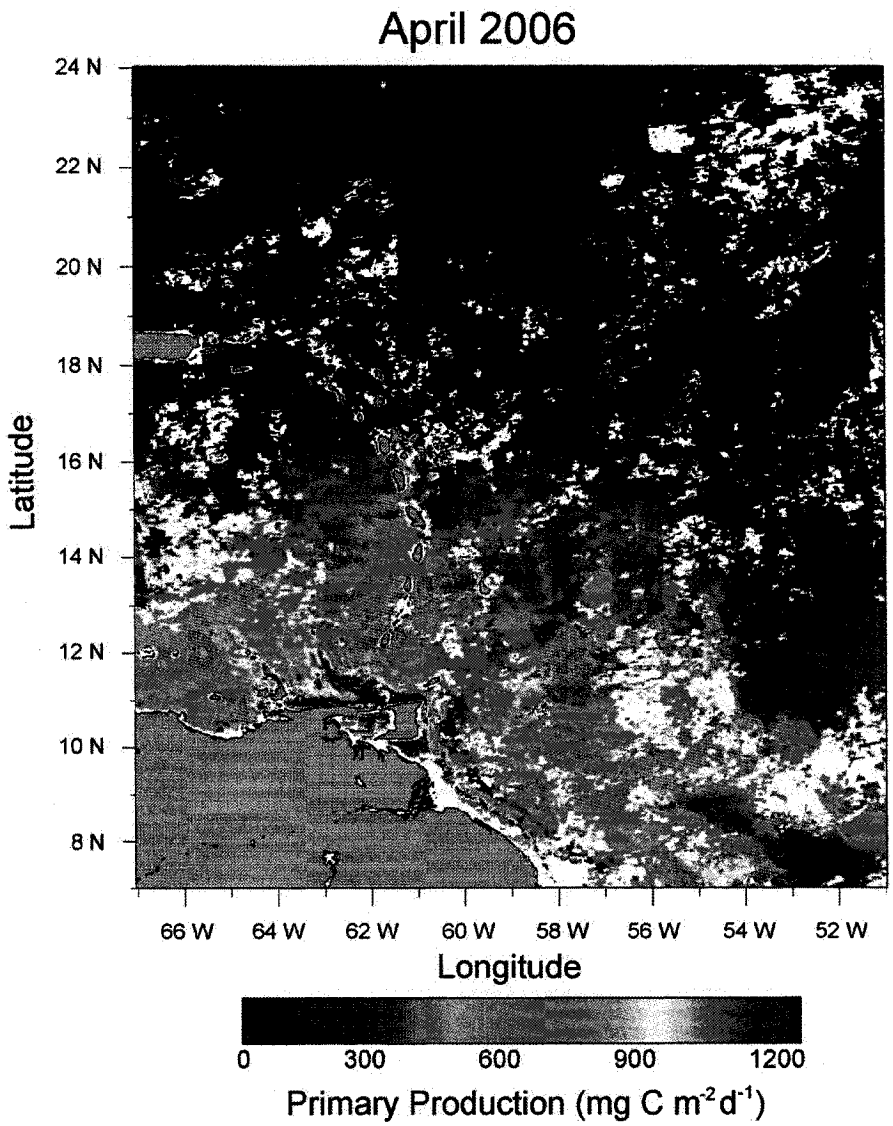

Figure G.4: Primary production with parameters assigned from three regions (coastal, north of 16°N and south of 16°N) for April 2006 for the LAPE region.

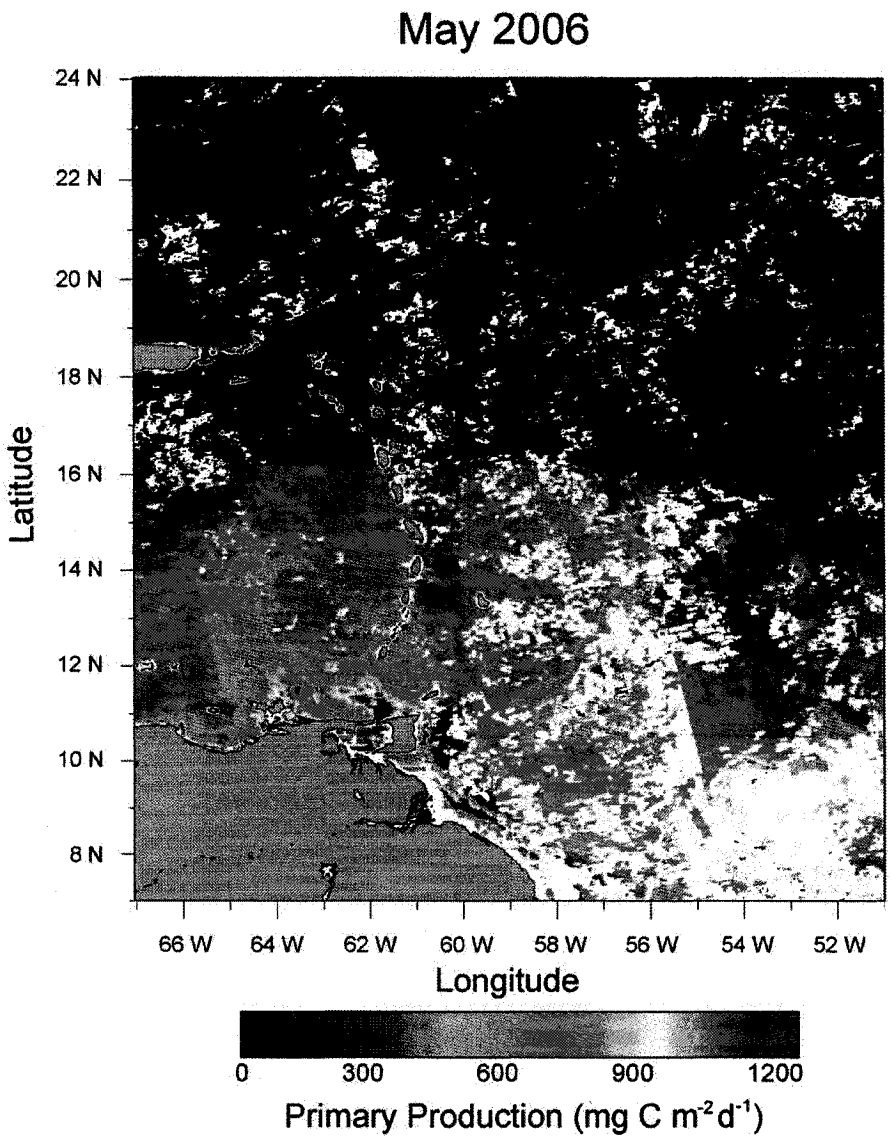

Figure G.5: Primary production with parameters assigned from three regions (coastal, north of 16°N and south of 16°N) for May 2006 for the LAPE region.

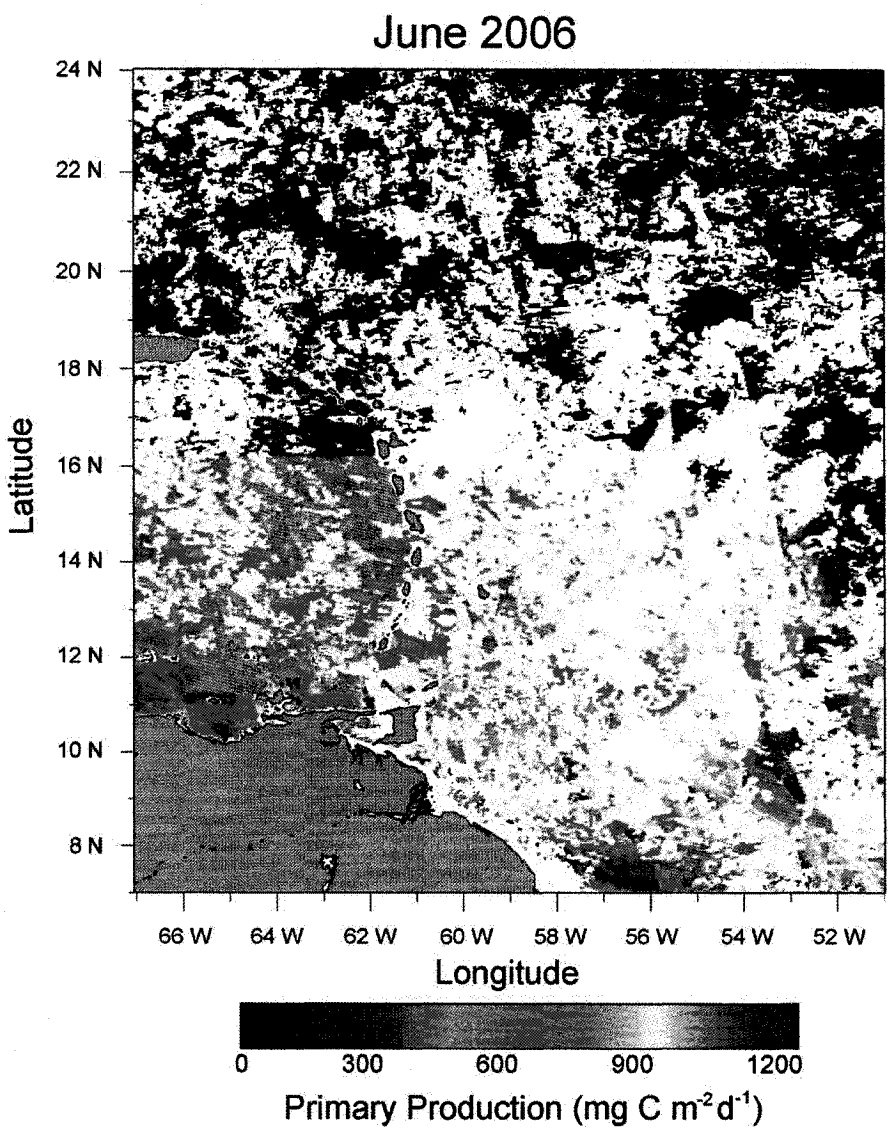

Figure G.6: Primary production with parameters assigned from three regions (coastal, north of 16°N and south of 16°N) for June 2006 for the LAPE region.

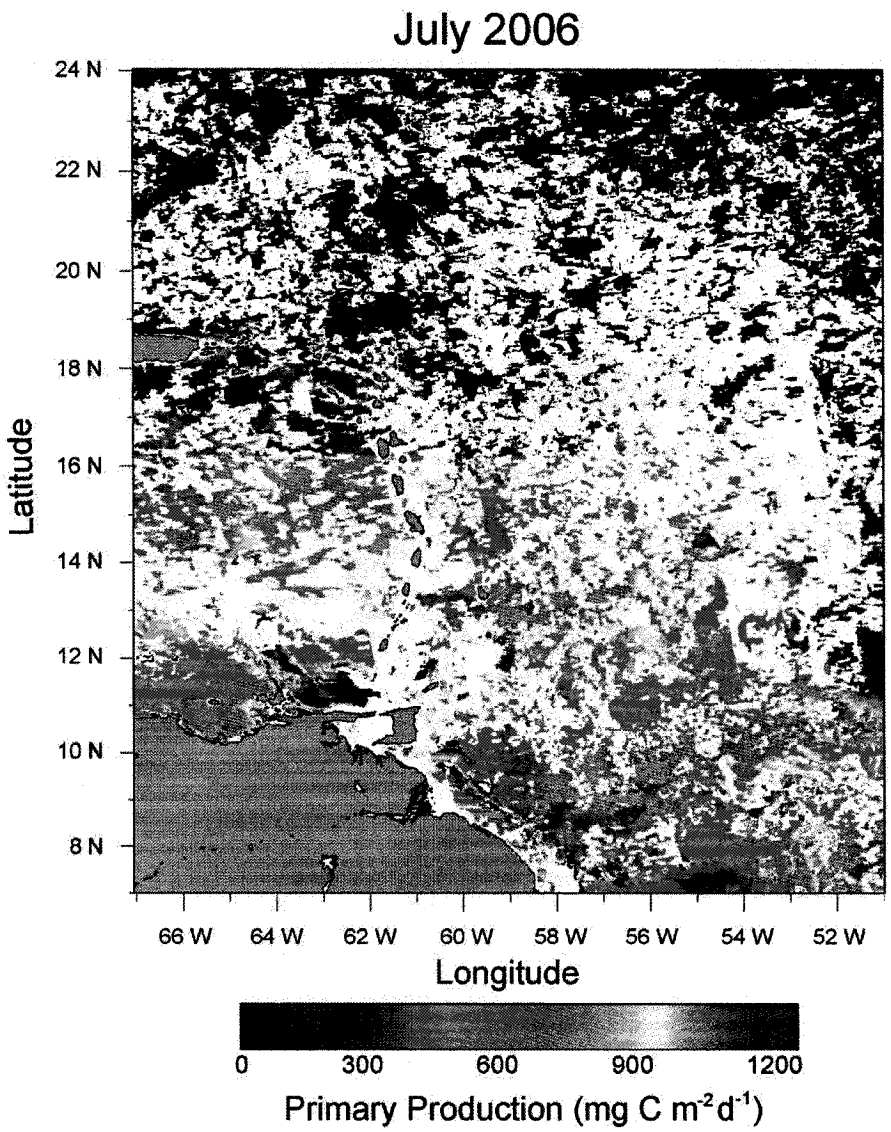

Figure G.7: Primary production with parameters assigned from three regions (coastal, north of 16°N and south of 16°N) for July 2006 for the LAPE region.

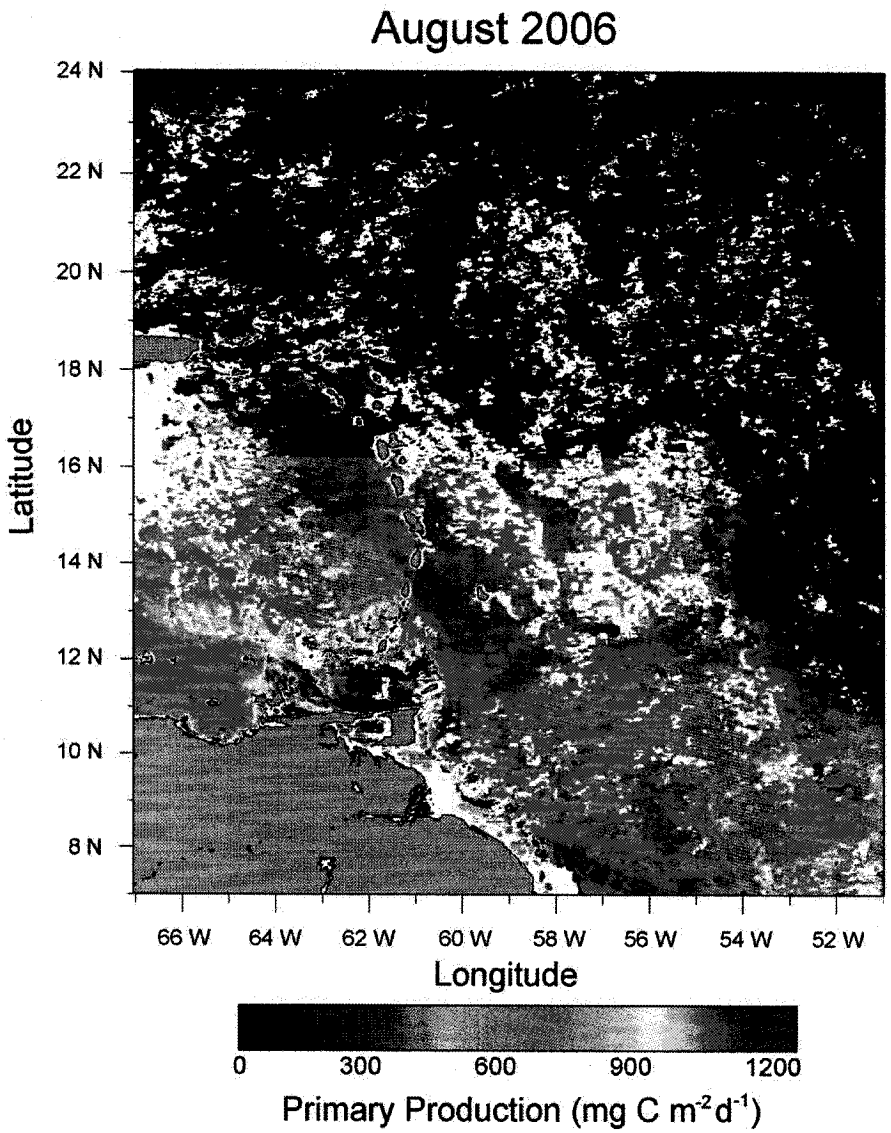

Figure G.8: Primary production with parameters assigned from three regions (coastal, north of 16°N and south of 16°N) for August 2006 for the LAPE region.

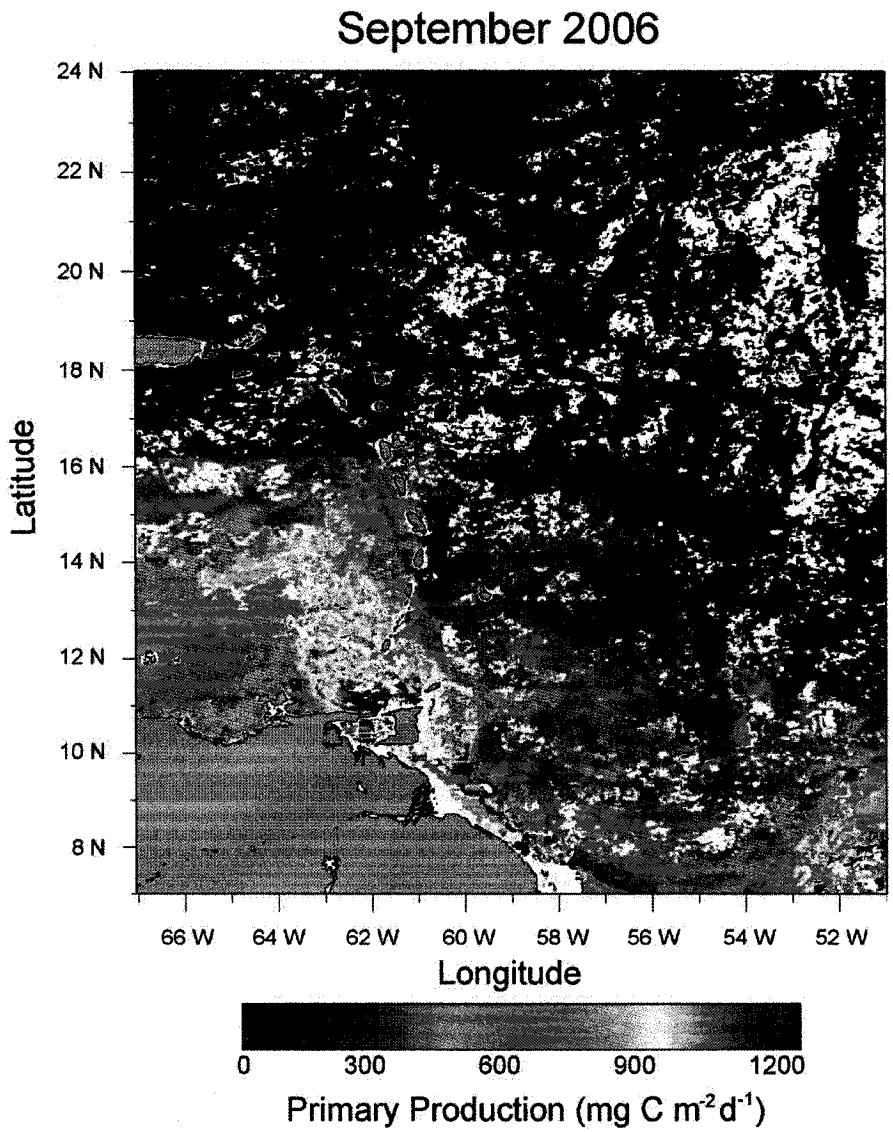

Figure G.9: Primary production with parameters assigned from three regions (coastal, north of 16°N and south of 16°N) for September 2006 for the LAPE region.

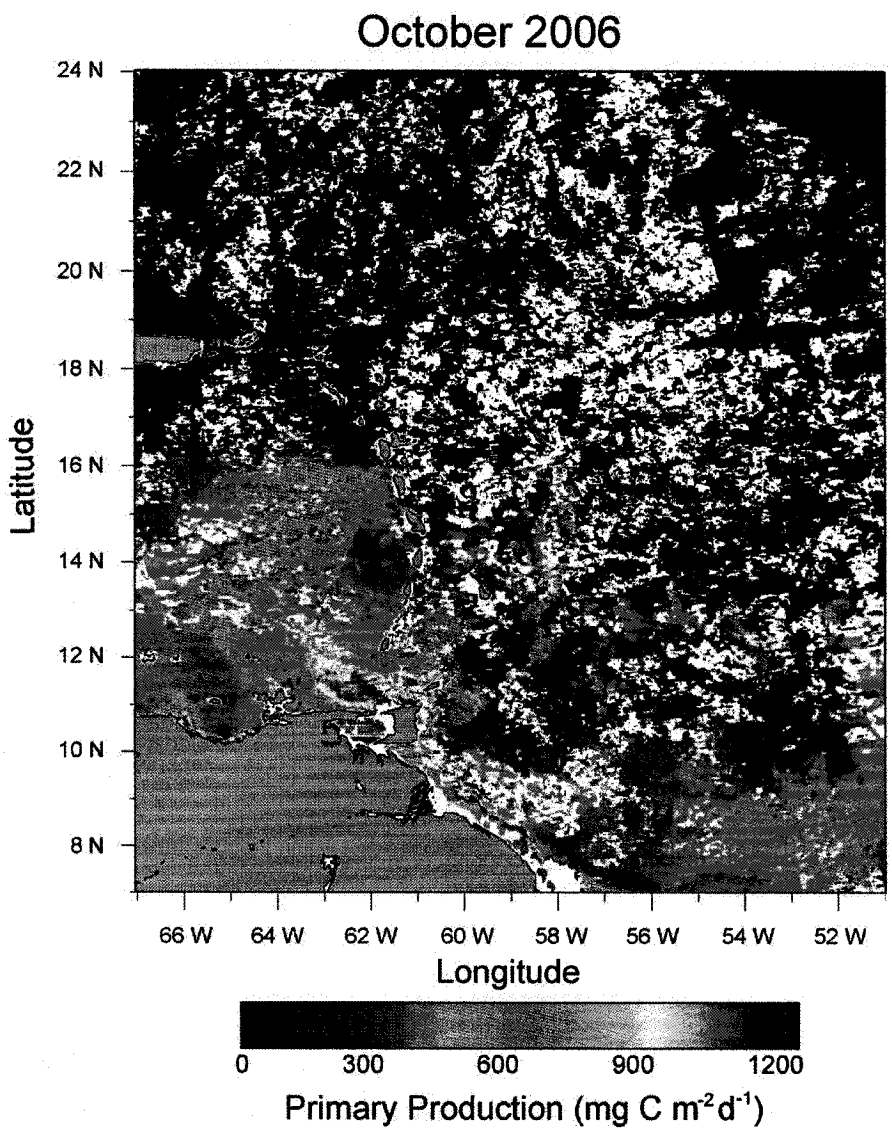

Figure G.10: Primary production with parameters assigned from three regions (coastal, north of 16°N and south of 16°N) for October 2006 for the LAPE region.

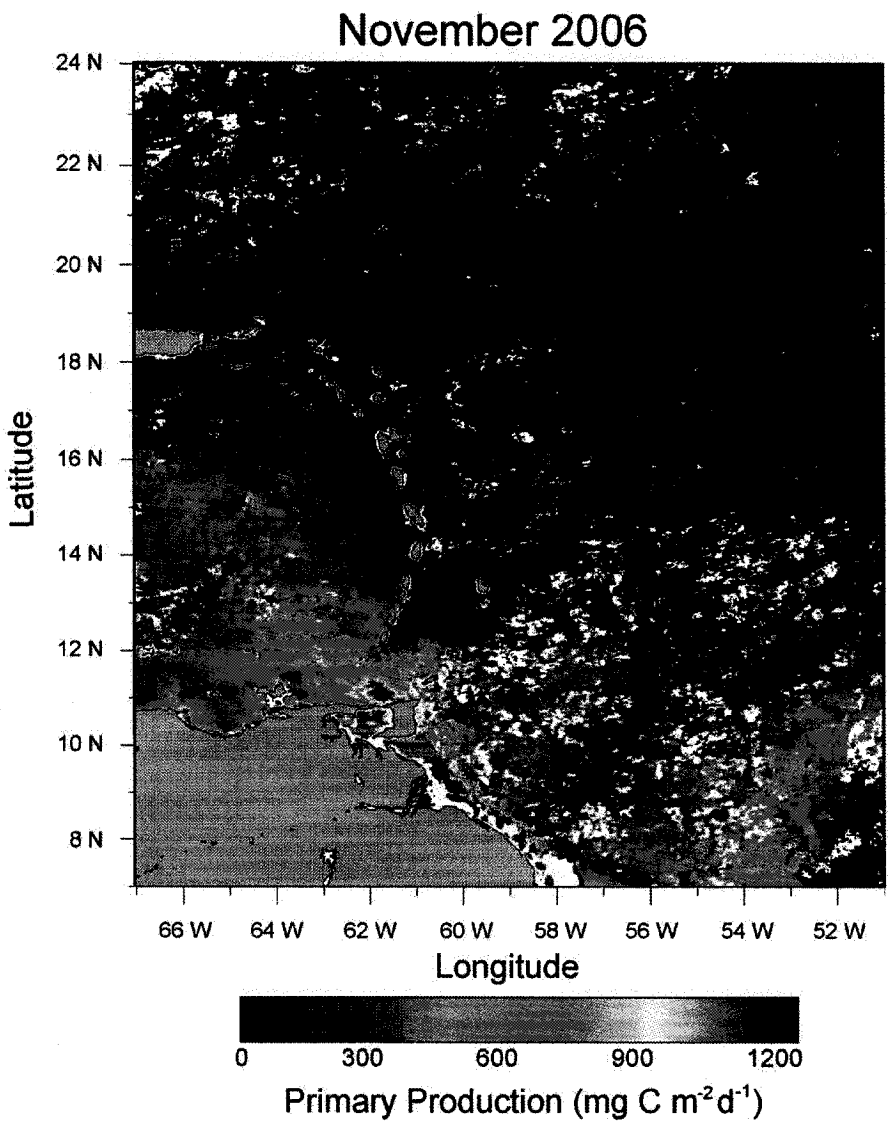

Figure G.11: Primary production with parameters assigned from three regions (coastal, north of 16°N and south of 16°N) for November 2006 for the LAPE region.

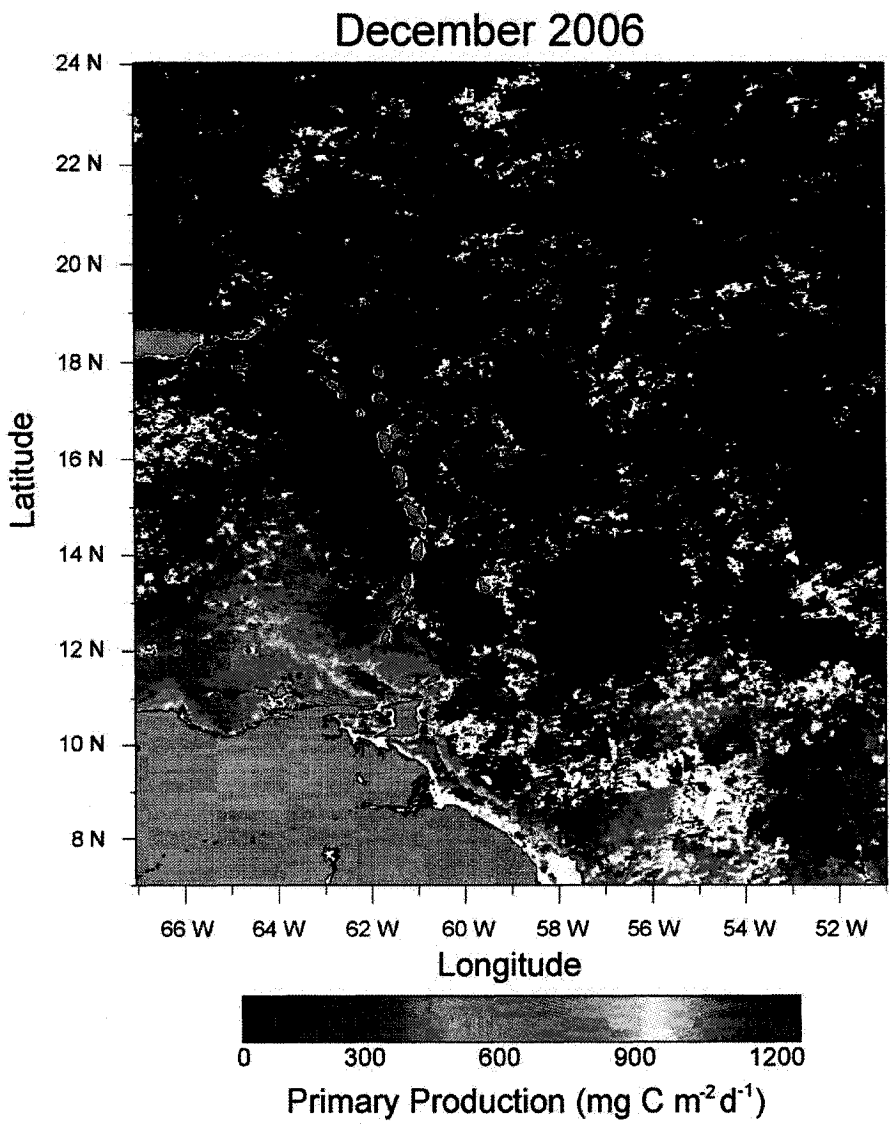

Figure G.12: Primary production with parameters assigned from three regions (coastal, north of 16°N and south of 16°N) for December 2006 for the LAPE region.

Appendix H

PRIMARY PRODUCTION ESTIMATED FROM REMOTE SENSING OF OCEAN COLOUR FOR THE LAPE REGION USING THE NEAREST NEIGHBOUR METHOD TO ASSIGN THE PARAMETERS

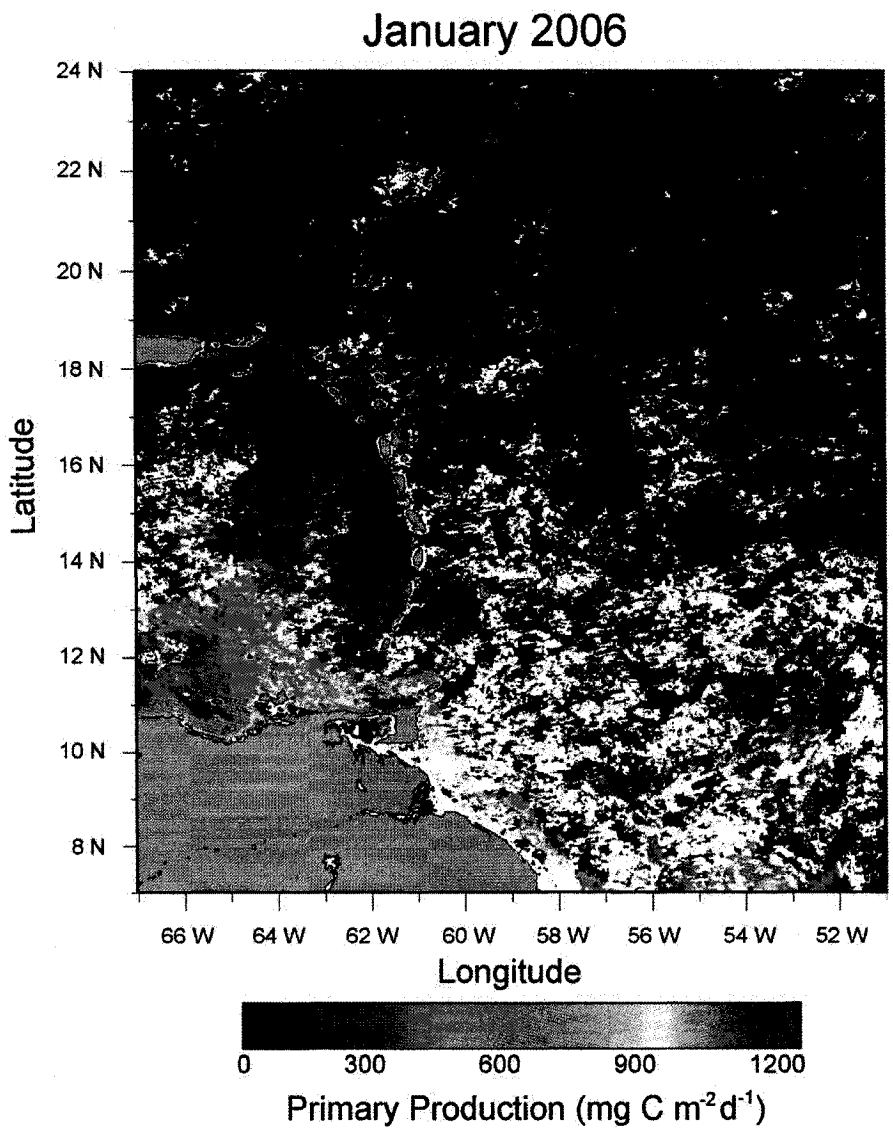

Figure H.1: Primary production estimated from remote sensing of ocean colour with parameters assigned using the Nearest-Neighbour Method for January 2006 for the LAPE region.

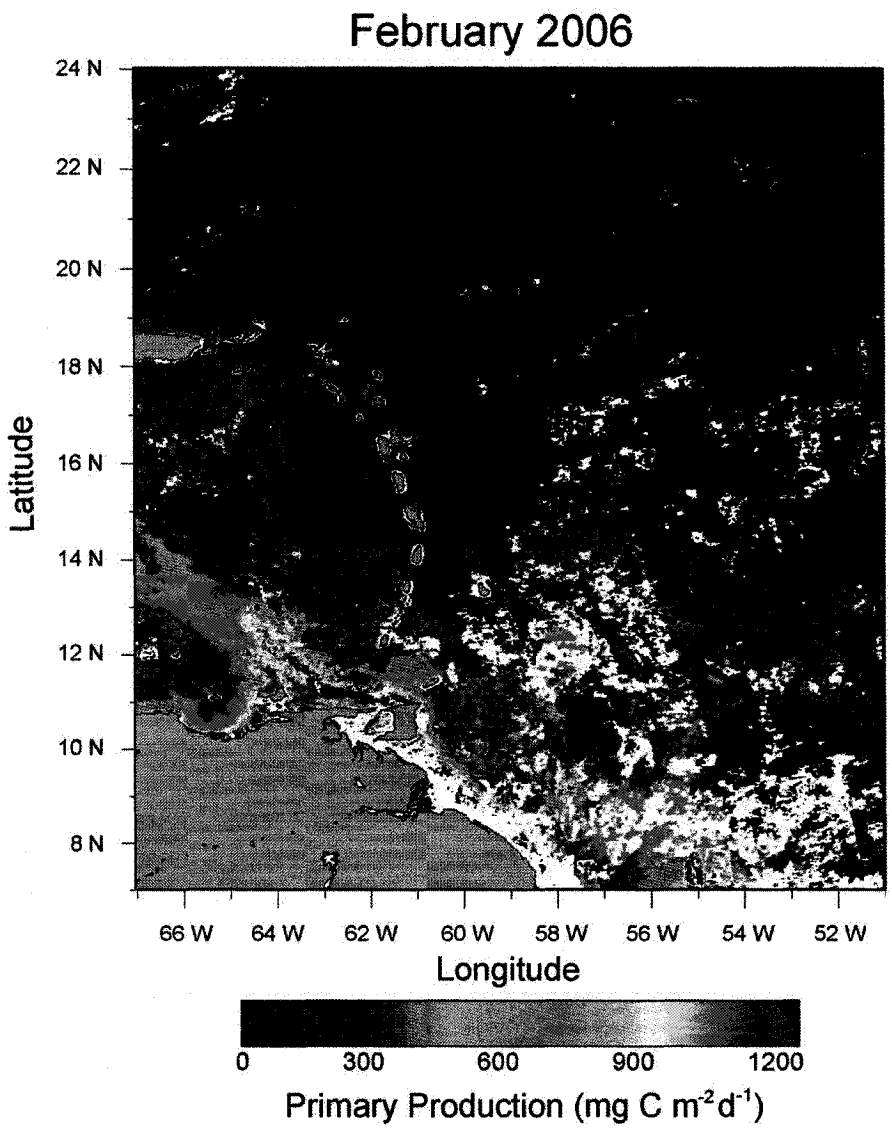

Figure H.2: Primary production estimated from remote sensing of ocean colour with parameters assigned using the Nearest-Neighbour Method for February 2006 for the LAPE region.

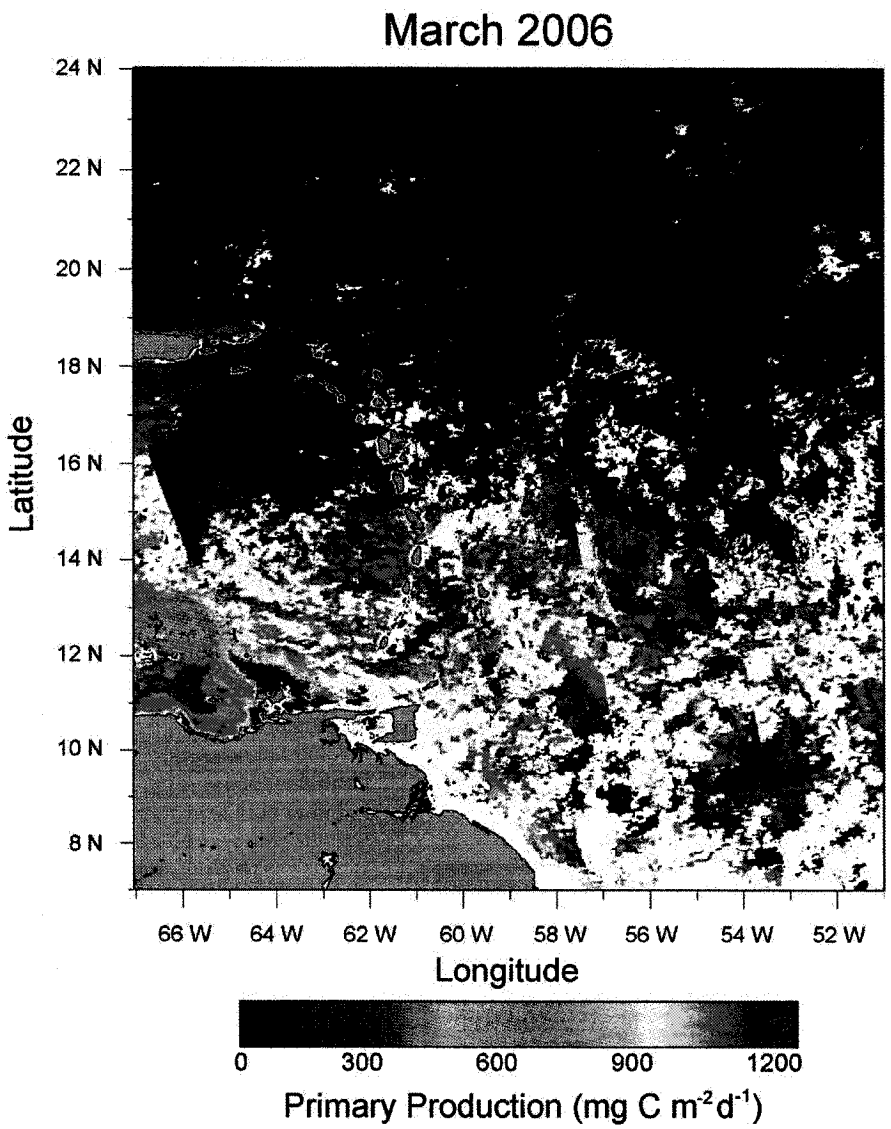

Figure H.3: Primary production estimated from remote sensing of ocean colour with parameters assigned using the Nearest-Neighbour Method for March 2006 for the LAPE region.

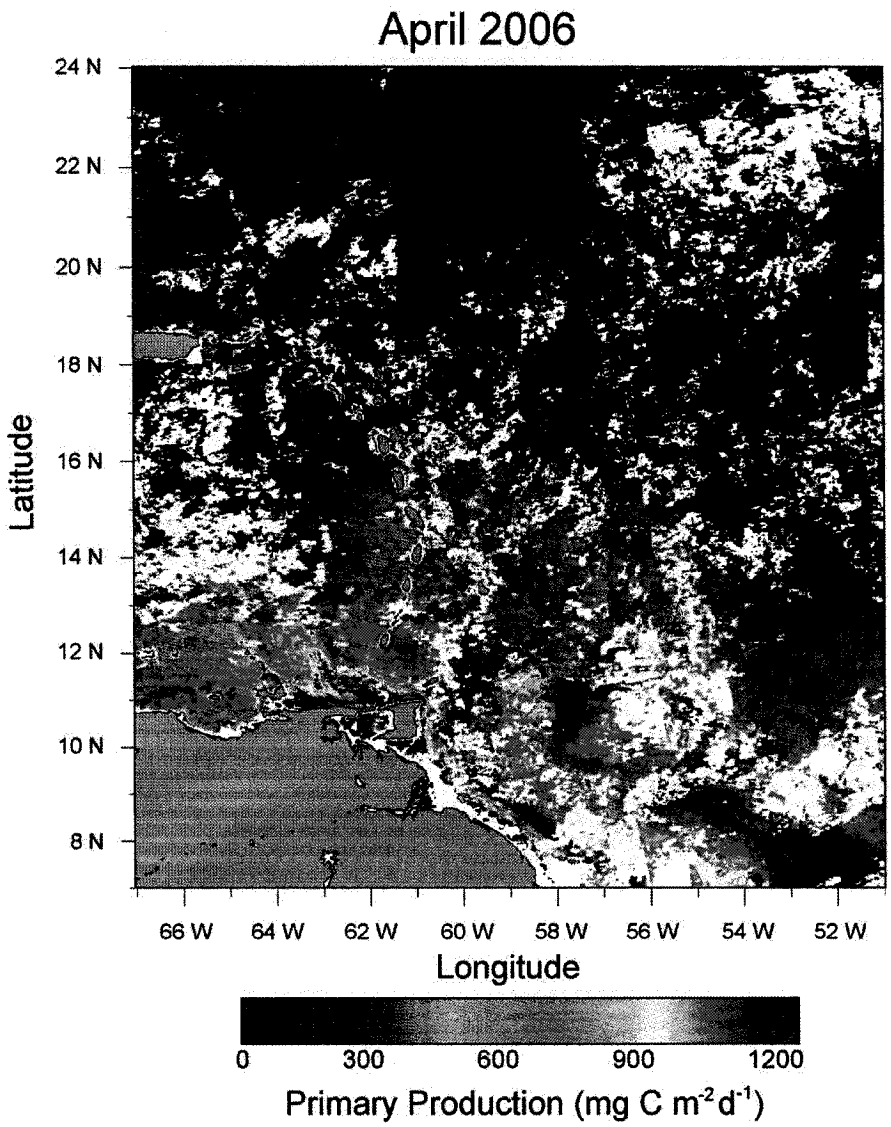

Figure H.4: Primary production estimated from remote sensing of ocean colour with parameters assigned using the Nearest-Neighbour Method for April 2006 for the LAPE region.

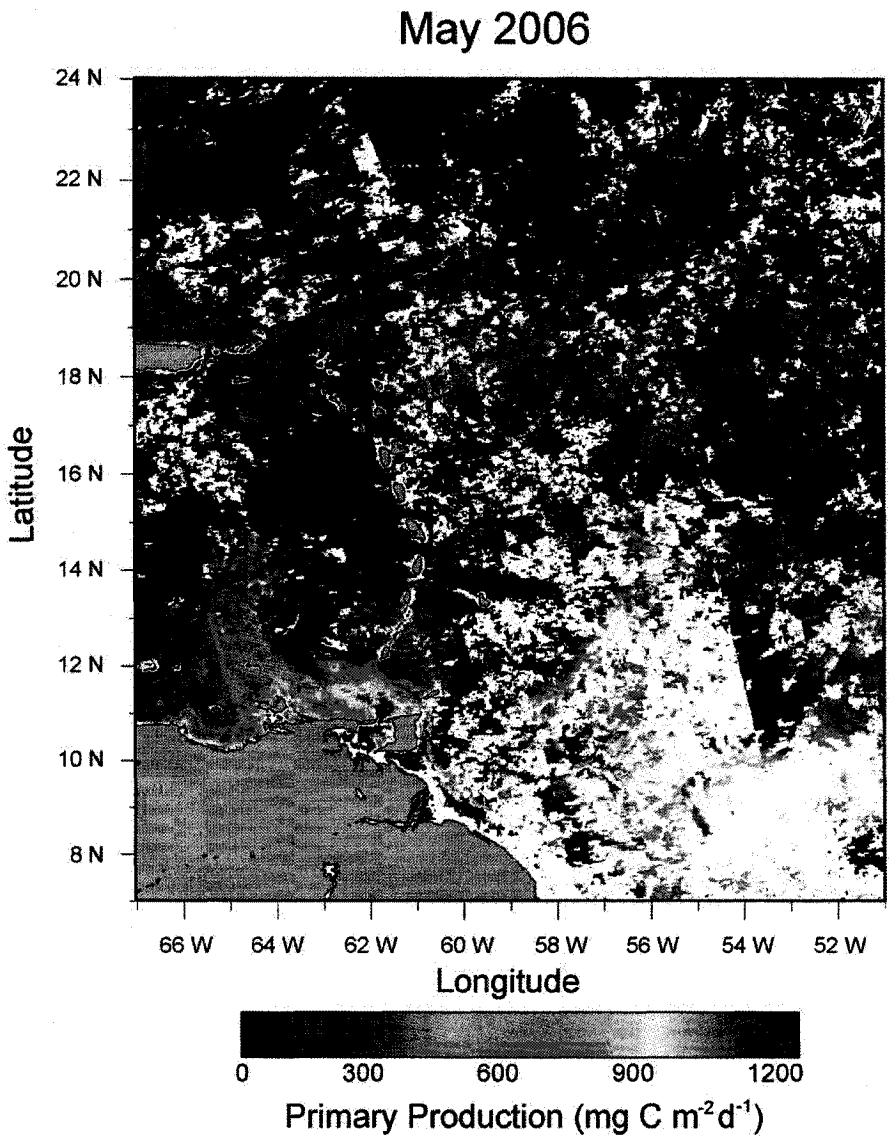

Figure H.5: Primary production estimated from remote sensing of ocean colour with parameters assigned using the Nearest-Neighbour Method for May 2006 for the LAPE region.

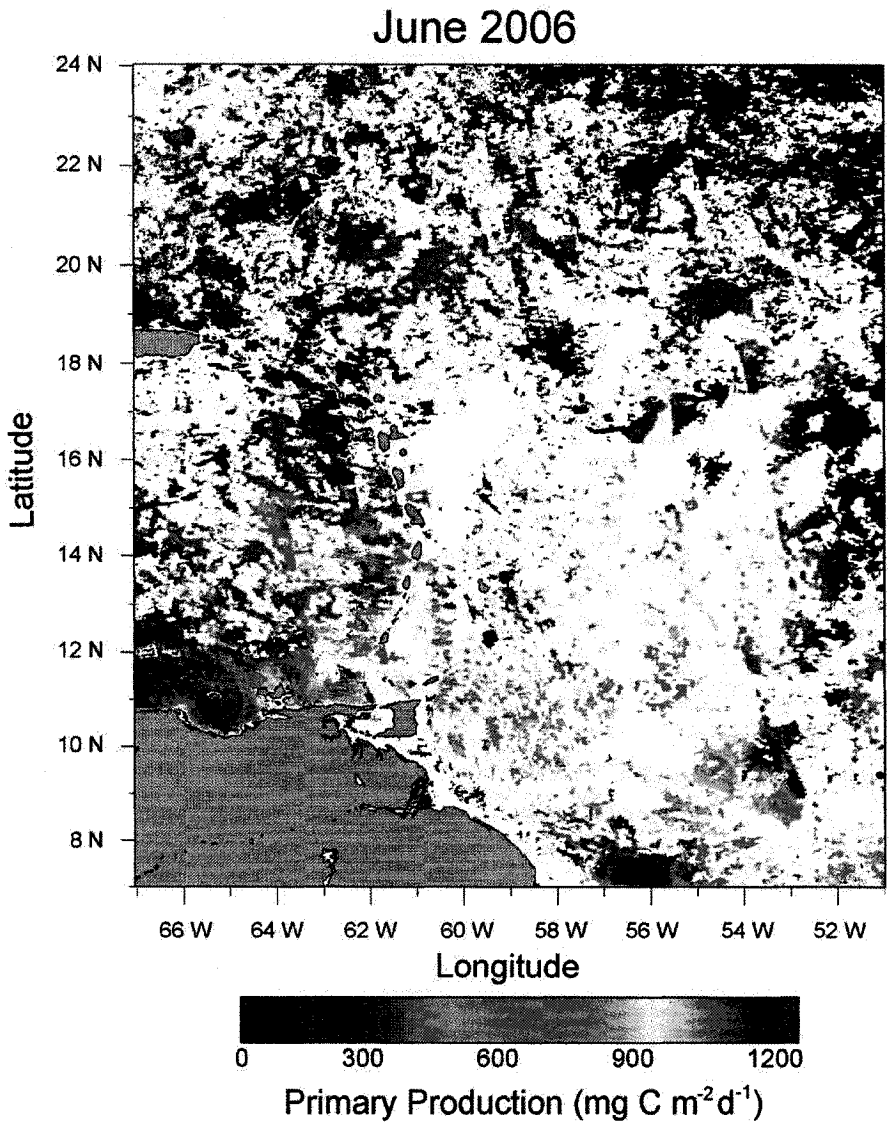

Figure H.6: Primary production estimated from remote sensing of ocean colour with parameters assigned using the Nearest-Neighbour Method for June 2006 for the LAPE region.

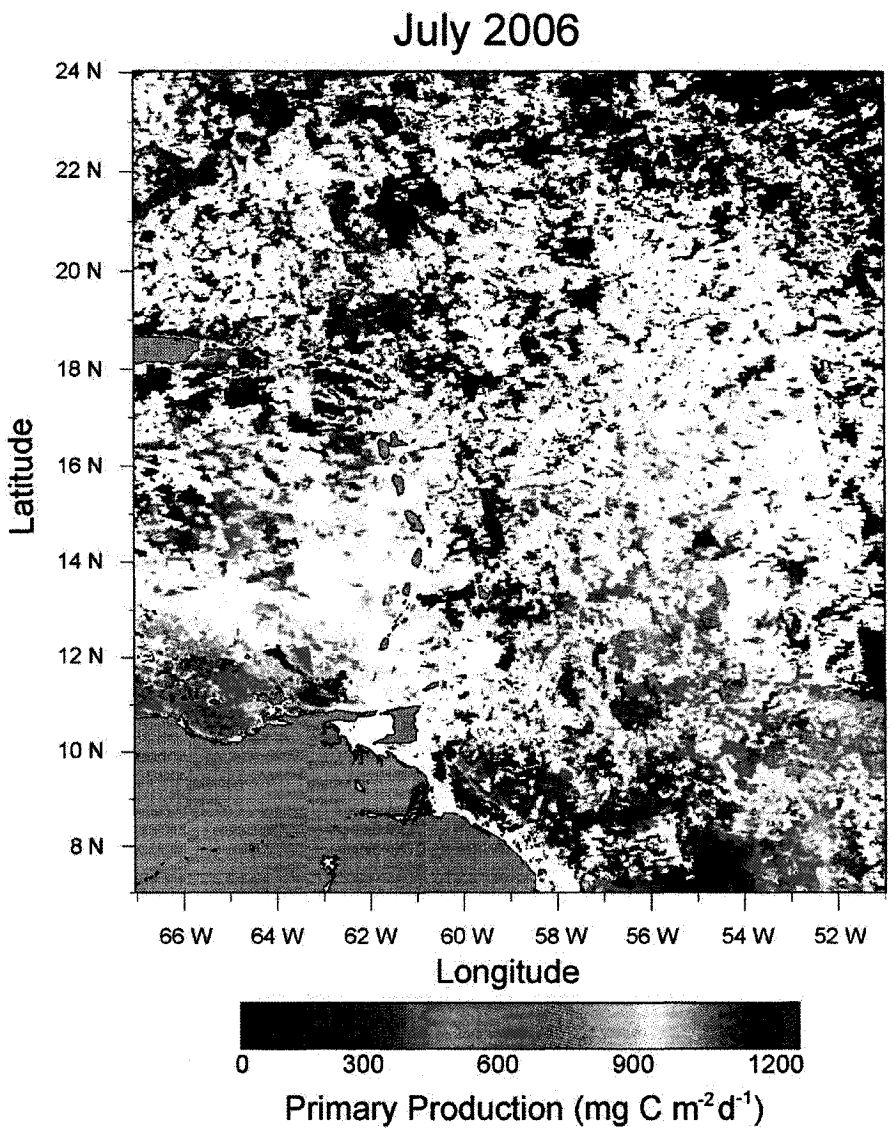

Figure H.7: Primary production estimated from remote sensing of ocean colour with parameters assigned using the Nearest-Neighbour Method for July 2006 for the LAPE region.

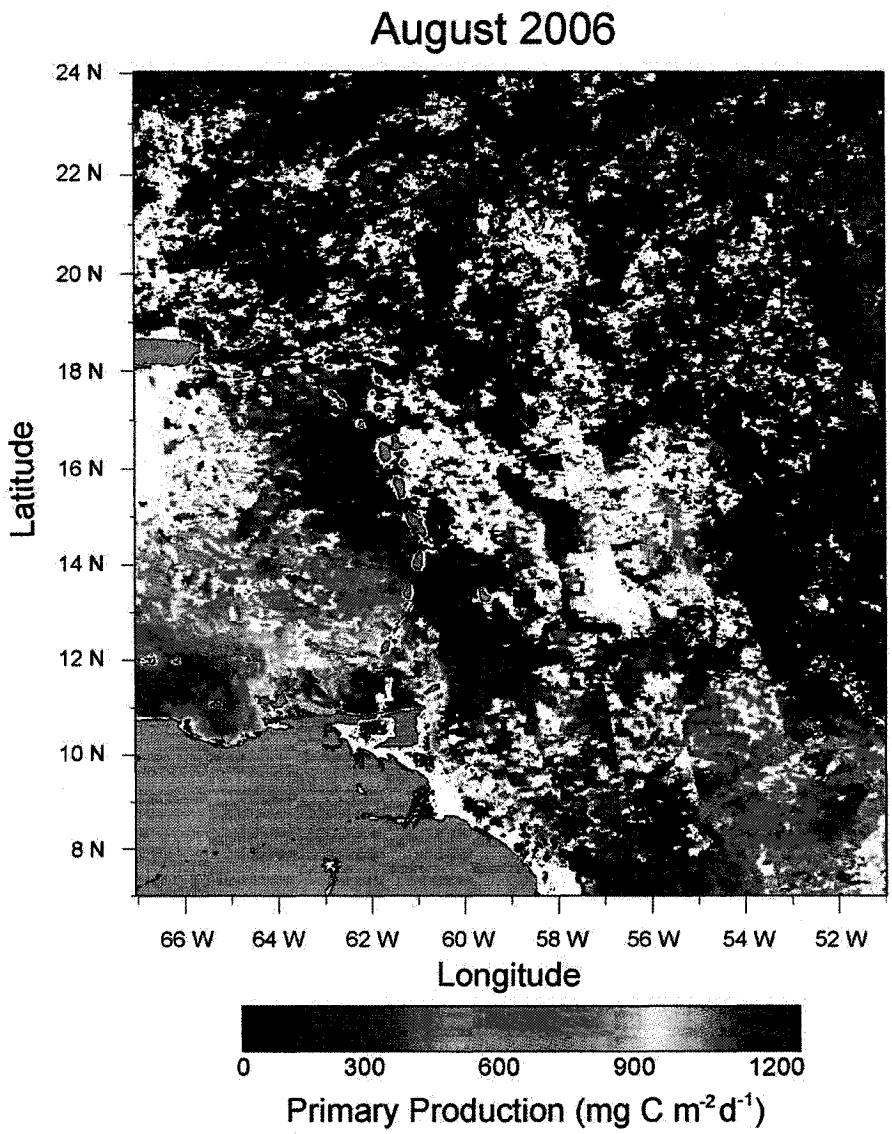

Figure H.8: Primary production estimated from remote sensing of ocean colour with parameters assigned using the Nearest-Neighbour Method for August 2006 for the LAPE region.

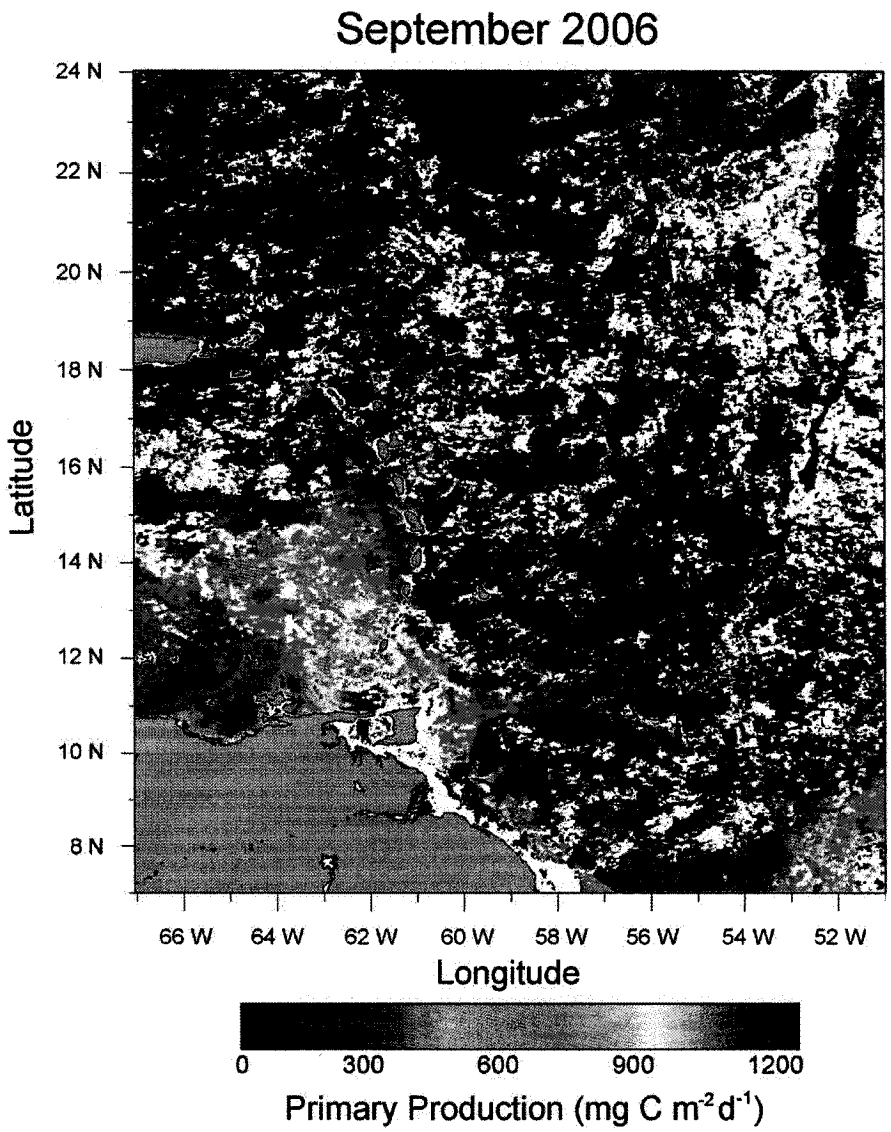

Figure H.9: Primary production estimated from remote sensing of ocean colour with parameters assigned using the Nearest-Neighbour Method for September 2006 for the LAPE region.

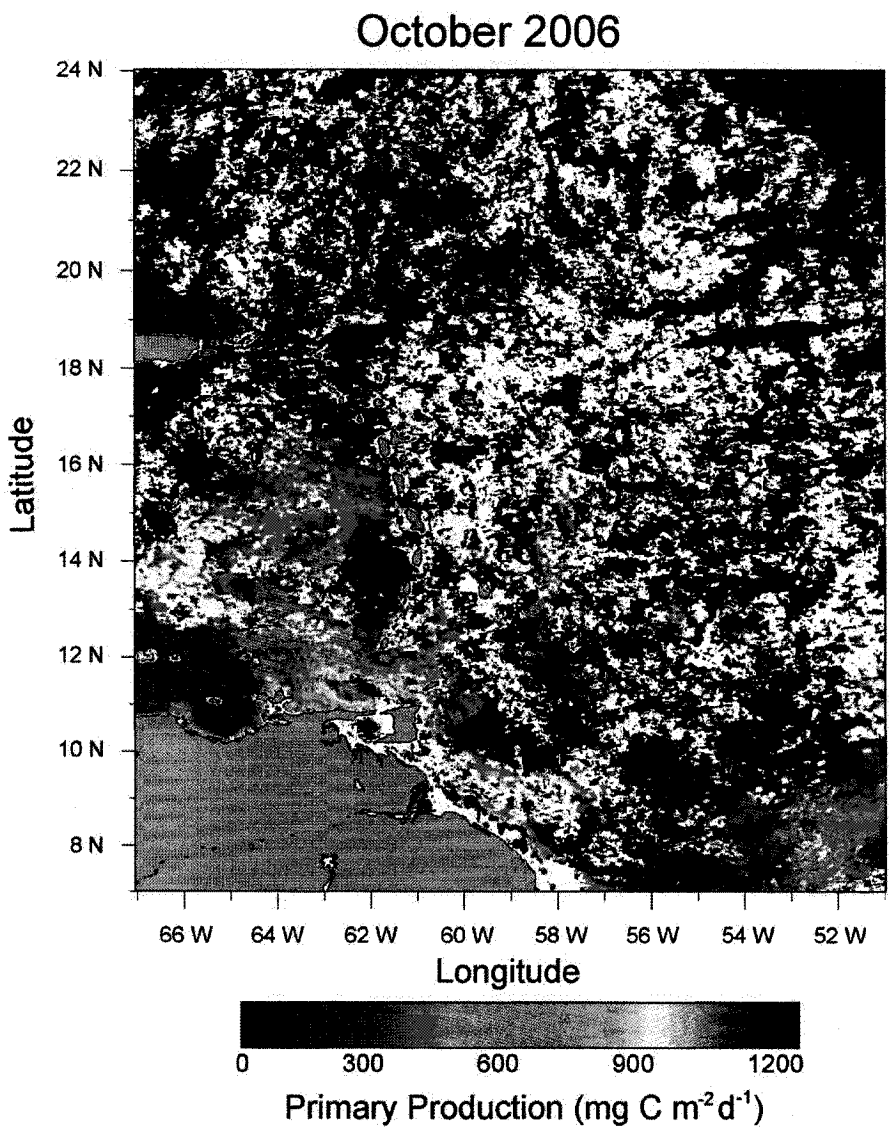

Figure H.10: Primary production estimated from remote sensing of ocean colour with parameters assigned using the Nearest-Neighbour Method for October 2006 for the LAPE region.

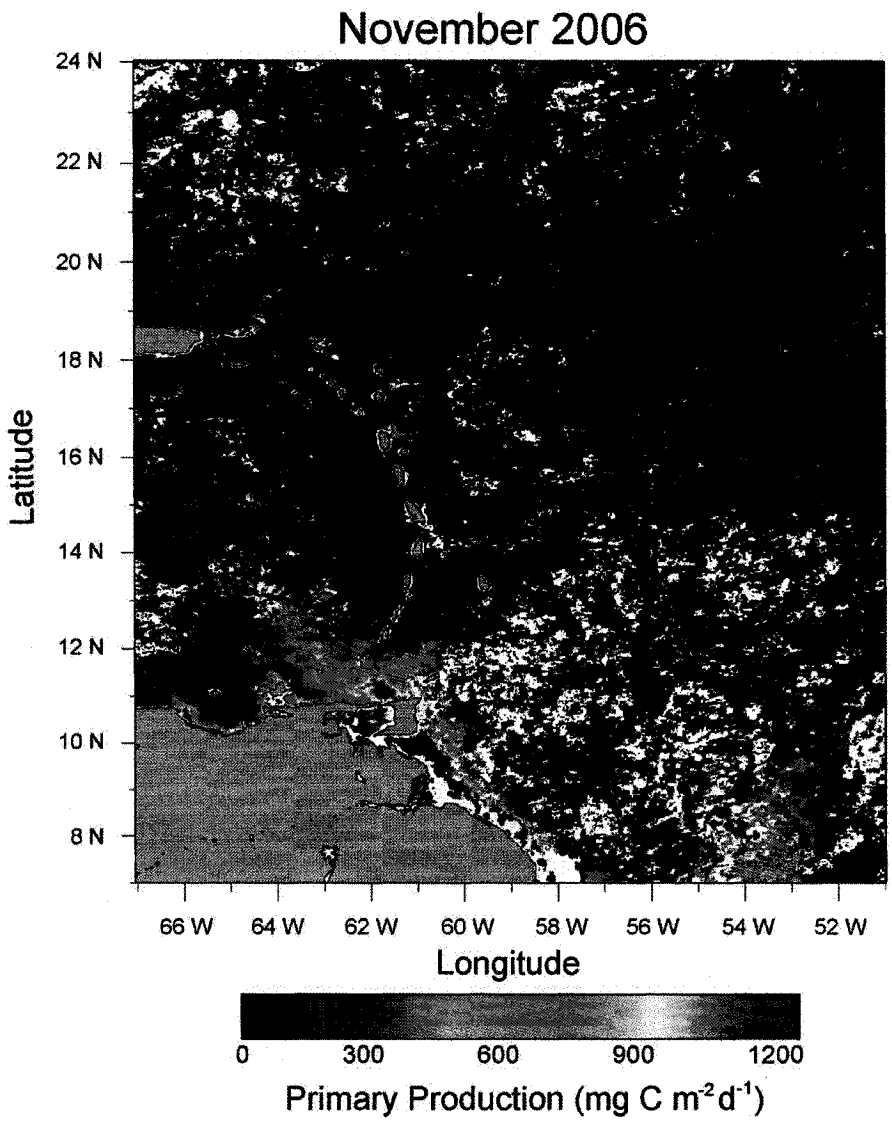

Figure H.11: Primary production estimated from remote sensing of ocean colour with parameters assigned using the Nearest-Neighbour Method for November 2006 for the LAPE region.

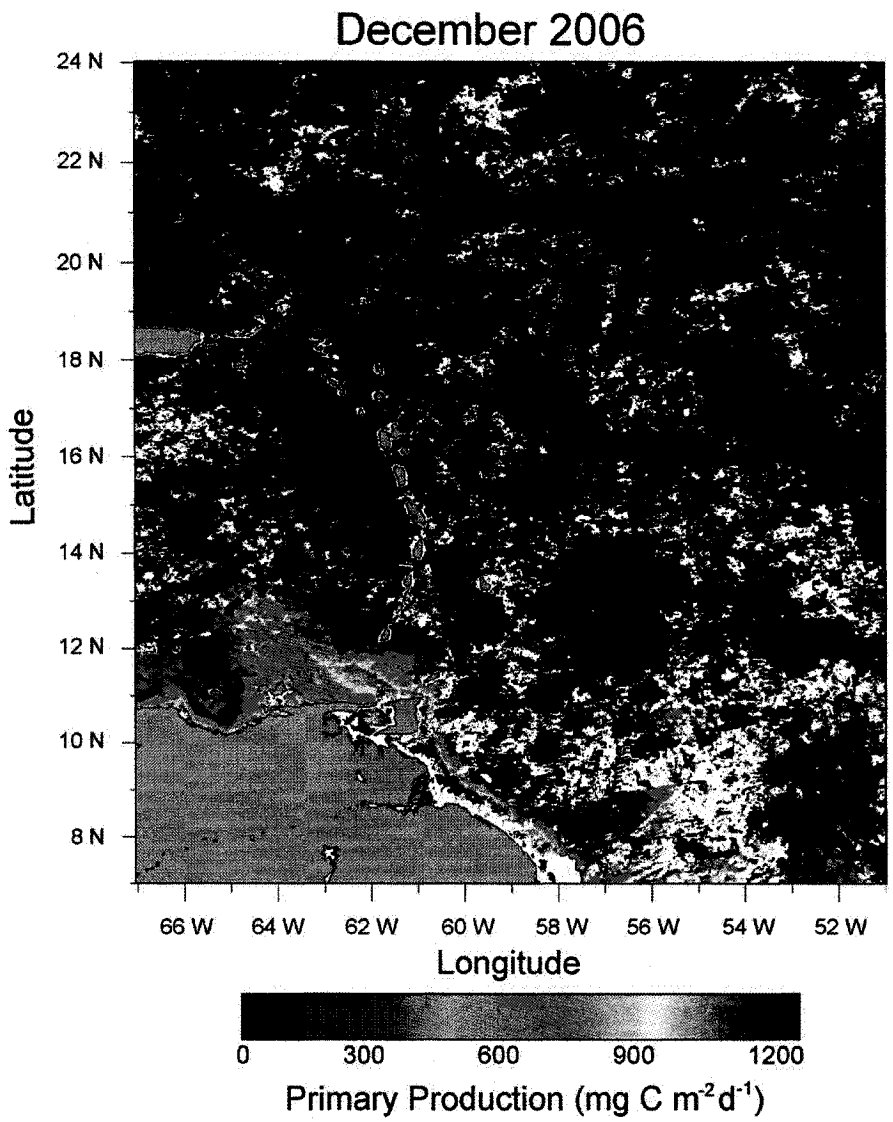

Figure H.12: Primary production estimated from remote sensing of ocean colour with parameters assigned using the Nearest-Neighbour Method for December 2006 for the LAPE region.

Appendix I

COPYRIGHT AGREEMENT LETTERS

I.1 Copyright Agreement Letter for Chapter 2 as a Technical Report for Food and Agriculture Organization.

There is no requirements from Food and Agriculture Organization for copyright agreement. The work presented in Chapter 2 has been supported by a grant from Food and Agriculture Organization (FAO) of the United Nation, in the context of the Lesser Antilles Pelagic Ecosystem (LAPE) project, project FI:GCP/RLA/140/JPN.